Development of AA2014&AA2219 Metal Matrix Nano Composites and Evaluation of their Mechanical and Tribological Characteristics

Submitted in partial fulfilment of the requirements

for the award of the degree of

Doctor of Philosophy

by

VISHNUMURTHY NALLAPATI

Roll No: 701239

Department of Mechanical Engineering
NATIONAL INSTITUTE OF TECHNOLOGY
WARANGAL – 506004
Telangana State, INDIA.

March – 2017

Development of AA2014&AA2219 Metal Matrix Nano Composites and Evaluation of their Mechanical and Tribological Characteristics

Submitted in partial fulfilment of the requirements

for the award of the degree of

Doctor of Philosophy

by

VISHNUMURTHY NALLAPATI

Roll No: 701239

Supervisor:

Dr. C.S.P. Rao

Professor

Co Supervisor:

Dr.N.Selvaraj

Professor

Department of Mechanical Engineering

NATIONAL INSTITUTE OF TECHNOLOGY

WARANGAL – 506004

Telangana State, INDIA.

March – 2017

THESIS APPROVAL FOR Ph.D.

This thesis entitled **"Development of AA2014&AA2219 Metal Matrix NanoComposites and Evaluation of their Mechanical and Tribological Characteristics"** by **Mr. Vishnu Murthy Nallapati** is approved for the degree of Doctor of Philosophy.

Examiners

_____

_____

_____

Supervisor(s)

Dr. C. S. P. Rao

(Supervisor)

Professor, Mechanical Engineering Department, NIT Warangal

Dr.N.Selvaraj

(Co Supervisor)

Professor, Mechanical Engineering Department, NIT Warangal

Chairman

Prof. S. Srinivasa Rao

Head, Mechanical Engineering Department, NIT Warangal

Dedicated
To
My Parents
&
My Beloved Sister(s)
Sreepada Sunita and Chandana Sujatha

NATIONAL INSTITUTE OF TECHNOLOGY
WARANGAL-506004.Telangana State,INDIA

CERTIFICATE

This is to certify the thesis entitled **"Development of AA2014&AA2219 Metal Matrix NanoComposites and Evaluation of their Mechanical and Tribological Characteristics"** submitted by **Mr. Vishnumurthy Nallapati** for, Roll No.701239 to **National Institute of Technology, Warangal** in partial fulfilment of the requirements for the award of the degree of **Doctor of Philosophy in Mechanical Engineering** is a record of bonafide research work carried out by him under my supervision and guidance. This work has not been submitted elsewhere for the award of any degree.

Signature of the Co-supervisor

Dr. N. Selvaraj
Professor
Department of Mechanical Engineering,
National Institute of Technology,
Warangal, Telangana.

Signature of the Supervisor

Dr. C.S.P.Rao
Professor &Head
Department of Mechanical Engineering,
National Institute of Technology,
Warangal, Telangana.

Place: Warangal.

Date:

NATIONAL INSTITUTE OF TECHNOLOGY
WARANGAL – 506 004, Telangana State, INDIA

DECLARATION

This is to certify that the work presented in the thesis entitled "**Development of AA2014&AA2219 Metal Matrix NanoComposites and Evaluation of their Mechanical and Tribological Characteristics**", is a bonafide work done by me under the supervision of **Dr. C.S.P. Rao**, Professor, Department of Mechanical Engineering, NIT Warangal, India and Co supervision of **Dr. N.Selvaraj**, Professor, Department of Mechanical Engineering, NIT Warangal, India and has not been submitted for the award of any degree to any other University or Institute.

I declare that this written submission represents my ideas in my own words and where ever others ideas or words are included have been adequately cited and referenced with the original sources. I also declare that I have adhered to all principles of academic honesty and integrity and have not misrepresented or fabricated or falsified any idea/data/fact/source in my submission. I understand that any violation of the above will cause for disciplinary action by the institute and can also evoke penal action from the sources which have thus not been properly cited or from whom proper permission has not been taken when needed.

Place: Warangal.
Date:

VishnuMurthy Nallapati
Roll No. 701239

ABSTRACT

Metal matrix nanocomposites are being increasingly used in the aerospace and automobile industries owing to their enhanced properties such as elastic modulus, hardness, tensile strength at room and elevated temperatures and wear resistance combined with significant weight savings over un-reinforced alloys and excellent thermal conductivity. Aluminum Metal Matrix nanocomposites are being used in place of cast iron and steel in automobile, mining and mineral sectors due to their lightweight and high strength. Aluminium alloys are preferred engineering material for automobile, aerospace and mineral processing industries for various high performing components that are being used for varieties of applications owing to their excellent properties. The commonly used reinforcements are fibers, whiskers and particulates. The advantages of particle reinforced composites over others are their formability with cost advantage and exhibit improved abrasion resistance and they find applications ranging from kitchen to automobile to space structures. The strength of these composites is proportional to the percentage volume and fineness of reinforced particles. These ceramic particle reinforced Aluminium alloy composites have led to a new generation of tailorable engineering materials with improved specific properties.

In most applications, there exist situations where two mating parts are in sliding contact with each other. Due to the relative motion of these sliding parts, there is an inevitable loss of material due to friction. In certain situations, if the extent of material wear is beyond a critical limit, there are possibilities of catastrophic failure of the components leading to huge material and economic losses. Wear is a complex phenomenon and is the most important reason for the damage and consequent failure of machine parts. A lot of experiments have to be conducted in order to study the wear behavior resulting in wastage of both man power and money. Hence, the prediction of wear properties is of utmost importance in the present industrial scenario to assess the life of sliding components in advance to avoid massive financial losses.

In the present study, AA2014/AA2219 nanocomposite castings were fabricated using the ultrasonic assisted stir casting technique. The AA2014/AA2219 alloy and

SiCp/Al_2O_3 nanoparticles of various sizes(50 nm and 150 nm) were used as the base alloy and the reinforcements respectively. Nano ceramic reinforcements were added into the molten metal and then dispersed by machanical impeller and then followed by ultrasonic assisted cavitation and acoustic streaming. Ultrasonic vibration has been used for degassing, purifying and refinement of metallic materials, because introducing the ultrasonic vibrational energy into a molten metal will induce nonlinear effects such as cavitation and acoustic streaming. The dispersion of nano reinforcements and removel of agglomerations in the liquid molten metal is an important application of ultrasonic assisted stir casting process. The nano reinforcements were in wetted condition, they can form agglomeration of nano particles by various physical and chemical nature of attractive forces including surface tension of liquid molten metal and van der Waals forces.

The attraction forces must be overcome in order to deagglomerate and disperse the particles into molten metal. The application of pressure gradient generated by ultrasonic waves breaks agglomarations formed by nano ceramic particles. Particles dispersion by ultrasonic waves creates microturbulences in the molten liquid pool, and also create small transient domains that would reach very high temperatures and pressures as well as extremely high heating and cooling rates. The shock force that takes place during ultrasonic cavitation process coupled with local high temperatures can break the nano reinforcement particle clusters and clean the surface of the particles. Ultrasonic vibration can improve the wettability between the nano reinforced ceramic particles and the liquid state base alloy, which can assist to distribute the nano ceramic reinforcement particles more uniformly into the molten metal. In present study,the mechanical properties and wear behaviour of AA2219/AA2014/SiC/Al_2O_3 based metal matrix nano composites were studied.

The hardness of the composites found to be increased with increase in filler content and the composites containing higher filler content exhibit higher hardness. The hardness of the AA2219/SiCp/50 nm composite material increases by an amount of 9.39% as the content of SiCp increases from 0 to 2Wt. % and in case ofAA2219/Al_2O_3/50 nm, AA2219/SiCp/150 nm, AA2219/Al_2O_3/150 nm, AA2014/SiCp/50 nm, AA2014/Al_2O_3/50 nm, AA2014/SiCp/150 nm and AA2014/Al_2O_3/150 nm, nanocomposites, the increase in hardness was found to be 5.9%, 7.45%, 5.09%, 8.28%, 3.1%, 6.6% and 1.9% respectively.

The ultimate tensile strength of the composites are found higher than that of base matrix and composites containing higher filler content exhibits superior tensile strength properties than other composites studied. The ultimate tensile strength of the AA 2219/SiCp/50 nm composite material increases by an amount of 35.14% as the content of SiCp increases from 0 to 2wt.% and in case of AA2219/Al_2O_3/50 nm, AA2219/SiCp/150 nm, AA2219/Al_2O_3/150 nm, AA2014/SiCp/50 nm, AA2014/Al_2O_3/50 nm, AA2014/SiCp/150 nm and AA2014/Al_2O_3/150 nm, nanocomposites, the increase in ultimate tensile strength was found to be 32.38%, 33.35%, 27.27%, 19.68%, 27.82%, 20.95% and 15.59% respectively. Taguchi L16 orthogonal array is used to conduct experiments for varying Input parameters namely applied a load, sliding distance, sliding velocity and weight % of nano ceramic particulates. The output parameter of the study is specific wear rate. The results of the experimentation were analyzed using Taguchi and Grey Relation Analysis techniques. ANOVA, GRA analysis on specific wear rate has been performed. Sliding distance, load and Wt.% of reinforcement parameters are having more influence on specific wear rate. Whereas sliding velocity influence is minimum. We found same regression models in both the cases. We also found that there is maximum error of 3% between experimental and regression values on the entire set of experimentation. Hence regression models can be used as an accurate model to predict specific wear rate of Aluminium MMNCs. The optimum wear test input parameters for minimum specific wear rate have been observed. According to Taguchi analysis the optimal process parameters for AA2219 based metal matrix nanocomposites are "L4-SD4-SV2-Wt.%1", and for AA 2014 based metal matrix nanocomposites are "L4-SD4-SV3-Wt.%1". Grey relational analysis (GRA) was also performed for multi-level optimization i.e. Minimization of the specific wear rate of all the eight metal matrix nanocomposites. According to Grey relational analysis the optimal process parameters for AA 2219 based metal matrix nanocomposites are "L4-SD4-SV2-Wt.%1", and for AA 2014 based metal matrix nanocomposites are "L4-SD4-SV3-Wt.%1". Hence both analysis techniques are in concurrence.

CONTENTS

LIST OF FIGURES

LIST OF TABLES

SYMBOLS

Symbol	Description
AA	Aluminium Alloy
Al	Aluminium
MMNC	Metal Matrix NanoComposite
UTS	Ultimate Tensile Strength
XRD	X Ray Diffraction
ANOVA	Analysis of Variance
Eq	Equation
WH	Wear Height
SiCp	Silicon carbide particulates
OA	Orthogonal Array
VOW	Volume of Wear
SWR	Specific Wear Rate
L	Load
SD	Sliding Distance
SV	Sliding Velocity
Wt.%	Weight Percentage
POD	Pin on disc
COF	Coefficient of Friction
S/N	Signal to noise ratio
km	Kilometer
s	Second

Chapter 1

Introduction

1.1 Engineering Materials

There are various types of engineering materials are available in the market and used in different applications. Design and development of new materials based on application and narrow path. The family of materials flow chart is shown in Figure 1.1. The engineering materials are Metals, Ceramics, Glasses, Polymers, Elastomers and Composites. The researchers were developed new materials, i.e., nanomaterials, hybrid materials, and hybrid nanomaterials by combining metals, ceramics, and polymers. However, the technology improved day by day and moved towards light weight, higher efficiency materials like composites. Composites divided into different types based on selection of matrix alloy or type of reinforcement used. There are metal matrix composites, polymer matrix composites, and ceramic matrix composites. The desirable properties are high strength, low density, stiffness, high-temperature stability; adjustable coefficients of thermal expansion, improved wear resistance, high electrical and thermal conductivity. Metal matrix composites have been applied in various applications for their flexibility in property customize based on specific requirement. The metal matrix composites in the market have been growing significantly because of the excellent properties of the metal matrix composites (BCC Research 2015). Figure 1.2. Shows the global consumption of metal matrix composites in different areas of applications. The total volume expected requirement is around 8000 tons in volume for the year 2019.

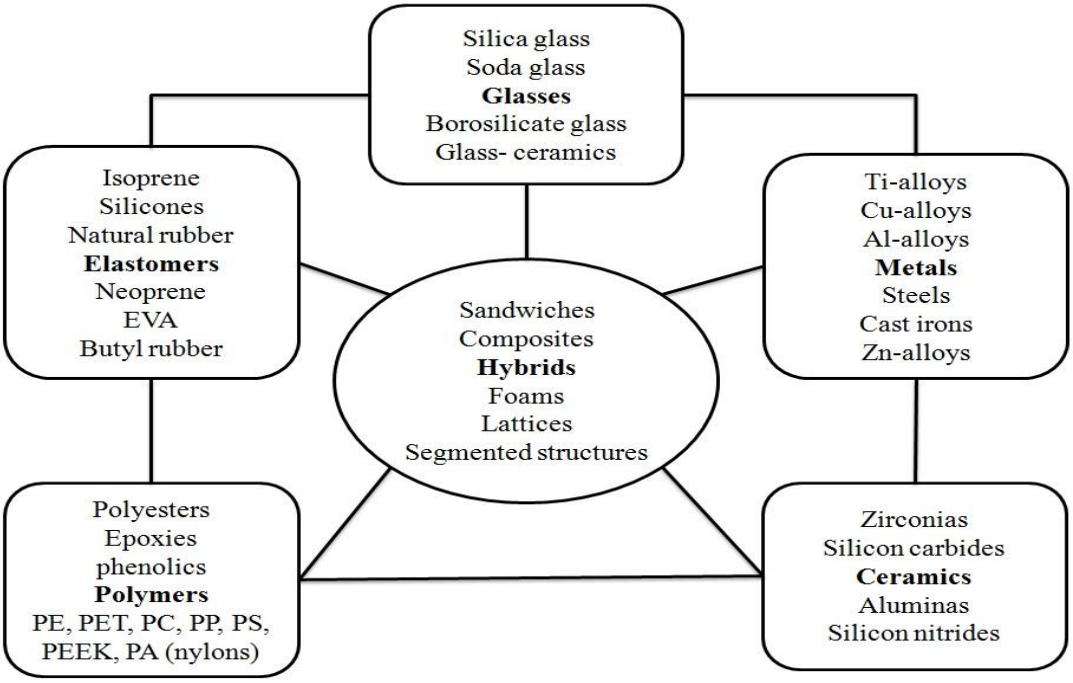

Figure 1.1. Basic families of metals, ceramics, polymers, glasses and elastomers

The increasing growth of the metal matrix composites market requires advanced technologies to mass produce metal matrix composites at low cost with high efficiency. However, there have been development activities in metal matrix composites, insufficient process stability, and reliability, and low economic efficiency still challenges the metal matrix composites manufacturing industry.

Figure 1.2 Global MMC market (2012-2019) (BCC Research 2015)

The materials and process charts of different materials were developed by GRANTA CES 2009. The process chart of Young's modulus versus density of different materials is shown in Figure 1.3. The process chart of Strength versus density of different materials is shown in Figure 1.4. From figures 1.3&1.4 the materials range was explained based on ratio of E to ρ .

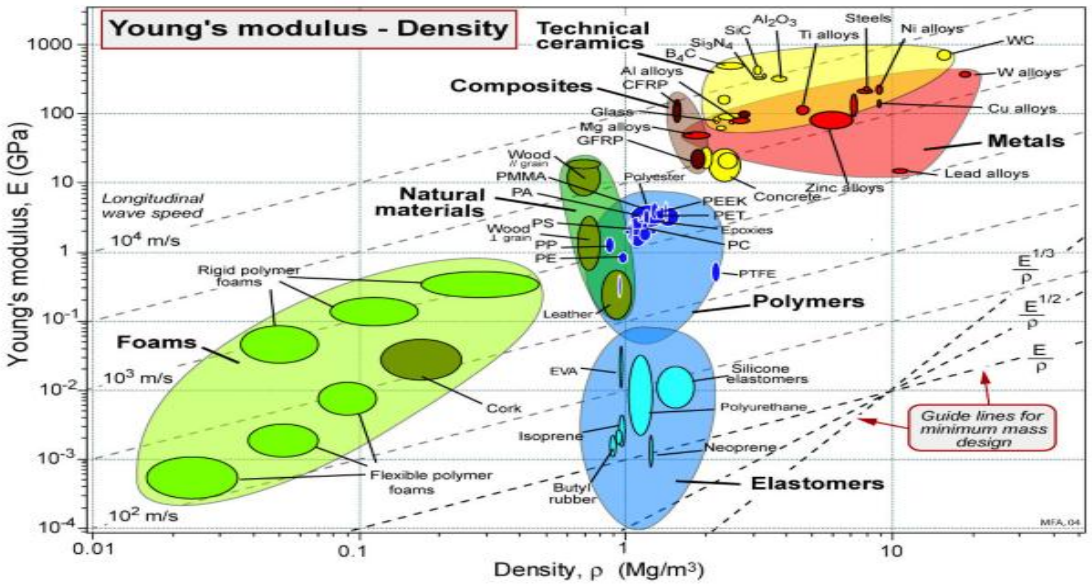

Figure 1.3. Process chart Density Vs Young's modulus (GRANTA CES 2009)

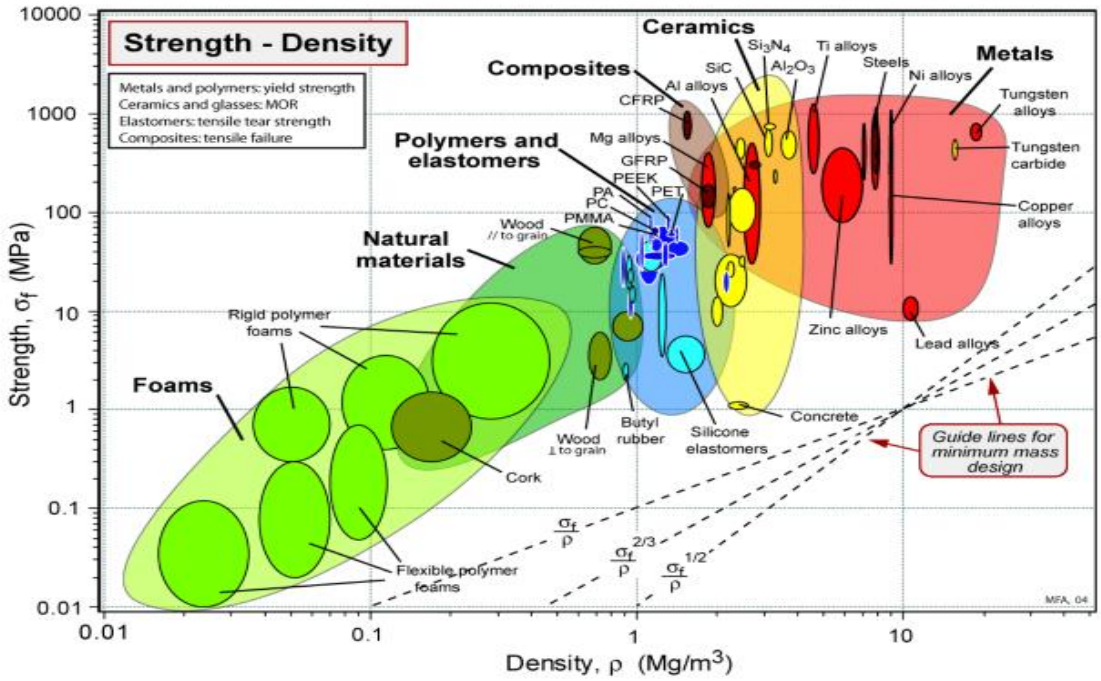

Figure 1.4 Process chart Density Vs Strength (GRANTA CES 2009)

1.2 Aluminium

Aluminium is boron group element having atomic number 13 in the periodic table. It is a third most abundant element in the earth's crust. It is most widely used element in the engineering applications apart from iron. It has excellent thermal conductivity, good electrical conductivity, and high reflectivity to light and heat. It has corrosion resistance under aggressive service conditions. Aluminium alloys offer a combination of mechanical and wear properties and low density. It is highly suitable for manufacturing of composite materials.

Sir Humphery Davy established aluminium in the year 1808. 17 years later the pellet of the metal was produced by Danish scientist. German scientist Wohler established outstanding characteristics lightness in the year 1845. Henri Saint-Clair Deville produced a solid bar in France in the year 1855. Later many low-cost production methods were improved. Researchers did constant research on product development throughout the 1960's, 70's, and 80's led to an endless range of consumer goods incorporating aluminium. Most of the applications aluminium used because of its lightness, high strength, formability, durability, and conductivity. Aluminium is unique in being highly economical to recycle. Aluminium is the third most abundant element in the earth crust. The crystal structure of the aluminium is face-centered cubic.

1.2.1 Aluminium Alloys

Aluminium metal is the backbone of the aerospace industries. Pure aluminium has certain limitations. However, researchers have shifted the research towards its alloys for better properties than aluminium. There are two types of alloy systems, i.e., wrought alloys and cast alloys. The aluminium alloys were classified given below:

1.2.1.1 Wrought alloys

- Unalloyed aluminium (1XXX)
- Aluminium-copper alloys (2XXX)
- Aluminium-manganese alloys (3XXX)
- Aluminium-silicon alloys (4XXX)
- Aluminium-magnesium alloys (5XXX)
- Aluminium-magnesium-silicon alloys (6XXX)

- Aluminium-zinc-magnesium alloys (7XXX)
- Aluminium- other elements (not covered by other series) (8XXX)

1.2.1.2 Cast alloys

- Unalloyed aluminium (1xx.x)
- Aluminium-copper (2xx.x)
- Aluminium-silicon, copper and/ or magnesium (3xx.x)
- Aluminium-silicon (4xx.x)
- Aluminium-magnesium (5xx.x)
- Aluminium-zinc (7xx.x)
- Aluminium-tin (8xx.x)
- Aluminium- (other elements) (9xx.x)

1.2.2 Designation of Aluminium Alloy (Temper)

Two systems designated the aluminium alloys one is Aluminium Association and European Normative aluminium wrought alloys. The wrought aluminium alloys classified in four digits by Aluminium Association (AA), Washington USA. The European reference for the alloys will be identified with the preface EN and AW. The temper designations flow chart as shown in Figure 1.5.

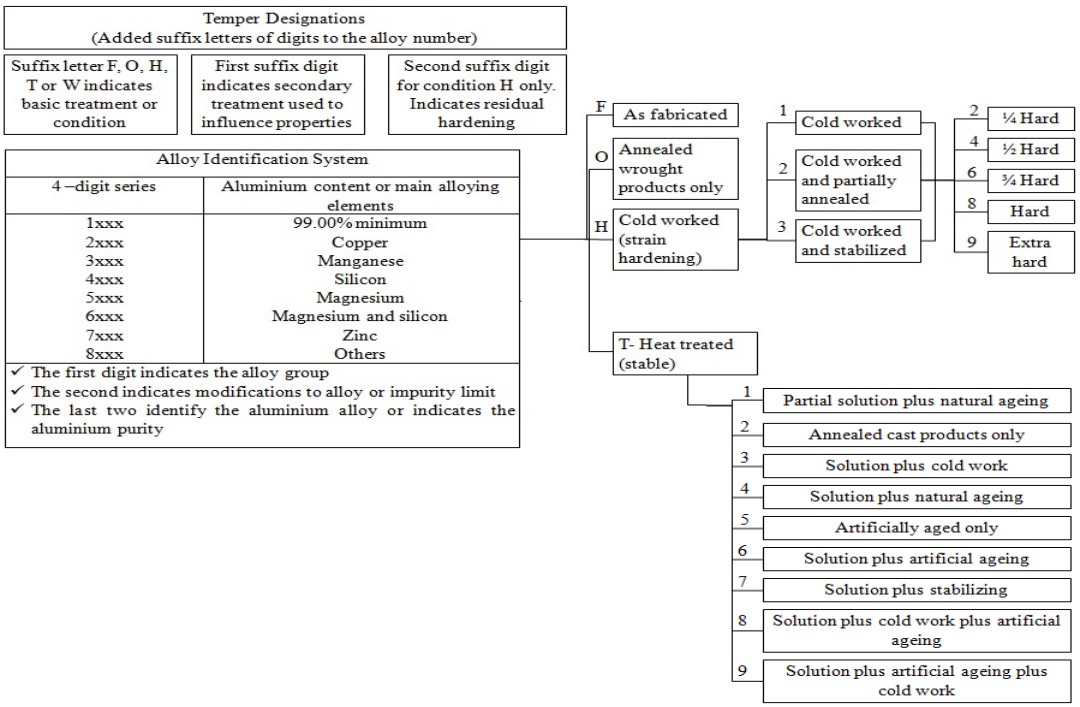

Figure 1.5 Aluminium Alloy Temper Designation flow chart

1.3 Composite Materials

Composite materials are made up of two or more constituents that are combined at a macroscopic level and are not soluble in each other. One constituent is reinforcing phase, and the other one is a matrix. The reinforcing material may be discontinuous or continuous in the form of particulates, whiskers, and fibers. The matrix materials are continuous. For example concrete is a composite material, it includes reinforced steel, concrete, and cement as a binding material.

1.4 Classification of Composite Materials

Composites classified into different types based on the type of reinforcements or the kind of matrix used. Matrix based composites are metal matrix composites (MMCs), ceramic matrix composites (CMCs) and polymer matrix composites (PMCs).

1.4.1 Metal Matrix Composites (MMCs)

Metal matrix composites used in different applications because of its high strength, fracture toughness, and stiffness than the polymers counterparts. Metal matrix composites can withstand elevated temperatures in the competitive environment than polymer composites. Most of metallic elements and alloys can use as matrix materials, and they require reinforcement materials which to be stable over a range of temperature and would be non-reactive too. Metals and alloys are mostly useful matrix materials. Only light metals are responsive, with their low density proving an advantage. Aluminium, Titanium, and Magnesium are the metal matrix currently in a trend, which are particularly useful for aerospace applications. The addition of high modulus ceramic reinforcements to the metallic matrix, they can offer high strength to the composites. The strength to weight ratios of resulting metal matrix composites can be greater than alloys. The melting point, mechanical and physical properties of the composite at various temperatures determine the service temperature of composites. Mostly metals, compounds, and ceramics can be used with matrix materials of low melting point alloys. The choice of reinforcements becomes more restrict with an increase in the melting temperature of matrix materials. The selection of strengthening materials becomes more restrict with an increase in the melting temperature of matrix materials.

1.5 Matrix

The matrix material is a homogeneous and monolithic completely continuous primary phase. Matrix material provides a continuous medium for holding and binding reinforcements together into a solid. It acts as protecting film to the reinforcements from aggressive environment service condition. It can transfer the load between the reinforcement from any external load. It gives a rigid form to the composite and provides texture. It can control chemical and electrical properties. It reduces the stress concentrations by providing an elastic response and redistribution of internal stress. It provides functionality and durability.

1.5.1 Types of Matrix

Titanium, copper, magnesium, nickel-based superalloys, aluminium and stainless steels used as matrices. The aluminium, titanium, magnesium alloy based matrices employed in composites for aerospace and automotive applications. Because of their high strength to weight ratio and light weight. Copper based matrix composites used for applications regarding electrical and thermal contacts. For high-temperature applications, nickel based super alloys and stainless steel matrix used. Because of their high melting point temperature. Aluminium alloys (AA 2014 and AA 2219) has received considerable attention for last two decades. The aluminium (AA 2219) alloy is readily weldable, used for aerospace, fuel tanks, and space shuttle and rocket booster applications. Both the alloys used in aircraft skin, aircraft fittings, ballistic armor, forged and machine components.

1.5.2 AA 2014

AA 2014 alloy is containing 4 % of copper; it is discovered by Alfred Wilm in the year 1903. It was designed by International Alloy Designation System created by Aluminum Association in the year 1970. It slowly hardens when left at room temperature for many days. It has high strength, excellent corrosion resistance, and mechanical properties.

1.5.3 Fabrication and Heat treatment of AA2014

- **Annealing**

  AA2014 can be annealed at 413°C (775°F) for 2 to 3 hours. The alloy is then cooled each hour between 10 and 260°C (50 and 500°F) that is followed by air cooling.

- **Cold Working**

  AA2014 can be cold worked in the T4 and T3 tempers. Tight bend radii is not recommended for this alloy.

- **Welding**

  The inert gas consumable arc method is recommended for welding AA2014. Filler rods of either 2017 alloy or 2014 alloy are used in the welding process. Fixturing is arranged for minimum strength as this alloy is subject to cracking during the welding process.

Table 1.1 Properties of AA2014

S.No	Properties	Metric
1.	Density	2.8 g/cm^3
2.	Melting point	510^{o}C
3.	Elastic Modulus	70- 80 GPa
4.	Poisson's ratio	0.33
5.	Thermal expansion	23 (10^{-6}/ºC)
6.	Thermal Conductivity	192 (W/mK)
7.	Ultimate tensile strength	190 - 480 Mpa

- **Forging**

  AA2014 can be forged between 399 and 454°C (750 and 850°F).

- **Forming**

  Conventional methods are used for forming AA2014. The forming process is performed in the T3 or T4 temper and tight bend radius is not recommended for this welding process.

- **Machinability**

  AA2014 has good machinability in the annealed condition and usage of kerosene or oil is recommended for this machining process. Usage of 20° side rake, 10° clearance and 15° top rake is ess ential for lathe cutting.

- **Heat Treatment**

  AA2014 is heat treated at 502°C (935°F) and then water quenched. T4 temper is produced as a result of this heat treatment.

- **Hot Working**

  AA2014 is hot worked in temperatures ranging 149 and 204°C (300 to 400°F).

- **Hardening**

  AA2014 is hardened by a precipitation heat treatment at 502°C (935°F). The alloy is then water quenched thus producing T4 temper. Additional cold work after the hardening process of this alloy produces other tempers. T6511 and T6510 tempers are produced by heat treatment at 160°C (320°F).

- **Applications**

  AA2014 is used in the manufacture of truck frames and aircraft structures.

1.5.4 AA 2219

AA 2219 alloy is containing 6% copper; it is discovered by Alfred Wilm in the year 1909. It was designed by International Alloy Designation System created by Aluminium Association in the year 1970. It has high strength, excellent corrosion resistance, and mechanical properties.

Table 1.2 Properties of AA2219

S.No	Properties	Metric
1.	Density	2.6-2.82 g/cm3
2.	Melting point	535^{o}C
3.	Elastic Modulus	70- 80GPa
4.	Poisson's ratio	0.33
5.	Thermal expansion	23 (10^{-6}/ºC)
6.	Thermal Conductivity	170 (W/mK)
7.	Ultimate tensile strength	170 - 310 Mpa

1.5.5 Fabrication and Heat treatment of AA2219

- **Machinability**

  AA2219 can be machined in the annealed condition. In the heat treated condition, this alloy is very difficult to machine. Oil base lubrication is used to perform machining operations.

- **Forming**

  AA2219 can be formed using conventional techniques.

- **Welding**

  AA2219 can be welded using resistance welding, and inert gas welding techniques with high precautions in order to prevent cracking. This process is followed by heat treatment in order to maintain the corrosion resistance property of this alloy.

- **Heat Treatment**

  AA2219 can be heat treated at 538°C (1000°F) followed by quenching in cold water.

- **Forging**

  AA2219 can be forged to maintain the corrosion resistance property.

- **Hot working**

  AA2219 should not be hot worked if they are not subjected to heat treatment in order to restore the corrosion resistance property of this alloy.

- **Cold working**

  AA2219 can be cold worked using conventional methods.

- **Annealing**

  AA2219 is annealed at 538°C (1000°F) for sufficient time followed by quenching in cold water.

- **Aging**

  AA2219 can be aged at 190°C (375°F) for varying time after annealing and quenching. Forgings can be aged at 190°C (375°F) for 18 h, and sheet or plate type product forms can be aged at 190°C (375°F) for 36 h followed by cooling in air.

- **Hardening**

  AA2219 is hardened by aging or cold working.

- **Applications**

  AA2219 is suitable for manufacturing structural components, which are used in high strength weldments and high temperature applications.

1.6 Reinforcement

Generally the reinforcing phase elements were Al_2O_3, SiC, SiO_2, Si_3N_4,SiC and BC of micro and nano average size particles was considered to improve the properties of the

matrix materials. Out of all these reinforceing materials mostly Al_2O_3 and SiC nano ceramic reinforceing materials gives the best results[16]. The nano alumina (Al_2O_3) reinforcements supplied by Sigma-Aldrich, Hyderabad, India. US research nanomaterials supplied the nano silicon carbide (SiC) reinforcements.

1.6.1 Purpose of Reinforcement

The purpose of reinforcement in the composite materials given below:

- ✓ To increase the strength of the composite
- ✓ To enhance the stiffness of the composite
- ✓ To improve the wear properties
- ✓ To improve the corrosion resistance
- ✓ To moderate the temperature resistance

1.6.2 Types of Reinforcements

In the fabrication of composites, the reinforcements can be particulates, fibers. The different types of reinforcing elements use in making composites depends on strength and kind of applications. Fibers can be continuous and discontinuous. Fiber reinforced composites has strength in their orientation direction.

1.6.3 Alumina (Al_2O_3)

Alumina (Al_2O_3) is widely used material in the engineering ceramics and which is cost effective. The high-performance ceramic material grade is readily available at low cost. The nano-size alumina had an excellent combination of properties and used in various applications.

1.6.3.1 Characteristics of Alumina (Al_2O_3)

The alumina (Al_2O_3) properties as following

- Excellent dielectric properties
- At elevated temperatures can cause resistance to alkali attack and strong acid
- High wear resistance and hardness
- High thermal conductivity
- High stiffness and strength

1.6.4 Silicon Carbide (SiC)

The silicon carbide is a ceramic compound. It had excellent abrasive properties and used in making grinding wheels. It is high melting point chemical compound. It can use in refractories and abrasives. It has excellent mechanical properties.

1.6.4.1 Characteristics of Silicon Carbide (SiC)

The silicon carbide (SiC) properties as following

- High thermal conductivity
- High strength and low density
- Low coefficient of thermal expansion
- High hardness
- High shock resistance
- Excellent corrosion resistance
- High elastic modulus

1.7 Aluminium Metal Matrix Nano Composites (AA-MMNCs)

The demand is globally increasing for new materials every day. There is a need for high efficiency and light materials in the automobile, structural construction works, helicopter, exit guide vanes of gas turbine engine, space shuttle, flywheels, military industries, and aerospace applications has lead to voluminous research in the evolution of aluminium nanocomposites. Metallic matrix based nanocomposites (MMNCs) possess numerous advantages over monolithic materials, alloys, and metal matrix composites (MMCs), including higher thermal conductivity than ceramic materials, high specific strength, high specific stiffness, low density and good wear resistance, and so forth. It is a promising approach to use nano-size ceramic reinforcements. Nanoparticulate reinforced metal matrix composites improved both physical and mechanical properties without affecting ductility. Currently, there are many fabrication techniques of metal matrix nanocomposites (MMNCs) are solid state and liquid state. Solid state includes Mechanical Alloying [1], Powder Metallurgy [2], Diffusion Bonding [3], Spray Deposition [4], Electroplating [5], Immersion Plating [6], Physical Vapour Deposition [7], Spark plasma sintering [8] and Chemical Vapour Deposition [9], etc. Liquid state processing includes Stir Casting [10], Compo Casting [11],

Laser Deposition [12], Squeeze Casting [13], and Melt Infiltration [14] etc. The mixing of nanosize ceramic reinforcements is normally lengthy, expensive and energy consuming. Ultrasonic assisted stirring and casting suitable manufacturing technique for minimizing the porosity and uniform reinforcement distribution. One of the best properties of ultrasonic assisted stirring moreover, casting for fabrication of nanocomposites can be obtained when the nano reinforcement is homogeneously dispersed in the alloy matrix, as approved by experiment and some of them are used in industry [15]. Ultrasonic assisted stir casting method can use in commercial casting processes due to its effects on the microstructure of metals, which include control of homogeneity, grain structure, refinement of secondary phases and uniform distribution of reinforcements [16].

In the present study, AA 2014/AA 2219 nanocomposite castings were fabricated using the ultrasonic assisted stirring and casting technique. The AA 2014/AA 2219 alloy and SiC/Al_2O_3 nanoparticles used as the matrix alloy and the reinforcement. Nano ceramic reinforcements were added into the molten metal and then dispersed by ultrasonic assisted cavitation and acoustic streaming. Ultrasonic vibration has used for degassing, purifying and refinement of metallic materials [17] because introducing the ultrasonic vibrational energy into a liquid will induce nonlinear effects such as cavitation and acoustic streaming. The dispersion of nano-reinforcements and removal of agglomerations in the molten liquid metal is an important application of ultrasonic apparatus. The nano-reinforcements were when in a wetted condition, then they can build agglomerates by various physical and chemical nature of attractive forces including surface tension of molten liquid metal and van der Waals forces.

The attraction forces must overcome to deagglomerate and disperse the particles into the liquid medium. Uniform dispersion and deagglomeration are paramount to use the full potential of the particles. Especially nano-reinforcements offer unusual characteristics, which can only exploit in the highly uniform dispersed state. The application of stress generated by ultrasonic cavitation breaks the nano reinforcement particle agglomerates apart. Also, the liquid pressed between the reinforcement particles. Dispersion by ultrasonic is a consequence of microturbulence caused by fluctuation of pressure and cavitation. Ultrasonic cavitation can create small transient domains that would reach very high

temperatures and pressures as well as extremely high heating and cooling rates. The shock force that takes place during ultrasonic cavitation processing coupled with high local temperatures can break the nano reinforcement particle clusters and clean the surface of the particles. Ultrasonic vibration can improve the wettability between the nano reinforcement particles and the metal matrix [18], which can assist to distribute the nano ceramic reinforcement particles more uniformly into the metal matrix. The mechanical properties and wear behaviour of Al-2014/Al-2219 alloy and SiC/Al_2O_3 nano-reinforced composites were studied.

Aluminium and its alloys are the most popular metal matrix for the composites. Because of their high strength to weight ratio, low density, high damping capacity, high thermal conductivity, excellent corrosion resistance and high electrical conductivity. Aluminium based metal matrix nanocomposites have used in several fields where low weight, thermal stability, and ductility are key requirements. Nowadays, the aluminium metal matrix nanocomposites are noticed many applications in aerospace, defense, automotive sectors and other engineering industries. The AA 2014 and AA 2219 alloys have received considerable attention for last two decades. The AA 2014 alloy used in bolted or riveted construction for truck body applications. The AA 2219 alloy is readily weldable, used for aerospace, fuel tanks, and space shuttle and rocket booster applications. Both the alloys used in aircraft skin, aircraft fittings, ballistic armor, forged and machine components.

Particulate reinforced aluminium based matrix nanocomposites represent an alternative and as advanced materials, because of their high strength to weight ratio, high specific heat capacity, high thermal conductivity and dimensional stability. Aluminium based metal matrix nanocomposites with excellent properties are tailor made with different manufacturing processes like mechanical stirring and ultrasonic assisted stir casting, squeeze casting, spark plasma sintering, powder metallurgy, etc. the experimental and theoretical studies have been carried out on the fundamental relationships between the microstructure, physical and mechanical properties of aluminium based metal matrix nanocomposites with different types of matrices, particulates and fibers as reinforcement. The selection of reinforcement type, volume fraction, and geometry was difficult to obtain the best

combination of minimum production cost. The particles can be used for reinforcement: oxides, nitrides, carbides, and borides.

1.8 Manufacturing Methods of Metal Matrix Nanocomposites

There are various fabrication or manufacturing processes being developed by the researchers for metal matrix nanocomposites. The methods were four types (i) liquid state process (ii) solid state process (iii) vapour deposition techniques (iv) semi-solid state method. The processing methods are shown in Table 1.3.

Table 1.3 Various fabrication methods for aluminium based metal matrix nanocomposites

Liquid state process	1) Stir Casting 2) Squeeze Casting 3) Compo Casting 4) Ultrasonic Cavitations based Solidification 5) Spray Deposition
Solid state process	1) Diffusion Bonding 2) Powder Metallurgy 3) Spark Plasma Sintering 4) Laser Deposition
Vapor Deposition	1) Physical Vapour Deposition

1.8.1 Stir Casting

Stir casting process introduced for to fabricate the metal matrix composites in the year 1968 [19]. S. Ray et al. manufactured by introducing alumina ceramic reinforcement particles into the aluminium alloy melt by stirring [19]. This process is suitable for fabricating composites with vol. % ≤ 30 of reinforcements. Mechanical stirring is the key element in stir casting process and the stirring parameters will affect the properties of the composite. The main disadvantage is the formation of porosity in the composites. To prevent the porosity it can be extruded at the end of the process. Schematic diagram of stir casting design setup is

shown in Figure 1.6. Stir casting process is limited because of non-uniform distribution of reinforcement particles in the matrix material.

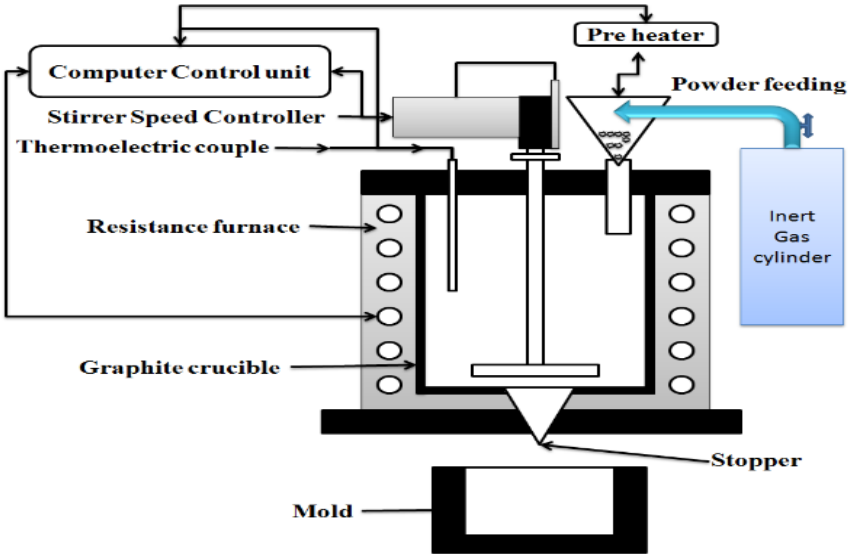

Figure 1.6. Stir casting design setup

1.8.2 Squeeze Casting

Squeeze casting [15] is the process of forcing molten liquid metal into a preform of particulates under controlled environment condition. The pressure is applied after forcing molten liquid metal into performing up to finishing the solidification process. The wettability of the matrix and reinforcement is better and the processing time is very less. The method involves melting of the matrix material in the crucible in a vacuum when the preform is heated separately. In this method complex and near net shapes are achieved. Making preforms with nano-reinforcing particles 's hard for squeeze casting method. The Squeeze casting setup is as shown in Figure 1.7.

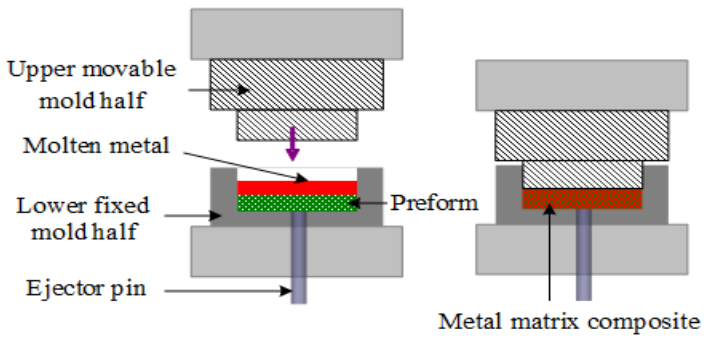

Figure 1.7 Squeeze casting setup

1.8.3 Compo Casting

The compo casting [11] is a process of incorporation of ceramic reinforcement particles in the semisolid metal matrix using mechanical mixing. In this method, the reinforcement particles are distributed uniformly with weak agglomeration. Operating temperatures are low in this process compared to the liquid state processing. Two major problems in this method (i) the reinforcement particles are not wetted to the liquid metal matrix and (ii) the dispersion is not uniform. The compo casting setup as shown in Figure 1.8.

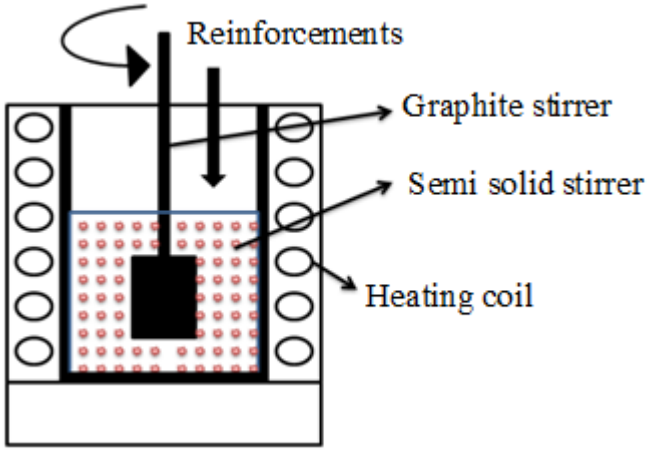

Figure 1.8. Compo casting setup

1.8.4 Ultrasonic Cavitations based Solidification

The ultrasonic cavitation method [16] is a process of distributing reinforcements uniformly in the liquid metal matrix by inducing the cavitations.

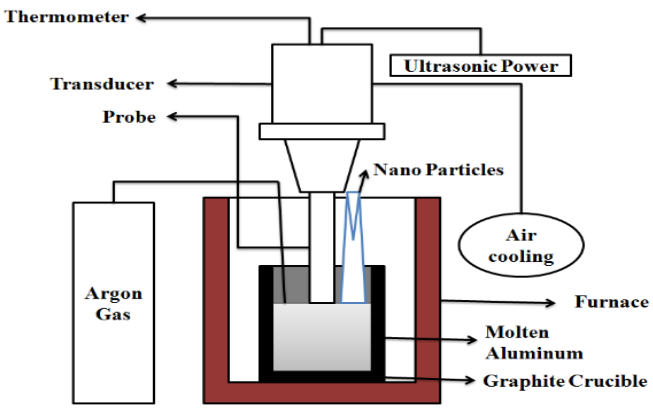

Figure 1.9. Ultrasonic assisted casting setup

In this process the induce the local high temperatures to break the nanoparticle clusters and clean the particle surface. During initial process, mechanical stirring can help to break the clusters by providing larger shear stress. The design of ultrasonic assisted casting setup as shown in Figure 1.9.

1.8.5 Spray Deposition

It is a process [4] of co-deposition of liquid metal droplets and ceramic particles onto a substrate. There two ways (i) depending on the droplet stream is produced from a molten bath (ii) continuous feeding of cold metal into a zone of rapid heat injection. Rapid solidification technique leads to limited chemical reactions between matrix and reinforcements. To improve chemical reactions, after rapid solidification, it is subjected to thermo-mechanical treatments. Which can modify the composite properties to a large extent Extrusion, forging, and rolling operations can improve mechanical properties by the distribution of reinforcements uniformly with less porosity.

1.8.6 Diffusion Bonding

It is a solid state process [3] for joining similar or dissimilar metals. This method is used to manufacture of fiber reinforced metal matrix composites from sheets, powder, foils, powder tape and wire of matrix material. The method of grouping reinforcement fibers and the matrix is determined by the fiber type and preform array process. The composite consolidation can be achieved by high pressure, in the normal direction of the ply surfaces and a sufficient temperature to produce atomic diffusion of the matrix alloy. This process is performed in a vacuum condition. A wide variety of metal matrices can be treated and volume fraction, fiber orientation can be controlled. The disadvantage of this process is long processing time. The diffusion bonding process as shown in Figure 1.10.

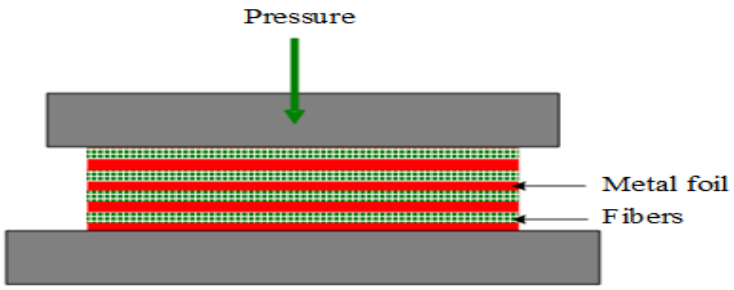

Figure 1.10 Diffusion bonding method

1.8.7 Powder Metallurgy

Powder metallurgy [2] is the process of mixing the matrix and reinforcement powders in a vial and making green compact specimens and then followed by sintering. This process can exploit the nano reinforcement particles and grain boundaries strengthening capability. It is a low-temperature process and the interphase kinetics precisely controlled. It is a unique part fabrication method, highly cost effective in producing complex parts at very close dimensional tolerances, with minimum scrap loss and fewer secondary machining processes. It involves complicated processes during the material fabrication. It is not ideal processing technique for mass production.

1.8.8 Spark Plasma Sintering

In this process, the spark discharges [8] in voids between the particles, generated by an instantaneous pulsed direct current which shall be treated through electrodes at the top and bottom punches of the graphite die, due to this the particle surface activated, purified and the self-heating phenomenon is generated between the particles [20]. It is not only for the production of dense bulk material within short processing duration, and to fabricate nanomaterials and to get real microstructures. The method is important because of getting enhanced properties, effective interface bonding, cleaner grain boundaries, and efficient shrinkage at the lower processing temperature and within a shorter sintering time to consolidate powders compared to other methods.

1.8.9 Laser Deposition

The laser is a process [12] of surface alloying with hard ceramic particles. The surface alloying can improve the wear properties and corrosion resistance of the material. The laser power can be controlled the deposition rate automatically. Using laser power the green compact specimens can be sintered. Different lasers are used to fuse the mixing powders according to energy requirements. Laser processing is described by its high energy density, low heat input, high heating and cooling rates that reduce its effect on a specimen. The laser process schematic diagram is shown in Figure 1.11.

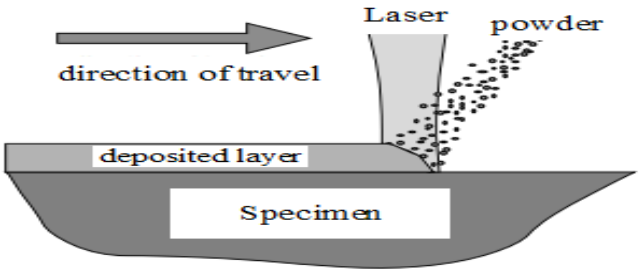

Figure 1.11 Laser process schematic diagram

1.8.10 Physical Vapor Deposition

Physical vapor deposition [7] is a process of depositing materials directly from the vapor phase on a substrate. It is used to manufacture of items which require in thin films for optical, mechanical, chemical and electronic functions. It is demanding and the deposition rate is very low. Coating of geometrically complex parts is complicated. The process is required very high temperatures and vacuums. It requires cooling water system to dissipate heavy heat loads. It is used for surface alloying of the substrate.

1.9 Tribology

Tribology is a concept of science and technology during interacting surfaces in relative motion; it is one of the core concepts in engineering design. It includes the study and collective character describing the field of wear, friction, and lubrication. The tribology design is relatively new, the importance of the constitutive parts of tribology is hoary. It is paramount economically and applicable to all fields such as biological systems, electromechanical, device technology, space engineering and nanodevices.

As compared to both lubrication and friction, the study on wear is relatively new. The importance of wear and the economic losses that followed has made the study of wear very pertinent. The wear and wear rate depend on upon many conditions such as elastic properties, material, surface asperity, the geometry of surfaces and surface roughness.

1.10 Testing of MMCs

1.10.1 Density Measurements

The density of the AA2219 & AA2014 alloy/ (Al_2O_3 or SiC) nanocomposites fabricated through the ultrasonic assisted and stir casting technique was measured using

Archimedes principle. It is a convenient method for measuring the volume of a regularly or irregularly shaped object. The density of the composite samples was examined using a high precision digital electronic weighing balance with an accuracy of 0.0001g. The sample dimensions were measured by measuring its dimensions using a micrometer and weighing its mass using balance. Six vertical measurements were made on each sample. Mass was measured on balance with five decimal point accuracy.

Procedure for measuring density

- Measure mass of the specimen in air (M_a) in grams
- Then submerge the sample completely in water and measure the mass (M_w) in grams
- The water displaced in grams (V = M_a-M_w) in grams. When (ρ_w=1 g/cm^2)

$$\rho = \frac{M_a}{M_a - M_w}$$

- By using the equation above to determine the density of specimen.

1.10.2 Hardness Test

The hardness of the fabricated nanocomposites indicates the mechanical properties of the samples. When surface properties concerned its importance to wear and friction processes, then measurement of hardness of the material is a quick method for to get the mechanical property.

Specifications
Microscope – magnification 800 to 1000X
Objects of 10X, 40/50X, 80/ 100X along with 10X eyepiece
Test load range- 10gf to 2000gf
Loading speed- 15 to 70 µm/sec
Dwell time – 5 to 99 sec
Indenters-square based pyramidal diamond with face angles 136° 0 min

Figure 1.12 Vickers Microhardness tester

The principle of hardness test technique is forcing an indenter into the specimen surface and measuring the dimensions of the indentation. The hardness of the ultrasonic assisted stirring and cast samples were performed Vickers micro hardness tester.

1.10.3 Tensile Strength Test

The tensile test of the aluminium alloy based nanocomposites is conducted as per American Society for Testing and Materials (ASTM-E8) standards. In this test, we can obtain the ultimate tensile strength and yield strength. The dimensions of the specimens prepared as per standards and are shown in Figure 1.13. This test was done with computerized strain rate based ultimate tensile testing machine at room temperature 25˚C as shown in Figure 1.14. It is used to test tensile stress and compressive strength of the materials. The results were recorded accurately with a break point. The stress at maximum is referred to as the ultimate tensile strength.

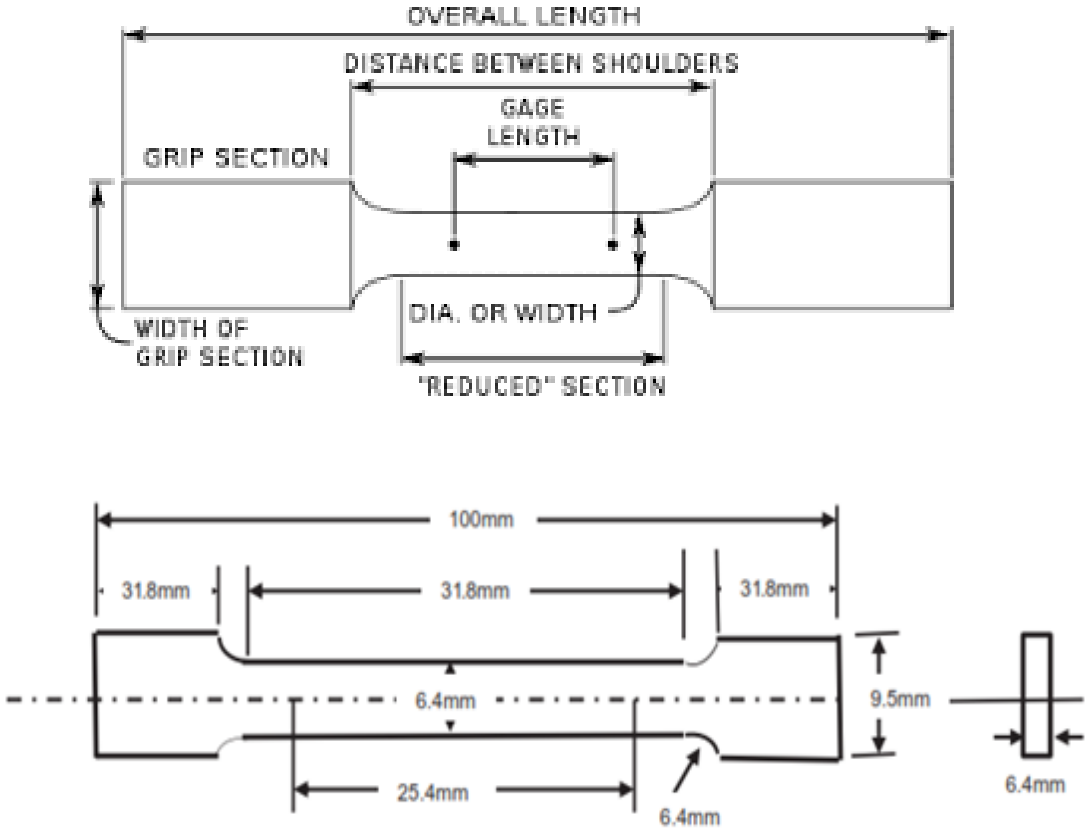

Figure 1.13 Dimensions of the tensile test specimen

Specifications

Electro Mechanical Tensile Testing Machine

Capacity -20 kN

Civil Engineering Department NIT W

Accuracy -In accordance ISO 7500-1 and EN 10002-2, Grade 0.5

Control-force and displacement closed loop controlled

Test speed- 0.001 mm/ min up to 1000/ 500 mm/ min

Crosshead travel- 1000/ 1100 mm

Power requirements- 3×400 V, 500 Hz

Figure 1.14 Electro Mechanical Tensile Testing Machine

1.10.4 Wear Test

The tribological tests were conducted for both the cast matrix alloy and its nanocomposites samples and studied their characteristics like wear height and coefficient of friction on wear testing machine. Table 1.4 gives the technical specifications of the wear test machine (POD) used and Figure 1.15 shows the apparatus and other peripheral units. The wear test samples were prepared in the form of cylindrical pins of diameter 6mm and pin height 25 mm, and the apparatus-disc material is high carbon EN31 steel.

The hardness value of the disc material is HRC60. The tribological tests are conducted according to **ASTM – G99 standard**. In each experiment, the wear height of the sample was recorded in microns by using LVDT control of 1.0 μm least count. During the wear test, the pin surface made contact with the disc surface and both surfaces are relatively moving in opposite directions in which disc is rotating, and the pin is in a stationary position.

Table 1.4 Technical Specifications of the POD Wear Testing Machine

Parameter	Specifications
Pin Dimensions	3 to 12 mm diameter and 10 to 50 mm length
Disc Dimensions	160 mm diameter and 8 to 12mm thickness
Wear track radius	8 mm to 125 mm diameter
Disc rotating speeds	100 to 1000 rpm
Sliding speed range	6 m/s to 26 m/s
Normal load	200N(maximum)
Frictional Force	0 to 200N(digital read out)
Wear height loss measurement	LVDT of 1.0 μm Least count
Input power	230V, 5A, I Phase,50Hz

Because of generation of high frictional force in between the two surfaces cylindrical pin loses the parent material in a vertically downward direction based on this wear height can be noted on the digital screen of LVDT. The load acting on the test specimen during the testing was varied from 5 to 20 N in steps of 5 N; the sliding distance was taken from 1km to 4km and is controlled by setting the timer on the machine at a velocity of 0.763 m/s. The surface roughness of the test pin specimen and the disc were maintained at 0.1 μm *R*a. From the POD experiment, the wear height practiced by the pin is measured in micrometers, and following parameters were calculated.

- ✓ Volume of Wear in mm^3= Cross-sectional Area of the pin X Height loss
- ✓ Weight Loss in grams = Volume of Wear X Density
- ✓ Specific Wear rate = Volume of Wear/(Sliding Distance X Load)

Different graphs were plotted of the various applied loads and reinforcements to distinguish the wear behavior of the metal matrix nanocomposites

- Volume of wear Vs Sliding Distance
- Weight Loss Vs Sliding Distance

- Specific Wear Rate Vs Sliding Distance

Composite Pin in Contact with the Disc

Control Unit of Wear Testing Machine

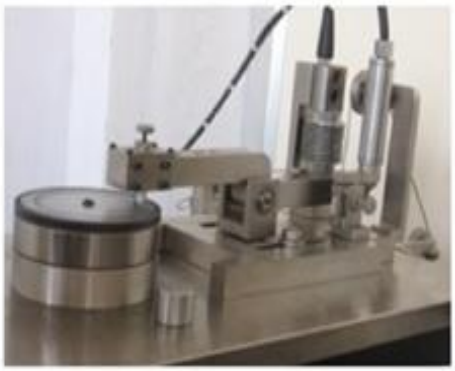

Pin on Disc with LVDT

Pin on Disc with Wear Debris

Figure 1.15 Pin on Disc Setup

1.11 Friction

Friction can be defined as the force resisting the relative motion of solid elemental surfaces, fluid layers each other. A force can prevent the object to move called friction force. In many engineering applications is required to reduce friction. What a body rolling on a horizontal surface is shown in Figure 1.16. N is normal force and f is friction force.

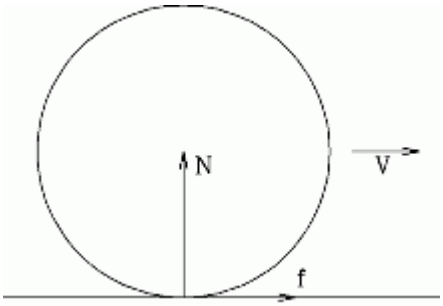

Figure 1.16 Body rolling on surface

1.11.1 Theories of Friction

There are three laws were attributed to dry friction.

- ✓ The force of friction is directly proportional to the applied load
- ✓ The force is independent of the apparent area of contact
- ✓ Kinetic friction is independent of the sliding velocity

1.11.1.1 Static and Dynamic Friction (Interlocking Theory)

The mathematical equation was developed by Leonard Euler (1707-1783) using geometrical resistance theory of dry friction. Euler's theory developed two terms for static and dynamic friction. Friction coefficient from the static condition and the dynamic friction coefficient is reduced by the kinetic term given below. Euler fell back to Galilei experiment of incline plane, and developed equations are provided below. In an incline, the plane block is moving as shown in Figure 1.17.

$$F_s = \frac{2s}{gt^2}F \quad \text{---------- (1)}$$

$$\mu = tan\theta - \frac{2s}{gt^2 cos\theta} \quad \text{---------- (2)}$$

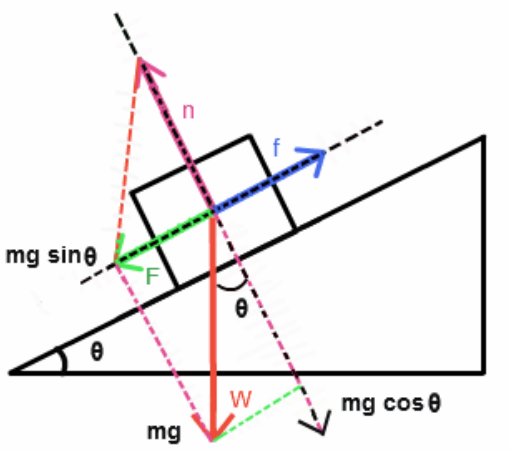

Figure 1.17 A block on incline plain

1.11.1.2 Rolling Friction

Rolling friction theory is proposed initially by Charles-Augustin Coulomb (1736-1806). The theory is, the frictional resistance of a rolling wheel or cylinder is proportional to the load and inversely proportional to the radius of the wheel. In this coulomb's description of rolling friction entirely neglected. Arsene Dupuis (1840) argued and proved that interfacial

rolling resistance and the material resisting leads to an inverse square root dependence of friction.

1.11.1.3 Inelastic Adhesion Concept of Friction

In the year 1954, Bowden and Tabor developed adhesion concept of friction by considering the traditional friction law of Amontons based on the projected area. They were considered real area over which the two sliding bodies are in contact.

1.11.1.4 Richard's Elastic Model of Friction

Archard suggested to the theory of Bowden and Tabor who assumed fully plastic deformation of the asperities. Archard explained friction could also occur if the asperities are only elastically deformed. Bowden and Tabor utilized the Archard suggestion and developed the Hertzian formalism for the contact radius.

1.12 Wear

The wear is the removal of material from a solid surface due to the mechanical action of another solid material. It is slow methodology but the continuous method of removal of materials from one or more elements. Wear is not an intrinsic material property. However, characteristics of the engineering system which depends on speed, load, environmental conditions, temperature, hardness, surface finish and presence of other inclusions.

1.12.1 Types of Wear

There are different types of wear; it is tough to describe types of wear which may likely occur in the tribomechanical system since these are very complex in nature. However, the unlubricated metal pair under sliding contact may be named as dry wear. There are four basic types of mechanisms are classified below.

1.12.1.1 Abrasive wear

Abrasive wear occurs when hard, rough surface element slides over a softer element, producing grooves on the latter. It is also caused by loose, abrasive particles rolling in between two soft sliding surfaces.

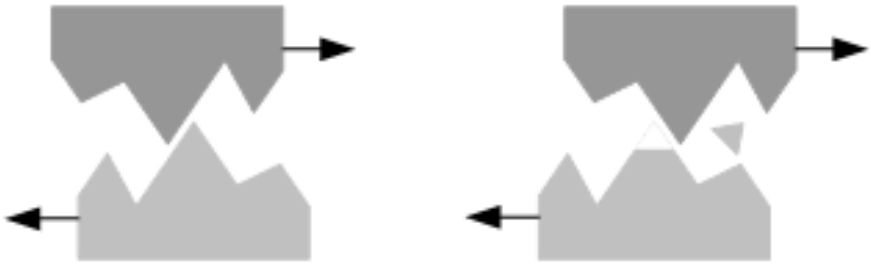

Figure 1.18 Two bodies abrasive wear

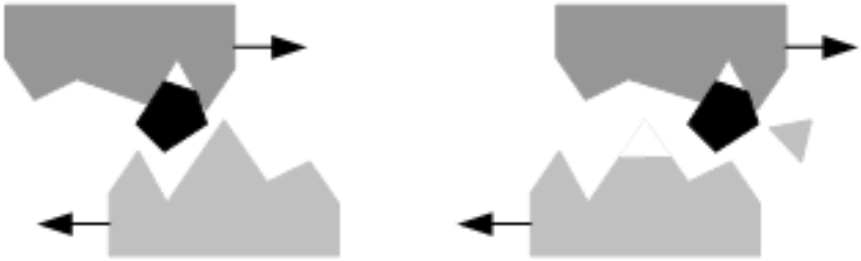

Figure 1.19 Three bodies abrasive wear

There is two types of abrasive wear (i) two-body abrasive wear (ii) three-body abrasive wear. It can be prevented by eliminating the hard, rough constituent. The two-body abrasive wear as shown in Figure 1.18 The three-body abrasive wear as shown in Figure 1.19

1.12.1.2 Adhesive wear

It is caused due to hard element surface sliding across a softer element surface. Since the two hard and soft surface contact through small asperities, adhesion occurs between theses asperities. During this condition, there is a plastic deformation at the contact areas at load application. The adhesive wear as shown in Figure 1.20.

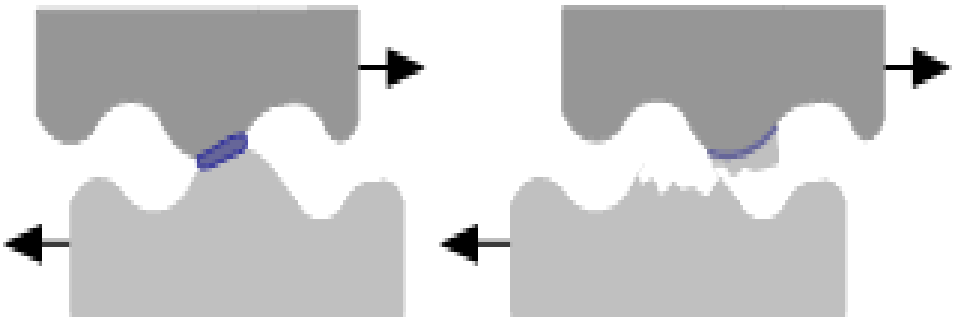

Figure 1.20 Adhesive wear

1.12.1.3 Surface-fatigue wear

This type wears produced due to repeated high-stress attendant on rolling condition, such as that of ball bearing rolling in a machine or metal wheels on tracks. The high stress causes subsurface cracks to form in either the moving or no motion component. As theses cracks grow, large particles separate from the surface and putting ensues. It is the most common form of wear affecting rolling elements such as gears, bearings. The surface-fatigue wear as shown in Figure 1.21.

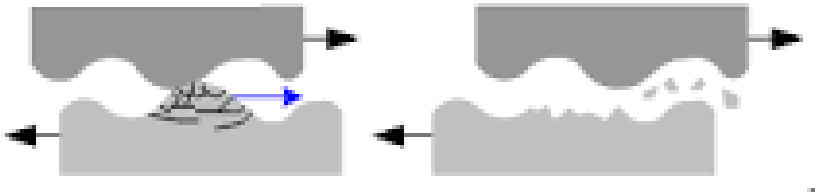

Figure 1.21 Surface-fatigue wear

1.12.1.4 Corrosive wear

It is caused when a gas or liquid chemically attacks a surface left exposed by the sliding process. When a surface corrodes, the products of corrosion tend to stay on the surface, thus slowing down further corrosion. The continuous sliding takes place; the sliding action removes the surface deposits that would otherwise protect against further corrosion, which thus takes place more rapidly. A surface that has experienced corrosive wear has a matte, relatively smooth appearance. The corrosion wears as shown in Figure 1.22.

Figure 1.22 Corrosion wear

1.13 Scope of the Present Research

The demand is increasing for new materials for to prevent pollution from automobile emissions. For to reduce the weight of the vehicle is required high strength to weight ratio materials. The need for high efficiency, low density and light weight new materials in the defense, engineering structures industries, aircraft, aerospace and automotive industries has

lead to huge research and development efforts in the development of aluminum-based metal matrix nanocomposites. The major disadvantage of metal matrix composites with the addition of micron size reinforcement particles in the matrix is improved strength and reduction of ductility. With the addition of nano-reinforcements in the aluminium, the matrix is improved strength and without affecting on ductility. However, the nanocomposite fabrication process is difficult to distribute reinforcements uniformly. There is a variety of reinforcing techniques is attracting interest in nanocomposite materials. This will go for the high-performance aluminium nanomaterials due to certain unique characteristics. There are different manufacturing methods which can apply for aluminium based composites. From these, mechanical stirring and ultrasonic assisted casting could be remarked as a highly efficient and economical method compared with other alternatives. The advantage of mechanical stirring and ultrasonic assisted casting is the uniformly in the reinforcement distribution without formation of clusters. This improves the structural properties but also the reproducibility level in the various properties.

Efforts have been made for to study the tribological behaviour of particle reinforced aluminium based nanocomposites. The reports have been showed significant improvements in mechanical and tribological properties compared to base alloys. The ductility is not affected, and strength is improved when ceramic nanoparticles are reinforced in the matrix.

- Fabrication of AA 2014/ SiC (50 nm & 150 nm), AA 2219 / SiC (50 nm & 150 nm), AA 2014 / Al_2O_3 (50 nm & 150 nm) and AA 2219 / Al_2O_3 (50 nm & 150 nm) nanocomposites manufactured by mechanical stirring and ultrasonic assisted casting.

- To study the mechanical and tribological behaviour of AA 2014/ SiC (50 nm & 150 nm), AA 2219 / SiC (50 nm & 150 nm), AA 2014 / Al_2O_3 (50 nm & 150 nm) and AA 2219 / Al_2O_3 (50 nm & 150 nm) nanocomposites.
- Characterization of AA 2014/ SiC, AA 2219/ SiC, AA 2014/ Al_2O_3 and AA 2219/ Al_2O_3 of nanocomposites by using Scanning Electron Microscope (SEM), X-Ray Diffraction (XRD) analysis.

- To study the effect of applied load, sliding distance on the friction and wear behaviour of the nanocomposites using Taguchi design of experiments, Gray relation analysis (GRA) and ANOVA analysis.
- To develop the mathematical model using a factorial method using MINITAB software and check the adequacy of the model by using the Analysis of Variance (ANOVA).

1.14 Organisation of the Thesis

CHAPTER – I present an introduction to composite materials, different fabrication process, and different optimization techniques, base alloy materials, and reinforcement materials.

CHAPTER – II provides a review of the literature on the work done in the field of fabrication and testing of Metal Matrix Nanocomposites and Identified gaps from literature. The objectives of the present work and experimentation problem formulation were presented.

CHAPTER –III give the complete details of the experimental setup, and the measurement of the output parameters for qualitative assessment of Ultrasonic assisted stir casting process.

CHAPTER-IV provides the full information about physical and mechanical properties including SEM and XRD studies of all Metal Matrix Nanocomposites.

CHAPTER –V Experimental results and analysis by Taguchi design method and Gray Relational Analysis.

CHAPTER-VI Wear Studies on Aluminium-SiC and Al_2O_3 reinforced metal matrix nanocomposites.

CHAPTER –VII present the conclusions drawn in this work and their industrial relevance**.**

- Future scope
- References

1.15 Summary

This thesis divided into seven chapters. Chapter 1 is an introduction to this dissertation to emphasize the focus of the work carried out. Chapter 2 reviews previous work on relevant areas of topics to this dissertation, such as brief introduction to the matrix material, fabrication methods of metal matrix nanocomposites and statistical analysis of Aluminium nanocomposites. Chapter 3, specifies the materials used in the present work. Experimental setup, sample preparation, experiment matrix and testing ASTM standard procedures are discussed. Chapter 4 reports the complete information about physical and

mechanical properties including SEM and XRD studies of all Metal Matrix Nanocomposites are presented..The statistical analysis of the AA 2014 / SiC (50 nm & 150 nm), AA 2219 / SiC (50 nm & 150 nm), AA 2014/ Al_2O_3 (50 nm & 150 nm) and AA 2219 / Al_2O_3 (50 nm & 150 nm) nanocomposites are summarized in Chapter 6. Chapter 6 reports the wear studies on metal matrix nanocomposites. In chapter 7, this dissertation is summarized, and specific conclusions drawn from the experimental and statistical analysis and the significance of this research work are presented. Future work is presented in this chapter.

Chapter 2

Literature Review

Literature available in the area of Al and Al-MMCs is abundant. About 200 papers related to the present area of work are referred and arranged in the following order. Aluminium and Aluminium alloys, Metal Matrix micro and nanocomposites, properties and interaction of various parameters on the property of Metal Matrix micro and nanocomposites.

2.1 Introduction

Metal matrix composites reinforced with micro-sized particles have been widely used in aerospace structural applications, automobile, and military industry because of its improved mechanical properties and tribological properties. Compared to the reinforced with micron sized particles, nano level particles gave good mechanical strength, hardness, and better ductile properties. Especially conventional metal matrix composites (AA6061) reinforced with nano level SiC at different weight percentages fabricated by ultrasonic cavitation based dispersion method and has been proved that, a considerable increase in the ultimate tensile strength (UTS) and hardness [21]. Recently alumina nano and micron powder size based metal matrix nano and micro composites were fabricated by equal channel angular press (ECAP), in that tensile strength, hardness is more for metal matrix nanocomposites than micron-sized metal matrix composites and also explained about brittleness, when compared to micron based metal matrix composites, nano-based metal matrix composites exhibits more ductile in nature [22]. Silicon carbide nanoparticles and nanographene sheets were distributed in the molten aluminium alloy (A356) by the semi-solid stirring process; ultrasonic pressure

gradient was applied into the melt and then followed by a vertical hydraulic press of 250 Tons held for 15s until solidification was completed. While stirring vortex was formed after 5mins at speed initiated 400rpm and temperature 605^{o}C, nanoparticles were wrapping by graphene nanosheets resulting in higher thermal conductivity [23]. Temperature also paramount phenomena in the fabrication process of metal matrix composites both nano level and micron level. Nowadays most of the researchers used ultrasonic based fabrication process, the current research work explains at various temperatures (700^{o}C, 725^{o}C, 750^{o}C and 775^{o}C), how ultrasonic power acts while dispersion of nano alumina powder at 1wt% in the hot molten metal (Aluminium based) and also proved increase of temperature, effects the increase of mechanical properties like ultimate tensile strength and hardness [24]. Aluminium matrix composites (A356) reinforced with TiB_2 nano and micron sized particles at different volume fractions of 20nm and 5μm was considered separately. Composites were fabricated at various casting temperatures (750,800 and 900^{o}C) by the mechanical stirring process. The porosity content of the metal matrix composites increased with increasing volume fraction and decreasing particle size of the ceramic particles. Moreover, the tensile strength was improved 43% and elongation 27% at 1.5 vol. % of TiB_2 [24, 25]. Pure aluminium nanopowder of size 15μm diameter and titanium oxide nanopowder of size 50nm was used to fabricate metal matrix nanocomposites by powder metallurgy route and found that tensile strength, hardness, and porosity were increased and ductility decreased with increasing of weight % of nanopowder [26].

The feasibility of Al/SiC nanocomposite manufacturing by the ultrasonic technique for the production of material of raw materials thixoforming. The aluminum (A356) it has manufactured the composites to a matrix with the addition of 0.2% by weight of SiC nanoparticles using an ultrasound method. Two different mechanisms for the addition of particles to the melt; the method capsulate Al double foil and the crucible investment approach, have been employed. Best results were obtained for the method capsulate double. Also, Ti and Nb probe tips have been attempted to provide ultrasonic vibration in the melt. It has been shown that Nb is a state-of-the-art equipment of ultrasonic probe promising for produce MMNCs to above 650°C, as is thermodynamically stable in comparison with the Ti [34].A few of the techniques for the development of metal matrix nanocomposites are

ultrasonic assisted stir casting [27], spark plasma sintering method [28], stir casting method [29], powder metallurgy method [30], spray atomization and co-deposition method [31], plasma spraying method [32] and squeeze casting method [33].The above methods are most important of which, liquid metallurgy technique has been explored to a great extent in current days.

2.2 Properties of Composite Materials

A composite material can be distinct as a combination of a matrix material and a reinforcement material, which when combined give superior properties to the properties of the individual components. In the case of a composite material, the reinforcement is fibers, whiskers or particulate's and serves to reinforce the matrix regarding resistance and rigidity. The physical properties of composite materials are not isotropic (independent of the direction of the applied force) in nature, but tend to be anisotropic (different depending on the guidance of the applied force or load). For example, the rigidity of a composite panel often depends on the orientation of the forces and/or moments applied. The rigidity of the board is also dependent on the design of the panel. For example, the fiber reinforcement and the matrix used the construction method of the panel against thermosetting, thermoplastic, type of weave, and the orientation of the fiber axis to the primary force. The main factors of the composites are to determine their properties such as weight fraction of reinforcement, homogeneity, microstructure and isotropy of the composite system.

In contrast, isotropic materials (e.g., aluminum or steel), standard wrought form, generally have the same stiffness despite the directional orientation of the applied forces. The relationship between the forces, moments, strains, curvatures for anisotropic material can be described with the properties of the following materials: Young's modulus, shear modulus, and Poisson's ratio, in relatively straightforward mathematical relationships. For the anisotropic material, it is the necessary mathematics of a second order tensor until constant material properties. For the particular case of orthogonal isotropy, there are three constants of different material properties for each of the Young's Modulus, shear modulus and the Poisson ratio, a total of 9 constants to describe the relationship between the forces, moments, strains and curvatures. The techniques that take advantage of anisotropic material properties

comprise mortise and tenon joints (natural composites such as wood) and Pi Joints in synthetic composites.

Strengthening of micron or nano range size of particles with the matrix of aluminum improves the quality of physical and mechanical properties of the composite materials. The distribution of nano-reinforcing particles of size also modifies the morphology interfacial characteristics and nanocomposites. In their study, AA 5083 alloy based micron and nano SiC composites have been invented by ultrasonic assisted stir casting method. Different weight % of particles of SiC taken in microns (3, 5, 8, and 10% by weight) and Nano (1, 2, 3 and 4 percent in weight) has been used for the synthesis of composite materials. SEM microstructure shows a uniform distribution of particles of SiC with agglomeration in some places. Various properties of composites as the resistance to traction, compressive strength, hardness, ductility, it has measured the density. The results revealed that the resistance to traction, the resistance to compression and the hardness of the composite materials increases with the increase of the weight % of the SiC particles and reduce the size of the particles [35]. However, the ductility of composites with micron level SiC particles was reduced to a great value with the strengthening of the weight % of the SiC. However with the addition of nano SiC particles only a small reduction in the ductility was observed. The application of ultrasonic vibration on the composite during the melting not only the structure of the refined grain of the matrix but also improved the distribution of nano-reinforcement of size.

2.2.1 Physical Property

2.2.1.1 Density

The density is the main physical property of the composites and was calculated theoretically by using the rule of the mixture [36] that shows the characteristics of composites. Composite consists, at least two phases of the matrix phase and the reinforcement phase are expressed either as weight fraction (w), which is commonly used in the properties evaluation. By connecting the weight fractions or volume fractions using density of the composite (ρ_c), the following relation (Eq 2. 1) is obtained:

$$\rho_c = \rho_p v_p + \rho_m v_m \quad \text{----------} \quad (2.1)$$

The above expression can be generalized, and its general form is known as rule of mixture and is as follows;

$$X_c = X_p v_p + X_m v_m \quad \text{----------} \quad (2.2)$$

Where subscript "p" shows particulates and "m" shows matrix material. Experimentally, the physical property called density of a composite is measured by displacement techniques using a physical balance with density measuring kit and as per ASTM: D 792-66 test method. Further, the density can be measured from porosity and perceptible density values (sample mass and dimensions) [37].

The density of the Al_2O_3 or SiC particle reinforced Al6061, and other aluminum alloys can be summarized as follows: the reinforcements Al_2O_3 or SiC increase the density of the core alloy when they are added to the alloy of the base to form the composite [38]. Also, the values of theoretical density correspondence with Density values measured of these composites and clearly show the no porosity. Furthermore, it is [39] reported that the density of Al2024- SiC composites of particles is superior to that of Al2024-SiC whisker reinforced composites for the same quantity of fraction of the volume.

2.2.1.2 Microstructure and XRD

The use of ultrasonic non-linear effects to disperse nano-sized ceramic particles in the molten metal has been studied and nanometric composites reinforced SiC particles of magnesium have manufactured AZ91D. The microstructure of composites has been investigated by electron microscopy at high resolution (SEM), X-ray picture spectroscopy (XPS) and high-resolution X-ray diffractometer (XRD) techniques. The experimental results show a distribution nearly uniform and good dispersion of the SiC nanoparticles in the magnesium matrix; although some of the small agglomerates (less than 300 nm) have been found in the matrix [40]. A detailed study reveals that the SiC nanoparticles were partially oxidized. Microhardness of composite materials has been significantly improved compared to that of pure AZ91D. The interaction between the SiC nanoparticles and the matrix was investigated. The interaction between the ultrasonic wave energy and nanoparticles was also discussed. The ultrasonic manufacturing methodology is striking too quickly produce a broad

range of nanoparticles reinforced metal matrix composite. Nano-sized SiC magnesium matrix reinforced nanocomposites, Mg-2Al-1SiC with 2% SiC and Mg-4Al-1Si with 2% of SiC, have been manufactured correctly by the ultrasonic cavitation, founded the dispersion of SiC nanoparticles in Mg-(2,4)Al-1Si melts with magnesium alloy. Compared to the Magnesium Alloy matrices, the mechanical properties whose resistance to traction and resistance to the rupture of the Mg-2Al-1Si/2% SiC and Mg-4Al-1Si/2% SiC nanocomposites were improved significantly, while the ductility of castings matrix in magnesium alloy has been retained. If there have been a few SiC micro-clusters in the microstructure of nanocomposites, the SiC nanoparticles have been dispersed and outside the areas of micro-clusters. Most of the micro-clusters were located along the grain boundaries while most nanoparticles of SiC distinct have been integrated into the interior of the grain. TEM study of the interface between the SiC nanoparticles and Mg-(2, 4) Al-1Si the metal matrix has suggested that the SiC adheres well to the metal of the matrices without forming an intermediate phase[41].

Some issues such as the grouping of particles of TiB_2, training of long rod-like Al_3Ti particles, as well as level of high porosity usually associated with the manufacture of in situ TiB_2p/Al-alloy composites conventional via stir casting using Ti and B as reagents. Ultrasonic vibration high intensity has been introduced in our research to resolve the above issues. The process involved that the original in place TiB_2p/Al-12If-4Cu sample with large groups of particles of TiB_2, large extended rod-like Al_3Ti particles, and the high porosity has been re-melted at 850^{o}C, and then ultrasonic vibration has been applied to the melt with an ultrasonic probe. The microstructural evolution of the samples treated by ultrasonic vibration with different time has been examined by using SEM. After treated by ultrasonic vibration for 12 min, large clusters of TiB_2 particles were broken into the TiB_2 particulate matter and efficiently have been dispersed uniformly in the matrix, and the large rod-like Al_3Ti particles have been transformed into blocky those with the size of 10 microns due to the effect of the ultrasonic agitation. In the meantime, the porosity in the composites has declined from approximately 6.5% to 0.86% due to the effect of degassing to ultrasound. Microhardness test suggested that a homogeneous microstructure of the composite was obtained after treatment to ultrasound. An effective approach to the assistance of ultrasonic vibrations at high intensity to optimize the microstructures of the particles strengthened al-alloy has been proposed and

composites the mechanism of the effect of vibration at high ultrasound intensity on the microstructural evolution of reinforcements, and the degassing of Composites has also been examined in our research[42].

2.2.2 Mechanical Properties

2.2.2.1 Hardness

The resistance offered by the material to form indentation is called as hardness. Most commonly used hardness measurement instruments are Rockwell's, Brinell's and Vickers's micro hardness testers. Theoretically, the hardness of the composite can be calculated by using the following expression [43];

$$H_c = v_r H_r + v_m H_m \quad \text{----------} \quad (2.3)$$

Where, H_c = hardness of the composite, H_r = hardness of the reinforcement,
H_m = hardness of the matrix, v_r = volume fraction of reinforcement,
v_m = volume fraction of the matrix.

The above expression is very much useful to approximate the hardness value. According to the aspect ratio of the reinforcement, phase influences the properties of the composite. This means, the low aspect ratio of the particle reinforcements gives the significant effect in hardness of the composite. Among different types of reinforcements (called fibers, whiskers, and particulates) particulates being low aspect ratio. [44].Some researchers proposed the effect of reinforcement on the hardness of the composite materials be explained as follows. Most commonly the particulate reinforcements being used SiC and Al_2O_3 to obtained higher hardness [45]. Nickel and copper coating reinforcement's leads to excellent interface characteristics, therefore hardness of the composite is being improved [46]. Dispersion of TiC particles in aluminum matrix gives better hardness to weight ratio and also produces thermodynamic stability [47] to the composite materials. Some of the researchers like Hutchings- 1994, Abdulhaqq-2006, and Lloyd-1984, explained the importance of hard ceramic particles in the preparation of metal matrix composites and also tells hardness increases as the weight percentage of the reinforcement content increases. Some of the reasons being obtained from Howell-1995, and Vencl A-2008, as the size of the reinforced particles, was decreased simultaneously hardness of the composite increased because of high

surface to volume ratio. Volume or weight fraction of reinforcement increases and particle size decreases relatively the hardness value increases; this was proved by Deuis-1996 and J.M. Wu-2000.Hardness was increased due to increase in strain energy at the periphery the reinforced particles dispersed in the base matrix [48]. Hardness improvement not only depends on particle size but also depends on hard ceramic particles, the structure of the composite and good bonding formed between reinforced material and matrix material [49]. The direct and easy method to measure the bond strength between matrix and reinforcement material is microhardness method.

2.2.2.1 Tensile Strength

As per the application prudent, mechanical properties of metal matrix composites have a great significance. Most of the researchers predicting the minimum and maximum values of the material property constants and tensile strength properties of the composites [50]. In 1998 P.H shipway proposed that aluminium based metal matrix composites be fabricated with a controlled addition of reinforcing material and selection of suitable manufacturing method. In 2001 M.D.Bermudez and 2003 T. Miyajima found that, no clear relation between mechanical properties of the MMC's, weight fraction and different combinations of reinforcements. H.Ribes-1990 and Ma Z Y-1997 has explained the relationship between the tensile strength, weight fraction and surface nature of reinforcements, Actually reduced the size (preferable nano size) of the reinforcement materials gives the better mechanical properties of the MMC's. Basically structure and physical properties of the reinforcements control the mechanical properties of the MMC's. Tensile strength and elastic modulus of the MMC's being increased, because of strong interface that transfers the load and distributed uniformly from the matrix material to the reinforcement material. Preheating the reinforcement materials is always gives the better interface bond strength and also uniform distribution of the particles in the molten base matrix metal [51]. The tensile strength of reinforcement materials (SiC, Al_2O_3, and TiC) was explained by Kassim S-1999 and Rajmesh Tyagi-2005, and TiB2 particulate being reinforced in aluminium based MMCs is establishing to improve the ductility on the increasing of weight percentage of the ceramic reinforcement material and decreases the size[52]. By comparing monolithic alloys with aluminum based MMCs reinforced with particulates have a lower elastic modulus, tensile strength and fatigue strength

[53]. After heat treatment the yield strength of the composites being increased due that reducing the cracking tendency [54] and also increases the precipitation hardening [55]. Out of many ceramic reinforcement particulate materials, SiC and Al_2O_3 are extensively in use, because of their right combination of density and hardness. SiC and Al_2O_3 are reinforced with aluminum based metal matrix composites shows the significant increase in its elastic modulus, hardness, tensile strength and wear properties [56]. Aluminium and TiO_2 based composites fabrication were very limited when compared to the SiC and $Al_2O_{3;}$ Anyway TiO_2 have excellent mechanical properties [57]. The reason behind the improvement of the tensile strength of the material is the addition of ceramic particles. According to Tresca yield criterion, the shear yield stress is half of the normal yield stress [58]. The yield stress of the MMCs may be calculated, using the expression;

$$P_m = c\sigma_y \text{ ---------- (2.4)}$$

Where P_m = hardness, c = constant and σ_y = Tensile yield stress.

2.3 Wear of Composite Materials

Wear is associated with relations between surfaces, and it is a continuous loss of material because of opposing surface force when two surfaces are contacting to each other [59]. Wear damage may occur in some forms out of which, micro-cracks and localized plastic deformation were explained by [60]. Wear is a multifaceted occurrence in which true mating area between two solid surfaces compared with the visible area of contact is consistently minuscule, limiting to the contact points between the surfaces. The applied load will be transferred to these surfaces, and through contact points and the confined to a small area, forces can be extremely high. Few of the factors are very significant for determining the wear rate; those are necessary surface properties, surface finish, load, speed, and temperature. Adhesive wear, abrasive wear, surface fatigue, Fretting wear, Erosive Wear, Corrosion and oxidation wear are the different types of wear. When two surfaces are in frictional contact can be observed that there is an adhesive wear between the surfaces and most commonly refers to surplus displacement and connection of wear debris. Hard, rough surface moves or slides along the softer surface resulting wear are abrasive wear. Surface fatigue is a procedure by which the surface of material is damaged by cyclic loading, which is a type of fatigue of

materials. Fretting wear is the repeated cyclic rasping between two surfaces. Over a period fretting, this will remove material from one or both surfaces in contact. Erosive wear can be defined as a very short sliding motion and is executed within a short time interval. Erosive wear is caused by the impact of particles of solid or liquid against the surface of an object. This kind of wear occurs in a variety of situations both lubricated and unlubricated contacts. The consecutive loss of material from the working surfaces of the physically interacting elements of a tribosystem known as wear rate being measured regarding volume loss or weight loss. The existing instruments for measuring frictional force and wear height loss are Pin-on-Disc, Pin-on-Cylinder and Thrust washers and such others. Sample geometry, applied a load, sliding distance, sliding velocity, temperature and humidity are the controlled factors, generally in laboratories; wear tests are conducted at room temperature under different controllable factors of various levels.

2.3.1 Factors Affecting Wear of Aluminum Composite Materials

Mechanical and physical factors can control the friction and wear performance of reinforced Al-MMCs, are the effect of normal load to the tribal contact, the sliding velocity, the sliding distance and reinforcement orientation, the environment, temperature, the surface finish and surface interaction such as the reinforcement type, size, shape and distribution of the reinforcement, the matrix microstructure and the reinforcement weight fraction [61]. One of the researchers, [62] while finding the wear rate of particulate reinforced MMCs under various applied load conditions, observed that three different wear regimes. Initially under very low load condition (regime I), in this regime, the particulates completely bare the total applied load in which the wear resistances of MMCs are better than Al-alloy. The wear of MMCs and Al-alloy were almost similar in regime-II. At higher loads (regime-III), the surface temperatures across a limiting value. In this regard, the material factors, the volume fraction of reinforcement has the strongest influence on the wear resistance [63]. Based on the shape, size and weight percentage of the reinforcement whiskers, fibers, and particles effects wear rate of MMCs. As the reinforcement weight percentage increases and reaches to maximum value gives the wear rate minimum value because of high surface to volume ratio and also depending on the type of reinforcement, matrix material and finally sliding conditions. From this analysis, tough to select the kind of reinforcement and weight fraction

that may give excellent wear properties [64]. Some researchers carried out experiments on the wear pattern of MMCs and a little bit investigation on MMNCs against various counter surfaces with different test conditions. In following sections, the influence of the various variables or parameters on the wear rate of MMCs and MMNCs are discussed.

2.3.2 Effect of Extrinsic (Mechanical and Physical) Factors

2.3.2.1 Applied Normal Load

Applied normal load greatly affects the wear rate of MMCs and it is the most significant factor controlling the wear behavior [65]. The specific wear rate changes with applied normal load, which is an Archard's law and is considerably less in MMCs [66]. The average wear height loss and volume of wear increases with increasing applied normal load [67]. Contact surface temperature also increases with increase in applied load. The wear rate is always proportional to the applied load and is calculated by using wear rate is equal to a function of applied normal load and reported [20, 68]. The wear rate is soft and steady and which is obtained below the applied normal load called as critical load decreases with temperature [69]. If the load is additionally increased gradually leads to unreinforced and reinforced MMCs and MMNCs ultimately grab. The convulsion event was accompanied by an unexpected increase in wear rate, noise, and vibration. This type of convulsion has been suggested to as galling convulsion [70]. One of the researchers has been reported that wear rate increases with the increase of applied normal load, the wear mechanism explains oxidation layer was formed at lower loads and adhesion and delamination was observed at higher loads [71]. The applied load is gradually increased on aluminium alloy leads to decrease the specific wear rate because the aluminium alloy was thermally softer material in nature when compared with the aluminium based composite materials and the strength of the composites is more at higher temperatures. Based on this reason, the specific wear rate is more in the case of aluminium alloys than aluminium based composites at higher loads. The particles act as a load bearing elements at low loads this clearly indicates the direct participation of aluminium alloy in the specific wear process is prohibited [72]. The chemical reaction of specimen wear surface with the counter surface is less at low loads, because the contact area is very less [73]. At low loads the wear debris size is very less almost in microns, but at higher loads, the wear debris size is colossal in order of millimeters [74]. The load

increased gradually, the quantity of wear debris gradually increased, and the size of the delamination is greater than before for the metal matrix composite. At higher loads, the worn wear surface called like classical ratcheting wears [75]. The change in specific wear rate found for many composites is quicker and temperature dependent and to be the output of void or cracking formation between the reinforcement and the matrix [76], both the reinforcement and matrix direct to fragmentation and delamination of the wear surface. Because of the fracture toughness of the composite, during sliding the composite could bear maximum load without more accurate wear rate [77].

2.3.2.2 Sliding Speed/Velocity/Distance

The increase of sliding velocity and sliding distance, the specific wear rate, and collective wear loss enhances for all the composites [78], and the tendency of the wear curve can be linear [79]. The sliding velocity effect the wear mechanism sturdily and at low sliding velocity, the specific wear rate of the composites is lower. This may occur because, at high velocity, the micro thermal softening [80] of metal matrix composites could take place and moreover decreases the bond strength of the reinforced particles with base matrix material [81]. At upper sliding velocity, specific wear rate is less for composites, due to the development of a solid transfer layer at the section of the worn faces. The quantity of components of the body in against the transfer layer is considered to increase the slip speed increases and the formation of a protective cover which tend to reduce the wear rate [82]. Kwok and Lim in 1999 reported that the immense specific wear occurs if the particles are smaller than the threshold value at greater velocities.

2.3.2.3 Effect of Temperature

The volume of wear increases significantly above a typical temperature between the transition from mild and severe wear [83]. Mild to severe wear occurs when the induced heating of friction increases the top contact surface temperature to a critical value [84] (about 0. four times the absolute temperature of fusion). More under normal pressure, the lesser is the transition temperature. The composite transition temperature is higher than the unloaded alloy, and the composite undergoes volume of minor wear [85]. The higher thermal conductivity of the frame helps to improve the wear resistance [86].

2.3.2.4 Surface Finish and Hardness of Counterpart

The surface roughness affects the wear rate. More roughness, the higher the wear rate [87]. The hardness of the surface is inversely proportional to the rate of wear and the counter material with a low hardness reduces the wear resistance because of the shared abrasion between the material and the against-wear surface of specimen [88]. The wear of the against-surface depends on of the wear mechanism of the composite material. An increase of the load usually results in an increased wear rate of both the composite axis and against the face. Increasing the weight percentage of reinforcement particles in the metal matrix composite reduces its wear rate, but increases the rate of the against-wear surface, so when the two-sided and against the composite wear are considered, a fraction of optimal volume particle exists in which wear is lower [89].

2.3.2.5 Nominal Contact Area

The dependence of the wear coefficient and the rate of the contact area of the nominal sample wear; nominal sample lower contact surface will wear a smaller coefficient value, volume asperity wear available is lower. It should also be noted that, in general, an increase in load or sliding speed also increases the volume loss and consequently the wear coefficient. According to the literature, it can be concluded that the values of wear coefficients obtained from the pin with a smaller area of nominal contact with were much lower on average by about 12% than the larger, due to the availability of small volumes of wear asperities. Hence we must exercise extreme caution in interpreting wear coefficient data obtained from different test methods or the use of different contact areas of the nominal sample [90].

2.3.3 Effect of Intrinsic (Material) Factors

2.3.3.1 Reinforcement Size and Shape

The wear resistance of a material depends on its hardness, strength, ductility, toughness, type of reinforcement, the volume fraction (V_f) and the particle size [91]. Particulate reinforcements are most effective in improving the wear resistance of MMCs provided that good interfacial bonding between the reinforcement and the matrix exist. The particulate reinforcing effect is to prevent plastic flow and adhesion of the matrix material.

Composite materials wear resistance is improved by preventing direct metal contacts which induce a deformation of the basement [92]. The addition of hard ceramic particles enhances the resistance to seizure, high temperatures. The particles allow significant effects of thermal softening without adverse effects on the wear behavior [93]. The frame also causes a higher hardness, a modulus of elasticity greater, more dynamic modulus, better damping capacity and the less thermal expansion coefficient of the matrix alloy [94]. The presence of the ceramic particles provide greater thermal stability, increased abrasion [95], and resistance to high temperature sliding wear and delays the transition from low to severe wear [96].

The wear rate decreases with decreasing grain size. This can be attributed to the strengthening of the aluminum grain boundaries leading to strain hardening. Such behavior can be attributed to the change in the form of grains of equiaxed to columnar (with an increase of grain size) the [97]. The reinforcing particles with a magnitude of a few micrometers have more to matrix bond strength, which supports the load efficiently and avoids the crack to initiate and propagate in the wear of the basement area. Therefore, the wear resistance of the composites is significantly improved [98]. The predominant friction mechanism for particle sizes below 13 μm adhesion involved and micro plowing, the latter being complemented by third hard abrasion SiC body with increasing particle size. Moreover, adhesion of micro cutting were the predominant wear mechanisms for small reinforcements, the higher wear rates observed in, the larger particle reinforced composite tribe being associated with the particulate-induced cracking increased delamination under the wear surface [99]. The role of second phase particles by providing localized areas of high-stress concentrations that have affected the flow stress and the wear rate [100]. The maximum wear resistance was obtained in microstructures associated with semi-consistent fine particles well dispersed. For materials characterized by carbides dispersed in a soft matrix, a decrease in the mean free path of the particles, by reducing the size of the carbide leads to better wear resistance. The wear resistance of composite materials, on the alloys, has been attributed to their effective distribution of particles of a comparatively diminutive size [101].

The main concern about Al-MMCs is that the greater the volume fraction and finer the size of the frame, the MMC are expensive. Therefore, it is necessary to reduce the cost component by optimizing the volume fraction and to avoid / minimize the use of fine particle

[102]. Al_2O_3 fine particles of the reinforcement strengthen the Al matrix and improve the wear resistance [103]. The residual alloy phase and the presence of a rigid ceramic skeleton allow blunting or lubricating properties of the alloy in the production of excellent tribological properties [104].

2.3.3.2 Effect of Different Types of Reinforcements

The reinforcement of SiC in the Al-MMCs is more resistant to breakage compared with $A1_2O_3$ and Si. SiC particles are more difficult than others reinforcements and provide a more effective barrier in the shear surface by the movement of 'adjacent steel-face against [105], and this is probably due to differences in particle form [106]. An additional disadvantage of Al-MMCs with reinforcing phases such as SiC and Al_2O_3 is the tendency of the frame to act as a second abrasive body against the counterface by increasing its wear rate [107].

Also, strengthening released as acts of wear debris as a third abrasive body on both surfaces. Both effects result in a higher wear rate for the whole system when MMC is used compared to the monolith, while the magnitude of this problem depends on the mechanical properties of the material surface against [108]. The presence of iron oxide remains in the wear track plays an important role since it has been reported as being beneficial to reduce the frictional resistance for MMCs reinforced by SiC or Al_2O_3 particles sliding against steel [109]. The slight wear debris consists mainly of iron oxide (Fe_2O_3), while severe wear debris consisted of Al_2O_3 phases, Al, Fe. Furthermore, the addition of Si-Fe particles of Al_2O_3 eutectic alloy and enhances the low transition of load to heavy wear of the alloy Al2024 by more than three times and the reduction of the friction coefficient [110].

The amalgamation of TiO_2 particles resulted in wear of the disk. The particle TiO_2 seems to reduce both the plastic flow of the matrix and the transfer of metal to the axis [111]. The Al356 reinforced TiC alloy was the hardest and had the lowest rate of wear and an increase in the load at which the transition to low wear high wear rate occurs [112]. An addition of particulate Al6061 alloy has shown that not only delays the transition of wear but also reduces the wear rate and friction coefficient [113]. The experimental results showed a significant improvement in wear resistance of B_4C particulate reinforced MMCs Al5083

[114]. Cryogenically treated composites may show a considerable reduction in wear rates with increased hardness and strength at higher applied loads [115]. The $MoSi_2$ and Cr_3Si reinforced alloys (Al2124, Al5056) had the lowest specific wear rate [116]. The wear resistance of the composite materials improved by incorporating TiB_2 reinforcing particles and refinement of the matrix grains is significantly improved mechanical properties of composite [117]. Also, the particles of TiB_2 significantly improve the wear performance of the alloy Al-4Cu. Arguably the TiB_2 particles not only protect the matrix because of their high hardness but also by generating rich debris fine iron which acts as an effective lubrication medium [118].

2.3.3.3 Effect of Reinforcements volume fraction

It has been reported that the wear resistance of the composite increases with increasing volume fraction of the reinforcement [119]. MMCs of wear resistance can be improved by increasing the volume fraction of the ceramic reinforcing phase by as much as 70% [120]. Also, the dry sliding wears resistance increases with the increase of the volume fraction of particles. At the high volume fraction, the higher coefficient of friction has been found, and there was almost no effect of the load on the friction coefficient [121]. The rate-face against increased wear material with an increase of the volume fraction of ceramic particles. This is mainly because the hardness and strength of the composites are higher and they increased with increasing filler content [122]. The volumetric wear rate increases with the load while it decreased with increasing volume fraction of filler [123]. This may be due to the reason that the addition of ceramic content resulted in a sharp decline in ductility [124] accompanied by an increase of the hardness can further increase the wear resistance of the composite materials. At any constant load, wear lower rate of increase in addition to SiC and improves load bearing Al alloy during sliding properties. SiC is adding increase limits the flow or deformation of the matrix material about the load [125]. Loss of cumulative volume and decreases in linear wear rate with the increase of the volume fraction of titanium carbide (TiC) made of pure aluminum. Friction coefficient means also decreases linearly due to a protective cover provided by the transfer layer with increasing volume fraction of TiC [126]. The increase of the volume fraction of TiC enhances the rate of the face against wear. Therefore, it is suggested that when the two against the face and composite wear are considered optimal volume fraction of particles exists in which wear is lower [127].

2.3.3.4 Effect of Interparticle Distance

The average distance between particles influences the microhardness, friction and wear properties. The poor dispersion of the particles is due to the agglomeration of particles in the matrix and can lead to a weakening of the mechanical properties. One can conclude that the reduction of particle agglomeration leads to a tendency to decrease the wear of composite material [128].

2.3.4 Composite Processing Parameters

2.3.4.1 Effect of Interfacial Bonding

The wear behavior of composite reinforced with hard particles depends mainly on the type interfacial bonding between the Al-matrix and the reinforcement. This is due to the strong interfacial bonding which plays an essential role in the transfer of charges from the matrix to the hard particles, which results in less wear of the material. In the case of poor interfacial bonding, the interface provides a nucleation site for crack and tends to remove the particle from the wear surface that tends to carry a greater loss [129]. For example, SiC coated Ni and Cu-dispersed Al-SiC composite lead to high-quality interface characteristics and have improved wear properties [130].

2.3.4.2 Effect of Porosity

The composite wear rate increases *in-situ* containing relatively lower reinforcement particles gradually with increasing the volume fraction of porosity in the critical porosity value of about 4% by volume, but beyond this level, wear rate increases faster. This could be attributed to the combined effect on the actual contact area and subsurface crack propagation. Also, the wear factor increases dramatically with the increase in porosity content in this group of in-situ composite distribution. Sometimes, the contributions of reinforcing particles in improving the wear resistance have been erased by increasing the content of porosity and hence it must be controlled in composite cast *in-situ*. However, a limited amount of porosity can be tolerated in the composite materials cast *in-situ* without significantly altering its resistance to wear. The composite wear rate cast *in-situ* containing relatively lower continuous porosity decreases with content more and more particles, more than expected by a decrease of the actual contact surface. It is therefore intended that blunting cracks in the surface porosity

may decrease wear debris generation as indicated by the reduction in wear coefficient with increasing the content of particles at a lower level of porosity [131].

Clusters of Li-reinforcement particles and the high porosity are usually present in the particles in situ reinforced metal matrix composites (MMC) manufactured by a conventional stir casting method. We have studied the effect of ultrasonic vibration on the microstructures of composite and particles of reinforced aluminum. The process involves the addition of titanium and graphite powders in pure aluminum melted at 850^{o}C. In the meantime, the ultrasonic vibration high intensity has been applied in the melt to disperse the particles formed in situ in the matrix. Microstructural Characterization has indicated that in situ formed Al_3Ti and SiC particles were uniformly distributed in the matrix and a homogeneous microstructure with a low porosity was obtained due to the effects of ultrasonic agitation and degassing. An effective approach to the assistance of ultrasonic vibrations at high intensity to optimize the microstructure of in situ particle of metal matrix composites reinforced was given first, and the mechanism of ultrasonic vibration has also been examined [132].

2.3.4.3 Effect of Wettability

The wettability of the reinforcement in the matrix and the interfacial resistance are related to another value of micro-hardness, the friction coefficient and the wear property of composite metal matrix. The decrease in the coefficient of friction value and the increase of the wear resistance is due to a better distribution of the particles in the matrix, which is due to the improvement of the wettability of the matrix of the reinforcing phase [133]. For example, to improve the wetting of the surface during molding, the graphite particles are coated with a layer of nickel [134].

2.3.5 Effect of Lubrication

Regarding the wear mechanisms in lubricated conditions, the degree of direct contact between the surfaces is minimal, and the wear progresses through debris layers [135]. For all materials, wear loss in the lubricated test declines constant load as hardness increases. However, for lubricated conditions, Al-MMCs with a higher hardness show more wear resistance [136]. Scratches and seizure problems can be treated incorporating solid lubricants, namely Graphite in Al-Si alloys reinforced with SiC or Al_2O_3 particles [137]. It was shown

that the addition of graphite flakes or particles in Al-alloys increased loads and speeds at which the seizure occurred in the boundary lubricated sliding and dry conditions [138]. The high galling resistance of Al matrix composite graphite has been attributed to the formation of the graphite layers on the contact surfaces which act as solid lubricants, which reduces the metal to metal contact between the sliding pairs [139]. Another important factor is that the lubricant used will serve as a cooling fluid between the two sliding surfaces avoiding the effects of increasing temperature of the metals in contact.

2.3.6 Effect of Load & Work Hardening

In the case of the alloy, the work hardening rate could be higher, and there are also all the abrasive scavenging Actions loose in the matrix, which results in relatively reduced wear rate in the alloy about the composite with the increase of the load[140]. Reduce the wear rate with the sliding distance is a more accurate indication of the efficiency of work hardening of the basement of the regions due to induced increase wear plastic deformation. The subsurface cure is evidenced by an increase in hardness in the basement area, compared to the unaffected mass [141]. Repeated with the dry sliding test, a hard working layer occurs on the wear surface, which promotes the wear strength of the composite. At the same time, the wear surface temperature increases after that. Accordingly, recrystallization occurs on the worn surface of the composite during the dry sliding, which results in the decrease of the wear surface hardness, which counteracts the effect of greatly promoting the wear resistance by the work hardening. Also, the oxidation layer formed on the sample wear surface is beneficial in improving the wear resistance [142].

2.3.7 Effect of Mechanical Mixed Layer

During sliding to higher wear rate, high temperature develops in the sliding surface due to which the sample softens and becomes plastic. It reacts with the oxygen available and forms of their respective oxides. The hard and brittle oxide formed on the surface of the sample becomes thicker and continuously covering the entire surface. The aluminum oxide film acts as an insulating part for the thermal conduction. Mechanically this mixed layer (MML) was responsible for the decrease in wear rate and friction MMCs [143]. The transfer of metallic inclusions from the surfaces against-surface on the composite wear surfaces is

another mechanism contributing to the increase in wear resistance of the composite [144]. This indicates that the inclusions act as additional reinforcement to the composite wear load carrying surface are of [145] and the specific wear rate decreased with increase in the thickness of MML [146]. Forms MML on the worn surface of the composite and serves as a protective layer [147] and a solid lubricant. In composite having a low volume fraction of the GMV is stable under weak and unstable loads under high loads. In the composite having the highest volume fraction of reinforcement, the MML is stable under high loads [148]. The MMLS are formed in the worn surfaces of a variety of sliding loads. The mixed layers had characteristics microstructure comprising a mixture of ultrafine-grained structures in which the constituents varied with sliding load [149]. The thickness of the transfer layer increases as the normal load increases [150]. Due to the presence of GMV, the rates of both the pin and the wear disc is lower at higher speeds. With speeds increasing the amount of training layer increases because of the higher temperatures generated [151]. The extent of coverage provided by this transfer layer is determined by the load, speed and environmental conditions of sliding and it increases with increasing load due to the heating by the increased friction and therefore a better compaction [152].

Once the MML is formed, it provides that the critical conditions before surface protection be achieved and debris off of the mixing layer, in agreement with observations of behavior to wear than the wear rate was less than an intermediate load range with the presence of MML. MML has not a uniform thickness over the whole of the wear track, and it had a corrugated shape in the cross section of the worn surface. The wear rate, therefore, is influenced by the formation and detachment of the MML in the load range used [153]. The formation of the tribo-layer delays mild to severe wear transition in Al-MMCs. Once the tribo-layer is removed from the contact surface, the bulk material is in direct contact with the against face, and it is difficult to form a new triboelectric layer on the hot and softened matrix [154]. Sliding further the MML separates from the pin surface due to delamination, leaving the surface of the new spindle, which causes the fall of the frictional force [155]. The results indicate that the different reinforcement type can generate MMLS. These observations suggest that the MML formed of material from three sources; against the face (Fe contributing with around 20% Fe), the matrix and particles [156].

Some features of the GMV, which can be used to distinguish it from the normal composite material, are: (A) a darker color than the normal composite material when observed under an optical microscope. (B) The presence of chemicals from the against-face. (C) A higher microhardness value in the LMM and the sudden change to low values outside GMV [157]. The hardness of GMV was considered much more challenging than the hardness of the matrix in the composite [158]. In fact, the GMV is independent of the hardness of the composite, and the value is comparable to the hardness of steel against-surface. Note that the GMV is formed in the non-reinforced material, mainly because no trace of iron is on the worn surface [159]. Hardness studies micro along the surface in a vertical section from the worn surface emission that the amplitude of the sample hardness decreases with the distance of the worn surface indicating that the closer to the under sol to the worn surface has been hardened due to the hardening effect that the remote area of the worn surface. The wear resistance of aluminum refined grains increases with decreasing grain size and grain aspect ratio (equiaxed) [160]. The formation of rich Tribo-iron oxidized layers on the contact surfaces[161]. Detailed surveys of tribo-layers on Al-Si Alloy worn surfaces were also presented[162]. The transition between the mild and severe wear regimes have been attributed to the removal of these layers [163]. Almost all surveys conducted to date on Tribo-layering and material transfer phenomena accompanying sliding wear of Al-Si alloys were carried out in an ambient atmosphere as a function of applied normal load and speed slip. SiC undergoes Tribo-chemical interaction during sliding and form SiO_2, which acts as a lubricant, especially at higher speeds [164].

The protective cover provided by MML is observed to increase with the volume fraction of TiC. This can be attributed to the greater hardness of the substrate having the relatively high amount of TiC, which is capable of holding a thick transfer layer of oxide as compared compacted on the low-hardness substrate [165]. When the reinforcement in the matrix has a wide size distribution, the wear rate and friction coefficient are found to be higher compared to composites containing mono-size reinforcement [166].

2.3.8 Effect of Heat Treatment

The alloy and the composites exhibit the minimum wear rate after heat treatment due to the improvement of hardness [167]. In the case of a cast alloy, the value of the constant

wear is greater than that of the heat-treated alloy and composite. During the process of wear, cracks are mainly nucleated at matrix interfaces and reinforcement. This resulted in a lower tendency to cracking of the composite surface to the cast alloy. The heat treatment has not radically changed the morphology, but the curing of the matrix by precipitation hardening took place, which led to greater hardness and strength [168].

The highest wear resistance was obtained for the heat-treatment state T6. Studies had determined that the maximum curing the matrix was obtained when the composite material was solubilized at a temperature of 560 ° C for 3 hours, quenched with ice water to 0 ° C and aging at a temperature 175 ° C for 7 hours. It was found that the T6 heat treatment of 7:00 was the one that provided the highest hardness matrix and so it was he who gave the MMC wear resistance [169]. The hardness and the yield strength of the composite material by T6 heat treatment would have the advantage of avoiding the formation of aluminum scrap and decreasing its transfer to the surface of the steel [170]. When aged at lower temperatures (between 50-150 ° C) hardness and resistance to abrasive wear of composites under-age were found to be relatively low. Elevation of the aging temperature to 200 ° C increases the hardness and abrasion resistance of the composite to the state of peak age. At temperature 250°C composites were too old, which resulted in a reduction in hardness and wear resistance due to the intermetallic precipitates coalescence [171]. Decreasing reinforced aluminum discontinuously (DRA) matrix strength via sub-aging and averaging heat treatment decreases the wear rate DRA in abrasion conditions by increasing the formation of a solid protective film [172].

2.4 Models for the Prediction of Wear Properties

In the automotive, aerospace, mining and minerals, there are situations where two coupling parts are in contact with the other slide. Due to the relative movement of these sliding parts, there is an inevitable loss of material. In some cases, if the wear rate of material beyond a significant threshold value, there is a potentially catastrophic failure of components leading to enormous economic losses. Extensive research has been conducted on the study of the tribological behavior of MMCs aluminum [173]. The most important reason for damage and consequent breakage of parts of the machine wear. Many experiments have to be

conducted to study the tribological behavior. This results in a waste of both the workforce and money [174]. Hence the prediction of the wear rate is of utmost importance in the current industrial scenario to assess the life of the sliding components in advance to avoid massive financial losses incurred due to wear.

2.4.1 Prediction of Wear Properties by Theoretical Models

JL Yang in 2003 proposed a new formulation of the wear coefficient be developed and tested experimentally, which was based on the equation of exponential volume and transitional wear equation of Archard. The wear equation was found to be a better predictor of wear coefficients steady state. Sharma 2001 SC developed a theoretical model to estimate the rate of sliding wear taking into account the friction of the heat effect on the wear properties at the contact surfaces, the reinforcing effect, a mechanical load, sliding distance and the speed on the wear rate, the coefficient of friction and sliding wear of transition. This theoretical model was proposed to estimate the rate of sliding wear of the two alloys and composite materials. S. Kumar-2008, have successfully developed a mathematical model to predict the composite specific wear rate Al7075-SiC by incorporating the effects of the weight fraction of the reinforcement size, applied load, speed and material hardness counter sliding surface. The developed model can be used effectively to predict the wear rate of the composite Al7075-SiC at 95% confidence, the behavior correlated Al alloy wear and composites regarding mechanical properties, microstructural characteristics, the applied load, and sharp size by an empirical equation. This equation shows the effect of the size and volume fraction of the reinforcing phase and the size of the abrasive particles on the alloy content of aluminum and composite wear. This suggests that the composite wear rate increases with increase in the size of the reinforcement and the composite phase may be subject to higher wear rates than the abrasive alloy if the size is greater than that of phase strengthening.

The wear resistance of model, developed for the MMCs according to the Taguchi method. The orthogonal network, the signal to noise ratio (S / N) and analysis of variance were used to find the optimal control parameters. The results showed that the size of the abrasive grain is the most powerful factor of abrasive wear, followed by the weight fraction of reinforcement. Optimum wear test conditions were verified with experience. It was observed that there was good agreement between the predicted and resistance to wear real. The wear

behavior through a statistical analysis of the wear rate measured at different operating conditions. The wear rate is expressed regarding the abrasive size and the load applied to a linear regression equation. Factorial design experience can be successfully used to describe the elevated stress rasping wear behavior of Al alloys and composites and develop empirical linear regression equations to predict the wear rates in selected experimental area. Also, some researchers also attempted to assess the wear coefficients using theoretical models Archard and Yang and concluded that the predicted values of the coefficient of wear are in close agreement with those experimental [175].

2.4.2 Prediction of Wear Properties of Composites by Taguchi Method and GRA

For the optimal selection of the parameters of the process, the method Taguchi has been widely adopted in the manufacturing industry to improve the process with a single characteristic of performance. However, traditional method cannot solve Taguchi multi-objective optimization problem. To overcome this issue, the Taguchi method coupled to the relational analysis Gray has a wide field of application in the area of manufacturing processes [176]. This approach can solve the problem of multi optimization-responses simultaneously [177]. Deng (1982) proposes the relational analysis to fulfill of gray the essential criteria mathematics to deal with a poor, incomplete and uncertain System [178]. Also, it is an efficient method to optimize the complex of reports between several replies [142]. The theories of the analysis gray relational have already aroused great interest among researchers [180]. The planning of experiences through the orthogonal matrix gray Taguchi has been used with success in the process of optimization in [146,162,154,159,112,119]. Using this method, complicated the multiple responses can be converted to normalized response called gray relational coefficient (GRC). The Gray-Taguchi method which is a combination of Taguchi method and GRA will improve a better response to complex problems in the manufacturing process [123]. It has carried out an analysis gray relational to combine the multiple responses to a single numeric score, classify these scores, and determine the parameters carburetion optimally. Confirmation tests have been carried out by using the experiences. The ANOVA carried out to study the more parameters of influence on the mechanical wear and other properties [128].

The metal matrix composite aluminum is a relatively new material that has proven its position in the automotive, aerospace and other engineering design applications because of its wear resistance and high hardness [129]. Need for improved tribological performance has led to the development and selection of new variants of the composite. This investigation concerns the study of dry sliding wear performance Al5083-10 weight. % SiC composites manufactured by an ultrasonic assisted stir casting method. Dry sliding wear tests were performed using the wear test by using Pin-on-Disk with normal loads of 10N, 20N, 30N, and sliding distance: 754 m, 1131 m, 1508 m and the sliding speed 0. 42 m / s, 0. 63 m / s, 0. 84 m / s at constant time of 30 minutes. Experiments were conducted by the design of experiments generated by Taguchi technique. A table L9 Orthogonal was selected for analysis of the output. Survey to find the influence of the applied load, sliding speed and sliding distance on the wear rate during wear process was performed using ANOVA and regression equation were developed for 10% SiC reinforced AMMCs Al-5083. The objective of the model was chosen as 'smaller is the best' features to analyze the dry sliding wear resistance. In this research, it was observed that the applied load has the highest influence, followed by the sliding distance and sliding speed. Finally, the experimental results were validated by confirmatory tests.

This study aimed the treatment parameters for the flat plate collector based on the orthogonal matrices. The treatment parameters of a flat plate collector are the key factors that affect its performance. These parameters include the material of the manifold tube, plate material endothermic, number of collector tubes, the diameter of the tube of the manifold, type of film of absorption and the thickness of the lower thermal insulation [131]. The quality characteristics include the coefficient of efficiency and factor of dissipation of the heat. Once the data on each quality characteristic are obtained from orthogonal matrices, analysis of the main effect and the ANOVA (analysis of variance) are conducted to determine the parameters which have significant effects on the quality characteristics. Gray generation then processes the data, and the Relational optimal combination of levels of treatment parameter is determined by gray relational analysis and entropy measure. Three confirmatory tests are conducted, and the results indicate that the average of the values of the effectiveness and dissipation of the heat coefficient factor are the responsibility of the 95% CI (Confidence

Interval), the experience has proven reliable and repeatable. According to the response graph of the GRG (gray), the absorption of a quality relational type of film is a major factor which affects the characteristics of quality; in other words, the overall quality can be effectively controlled by controlling the only parameter.

The influence of stone dust of size (10-30 μm) and the mass fraction (5% - 15%) on the density, hardness and wear by dragging dry behavior Al 6061/rock dust processed via stir casting has been studied. The behavior of the wear of the developed metal matrix composite has been characterized in different loads conditions, slip speed and distances using the pin-on-disk configuration [136]. The experiments were conducted based on the Taguchi L27 orthogonal matrix, and the influence of process parameters on the rate of wear has been studied with the aid of the ANOVA. The experimental results show that the applied load and the strengthening of the size are the main parameters that affect the rate of wear specific for all samples, followed by the mass fraction of reinforcement, slip speed and distance of slip at the level of 47.61%, 28.57%, 19.04%, 9.52%, and 4.76%, respectively. The regression equation developed was tested for its accuracy and obvious fact that it can be used to predict the rate of wear with a minimum of error. With the help of SEM images, worn surfaces of the composite novel studied and the analysis shows that the resistance to wear of aluminum alloys can be improved with the addition of rock dust as reinforcement.

The optimization of process parameters for soft carburization Steel in using the method Taguchi based on gray. The design of experiments has been conducted by an orthogonal matrix L9 (34). Nine experiments were performed, and mechanical & properties of wear have been selected as the target of quality. A combination of settings of optimized cementation process has been obtained through the use of gray relational analysis. By analyzing the quality gray relational, we find the degree of influence of each factor on the quality target. In this study, we concluded that the temperature was the most carburetion dominated factor, which affects the mechanical and especially of the wear properties of mild steel cementation. Finally, a confirmatory test has been carried out according to the optimal settings planned and has found the success of the implementation of gray Taguchi approach.

2.5 Identified Gaps in the Literature / Motivation

After a comprehensive study of the existing literature, some gaps have been observed in fabrication metal matrix nanocomposites and optimization of process parameters for a desired output response.

- The fabrication process of AA2219, AA2014 with SiC and Al_2O_3 based metal matrix nanocomposites of using stir casting and use of ultrasonic cavitation and acoustic streaming for stirring is unexplored.
- Very few works are available on optimization of process parameters for a desired output response(s).
- Multiple objective optimizations for optimization of more than one response is still not much explored.

Thus present work aims at "Development of AA2014&AA2219 Metal Matrix Nano-Composites and evaluation of their Mechanical and Tribological Characteristics" has been undertaken keeping into mind the following problems mentioned as objective of the research work (section 2.6). Thus the present research work deals with fabrication process called Ultrasonic assisted stir casting and optimization of process parameters (load, sliding distance, and sliding velocity and the weight percentage of nano ceramic particles) for output response specific wear rate.

2.6 Objective of the Research Work

Metal matrix composites are being increasingly used in the aerospace and automobile industries owing to their enhanced properties such as elastic modulus, hardness, tensile strength at room and elevated temperatures and wear resistance combined with significant weight savings over unreinforced alloys and excellent thermal conductivity. Aluminum Metal Matrix Composites are being used in place of cast iron and steel in an automobile, mining and mineral sectors due to their lightweight and high strength. Al-alloys are preferred engineering material for automobile, aerospace and mineral processing industries for various high performing components that are being used for varieties of applications owing to their excellent properties. The commonly used reinforcements are fibers, whiskers, and particulates. The advantages of particle-reinforced composites over others are their formability with cost advantage and exhibit improved abrasion resistance, and they find

applications ranging from kitchen to automobile to space structures. The strength of these composites is proportional to the percentage volume and fineness of reinforced particles. This ceramic particle reinforced Al alloy composites have led to a new generation of tailorable engineering materials with improved specific properties.

In most applications, there exist situations where two mating parts are in sliding contact with each other. Due to the relative motion of these sliding parts, there is an inevitable loss of material due to friction. In certain situations, if the extent of material wear is beyond a critical limit, there are possibilities of catastrophic failure of the components leading to huge material and economic losses. Wear is a complex phenomenon and is the most important reason for the damage and consequent failure of machine parts. Many experiments have to be conducted to study the wear behavior resulting in wastage of both workforce and money. Hence, the prediction of wear properties is of utmost importance in the present industrial scenario to assess the life of sliding components in advance to avoid massive financial losses.

- To investigate the effect of process parameters like load, sliding distance, sliding speed and weight percentage of nano ceramic particles in wear test(pin on disc) of metal matrix nanocomposites namely AA2219/SiC/Al_2O_3(50nm,150nm) and AA2014/ SiC/Al_2O_3(50nm,150nm) on specific wear rate, volume of wear, weight loss, coefficient of friction, wear height.
- To fabricate AA2014 &AA2219 MMNCs using ultrasonic assisted stir casting method at ultrasonic frequency of 20kHz with different wt.% of SiC/Al_2O_3 with different particle sizes indepently.
- Optimization of process parameters using Taguchi method on wear test (pin on disc) of metal matrix nanocomposites namely AA2219/SiC/Al_2O_3 (50nm, 150nm) and AA2014/ SiC/Al_2O_3 (50nm, 150nm) as output response specific wear rate.
- Development of mathematical models for performance measurement (specific wear rate) with metal matrix nanocomposites AA2219/SiC/Al_2O_3 (50nm, 150nm) and AA2014/ SiC/Al_2O_3 (50nm, 150nm) using Regression analysis.

- Multi- objective optimization of process parameters using Grey Relational Analysis in wear studies metal matrix nanocomposites namely AA2219/SiC/Al_2O_3 (50nm, 150nm) and AA2014/ SiC/Al_2O_3 (50 nm, 150 nm).
- Comparison of results of metal matrix nano composites AA2219/SiC/Al_2O_3 (50 nm, 150nm) and AA2014/ SiC/Al_2O_3 (50 nm, 150 nm).
- To study the microstructure and perform microstructural analysis using SEM and XRD.

2.7 Problem formulation / Statement

In the present study, AA2014/AA2219 nanocomposite castings were fabricated using the ultrasonic assisted stir casting technique. The AA2014/AA2219 alloy and SiC/Al_2O_3 nanoparticles of various sizes (50nm and 150nm) were used as the base alloy and the reinforcements respectively. Nano ceramic reinforcements were added into the molten metal and then dispersed by the mechanical impeller and then followed by ultrasonic assisted cavitation and acoustic streaming. Ultrasonic vibration has been used for degassing, purifying and refinement of metallic materials because introducing the ultrasonic vibrational energy into a molten metal will induce nonlinear effects such as cavitation and acoustic streaming. The dispersion of nano-reinforcements and removal of agglomerations in the molten liquid metal is an important application of ultrasonic assisted stir casting process. The nano-reinforcements were in wetted condition; they can form an agglomeration of nanoparticles by various physical and chemical nature of attractive forces including surface tension of molten liquid metal and van der Waals forces. The attraction forces must be overcome to deagglomerate and disperse the particles into molten metal. The application of pressure gradient generated by ultrasonic waves breaks agglomerations formed by ceramic nanoparticles. Particles dispersion by ultrasonic waves creates microturbulence in the molten liquid pool, and also create small transient domains that would reach very high temperatures and pressures as well as extremely high heating and cooling rates. The shock force that takes place during ultrasonic cavitation process coupled with high local temperatures can break the nano reinforcement particle clusters and clean the surface of the particles. Ultrasonic vibration can improve the wettability between the nano-reinforced ceramic particles and the liquid state base alloy, which can assist to distribute the nano ceramic reinforcement particles more uniformly into the molten metal.

In the present study, the mechanical properties and wear behavior of AA2219/AA2014/SiC/Al_2O_3 based metal matrix nanocomposites have been investigated.

2.8 Overall Work Plan Structure

The work done has been presented in the following schematic figure 2.1 which is a self explanting. The selection of matrix material, nano-reinforcements, fabrication process, testing, and followed by analysis of wear properties of AA 2219 & AA 2014 based nanocomposites.

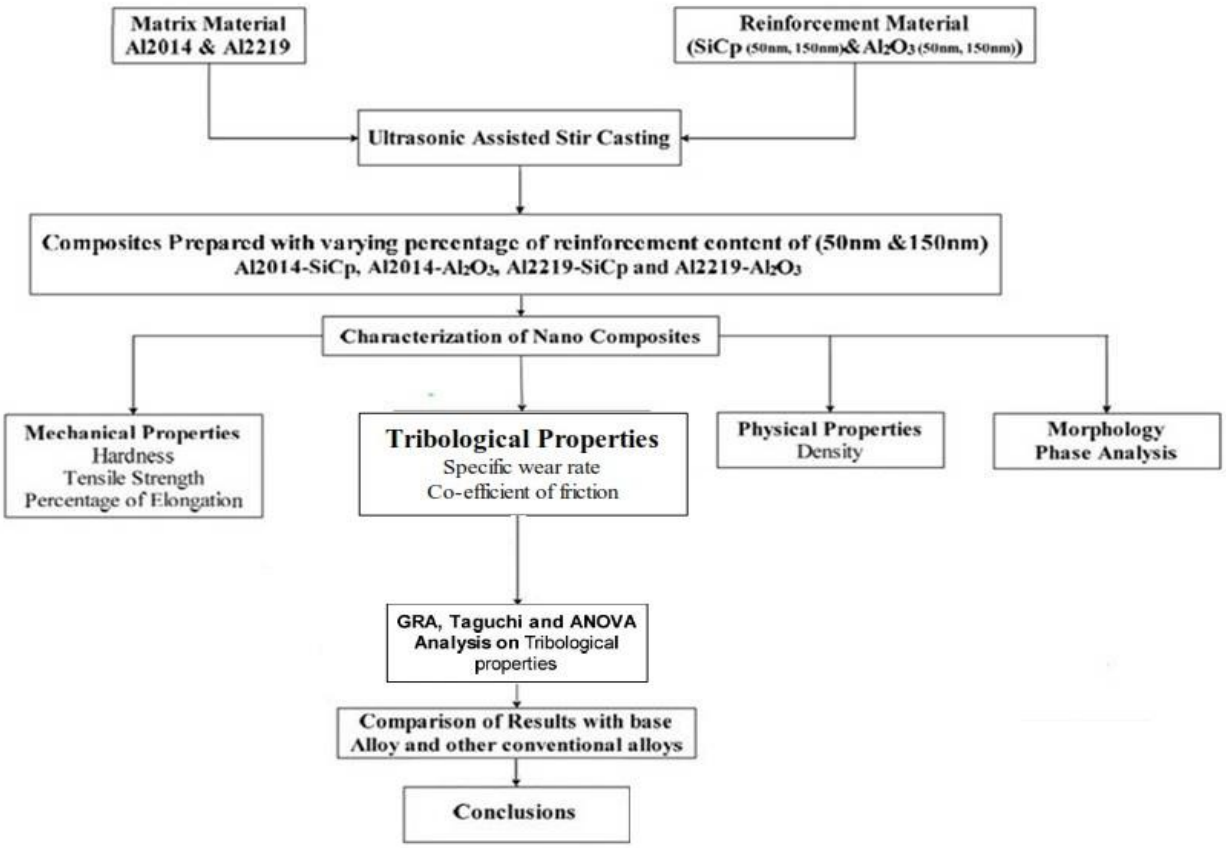

Figure 2.1 Schematic of work done in this thesis

Taguchi, ANOVA and GRA using Minitab software [162] from the above; Taguchi, ANOVA, and GRA can be successfully implemented for the prediction of mechanical and tribological properties of various composite materials. There are very few researchers who have attempted to study and develop the Taguchi, ANOVA, and GRA model for the prediction of tribological properties of Al-MMCs; hence the present work is undertaken**.**

Chapter 3

Methodology and Experimentation

3.1 Introduction

In this chapter, the author would present the fabrication of AA2014/SiC, AA2014/Al_2O_3, AA2219/SiC and AA2219/Al_2O_3 metal matrix nanocomposites. Ultrasonic stir casting method is used for processing of aluminium MMNCs. The procedures adopted for characterization of these components is also presented. Two types of aluminium alloys such as AA2219 & AA2014 were considered as base materials for MMNCs. A notation is followed for describing each combination alloy nanocomposites. AA2219/SiC/50 nm: means Al2219 alloy reinforced with 50 nm silicon carbide particulates.

3.2 Materials used for Aluminium MMNCs:

Many research studies [38] on aluminium MMNCs indicated that addition of micro/nano sized ceramic powders and such aluminium MMNCs have improved the properties compared to base metal. Such as strength, corrosion resistance, density, excellent wear resistance, and high stiffness. The micron size of ceramic reinforcements have been added to the aluminium based alloy matrix by the researchers [41] show better in the yield strength and ultimate tensile strength but reduce the ductility with an increase of weight percentage of reinforcements in the alloy matrix. Many of the researchers have been identified the improvement of properties with the addition of nanosize ceramic reinforcements to the aluminium matrix, resulted in no effect on ductility. Aluminium alloys like AA2014 and

AA2219 have received significant attention for last two decades [53]. The AA2014 is used in bolted or riveted construction for truck body applications [51]. The AA2219 is readily weldable, used for aerospace, fuel tanks, and space shuttle and rocket booster applications. Both the alloys are used in aircraft skin, aircraft fittings, ballistic armor, forged and machine components [55]. There is no study reported on use of nano silicon carbide (SiC) and alumina (Al_2O_3) as reinforcements in aluminium (AA2219 & AA2014) based metal matrix nanocomposites. The nano alumina and nano silicon carbide reinforced aluminium alloy matrix have shown improved stiffness and strength over the alloys without effecting on ductility. The silicon carbide and alumina possess outstanding characteristics high-temperature resistance, high strength, excellent wear resistance and high corrosion resistance.

Table 3.1 Chemical composition of AA2219 & AA2014 alloy in weight %

Alloy Name	**Cu**	**Fe**	**Cr**	**Mg**	**Mn**	**Si**	**Ti**	**Ni**	**V**	**Zn**	**Zr**	**Al**
AA2219	6.1	0.3	--	0.02	0.4	0.2	0.02	0	0.1	0.15	0.25	**Bal**
AA2014	4.9	0.5	0.1	0.8	1.2	0.9	0.15	0.1	--	--	0.1	**Bal**

Table 3.2 The physical properties of AA2014 and AA2219

Physical property	AA2014	AA2219
Density (g/cm^3)	2.80	2.84
Modulus of Elasticity (GPa)	71	73
Thermal Conductivity (W/m. K)	138	130
Thermal Expansion (K^{-1})	23×10^{-6}	22.5×10^{-6}
Melting Point(˚C)	535	550
Electrical Resistivity (Ω. m)	0.045×10^{-6}	0.057×10^{-6}

The AA2219 and AA2014 alloy used in this work were supplied by Rohit Super Forge Private Limited, Hyderabad, India. The chemical composition and physical properties of AA2219 and AA2014 are given in Table 3.1 and Table 3.2 respectively.

The ceramic nano-reinforcing material with size of 50 nm and 150 nm were considered in this research work. The properties of these nano powders are listed in Table 3.3. Alumina has excellent dielectric properties, high wear resistance, good thermal conductivity and good

stiffness. It is having a melting point 2072˚C and of density 3.95 g/ cm^3. The alumina was supplied by Sigma-Aldrich, Hyderabad, India. The ceramic nano-reinforcing material was Silicon carbide (SiC) of size 50 nm and 150 nm was taken in this research work. Silicon carbide has high wear resistance, excellent abrasiveness, high thermal conductivity and good shock resistance. It is having a melting point 2730˚C and of density 3.217 g/ cm^3. The Silicon carbide was supplied by US Research Nanomaterials, USA.

Table 3.3 properties of nano powders

Material	Density (g/cm^3)	Melting Point(˚C)
SiC	3.95	2072
Al_2O_3	3.217	2730

Table 3.4 The list various types of nanocomposites were fabricated

S. No	Base Material	Reinforcement	Size of Reinforcement (nm)	Designation of MMNC
1	AA 2219	(0, 0.5, 1, 1.5 & 2) Wt. % SiC	50	AA2219/SiC/50 nm
2	AA 2219	(0, 0.5, 1, 1.5 & 2) Wt. % SiC	150	AA2219/Al_2O_3/50 nm
3	AA 2219	(0, 0.5, 1, 1.5 & 2) Wt. % Al_2O_3	50	AA2219/SiC/150 nm
4	AA 2219	(0, 0.5, 1, 1.5 & 2) Wt. % Al_2O_3	150	AA2219/Al_2O_3/150 nm
5	AA 2014	(0, 0.5, 1, 1.5 & 2) Wt. % SiC	50	AA2014/SiC/50 nm
6	AA 2014	(0, 0.5, 1, 1.5 & 2) Wt. % SiC	150	AA2014/Al_2O_3/50 nm
7	AA 2014	(0, 0.5, 1, 1.5 & 2) Wt. % Al_2O_3	50	AA2014/SiC/150 nm
8	AA 2014	(0, 0.5, 1, 1.5 & 2) Wt. % Al_2O_3	150	AA2014/Al_2O_3/150 nm

Therefore, the present study concentrated on the fabrication of AA 2014, and AA 2219 with different weight percentages of reinforcements of Al_2O_3 and SiC nanocomposites.

Table 3.4 gives the different composites of aluminium MMNCs. The morphology and mechanical properties and tribological properties of the nanocomposites were reported. A notation is followed for describing each combination alloy nanocomposites. AA2219/SiC/50 nm: means Al2219 alloy reinforced with 50 nm silicon carbide particulates.

3.3 Experimental Setup

The experimental setup for the manufacturing nanocomposite material is shown in Figure 3.1. The setup consists of ultrasonic probe, ultrasonic control unit, ultrasonic generator, electric resistance heating furnace, furnace control unit, mechanical stirring unit, a cooling unit for ultrasonic probe and pre-heating electric furnace. The temperature limit of the furnace is up to 1000˚C. The frequency of the ultrasonic probe was used 20 KHz for fabrication of aluminium based nanocomposites of various weight percentages. An individually designed graphite crucible with a capacity of 2kg was used for melt processing.

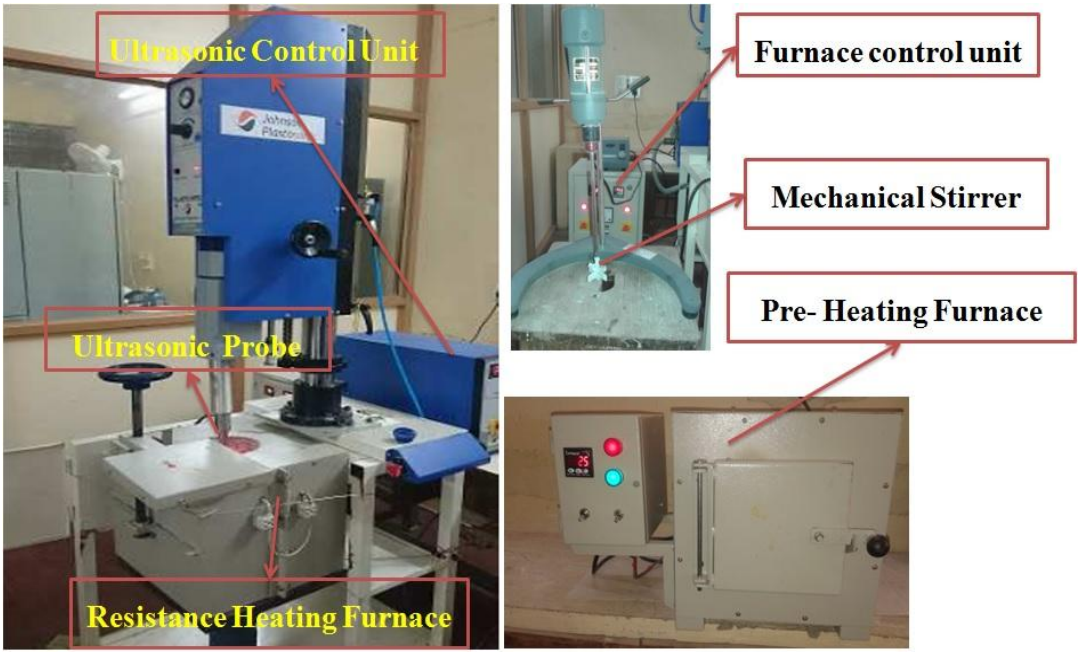

Figure 3.1. Ultrasonic cavitation assisted stir casting experimental setup (NITW)

The crucible is designed in such way that it easily occupies the space provided in the ultrasonic setup. Adjustable speed electrical motor with a mechanical stirrer was used to generate vortex motion in the molten slurry. The ultrasonic generator with 20kW power was used to generate 28 kHz frequency for slurry processing. The piezoelectric transducer

converts electrical pulse on and off signals into mechanical vibrations. The pulse on and pulse of time for each cycle is 0.1s. The stepped type ultrasonic probe which is also called as sonotrode as shown in Figure 3.1 is used for molten slurry processing. The ultrasonic horn is made of titanium and has a flat radiating surface. Titanium has negligible solubility in liquid state AA2014, resulting in a long lifespan and minimum contamination. The top portion of the horn 85mm in length and 35 mm in diameter is connected to the ultrasonic transducer, and the bottom portion has 185 mm length and 20 mm diameter, which is immersed in liquid alloy during ultrasonic stir processing. A thermocouple was used to monitor the temperature of the molten slurry. Compressed air was used for cooling purpose and controls the up and down movement of the ultrasonic horn. The molten metal surface was exposed to the atmosphere for producing optimal cavitation effect inside the molten metal.

3.4 Experimental Procedure for Fabrication of Nano-Composites

Experiments were conducted to study the effect of ultrasonic cavitation phenomena on processing the molten aluminium alloy 2014 by changing the weight percentages of silicon carbide and alumina nanoparticles of various sizes 50 nm and 150 nm. In each experiment, 700g of AA2014 was melted in a graphite crucible (inner diameter: 70mm) at 760^{o}C and blocked for about 30min. Initially, molten alloy was mechanically stirred to obtain the homogeneous mixture and then the silicon carbide or alumina nanoparticles pallets made of aluminium foil were slowly dropped into the molten metal from the top of the crucible with different combinations. Mechanical stirring was done at 600rpm about 15min for pre-mixing the nanoparticles and also to travel the ultrasonic waves uniformly inside the homogeneous molten slurry. After finishing the mechanical stirring process, the impeller was taken out from the molten slurry and then ultrasonic probe was dipped into the molten slurry at 25mm depth, and ultrasonic wave generator (Johnson Plasmonic Ltd., Bangalore, India) was switched on. When the pressure gradient of the ultrasonic waves is more to that of liquid aluminum alloy bonding energy, it breaks the bonds and developed an enormous amount of energy. While the hydrogen bubbles collapse they disperse the nanoparticles in all directions randomly, this phenomenon is also called as cavitation. Hence the formation of agglomerations was significantly reduced after effective ultrasonic processing. The ultrasonic cavitation process is allowed for 15min was used for melt processing. During ultrasonic cavitation process, the

viscosity of the molten aluminium alloy slightly increases due to the addition of silicon or alumina nanoparticles. Thus after effective ultrasonic cavitation, a higher casting temperature of 780^{o}C was used to make sure the better flowability of the slurry into the preheated steel die. An ingot of diameter 30mm and length 150mm was prepared.

In this present work AA2014/SiC/Al_2O_3 and AA2219/SiC/Al_2O_3 metal matrix nanocomposites with various weight percentages (0.5,1,1.5 & 2) of SiC and Al_2O_3 nanoparticles of different sizes 50 nm and 150 nm were fabricated by ultrasonic assisted stir casting method. Ceramic NPs beyond 2Wt.% were not considered in this work due to formation of clusters at higher percentage SiC/Al_2O_3 particles.

Table 3.5 (a) Aluminium based metal matrix nanocomposites:

Alloy name	AA 2219															
Name of nano ceramic powder	SiC								Al_2O_3							
Size of nano ceramic powder	50 nm				150 nm				50 nm				150 nm			
Weight % of nano ceramic powder	0.5	1	1.5	2	0.5	1	1.5	2	0.5	1	1.5	2	0.5	1	1.5	2
Number of MMNC's Based on Weight % of nano ceramic powder	1	2	3	4	5	6	7	8	9	10	11	12	13	14	15	16
Number of MMNC's Based on size& type of nano ceramic powder	1.) AA 2219/ SiC/50 nm				2.) AA 2219/ SiC/150 nm				3.) AA 2219/ Al_2O_3/50 nm				4.) AA 2219 Al_2O_3/150 nm			

The scheme of carrying out experiments was selected and the experiments were conducted on different aluminium based metal matrix nanocomposites (AA MMNC's as

shown in Table 3.5(a) & (b) to study the influence of process parameters on the output responses e.g. wear height (WH), volume of wear (VOW), specific wear rate (SWR). In the present study load (L), sliding distance (SD), sliding velocity (SV) and weight percentage (Wt. %) of ceramic nanoparticles of silicon carbide (SiC) and alumina (Al_2O_3) of different particle sizes (50 nm&150 nm) are the independent parameters.

Whereas dependent parameters are WH, VOW & SWR. Here the dependent parameters are mathematically proportional to each other; that is why to investigate any one of the dependent parameters the same must reflect other dependent parameters. In this present work mainly concentrated on dependent parameter SWR. The experimental results are discussed subsequently in chapter 6.

Table 3.5(b) Aluminium based metal matrix nanocomposites

Alloy name	AA 2014															
Name of nano ceramic powder	SiC								Al_2O_3							
Size of nano ceramic powder	50 nm				150 nm				50 nm				150 nm			
Weight % of nano ceramic powder	0.5	1	1.5	2	0.5	1	1.5	2	0.5	1	1.5	2	0.5	1	1.5	2
Number of MMNC's Based on Weight % of nano ceramic powder	1	2	3	4	5	6	7	8	9	10	11	12	13	14	15	16
Number of MMNC's Based on size & type of nanopowder	1.) AA 2014/ SiC/50 nm				2.) AA 2014/ SiC /150 nm				3.) AA 2014/ Al_2O_3/50 nm				4.) AA 2014 Al_2O_3/150 nm			

Selection of Orthogonal Array and Process Parameters

For the current experimental work, four process parameters each at four levels have been decided. It is desirable to have four levels of process parameters to reflect the actual behavior of output parameters of the study. The process parameters, their corresponding symbols and the levels of the individual process parameters are given in Table 3.6.

Table 3.6 Levels of Various Process Parameters in wear test Process

S. No.	Process parameters	Units	Symbol	Levels			
				L1	L2	L3	L4
1	Load	N	L	5	10	15	20
2	Sliding distance	m	SD	1000	2000	3000	4000
3	Sliding speed	m/s	SV	0.733	1.0989	1.465	1.832
4	Weight percentage	Wt. %	Wt. %	0.5	1	1.5	2

The wear experiments were conducted to investigate the influence of input parameters over the output response characteristic with aluminium based metal matrix nanocomposites (AA MMNC's as shown in Table 3.7; SWR is the response.

Table 3.7 Taguchi's L16 Standard Orthogonal Array

S. No	L	SD	SV	Wt. %	Response (Raw data)			Average WH (μm)	VOW (mm^3) 10e-3	SWR (mm^3/ Nm)	S/ N Ratio
					WH1 (μm)	WH2 (μm)	WH3 (μm)				
1	5	1000	0.733	0.5							
2	5	2000	1.0989	1							
3	5	3000	1.465	1.5							
4	5	4000	1.832	2							
5	10	1000	1.0989	1.5							
6	10	2000	0.733	2							
7	10	3000	1.832	0.5							
8	10	4000	1.465	1							
9	15	1000	1.465	2							
10	15	2000	1.832	1.5							
11	15	3000	0.733	1							
12	15	4000	1.0989	0.5							
13	20	1000	1.832	1							
14	20	2000	1.465	0.5							
15	20	3000	1.0989	2							
16	20	4000	0.733	1.5							

- WH1, WH2 &WH3 represent response values for three repetitions of each trial.

The effect of process parameters on SWR regarding response plots, residual plots, analysis of variance (ANOVA) tables and response tables are presented in the following sections. Orthogonal Array (OA) L16 experiments were conducted using Taguchi experimental design methodology shown in Table 3.7 and each experiment was repeated three times for obtaining S/N values. Minitab statistical software is utilized for the above study. Detailed full factorial experiments were also conducted and the results of the experiments are included in Appendix I.

3.5 Materials Characterization

Aluminium nanocomposites thus fabricated and further analyzed for hardness, density, phase and morphology analysis and SEM pictures, wear testing and friction measurement. They are explained in detail in the following subsection.

3.5.1 Sample Preparation for SEM Analysis

The sample preparation includes sectioning, grinding, polishing and etching. To avoid cold working and to alter the microstructure, metallographic specimens of ultrasonic cavitation-assisted and stirring samples can be cut with a low-speed saw and cooled by a liquid coolant during cutting. Then the samples were prepared using standard hand polishing using 220, 300, 600, 800 and 1000-grit and followed by I/0, II/0, III/0 and IV/0 silicon carbide papers. Specimens were then cloth finish-polished using 1 µm diamond paste suspended in distilled water to obtain mirror like surface. For microstructural features, the polished specimens were etched with Keller etching chemical solution for 10 to 40 seconds. The etching allows the aluminium alloy matrix to dissolve while leaving the silicon particles elevated above the matrix level. After they were cleaned with water and dried with acetone, etch-polish-etch procedures were used to attain real microstructure.

3.5.2 X-ray Diffraction (XRD) Analysis

To identify the phases formation in the prepared Al-2219/ (SiC or Al_2O_3) & Al-2014 (SiC or Al_2O_3) nanocomposites X-ray Diffraction (XRD) technique is used. It is a non-destructive and universal technique for characterizing crystalline materials. The technique is used to obtain the information of crystallographic structures, chemical composition and physical properties of the investigated specimens. In X-ray diffraction, the electromagnetic

radiation with wavelength 1.54 A˚ in order typically and elastically scatters on the electron cloud of the atom in a crystal. The X-rays causes the scattered X-rays to interfere constructively or destructively, depending on the wavelength of X-rays and distance between lattice planes of atoms, in the crystal structure. The XRD setup (National Institute of Technology Warangal, India) image as showed in Figure 3.3. The Bragg's law stated and followed the interference of these waves is given below:

$$n\lambda = 2d_{hkl}\ sin\emptyset \text{ ---------- (1)}$$

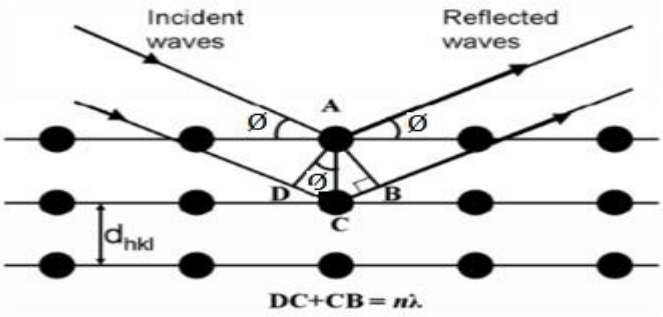

Figure 3.2. Schematic description of Bragg's Law

Where: λ- wavelength, n-integer, 2∅ - angle between the transmitted and scattered beam directions, d_{hkl}- lattice spacing for a particular set of Miller (hkl) indices [46].

Figure 3.3. XRD equipment NIT Warangal Modal PANalytical

The Schematic description of Bragg's Law is shown in Figure 3.2. By varying the incidence angle of the incoming X-ray beam by a ∅ and scattering angle by 2∅ the scattered intensity is measured as a function of the latter. In our Institute laboratory, the XRD setup is used where the sample remains in a fixed position while both X-ray source and detector rotate by∅, clockwise and anticlockwise, respectively. These precise movements are performed by a goniometer which is a main part of the diffract meter.

3.5.3 Scanning Electron Microscopy (SEM) for Morphology and Topography Analysis

Scanning electron microscopy (SEM) is an instrument used for examining the morphology, surface topography, and chemical composition of the specimen. The sample crystallographic information can get from SEM instrument. From the tungsten filament, the electron beam generates and focused by the several magnetic lenses, and hits the sample. The electron from the beam collides with the electrons from the sample. That creates an elastic scattering high energetic BSE are reflected back in backscattered mode. Due to inelastic collisions, SE with lower energy is emitted. The SEM setup used (National Institute of Technology Warangal, India) is shown in Figure 3.4.

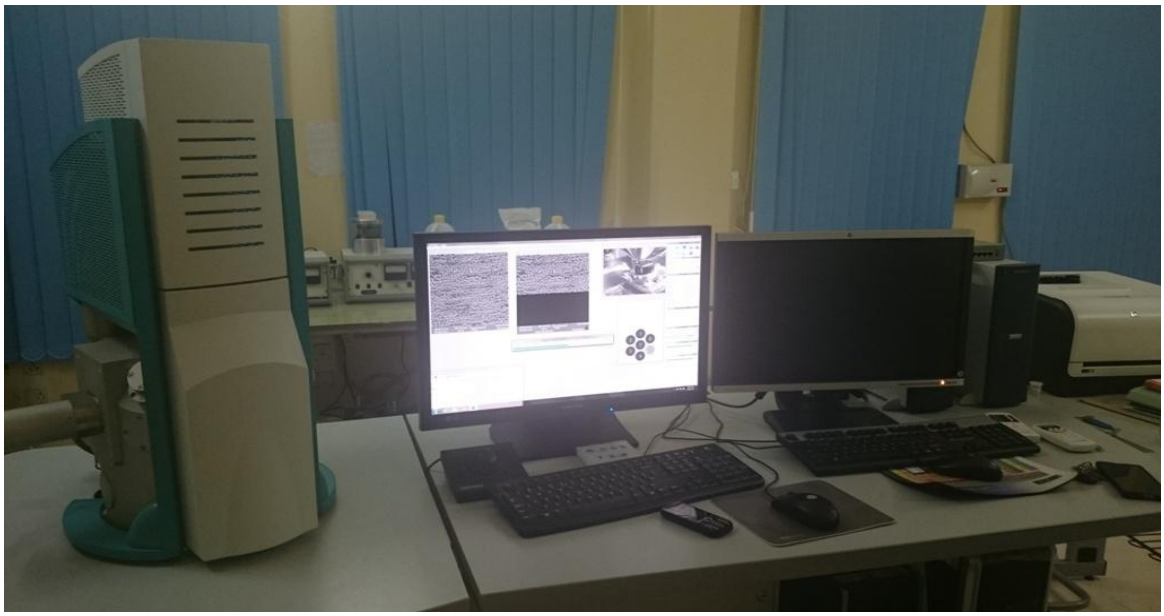

Figure 3.4. SEM equipment at NIT Warangal

3.6 Testing Methods

3.6.1 Density Measurements

The density of the AA2219 & AA2014 alloy/ (Al_2O_3 or SiC) nanocomposites fabricated through the ultrasonic assisted and stir casting technique was measured using Archimedes principle. It is a convenient method for measuring the volume of a regularly or irregularly shaped object. The density of the composite samples was examined using a high precision digital electronic weighing balance with an accuracy of 0.0001g. The sample dimensions were measured by measuring its dimensions using a micrometer and weighing its mass using balance. Six vertical measurements were made on each sample. Mass was measured on balance with five decimal point accuracy.

Procedure for measuring density

- Measure mass of the specimen in air (M_a) in grams
- Then submerge the sample completely in water and measure the mass (M_w) in grams
- The water displaced in grams ($V = M_a - M_w$) in grams. When (ρ_w=1 g/cm^2)

$$\rho = \frac{M_a}{M_a - M_w}$$

- By using the equation above to determine the density of specimen.
- The densities measured for all combination of aluminium MMNCs have been given in chapter 4. Each experiment is conducted four repeated times and consider the average of four results. The outcome results are repeatable in a significant manner and did not change above 0.05% from the mean value.

3.6.2 Hardness Test

The hardness of the fabricated nanocomposites indicates the mechanical properties of the samples. When surface properties concerned its importance to wear and friction processes, then measurement of hardness of the material is a quick method for to get the mechanical property. The principle of hardness test technique is forcing an indenter into the specimen surface and measuring the dimensions of the indentation. The hardness of the ultrasonic assisted stirring and cast samples were performed Vickers micro hardness tester.

Specifications
Microscope – magnification 800 to 1000X
Objects of 10X, 40/50X, 80/ 100X along with 10X eyepiece
Test load range- 10gf to 2000gf
Loading speed- 15 to 70 µm/sec
Dwell time – 5 to 99 sec
Indenters-square based pyramidal diamond with face angles 136˚ 0 min

Figure 3.5 Vickers Microhardness tester

3.6.3 Tensile Strength Test

The tensile test of the aluminium alloy based nanocomposites is conducted as per American Society for Testing and Materials (ASTM-E8) standards. In this test, we can obtain the ultimate tensile strength and yield strength. The dimensions of the specimens prepared as per standards and are shown in Figure 3.6. This test was done with computerized strain rate based ultimate tensile testing machine at room temperature 25˚C as shown in Figure 3.7. It is used to test tensile stress and compressive strength of the materials. The results were recorded accurately with a break point. The stress at maximum is referred to as the ultimate tensile strength.

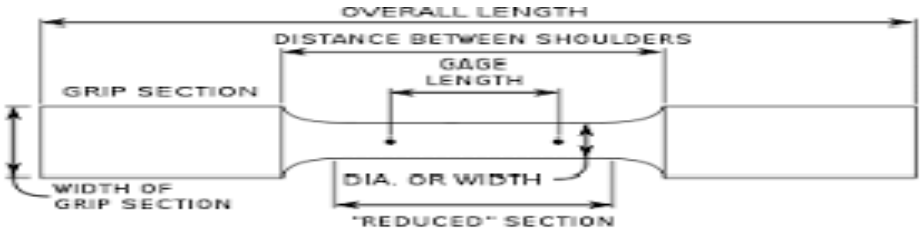

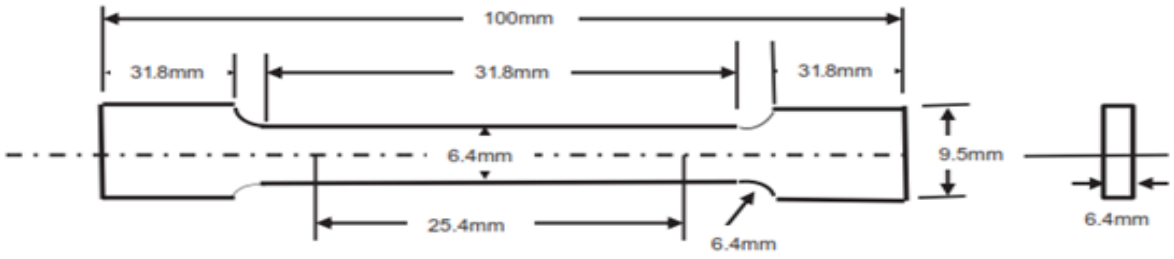

Figure 3.6. Dimensions of the tensile test specimen

Specifications

Electro Mechanical Tensile Testing Machine

Capacity -20 kN

Civil Engineering Department NIT W

Accuracy -In accordance ISO 7500-1 and EN 10002-2, Grade 0.5

Control-force and displacement closed loop controlled

Test speed- 0.001 mm/ min up to 1000/ 500 mm/ min

Crosshead travel- 1000/ 1100 mm

Power requirements- 3×400 V, 500 Hz

Figure 3.7. Dimensions of the tensile test specimen

3.6.4 Wear Test

The tribological tests were conducted for both the cast matrix alloy and its nanocomposites samples and studied their characteristics like wear height and coefficient of friction on wear testing machine. Table 3.8 gives the technical specifications of the wear test machine (POD) used and Figure 3.8 shows the apparatus and other peripheral units. The wear test samples were prepared in the form of cylindrical pins of diameter 6mm and pin height 25

mm, and the apparatus-disc material is high carbon EN31 steel. The hardness value of the disc material is HRC60. The tribological tests are conducted according to **ASTM – G99 standard**. In each experiment, the wear height of the sample was recorded in microns by using LVDT control of 1.0μm least count. During the wear test, the pin surface made contact with the disc surface and both surfaces are relatively moving in opposite directions in which disc is rotating, and the pin is in a stationary position.

Table 3.8 Technical Specifications of the POD Wear Testing Machine

Parameter	Specifications
Pin Dimensions	3 to 12mm diameter and 10 to 50mm length
Disc Dimensions	160mm diameter and 8 to 12mm thickness
Wear track radius	8mm to 125mm diameter
Disc rotating speeds	100 to 1000 rpm
Sliding speed range	6 m/s to 26 m/s
Normal load	200N(maximum)
Frictional Force	0 to 200N(digital read out)
Wear height loss measurement	LVDT of 1.0μm Least count
Input power	230V, 5A, I Phase,50Hz

Because of generation of high frictional force in between the two surfaces cylindrical pin loses the parent material in a vertically downward direction based on this wear height can be noted on the digital screen of LVDT. The load acting on the test specimen during the testing was varied from 5 to 20 N in steps of 5 N; the sliding distance was taken from 1km to 4km and is controlled by setting the timer on the machine at a velocity of 0.763 m/S. The surface roughness of the test pin specimen and the disc were maintained at 0.1 μm *R*a. From the POD experiment, the wear height practiced by the pin is measured in micrometers, and following parameters were calculated.

- ✓ Volume of Wear in mm^3= Cross-sectional Area of the pin X Height loss
- ✓ Weight Loss in grams = Volume of Wear X Density

✓ Specific Wear rate = Volume of Wear/(Sliding Distance X Load)

Different graphs were plotted of the various applied loads and reinforcements to distinguish the wear behavior of the metal matrix nanocomposites (presented in Chapter 6)

- Volume of wear Vs Sliding Distance
- Weight Loss Vs Sliding Distance
- Specific Wear Rate Vs Sliding Distance

Composite Pin in Contact with the Disc

Control Unit of Wear Testing Machine

Pin on Disc with LVDT

Pin on Disc with Wear Debris

Figure 3.8 Pin on Disc Setup

Immediately before testing, and before measuring or weighing, clean and dry the specimens. Take care to remove all dirt and foreign matter from the specimens. Use non-chlorinated, non-film-forming cleaning agents and solvents. Dry materials with open grains to remove all traces of the cleaning fluids that may be entrapped in the material. Steel (ferromagnetic) specimens having residual magnetism should be demagnetized. Report the methods used for cleaning. Measure appropriate specimen dimensions to the nearest 2.5 μm or weigh the specimens to the nearest 0.0001 g. Insert the pinned specimen securely in its holder and, if necessary, adjust so that the specimen is perpendicular to the disk surface when in contact, to maintain the necessary contact conditions. Add the proper mass to the system lever or bale to develop the selected force pressing the pin against the disk. Start the motor and adjust the speed to the desired value while holding the pinned specimen out of contact with the disk. Stop the motor. Set the revolution counter (or equivalent) to the desired number

of revolutions. Begin the test with the specimens in contact under load. The test is stopped when the desired number of revolutions is achieved. Tests should not be interrupted or restarted. Remove the specimens and clean off any loose wear debris. Note the existence of features on or near the wear scar such as protrusions, displaced metal, discoloration, microcracking, or spotting. Premeasured the specimen dimensions to the nearest 2.5μm or reweigh the specimens to the nearest 0.0001 g, as appropriate. Repeat the test with additional specimens to obtain sufficient data for statistically significant results.

Specific Wear Rate, K:

$$K = \frac{\text{(Volume of Wear)}}{\text{(Applied Load) x (Sliding Distance)}}$$

Where, Volume of Wear = (π x (Radius of pin point) ^{2} x Depth of penetration), Sliding Distance = (2 x π x Radius of wear circle), S.I. Unit of Specific Wear Rate, K is (mm) ^{3}/ (N-m).

3.6.5 Samples for mechanical Testing

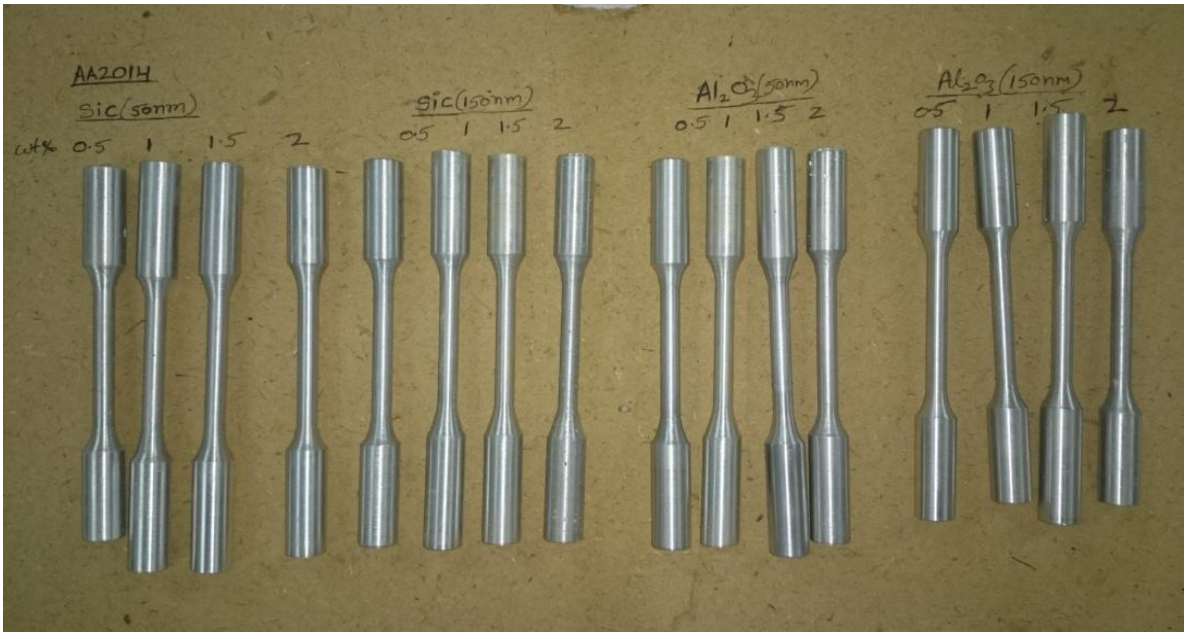

Figure 3.9 Tensile testing specimens of AA 2014 &AA 2219/SiC (150 nm, 50 nm), AA 2014&AA 2219/Al2O3 (150 nm, 50 nm)

Figure 3.10 Hardness specimens of AA 2014 &AA 2219/SiC (150 nm, 50 nm), AA 2014&AA 2219/Al_2O_3 (150 nm, 50 nm).

3.6.6 Samples for Wear Testing

a.)

b.)

Figure 3.11 Wear test specimens of (a) AA 2014 &AA 2219/SiC (150 nm, 50 nm), (b) AA 2014&AA 2219/Al_2O_3 (150 nm, 50 nm).

3.7 Summary

The base metal matrix aluminium alloys (AA2219&AA2014) reinforced with silicon carbide & Alumina Nanocomposites are casted using the ultrasonic assisted stir casting process and these various samples of Aluminium MMNCs were prepared. The samples were prepared for various tribological and mechanical tests according to ASTM standards. The morphology, topography, phases and chemical composition of the various nanocomposites are analyzed using SEM and XRD. The mechanical properties were measured by the ultimate tensile strength, hardness, and yield strength tests on the tensile testing machine and Vickers microhardness tester. The wear tests were conducted on a pin on disc setup against the counter body material. The wear surface of the nanocomposites was examined using SEM.

Chapter 4

Evaluation of Mechanical Properties

This chapter deals with evaluation of properties of aluminium MMNCs fabricated by Ultrasonic assisted stir casting method. The properties such as density, ultimate tensile strength, hardness were evaluated for the following composites and their micro structures were also studied.

1.) AA2219/SiC/50 nm

2.)AA2219/Al_2O_3/50 nm

3.)AA2219/SiC/150 nm

4.)AA2219/Al_2O_3/150 nm

5.)AA2014/SiC/50 nm

6.)AA2014/Al_2O_3/50 nm

7.) AA2014/SiC/150 nm

8.) AA2014/Al_2O_3/150 nm.

4.1 AA 2219/ SiC /50 nm Composites

The density, UTS and hardness were measured for AA2219/SiC/50 nm samples as per the standards and presented in Table 4.1. The various samples were prepared charging SiC/50 nm wt.% particulates in base AA2219 from 0 to 2wt.% using ultrasonic assisted stir casting process.

Table 4.1 Mechanical Properties of AA2219/SiC/50 nm

S.No	Material	Density value(g/cm^3)		UTS	Hardness	% of Elongation
		Theoretical	Experimental			
1.	AA2219	2.84	2.84	169.79	149.38	17.7
2.	AA2219/0.5wt.% SiC	2.8416	2.8405	222.85	156.70	13.6
3.	AA2219/1 wt.% SiC	2.8433	2.8427	233.46	160.48	12.7
4.	AA2219/1.5wt.% SiC	2.8448	2.8439	240.54	160.26	11.9
5.	AA2219/2 wt.% SiC	2.8465	2.8455	261.76	162.88	11.3

4.1.1 Density of AA 2219 / SiC / 50 nm Composites

The theoretical density of the composite has been calculated using the rule of the mixture. Figure 4.1 shows the theoretical and the experimental density values of the AA 2219/ SiC /50 nm based MMNCs containing 0 to 2wt% of nano SiC reinforcement contents. It is found that the density of the AA2219/SiC MMNC is greater than that of the base metal matrix material (AA 2219). The density of AA 2219/ SiC /50 nm also increases by increase in wt. %

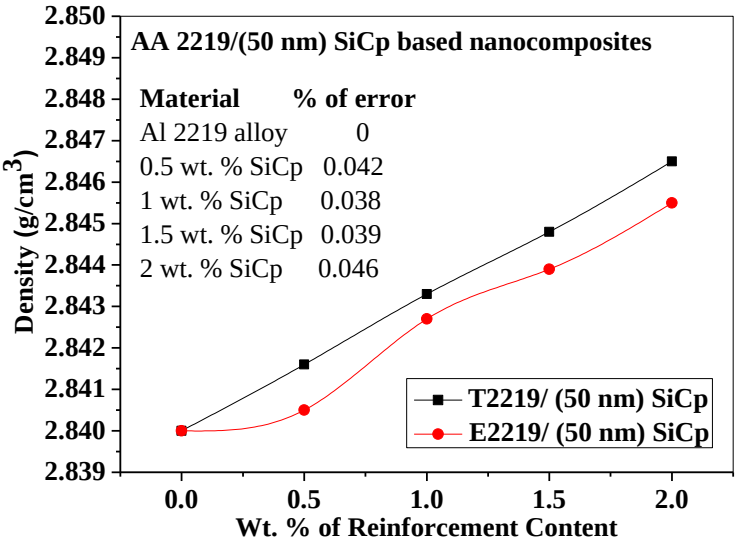

Figure 4.1 Theoretical densities and Experimental Densities for varying wt% of nano SiC in AA 2219 alloy.

of Particulate reinforcement. An average of 0.2 to 0.25% improvements in the density is observed above the base alloy. Additionally, the experimental densities and the theoretical densities are in line with each other confirming the appropriateness of the ultrasonic assisted

stir casting method for the successful fabrication of AA 2219/ SiC /50 nm based MMNCs at different weight percentages. An average of 0.042% of deviation of densities observed between theoretical and practical values.

4.1.2 Microstructure Studies of AA 2219/ SiC /50 nm Composites

The scanning electron microscopy images of the MMNC (AA 2219/ SiC /50 nm) at different levels of reinforcement are given in Figure 4.2 (a, b,c&d)

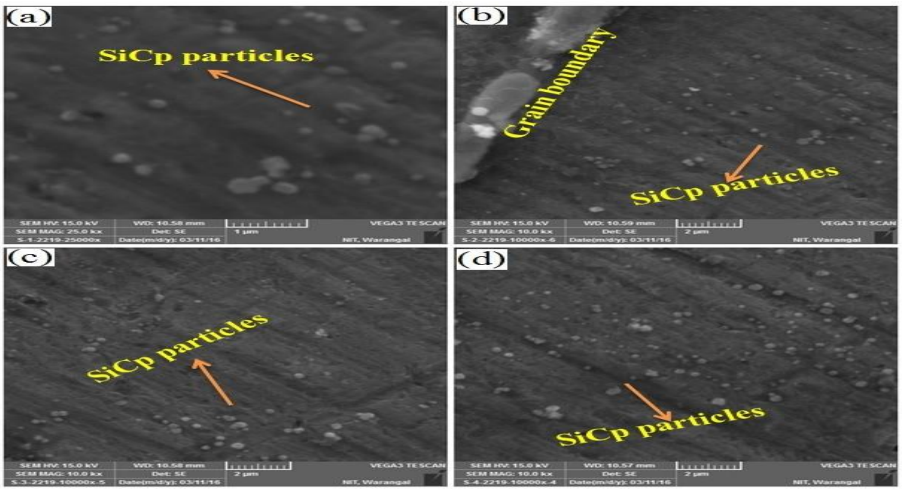

Figures 4.2. SEM images of AA 2219/ SiC /50 nm alloy and its nanocomposites (a) 0.5 wt. % of SiC, (b) 1 wt. % of SiC, (c) 1.5 wt. % of SiC, and (d) 2 wt. % of SiC

Microstructural SEM images presented in Figures 4.2. (a, b, c & d) show an uniform distribution of nano SiC particulates throughout the metal matrix composite (AA 2219).

4.1.3 Hardness of AA2219/SiC/50 nm

The variation of Vickers's Microhardness of AA2219/SiC/50 nm MMNC with increased wt.% of nano SiC reinforcement content is given in Table 4.1 and also shown in Figure 4.3. From the Figure 4.3, it can be observed that the hardness value of the MMNCs (AA 2219/ SiC /50 nm) is more than that of its base aluminium alloy (AA 2219). Moreover, it is also found that as the wt.% of nano SiC amount increases the hardness also increases by

significant amounts. The MMNCs containing 2wt% reinforcement content exhibits greater hardness value. The hardness value of the AA 2219/ SiC /50 nm MMNC material increases by 8.3% as the reinforcement content of nano SiC raises from 0 to 2wt. %.

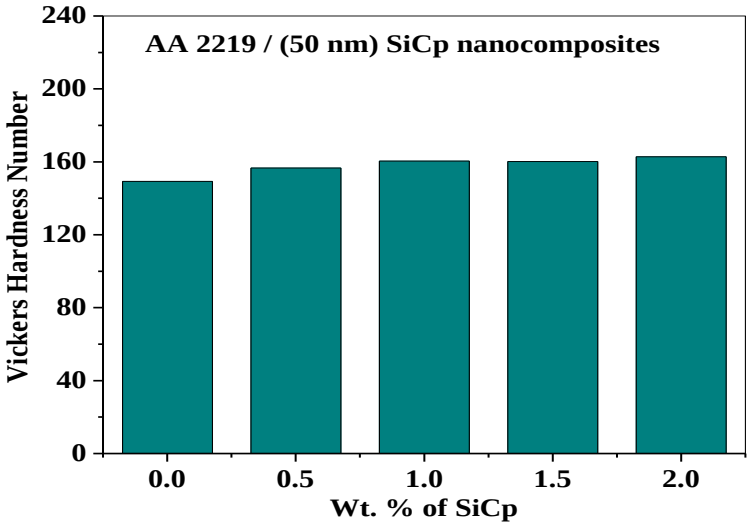

Figure 4.3. Variation of Vicker's Micro Hardness number of AA 2219 and its nanocomposites

4.1.4 Ultimate Tensile Strength (UTS) of AA 2219/ SiC /50 nm Composites

The variation of the ultimate tensile strength of AA 2219/ SiC /50 nm MMNC has given in Table 4.1 and also shown in Figure 4.4. UTS of samples increases with the increase of weight percentage of nano SiC reinforced particulates. Theoretically when hardness increases the UTS of the material also increases [Tom Chandler]. A relation existing between hardness(H) and UTS is H=(UTS)/k ; where "k" depends on material condition and type.

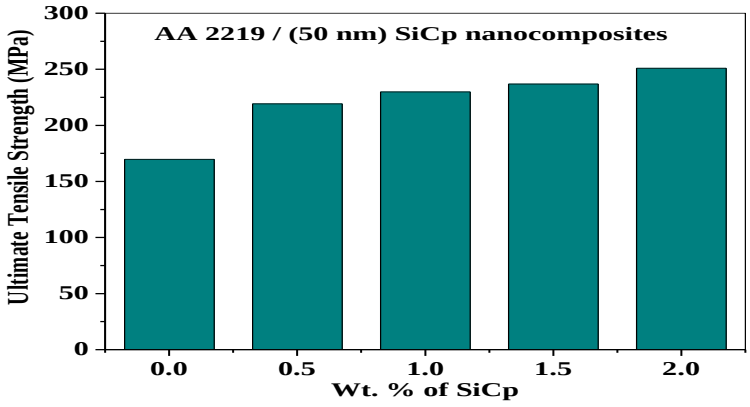

Figure 4.4. Variation in UTS of AA 2219 and its Nano SiC reinforced Composites

The UTS of the AA 2219/ SiC /50 nm MMNC increases as the weight percentage of the nano ceramic SiC particulate phase increase from 0 to 2wt%. The UTS of the metal matrix nanocomposite increases by 23.81% as the reinforcement content of nano SiC particulates raise from 0 to 2 wt%.

4.1.5 Ductility or Percentage Elongation of AA 2219/ SiC /50 nm Composites

The consequence of nano SiC reinforced content on the ductility of AA 2219/ SiC /50 nm MMNC was calculated with respect to the percentage of elongation and the result is presented in Table 4.1 and also depicted in Figure 4.5. The percentage of elongation of the metal matrix nanocomposites is found less as compared with the base material(AA2219), and AA2219/SiC/50 nm MMNC containing highest reinforcement(2wt.%) exhibits the lowest percentage of elongation. It can be seen from the Figure 4.5 ductility of the MMNC decreases gradually with the increase of reinforced nano SiC particulates. The ductility has been found decreased by an amount of 23.02% as the reinforced nano SiC content is increased from 0 to 2 wt%.

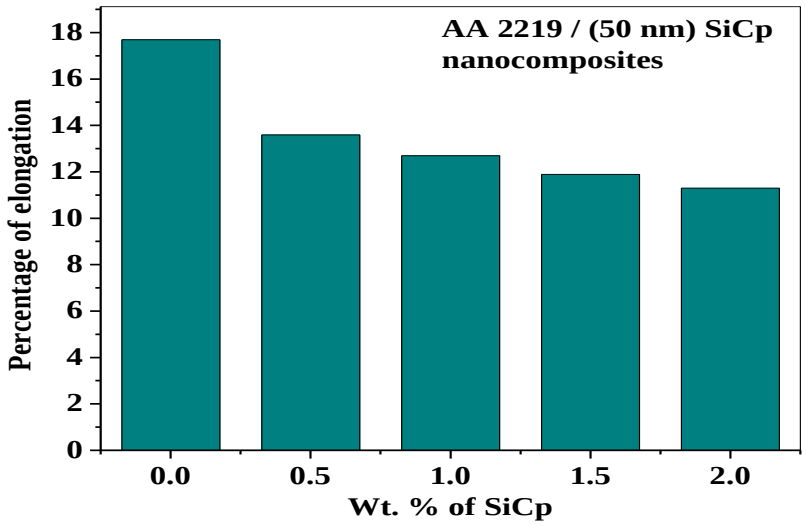

Figure 4.5 Variation in the Ductility of AA 2219 and its nano SiC reinforced Composites

4.2 AA 2219/ Al_2O_3 /50 nm Composites

The density, UTS, hardness and SEM analysis is done for AA2219/Al_2O_3/50 nm composite prepared by Ultrasonic assisted stir casting method and this results are presented in Table 4.2

Table 4.2 Mechanical Properties of AA2219/Al_2O_3/50 nm

S.No	Material	Density value(g/cm^3)		UTS	Hardness	% of Elongation
		Theoretical	Experimental			
1.	AA2219	2.84	2.84	169.79	149.38	17.7
2.	AA2219/0.5 wt.% Al_2O_3	2.8438	2.8429	219.28	153.72	15.5
3.	AA2219/1wt.% Al_2O_3	2.8476	2.8463	229.89	157.22	14.6
4.	AA2219/1.5wt. % Al_2O_3	2.8513	2.8501	236.96	158.50	14.2
5.	AA2219/2wt.% Al_2O_3	2.8551	2.8539	251.11	159.32	14.1

4.2.1 Density of AA 2219/ Al_2O_3/50 nm Composites

Figure 4.6 shows the theoretical and the experimental density values of the AA 2219/ Al_2O_3 /50 nm based MMNCs containing 0 to 2wt% of nano Al_2O_3 reinforcement contents. It is found that the density of the MMNC is greater than that of the base metal matrix material (AA2219). The density of the MMNC (AA 2219/ Al_2O_3 /50 nm) also increases by increase in wt. % particulate reinforcement. An average of 0.2 to 0.25% improvements in the density is observed above base alloy. Additionally, the experimental densities and the theoretical densities are in line with each other confirming the appropriateness of the ultrasonic assisted stir casting for the successful fabrication of AA 2219/ Al_2O_3/50 nm based MMNCs at different weight percentages. An average of 0.042% of deviation of densities observed between theoretical and practical values.

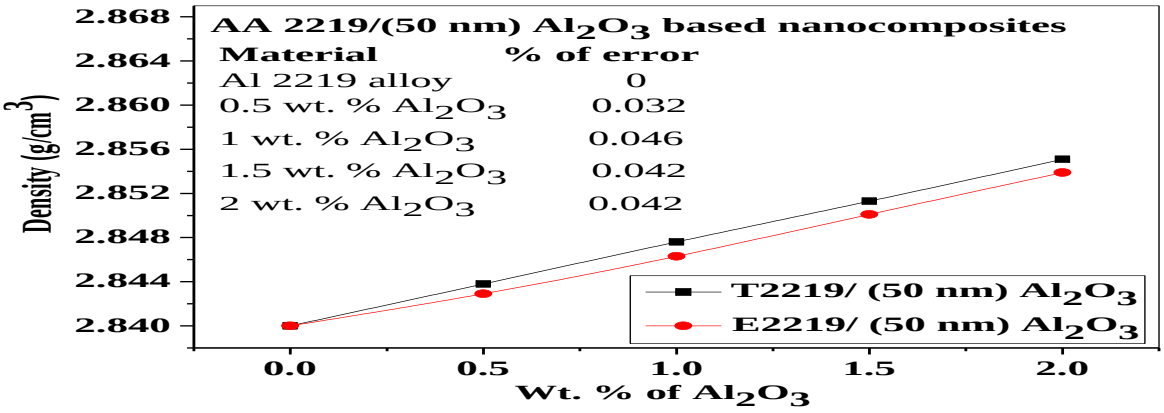

Figure 4.6 Theoretical densities and Experimental Densities for varying wt% of nano Al_2O_3 in AA 2219 alloy.

4.2.2 Microstructure Studies of AA 2219/ Al_2O_3 /50 nm Composites

The scanning electron microscopy images of the MMNC (AA 2219/ Al_2O_3 /50 nm) at different levels of reinforcement are given in 4.7 (a, b,c&d). Microstructural SEM images presented in Figures 4.7 (a, b, c & d) show a considerable amount of uniform distribution of nano SiC particulates throughout the metal matrix composite (AA 2219).

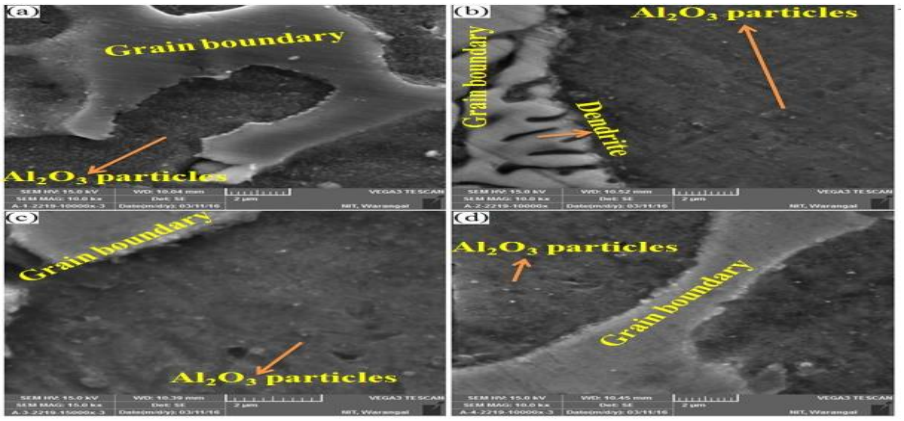

Figures 4.7(a, b, c & d) SEM images of AA 2219/ Al_2O_3 /50 nm alloy and its nano SiC Composites.

4.2.3 Hardness of MMNC AA 2219/ Al_2O_3 (50 nm)

The variation of Vicker's Microhardness of MMNCs with increased wt% of nano Al_2O_3 reinforcement content is given in Table 4.2 and also shown in Figure 4.8.

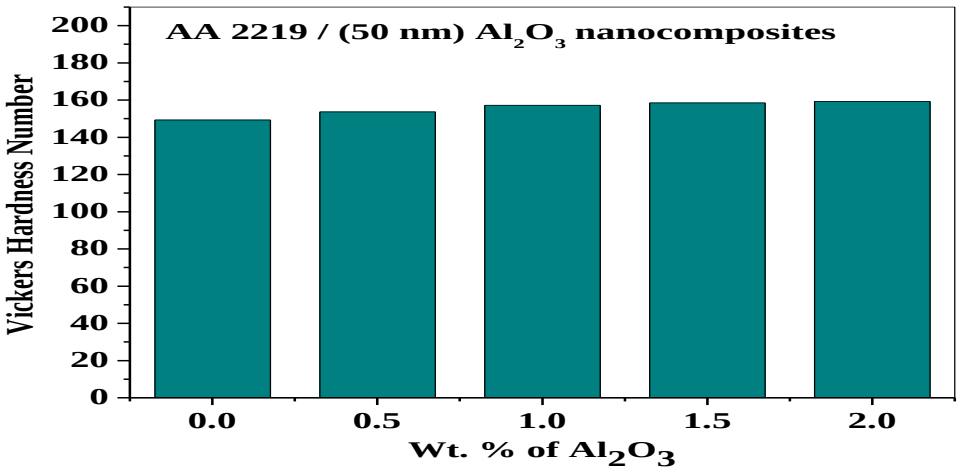

Figure 4.8. Variation in Vickers's Micro Hardness of AA 2219 and its nano Al_2O_3 (50 nm) reinforced MMNCs

From the Figure 4.8, it can be observed that the hardness value of the MMNCs (AA 2219/ Al_2O_3 /50 nm) is more than that of its base metal matrix composite (AA 2219). Moreover, it is also found that as the wt% nano Al_2O_3 amount increases the hardness of the composite also increases by significant amounts. The MMNCs containing 2wt% reinforcement content exhibits greater hardness value. The hardness value of the MMNCs (AA 2219/Al_2O_3/50 nm) material increases by the quantity of 6.24% as the reinforcement content of nano Al_2O_3 rises from 0 to 2wt%.

4.2.4 Ultimate Tensile Strength (UTS) of AA 2219/ Al_2O_3 /50 nm Composites

the variation of the ultimate tensile strength of MMNCs (AA 2219/ Al_2O_3 /50 nm) has given in Table 4.2 and also shown in Figure 4.9. It increases with the increase of weight percentage of nano Al_2O_3 reinforced particulates. Theoretically when hardness increases the UTS of the material also increases [Tom Chandler]. A relation existing between hardness (H) and UTS is H= (UTS)/k; where "k" depends on material condition and type.

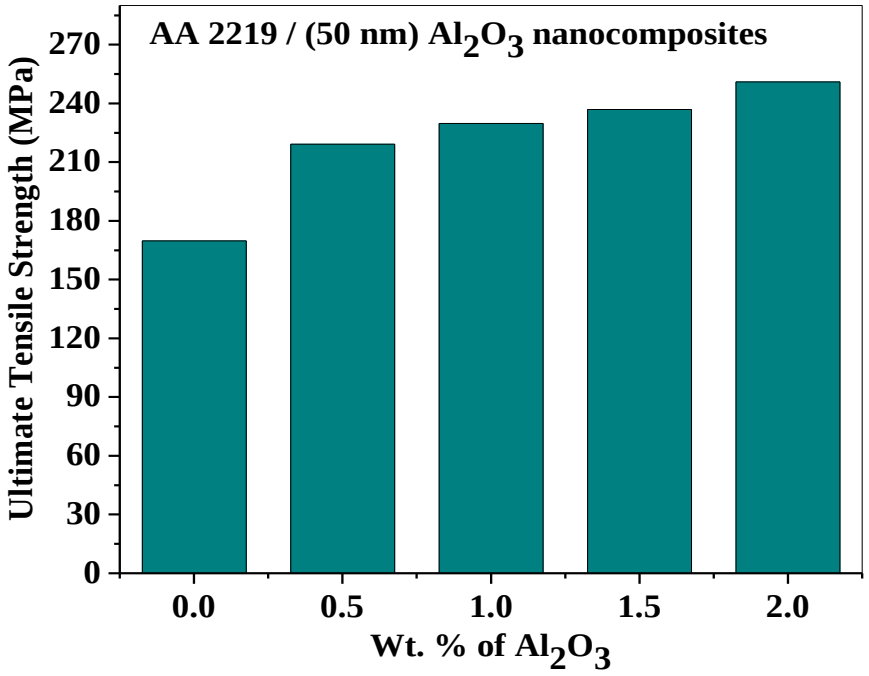

Figure 4.9 Variation in UTS of AA 2219 and its nano Al_2O_3 reinforced Composites

The UTS of the MMNCs (AA 2219/ Al_2O_3 /50 nm) increased as the weight percentage of the nano ceramic Al_2O_3 particulate phase raised from 0 to 2wt% because of uniform distribution

of the reinforced nano alumina particles as explained in the above section called microstructural studies. The UTS of the metal matrix nanocomposite increases by the quantity of 22.57% as the reinforcement content of nano Al_2O_3 particulates rises from 0 to 2 wt%.

4.2.5 Ductility or Percentage Elongation of AA 2219/ Al_2O_3 /50 nm Composites

The consequence of nano SiC reinforced content on the ductility of MMNCs (AA 2219/ Al_2O_3 /50 nm) was calculated with respect to the percentage of elongation and the result is presented in Table 4.2 and also shown in Figure 4.10. The percentage of elongation of the metal matrix nanocomposites is established to be lesser value as compared with the base metal matrix material (AA2219), and MMNCs containing highest reinforced content exhibits the lowest percentage of elongation than the other MMNCs of AA 2219/ Al_2O_3/50 nm premeditated. It can be seen from the Figure 4.10 ductility of the MMNCs decreases gradually with the increase of reinforced nano Al_2O_3 particulates. The ductility of MMNCs being decreased by an amount of 12.26% as the reinforced nano Al_2O_3 content is raised from 0 to 2 wt%

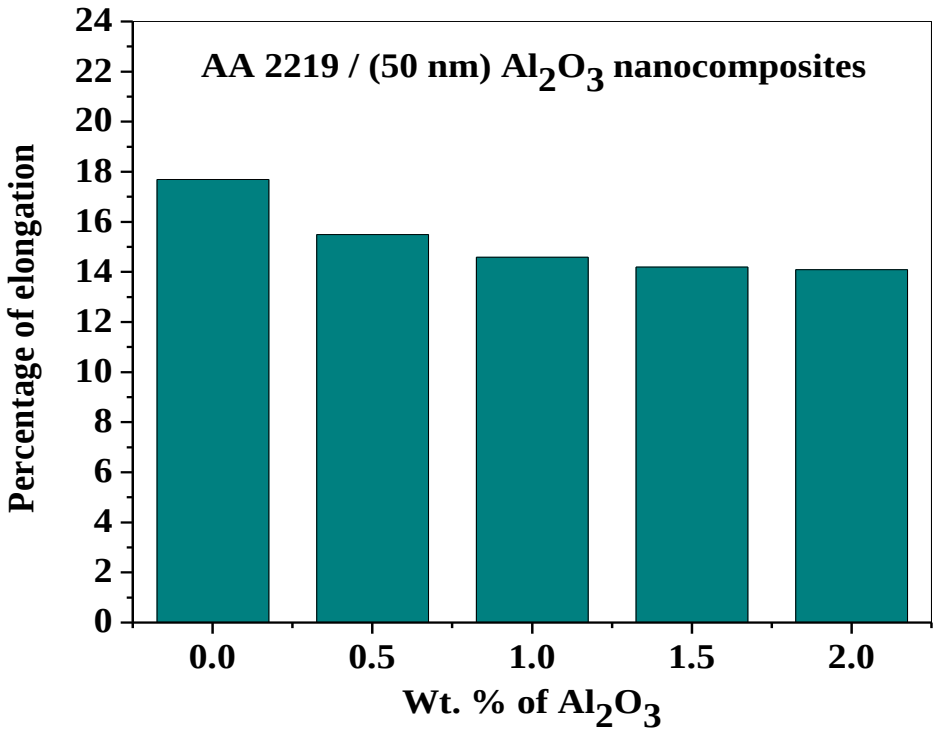

Figure 4.10 Variation in the Ductility of AA 2219 and its Nano Al_2O_3 reinforced Composites

4.3 Results and Discussions for AA 2219/ SiC /150 nm Composites

The density, UTS, hardness and SEM analysis is done for AA2219/SiC/150 nm composite prepared by Ultrasonic assisted stir casting method and this results are presented in Table 4.3

Table 4.3 Mechanical Properties of AA2219/SiC/150 nm

S.No	Material	Density value(g/cm^3)		UTS	Hardness	% of Elongation
		Theoretical	Experimental			
1.	AA2219	2.84	2.84	169.79	149.38	17.7
2.	AA2219/0.5wt. % SiC	2.8416	2.8404	212.24	154.96	13.5
3.	AA2219/1 wt.% SiC	2.8433	2.8422	222.85	159.04	12.6
4.	AA2219/1.5wt. % SiC	2.8448	2.8437	229.92	159.10	11.6
5.	AA2219/2 wt.% SiC	2.8465	2.8452	254.69	161.82	10.9

4.3.1 Density of AA 2219/ SiC /150 nm Composites

Figure 4.11 shows the theoretical and the experimental density values of the AA 2219/ SiC /150 nm based MMNCs containing 0 to 2wt% of nano SiC reinforcement contents. It is found that the density of the MMNCs is greater than that of the base metal matrix material (AA 2219).

The density of the MMNC (AA 2219/ SiC /150 nm) also increases by increase in wt. % particulate reinforcement. An average of 0.2 to 0.25% improvements in the density is observed above base alloy. Additionally, the experimental densities and the theoretical densities are in line with each other confirming the appropriateness of the ultrasonic assisted stir casting for the successful fabrication of AA 2219/ SiC /150 nm based MMNCs at different weight percentages. An average of 0.042% of deviation of densities observed between theoretical and practical values.

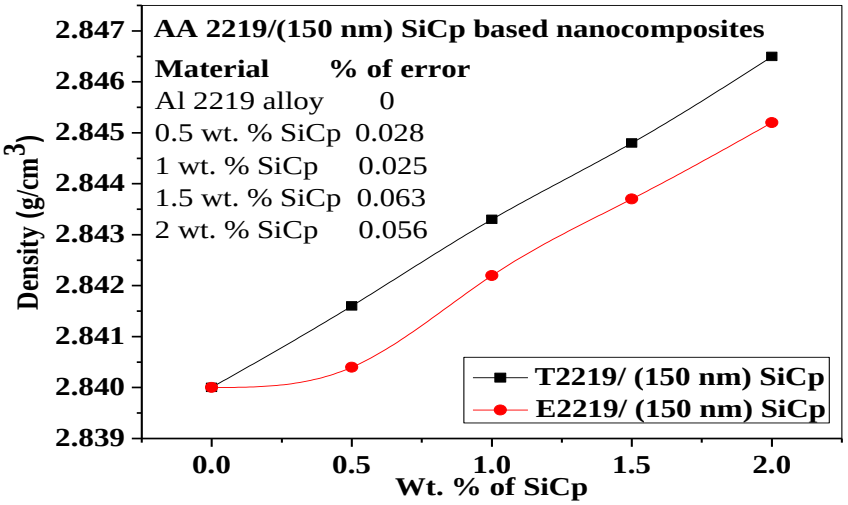

Figure 4.11. Theoretical densities and Experimental Densities for varying wt% of nano SiC in AA2219 alloy

4.3.2 Microstructure Studies of AA 2219/ SiC /150 nm Composites

The scanning electron microscopy images of the MMNCs (AA 2219/ SiC /150 nm) at different levels of reinforcement are given in 4.12 (a, b,c&d). Microstructural SEM images presented in Figures 4.12. (a, b, c & d) show a considerable amount of uniform distribution of nano SiC particulates throughout the metal matrix composite (AA 2219).

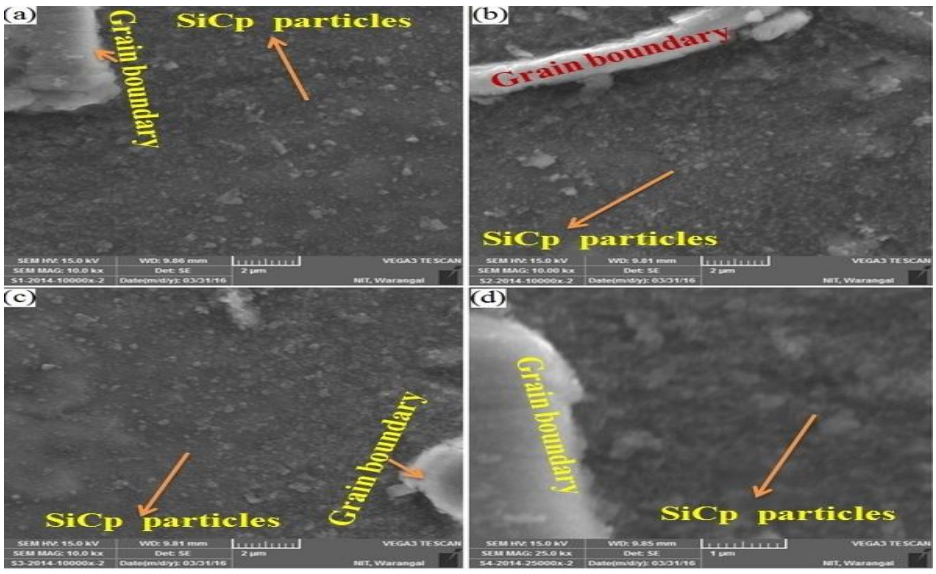

Figure 4.12(a, b, c &d) SEM images of AA 2219/ SiC /150 nm alloy and its nano SiC Composites

4.3.3 Hardness of AA 2219/ SiC /150 nm

The variation of Vicker's Microhardness of MMNC with increased wt.% of nano SiC reinforcement content is given in Table 4.3 and also shown in Figure 4.13.

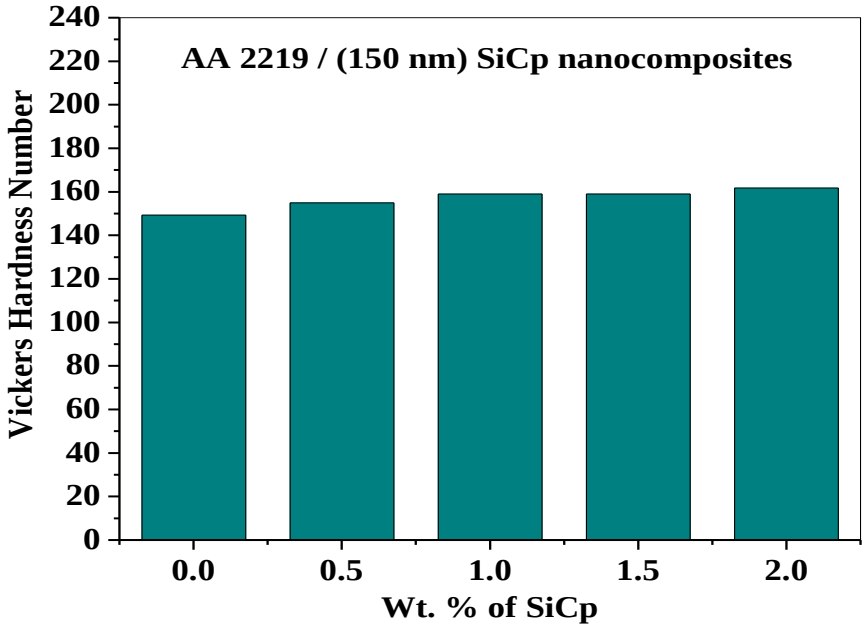

Figure 4.13. Variation in Vicker's Micro Hardness of AA 2219 and its nano SiC (150 nm) reinforced MMNCs

From the Figure 4.13; it can be observed that the hardness value of the MMNCs (AA 2219/ SiC /150 nm) is more than that of its base metal matrix composite (AA 2219). Moreover,it is also found that as the wt.% nano SiC amount increases the hardness of the composite also increases by significant amounts. The MMNCs containing 2wt% reinforcement content exhibits greater hardness value. The hardness value of the MMNCs (AA 2219/ SiC /150 nm**),** material increases in the quantity of 7.68% as the reinforcement content of nano SiC, raises from 0 to 2wt%.

4.3.4 Ultimate Tensile Strength (UTS) of AA 2219/ SiC /150 nm Composites

The ultimate tensile strength of nanocomposites is given in Table 4.3 and also shown in Figure 4.14, the variation of the ultimate tensile strength of MMNC (AA 2219/ SiC /150 nm) increases with the increase of weight percentage of nano SiC reinforced particulates. Theoretically when hardness increases the UTS of the material also increases [Tom Chandler]. A relation existing between hardness(H) and UTS is H=(UTS)/k ; where "k" depends on material

condition and type. The UTS of the MMNC (AA 2219/ SiC /150 nm) increased as the weight percentage of the nano ceramic SiC particulate phase raised from 0 to 2wt% because of uniform distribution of the reinforced nano silicon carbide particles as explained in the above section called microstructural studies. The UTS of the metal matrix nanocomposite increases by the quantity of 20% as the reinforcement content of nano SiC particulates raise from 0 to 2 wt%.

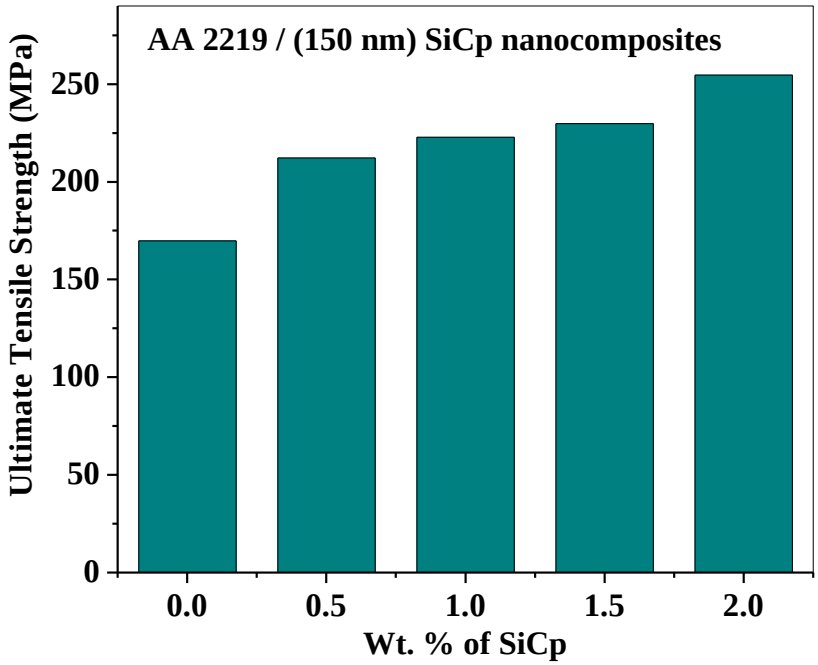

Figure 4.14 Variation in UTS of AA 2219 and its nano SiC reinforced Composites

4.3.5 Ductility or Percentage Elongation of AA 2219/ SiC /150 nm Composites

The consequence of nano SiC reinforced content on the ductility of MMNC (AA 2219/ SiC /150 nm) was calculated with respect to the percentage of elongation and the result is presented in Table 4.3 and also shown in Figure 4.15. The percentage of elongation of the metal matrix nanocomposites is established to be lesser value as compared with the base metal matrix material(AA2219), and MMNCs containing highest reinforced content exhibits the lowest percentage of elongation than the other MMNCs of AA 2219/ SiC /150 nm premeditated.

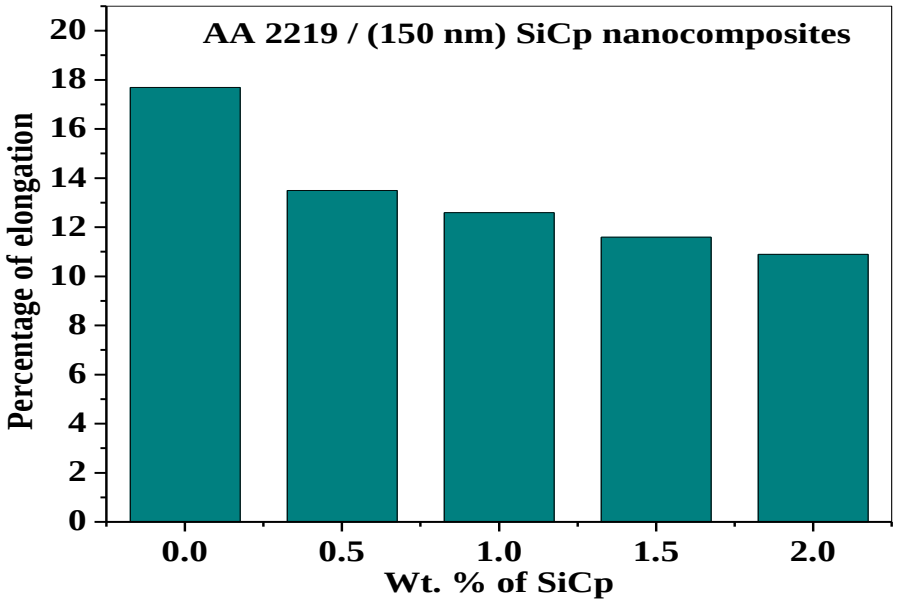

Figure 4.15 Variation in the Ductility of AA2219 and its Nano SiC reinforced Composites.

It can be seen from the Figure 4.10 ductility of the MMNC decreases gradually with the increase of reinforced nano SiC particulates. The ductility of MMNC being decreased by an amount of 23.58% as the reinforced nano SiC content is raised from 0 to 2 wt%.

4.4 AA 2219/ Al_2O_3 /150 nm Composites

The density, UTS, hardness and SEM analysis is done for AA2219/Al_2O_3/150 nm composite prepared by Ultrasonic assisted stir casting method and this results are presented in Table 4.4

Table 4.4 Mechanical Properties of AA2219Al_2O_3/150 nm

S.No	Material	Density value(g/cm^3)		UTS	Hardness	% of Elongation
		Theoretical	Experimental			
1.	AA2219	2.84	2.84	169.79	149.38	17.7
2.	AA2219/0.5wt. % Al_2O_3	2.844	2.8432	205.16	152.26	14.8
3.	AA2219/1 wt.% Al_2O_3	2.848	2.8473	215.77	155.62	14.1
4.	AA2219/1.5wt. % Al_2O_3	2.852	2.8502	226.39	155.50	13.8
5.	AA2219/2 wt.% Al_2O_3	2.8559	2.8543	233.46	157.70	13.4

4.4.1 Density of AA 2219/ Al_2O_3/150 nm Composites

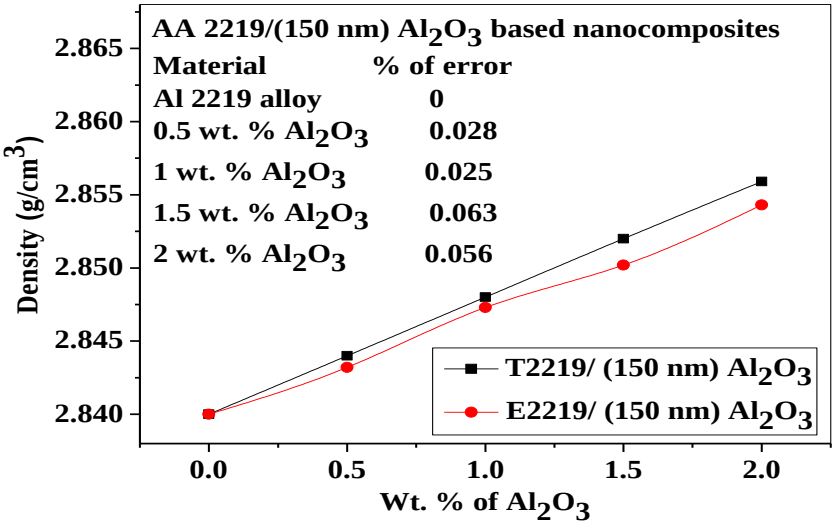

Figure 4.16. Theoretical densities and Experimental Densities for varying wt% of nano Al_2O_3 in AA2219 alloy

Figure 4.16 shows the theoretical and the experimental density values of the AA 2219/ Al_2O_3 /150 nm based MMNCs containing 0 to 2wt% of nano Al_2O_3 reinforcement contents. It is found that the density of the MMNCs is greater than that of the base metal matrix material (AA 2219). The density of the MMNC (AA 2219/Al_2O_3/150 nm) also increases by increase in wt. % particulate reinforcement. An average of 0.2 to 0.25% improvements in the density is observed above base alloy. Additionally, the experimental densities and the theoretical densities are in line with each other confirming the appropriateness of the ultrasonic assisted stir casting for the successful fabrication of AA 2219/ Al_2O_3/150 nm based MMNCs at different weight percentages. An average of 0.042% of deviation of densities observed between theoretical and practical values.

4.4.2 Microstructure Studies of AA 2219/ Al_2O_3 /150 nm Composites

The scanning electron microscopy images of the MMNC (AA 2219/ Al_2O_3 /150 nm) studied at different levels of reinforcement are given in 4.17 (a, b,c&d). Microstructural SEM images presented in Figures 4.17(a, b, c & d) show a considerable amount of uniform distribution of nano SiC particulates throughout the metal matrix composite (AA 2219).

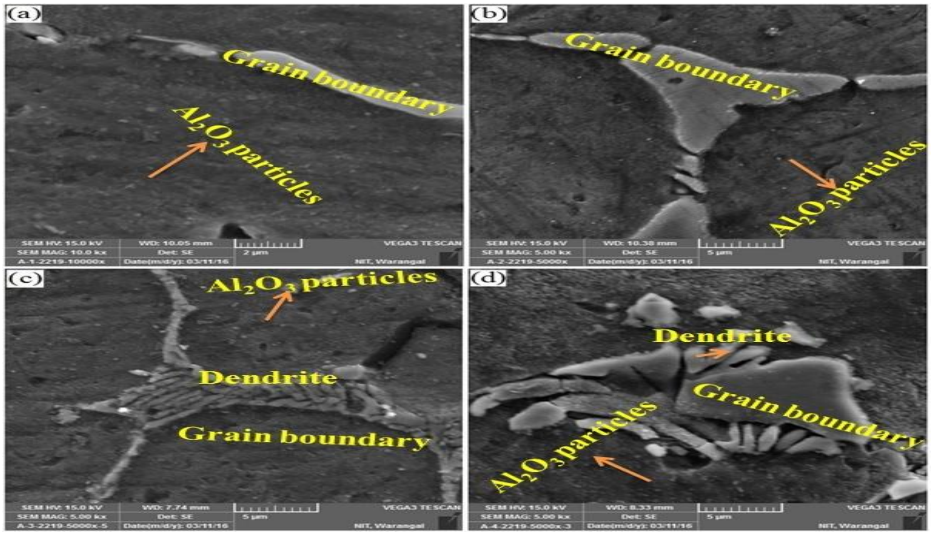

Figure 4.17(a, b, c & d) SEM images of AA 2219/ Al_2O_3 /150 nm alloy and its nano Al_2O_3 Composites

4.4.3 Hardness of AA 2219/ Al_2O_3 /150 nm

The variation of Vicker's Microhardness of MMNCs with increased wt.% of nano Al_2O_3 reinforcement content is given in Table 4.4 and also shown in Figure 4.18.

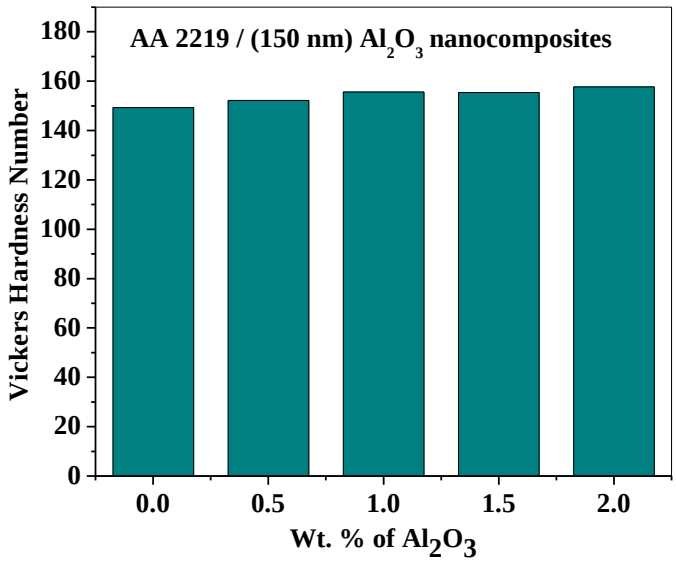

Figure 4.18 Variation in Vickers's Micro Hardness of AA 2219 and its nano Al_2O_3 (150 nm) reinforced MMNCs

From the Figure 4.18; it can be observed that the hardness value of the MMNCs (AA 2219/ Al_2O_3 /150 nm) is more than that of its base metal matrix composite (AA 2219). Moreover, it

is also found that as the wt.% nano Al_2O_3 amount increases the hardness of the composite also increases by significant amounts. The MMNCs containing 2wt% reinforcement content exhibits greater hardness value. The hardness value of the MMNCs (AA 2219/Al_2O_3/150 nm) material increases by the quantity of 5.28% as the reinforcement content of nano Al_2O_3 rises from 0 to 2wt%.

4.4.4 Ultimate Tensile Strength (UTS) of AA 2219/ Al_2O_3 /150 nm Composites

The ultimate tensile strength of nanocomposites is given in Table 4.4 and also shown in Figure 4.19, demonstrates the variation of the ultimate tensile strength of MMNCs (AA 2219/ Al_2O_3 /50 nm) increases with the increase of weight percentage of nano Al_2O_3 reinforced particulates. Theoretically when hardness increases the UTS of the material also increases [Tom Chandler]. A relation existing between hardness(H) and UTS is H=(UTS)/k ; where "k" depends on material condition and type. The UTS of the MMNCs (AA 2219/ Al_2O_3 /50 nm) increased as the weight percentage of the nano ceramic Al_2O_3 particulate phase raised from 0 to 2wt% because of uniform distribution of the reinforced nano alumina particles as explained in the above section called microstructural studies. The UTS of the metal matrix nanocomposite increases by the quantity of 17.24% as the reinforcement content of nano Al_2O_3 particulates rises from 0 to 2 wt%.

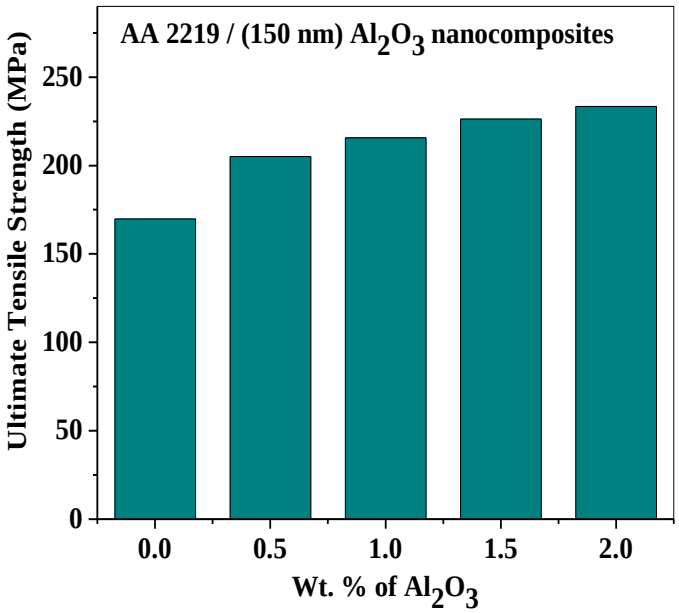

Figure 4.19 Variation in UTS of AA 2219 and its Nano Al_2O_3 reinforced Composites

4.4.5 Ductility or Percentage Elongation of AA 2219/ Al_2O_3 /150 nm Composites

The consequence of nano Al_2O_3 reinforced content on the ductility of MMNC (AA 2219/ Al_2O_3 /150 nm) was calculated with respect to the percentage of elongation and the result is presented in Table 4.6 and also shown in Figure 4.20. The percentage of elongation of the metal matrix nanocomposites is established to be lesser value as compared with the base metal matrix material (AA 2219), and MMNCs containing highest reinforced content exhibits the lowest percentage of elongation than the other MMNCs of AA 2219/ Al_2O_3/150 nm premeditated. It can be seen from the Figure 4.20 ductility of the MMNCs decreases gradually with the increase of reinforced nano Al_2O_3 particulates. The ductility of MMNCs being decreased by an amount of 16.04% as the reinforced nano Al_2O_3 content is raised from 0 to 2 wt%.

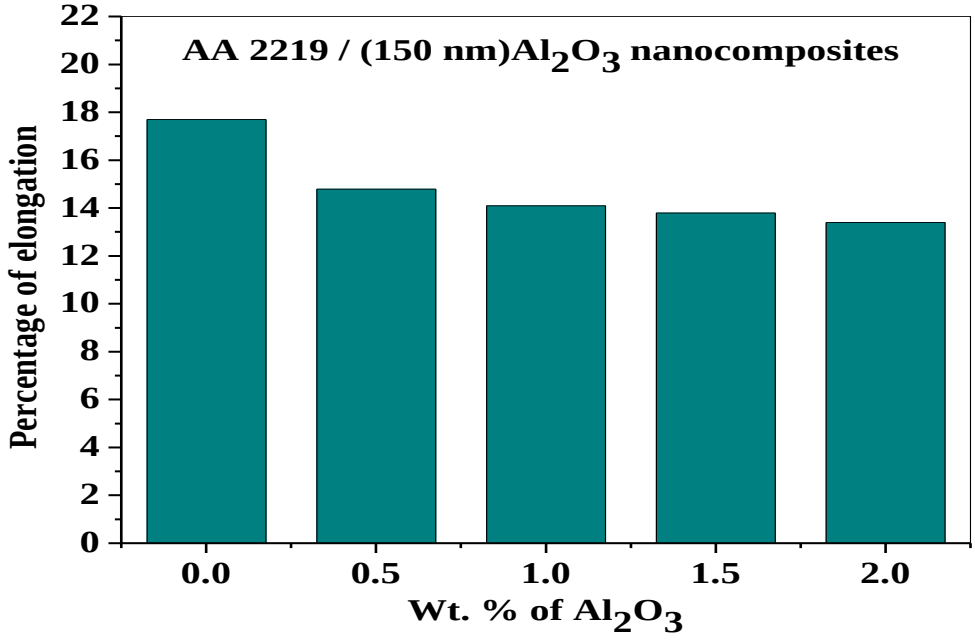

Figure 4.20 Variation in the Ductility of AA 2219 and its Nano Al_2O_3 reinforced Composites

4.5 AA 2014/ SiC /50 nm Composites

The density, UTS, hardness and SEM analysis is done for AA2014/SiC/50 nm composite prepared by Ultrasonic assisted stir casting method and this results are presented in Table 4.5

Table 4.5 Mechanical Properties of AA2014/SiC/50 nm

S.No	Material	Density value(g/cm^3)		UTS	Hardness	% of Elongation
		Theoretical	Experimental			
1.	AA2014	2.80	2.80	176.16	154.32	12.90
2.	AA2014/0.5wt.% SiC	2.8018	2.8004	198.09	159.32	11.73
3.	AA2014/1 wt.% SiC	2.8036	2.8022	208.70	164.24	11.30
4.	AA2014/1.5wt.% SiC	2.8053	2.8044	226.39	166.3	10.90
5.	AA2014/2 wt.% SiC	2.8071	2.8065	244.07	165.54	10.46

4.5.1 Density of AA 2014/ SiC /50 nm Composites

Figure 4.21 shows the theoretical and the experimental density values of the AA 2014/ SiC /50 nm based MMNCs containing 0 to 2wt% of nano SiC reinforcement contents. It is found that the density of the MMNCs is greater than that of the base metal matrix material (AA 2014). The density of the MMNC (AA 2014/ SiC /50 nm) also increases by increase in wt. % particulate reinforcement. An average of 0.2 to 0.25% improvement in the density is observed above base alloy. Additionally, the experimental densities and the theoretical densities are in line with each other confirming the appropriateness of the ultrasonic assisted stir casting for the successful fabrication of AA 2014/ SiC /50 nm based MMNCs at different weight percentages. An average of 0.042% of deviation of densities observed between theoretical and practical values.

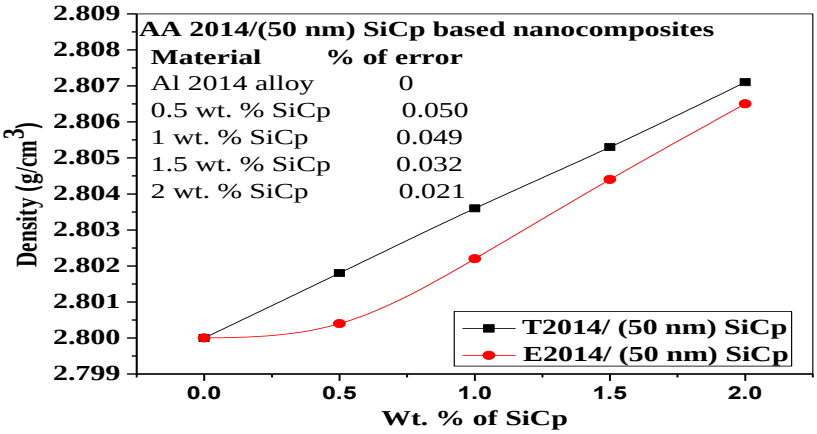

Figure 4.21 Theoretical densities and Experimental Densities for varying wt% of nano SiC in AA 2014 alloy

4.5.2 Microstructure Studies of AA 2014/ SiC /50 nm Composites

The scanning electron microscopy images of the MMNCs (AA 2014/ SiC /50 nm) studied at different levels of reinforcement are given in 4.22 (a, b,c&d). Microstructural SEM images presented in Figures 4.22 (a, b, c & d) show a considerable amount of uniform distribution of nano SiC particulates throughout the metal matrix composite (AA 2014).

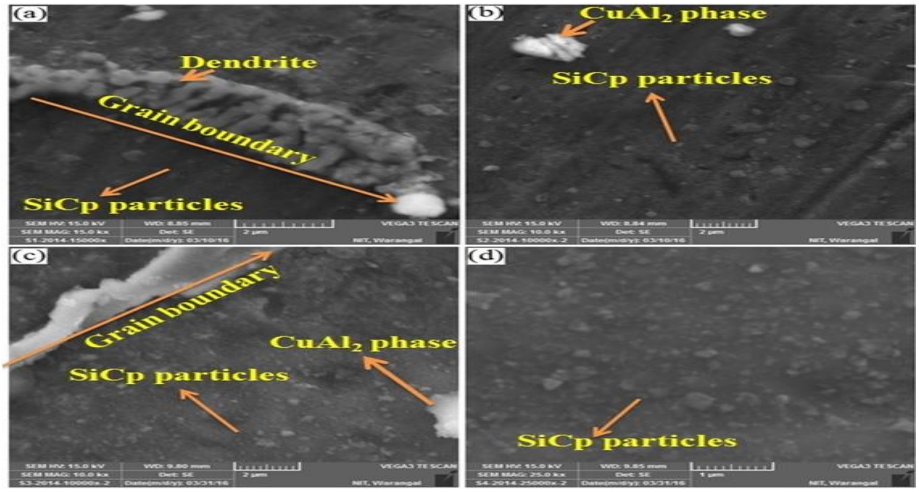

Figures 4.22 (a, b, c & d) SEM images of AA 2014/ SiC /50 nm alloy and its nano SiC Composites

4.5.3 Hardness of AA 2014/ SiC /50 nm

The variation of Vicker's Microhardness of MMNCs with increased wt.% of nano SiC reinforcement content is given in Table 4.5 and also shown in Figure 4.23.

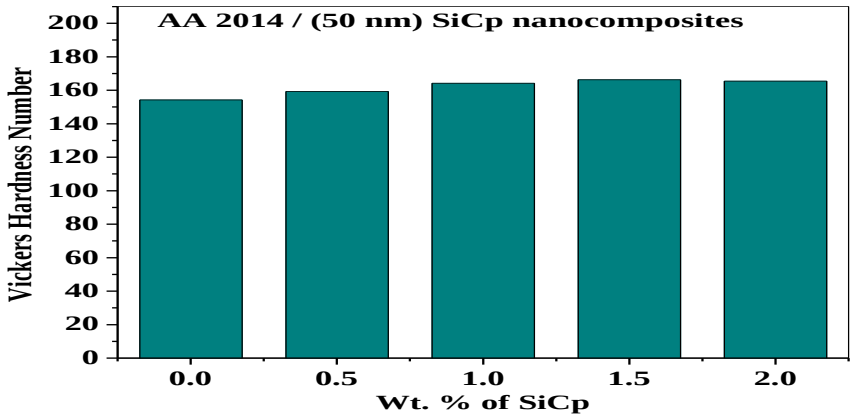

Figure 4.23 Variation in Vicker's Micro Hardness of AA 2014 and its nano SiC (50 nm) reinforced MMNCs

From the Figure 4.23; it can be observed that the hardness value of the MMNCs (AA 2014/ SiC /50 nm) is more than that of its base metal matrix composite (AA 2014). Moreover, it is also found that as the wt.% nano SiC amount increases the hardness of the composite also increases by significant amounts. The MMNCs containing 2wt% reinforcement content exhibits greater hardness value. The hardness value of the MMNCs AA 2014/ SiC /50 nm material increases by the quantity of 6.78% as the reinforcement content of nano SiC raises from 0 to 2wt%.

4.5.4 Ultimate Tensile Strength (UTS) of AA 2014/ SiC /50 nm Composites

The variation of the ultimate tensile strength of MMNCs AA 2014/ SiC /50 nm has given in Table 4.5 and also shown in Figure 4.24 increases with the increase of weight percentage of nano SiC reinforced particulates. The UTS of the MMNCs AA 2014/ SiC /50 nm increased as the weight percentage of the nano ceramic SiC particulate phase raised from 0 to 2wt% because of uniform distribution of the reinforced nano silicon carbide particles as explained in the above section called microstructural studies. The UTS of the metal matrix nanocomposite increases by the quantity of 27.08% as the reinforcement content of nano SiC particulates raise from 0 to 2 wt%.

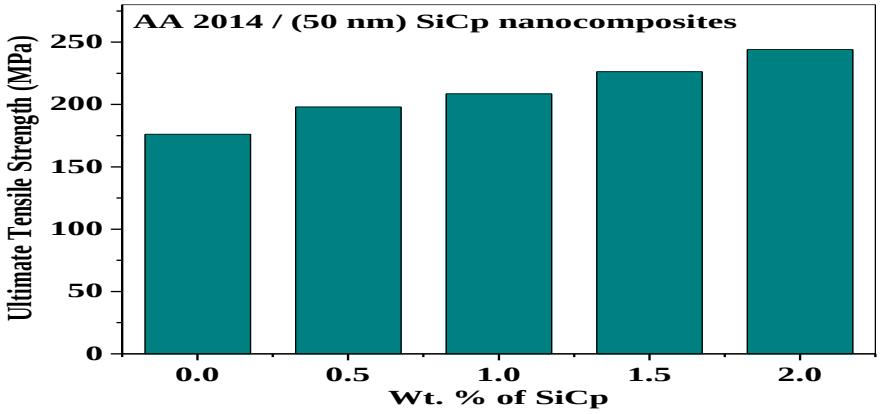

Figure 4.24 Variation in UTS of AA 2014 and its Nano SiC reinforced Composites

4.5.5 Ductility or Percentage Elongation of AA 2014/ SiC /50 nm Composites

Figure 4.25 explains the consequence of nano SiC reinforced content on the ductility of MMNCs (AA 2014/ SiC /50 nm) was calculated regarding the percentage of elongation of MMNCs. The percentage of elongation of the metal matrix nanocomposites is established to

be lesser value as compared with the base metal matrix material (AA 2014), and MMNCs containing highest reinforced content exhibits the lowest percentage of elongation than the other MMNCs of AA 2014/ SiC /50 nm premeditated. It can be seen from the Figure 4.25 ductility of the MMNC decreases gradually with the increase of reinforced nano SiC particulates. The ductility of MMNC being decreased by an amount of 23.57% as the reinforced nano SiC content is raised from 0 to 2 wt%.

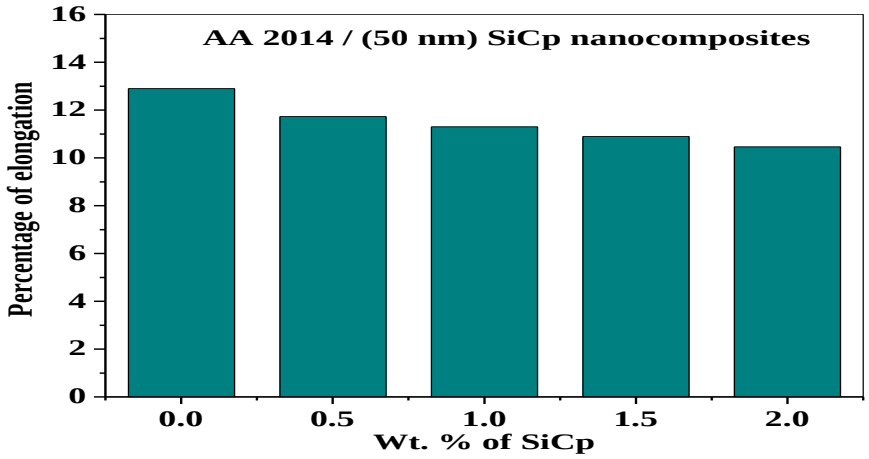

Figure 4.25 Variation in the Ductility of AA 2014 and its Nano SiC reinforced Composites

4.6 AA 2014/ Al_2O_3 /50 nm Composites

The density, UTS, hardness and SEM analysis is done for AA2014/Al_2O_3/50 nm composite prepared by Ultrasonic assisted stir casting method and this results are presented in Table 4.6.

Table 4.6 Mechanical Properties of AA2014/ Al_2O_3/50 nm

S.No	Material	Density value(g/cm^3)		UTS	Hardness	% of Elongation
		Theoretical	Experimental			
1.	AA2014	2.80	2.80	176.16	154.32	12.90
2.	AA2014/0.5wt. % Al_2O_3	2.8039	2.8032	183.94	155.32	12.4
3.	AA2014/1 wt.% Al_2O_3	2.8078	2.8071	198.08	156.62	11.6
4.	AA2014/1.5wt. % Al_2O_3	2.8117	2.8103	208.70	157.94	11.1
5.	AA2014/2 wt.% Al_2O_3	2.8155	2.8144	219.31	160.54	10.8

4.6.1 Density of AA 2014/ Al_2O_3/50 nm Composites

Figure 4.26. shows the theoretical and the experimental density values of the AA 2014/ Al_2O_3 /50 nm based MMNCs containing 0 to 2wt% of nano Al_2O_3 reinforcement contents. It is found that the density of the MMNCs is greater than that of the base metal matrix material (AA 2014). The density of the MMNC (AA 2014/ Al_2O_3 /50 nm) also increases by increase in wt. % particulate reinforcement. An average of 0.2 to 0.25% improvement in the density is observed above base alloy. Additionally, the experimental densities and the theoretical densities are in line with each other confirming the appropriateness of the ultrasonic assisted stir casting for the successful fabrication of AA 2014/ Al_2O_3/50 nm based MMNCs at different weight percentages. An average of 0.042% of deviation of densities observed between theoretical and practical values.

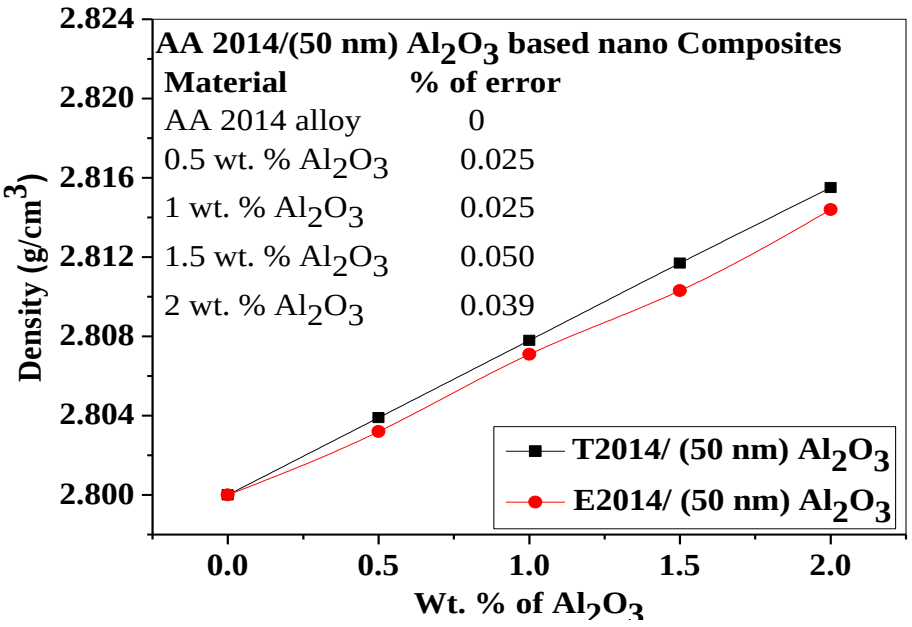

Figure 4.26 Theoretical densities and Experimental Densities for varying wt% of nano Al_2O_3 in AA 2014 alloy

4.6.2 Microstructure Studies of AA 2014/ Al_2O_3 /50 nm Composites

The scanning electron microscopy images of the MMNCs (AA 2014/ Al_2O_3 /50 nm) studied at different levels of reinforcement are given in 4.27 (a, b,c&d).

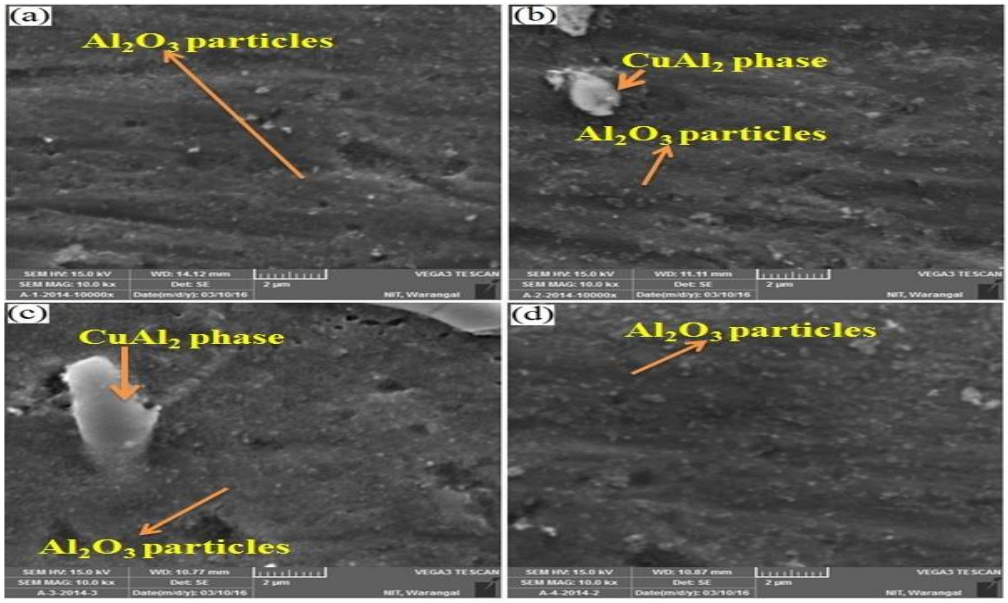

Figures 4.27(a, b, c & d) SEM images of AA 2014/ Al_2O_3 /50 nm alloy and its nano Al_2O_3 Composites.

Microstructural SEM images presented in Figures 4.27 (a, b, c & d) show a considerable amount of uniform distribution of nano SiC particulates throughout the metal matrix composite (AA 2014).

4.6.3 Hardness of AA 2014/ Al_2O_3 /50 nm

The variation of Vicker's Microhardness of MMNCs with increased wt% of nano Al_2O_3 reinforcement content is given in Table 4.6 and also shown in Figure 4.28.

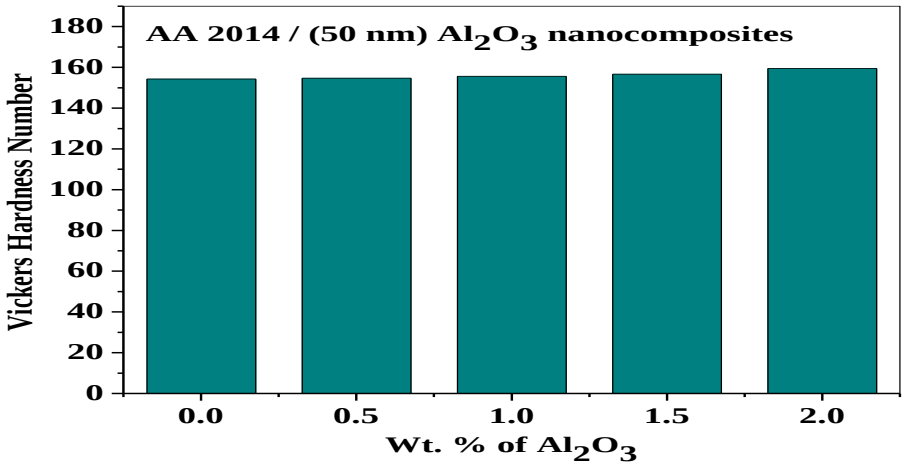

Figure 4.28 Variation in Vickers's Micro Hardness of AA 2014 and its nano Al_2O_3 (50 nm) reinforced MMNCs

From the Figure 4.28, it can be observed that the hardness value of the MMNCs (AA 2014/ Al_2O_3 /150 nm) is more than that of its base metal matrix composite (AA 2014). Moreover, it is also found that as the wt. % of nano Al_2O_3 amount increases the hardness of the composite also increases by significant amounts. The MMNCs containing 2wt% reinforcement content exhibits greater hardness value. The hardness value of the MMNC (AA 2014/Al_2O_3/50 nm) material increases by the quantity of 3.87% as the reinforcement content of nano Al_2O_3 rises from 0 to 2wt%.

4.6.4 Ultimate Tensile Strength (UTS) of AA 2014/ Al_2O_3 /50 nm Composites

The ultimate tensile strength of the nanocomposites is given in Table 4.6 and also shown in Figure 4.29; it shows the variation of the ultimate tensile strength of MMNCs (AA 2014/ Al_2O_3 /50 nm) increases with the increase of weight percentage of nano Al_2O_3 reinforced particulates. Theoretically when hardness increases the UTS of the material also increases [Tom Chandler]. A relation existing between hardness(H) and UTS is H=(UTS)/k ; where "k" depends on material condition and type.

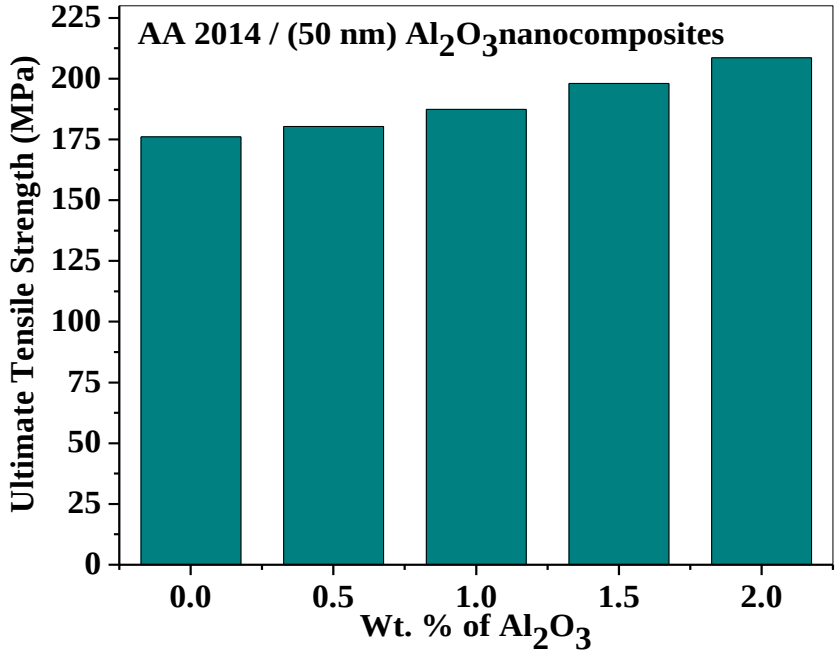

Figure 4.29 Variation in UTS of AA 2014 and its nano Al_2O_3 reinforced Composites

The UTS of the MMNCs (AA 2014/ Al_2O_3 /50 nm) increased as the weight percentage of the nano ceramic Al_2O_3 particulate phase raised from 0 to 2wt% because of uniform distribution

of the reinforced nano alumina particles as explained in the above section called microstructural studies. The UTS of the metal matrix nanocomposite increases by the quantity of 19.68% as the reinforcement content of nano Al_2O_3 particulates rises from 0 to 2 wt%.

4.6.5 Ductility or Percentage Elongation of AA 2014/ Al_2O_3 /50 nm Composites

The consequence of nano Al_2O_3 reinforced content on the ductility of MMNCs (AA 2014/ Al_2O_3 /50 nm) was calculated with respect to the percentage of elongation and the result is presented in the Table 4.6 and also shown in Figure 4.30. The percentage of elongation of the metal matrix nanocomposites is established to be lesser value as compared with the base metal matrix material (AA 2014), and MMNCs containing highest reinforced content exhibits the lowest percentage of elongation than the other MMNCs of AA 2014/ Al_2O_3/50 nm premeditated. It can be seen from the Figure 4.30 ductility of the MMNCs decreases gradually with the increase of reinforced nano Al_2O_3 particulates. The ductility of MMNCs being decreased by an amount of 19.75% as the reinforced nano Al_2O_3 content is raised from 0 to 2 wt%.

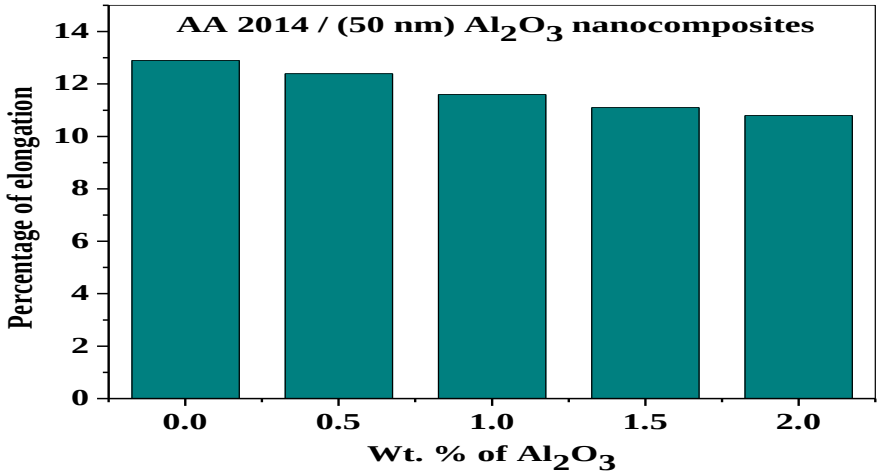

Figure 4.30 Variation in the Ductility of AA 2014 and its Nano Al_2O_3 reinforced Composites

4.7 AA 2014/ SiC /150 nm Composites

The density, UTS, hardness and SEM analysis is done for AA2014/SiC/150 nm composite prepared by Ultrasonic assisted stir casting method and this results are presented in Table 4.7

Table 4.7 Mechanical Properties of AA2014/ SiC/150 nm

S.No	Material	Density value(g/cm^3)		UTS	Hardness	% of Elongation
		Theoretical	Experimental			
1.	AA2014	2.80	2.80	176.16	154.32	12.90
2.	AA2014/0.5wt.% SiC	2.8018	2.8007	191.01	158.24	11.57
3.	AA2014/1 wt.% SiC	2.8036	2.8024	198.09	162.9	11.07
4.	AA2014/1.5wt.% SiC	2.8053	2.8042	208.70	165.22	10.70
5.	AA2014/2 wt.% SiC	2.8071	2.8063	222.85	163.38	10.16

4.7.1 Density of AA 2014/ SiC /150 nm Composites

Figure 4.31 shows the theoretical and the experimental density values of the AA 2014/ SiC /150 nm based MMNCs containing 0 to 2wt% of nano SiC reinforcement contents. It is found that the density of the MMNCs is greater than that of the base metal matrix material (AA 2014). The density of the MMNC (AA 2014/ SiC /50 nm) also increases by increase in wt. % particulate reinforcement. An average of 0.2 to 0.25% improvement in the density is observed above base alloy. Additionally, the experimental densities and the theoretical densities are in line with each other confirming the appropriateness of the ultrasonic assisted stir casting for the successful fabrication of AA 2014/ SiC /150 nm based MMNCs at different weight percentages. An average of 0.042% of deviation of densities observed between theoretical and practical values.

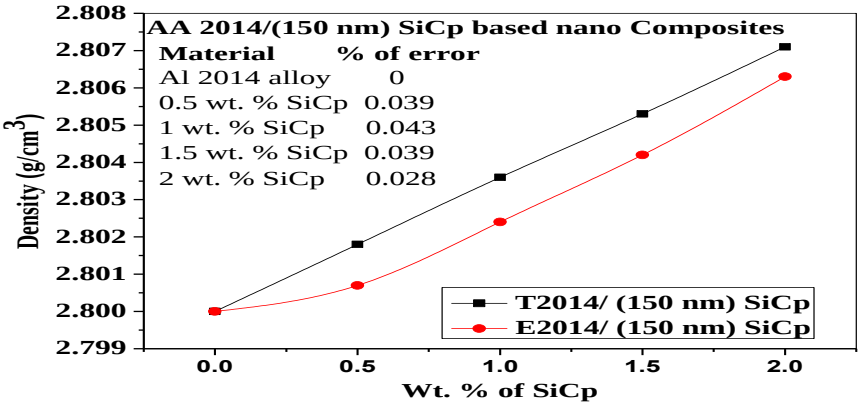

Figure 4.31 Theoretical densities and Experimental Densities for varying wt% of nano SiC in AA 2014 alloy

4.7.2 Microstructure Studies of AA 2014/ SiC /150 nm Composites

The scanning electron microscopy images of the MMNCs (AA 2014/ SiC /150 nm) studied at different levels of reinforcement are given in 4.32 (a, b,c&d). Microstructural SEM images presented in Figures 4.32 (a, b, c & d) show a considerable amount of uniform distribution of nano SiC particulates throughout the metal matrix composite (AA 2014).

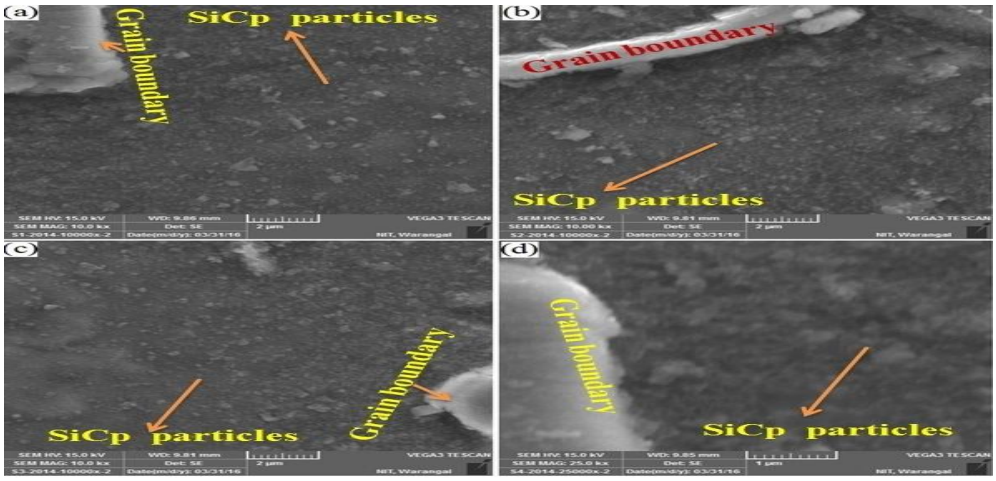

Figures 4.32(a, b, c &d) SEM images of AA 2014/ SiC /150 nm alloy and its nano SiC Composites.

4.7.3 Hardness of MMNC AA 2014/ SiC /150 nm

The variation of Vicker's Microhardness of MMNCs with increased wt.% of nano SiC reinforcement content is given in table and also shown in Figure 4.33.

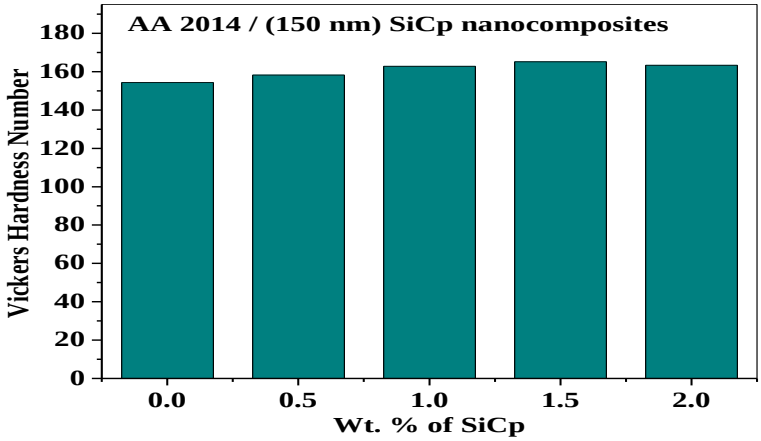

Figure 4.33. Variation in Vicker's Micro Hardness of AA 2014 and its nano SiC (150 nm) reinforced MMNCs

From the Figure 4.33, it can be observed that the hardness value of the MMNCs (AA 2014/ SiC /150 nm) is more than that of its base metal matrix composite (AA 2014). Moreover, it is also found that as the wt.% nano SiC amount increases the hardness of the composite also increases by significant amounts. The MMNC containing 2wt% reinforcement content exhibits greater hardness value. The hardness value of the MMNCs (AA 2014/ SiC /150 nm)**,** material increases in the quantity of 5.24% as the reinforcement content of nano SiC, raises from 0 to 2wt%.

4.7.4 Ultimate Tensile Strength (UTS) of AA 2014/ SiC /150 nm Composites

The ultimate tensile strength of the nanocomposites is given in Table 4.7 and also shown in Figure 4.34, shows the variation of the ultimate tensile strength of MMNCs (AA 2014/ SiC /150 nm) increases with the increase of weight percentage of nano SiC reinforced particulates. Theoretically when hardness increases the UTS of the material also increases [Tom Chandler]. A relation existing between hardness(H) and UTS is H=(UTS)/k ; where "k" depends on material condition and type. The UTS of the MMNC (AA 2014/ SiC /150 nm) increased as the weight percentage of the nano ceramic SiC particulate phase raised from 0 to 2wt% because of uniform distribution of the reinforced nano silicon carbide particles as explained in the above section called microstructural studies. The UTS of the metal matrix nanocomposite increases by the quantity of 46% as the reinforcement content of nano SiC particulates rise from 0 to 2 wt%.

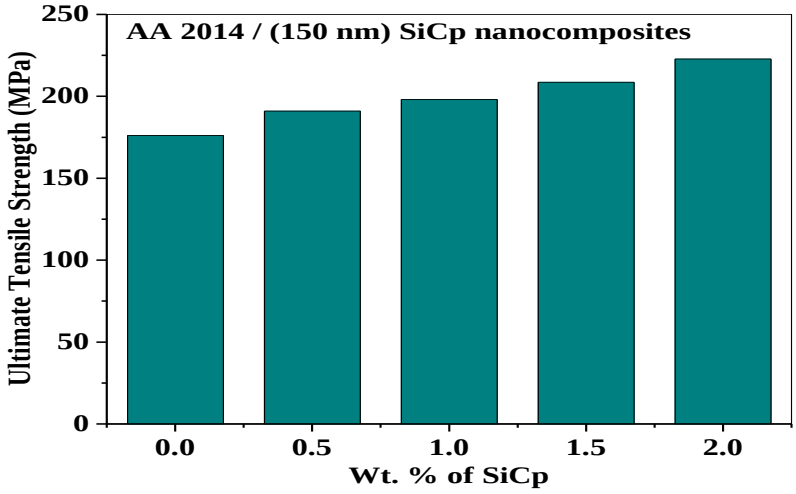

Figure 4.34 Variation in UTS of AA 2014 and its Nano SiC reinforced Composites.

4.7.5 Ductility or Percentage Elongation of AA 2014/ SiC /150 nm Composites

The consequence of nano SiC reinforced content on the ductility of MMNCs (AA 2014/ SiC /150 nm) was calculated with respect to the percentage of elongation and the result is presented in Table 4.7 and also shown in Figure 4.35. The percentage of elongation of the metal matrix nanocomposites is established to be lesser value as compared with the base metal matrix material (AA 2014), and MMNCs containing highest reinforced content exhibits the lowest percentage of elongation than the other MMNCs of AA 2014/ SiC /150 nm premeditated. It can be seen from the Figure 4.30 ductility of the MMNC decreases gradually with the increase of reinforced nano SiC particulates. The ductility of MMNCs being decreased by an amount of 21.39% as the reinforced nano SiC content is raised from 0 to 2 wt%.

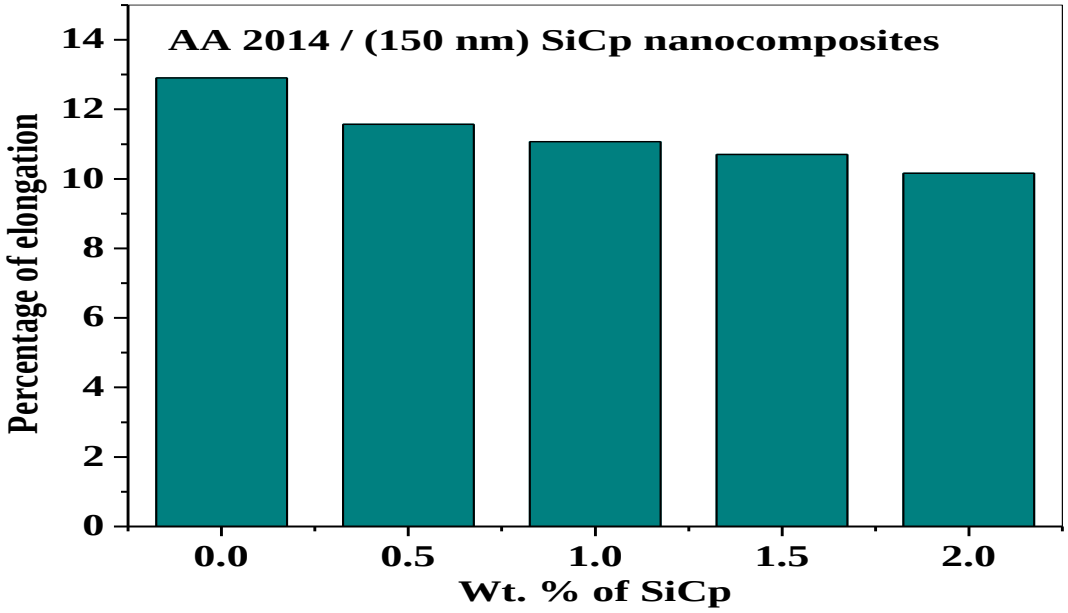

Figure 4.35 Variation in the Ductility of AA 2014 and its Nano SiC reinforced Composites

4.8 AA 2014/ Al_2O_3 /150 nm Composites

The density, UTS, hardness and SEM analysis is done for AA2014/Al_2O_3/150 nm composite prepared by Ultrasonic assisted stir casting method and this results are presented in Table 4.8.

Table 4.8 Mechanical Properties of AA2014/ Al_2O_3/150 nm

S.No	Material	Density value(g/cm^3)		UTS	Hardness	% of Elongation
		Theoretical	Experimental			
1.	AA2014	2.80	2.80	176.16	154.32	12.90
2.	AA2014/0.5wt.% Al_2O_3	2.8041	2.8032	180.40	154.72	12.27
3.	AA2014/1 wt.% Al_2O_3	2.8082	2.8074	187.48	155.66	11.40
4.	AA2014/1.5wt.% Al_2O_3	2.812	2.8102	198.08	156.72	11.03
5.	AA2014/2 wt.% Al_2O_3	2.816	2.8151	208.70	159.54	19.67

4.8.1 Density of AA 2014/ Al_2O_3/150 nm Composites

Figure 4.36 shows the theoretical and the experimental density values of the AA 2014/ Al_2O_3 /50 nm based MMNCs containing 0 to 2wt% of nano Al_2O_3 reinforcement contents. It is found that the density of the MMNC is greater than that of the base metal matrix material (AA 2014). The density of the MMNC (AA 2014/ Al_2O_3 /150 nm) also increases by increase in wt. % particulate reinforcement. An average of 0.2 to 0.25% improvements in the density is observed above base alloy. Additionally, the experimental densities and the theoretical densities are in line with each other confirming the appropriateness of the ultrasonic assisted stir casting for the successful fabrication of AA 2014/ Al_2O_3/150 nm based MMNCs at different weight percentages. An average of 0.042% of deviation of densities observed between theoretical and practical values.

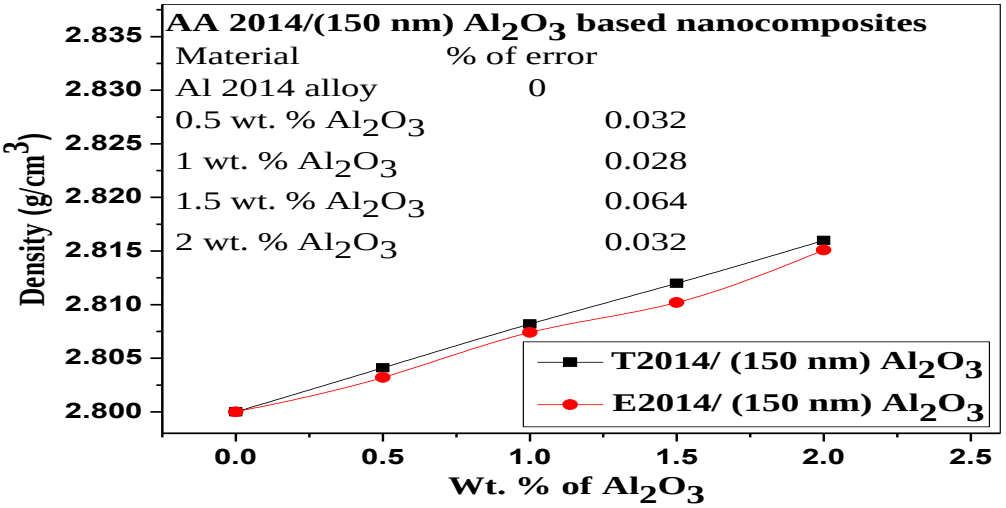

Figure 4.36. Theoretical densities and Experimental Densities for varying wt% of nano Al_2O_3 in AA 2014 alloy

4.8.2 Microstructure Studies of AA 2014/ Al_2O_3 /150 nm Composites

The scanning electron microscopy images of the MMNCs (AA 2014/ Al_2O_3 /150 nm) studied at different levels of reinforcement are given in 4.37(a, b,c&d).

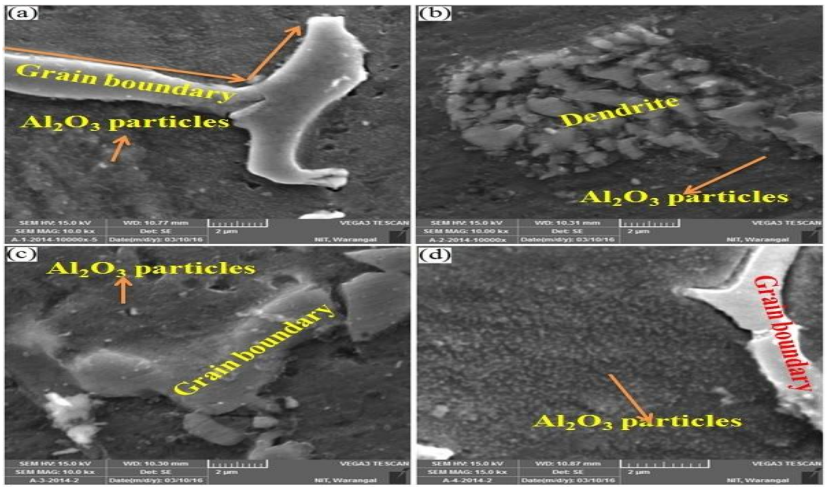

Figures 4.37(a, b, c & d) SEM images of AA 2014/ Al_2O_3 /150 nm alloy and its nano Al_2O_3 Composites.

Microstructural SEM images presented in Figures 4.37(a, b, c & d) show a considerable amount of uniform distribution of nano SiC particulates throughout the metal matrix composite (AA 2014).

4.8.3 Hardness of AA 2014/ Al_2O_3 /150 nm

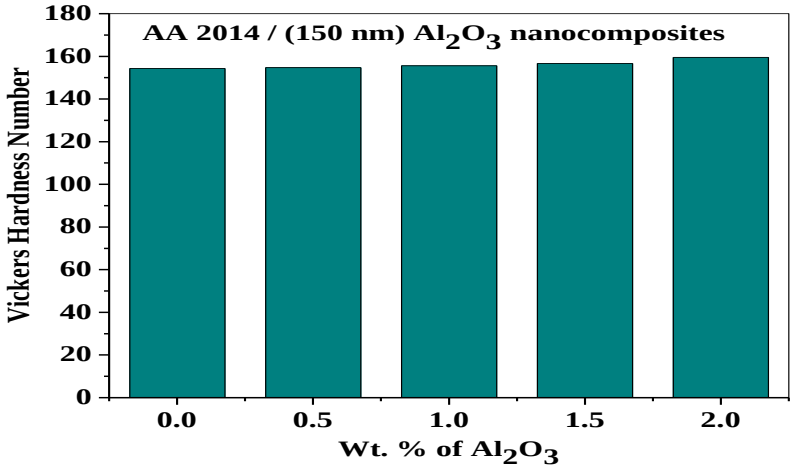

Figure 4.38 Variation in Vickers's Micro Hardness of AA 2014 and its nano Al_2O_3 (150 nm) reinforced MMNCs

The variation of Vicker's Microhardness of MMNCs with increased wt.% of nano Al_2O_3 reinforcement content is given in Table 4.8 and also shown in Figure 4.38. From the Figure 4.38, it can be observed that the hardness value of the MMNCs (AA 2014/ Al_2O_3 /150 nm) is more than that of its base metal matrix composite (AA 2014). Moreover, it is also found that as the wt.% nano Al_2O_3 amount increases the hardness of the composite also increases by significant amounts. The MMNCs containing 2wt% reinforcement content exhibits greater hardness value. The hardness value of the MMNCs (AA 2014/Al_2O_3/150 nm) material increases by the quantity of 3.27% as the reinforcement content of nano Al_2O_3 rises from 0 to 2wt%.

4.8.4 Ultimate Tensile Strength (UTS) of AA 2014/ Al_2O_3 /150 nm Composites

The ultimate tensile strength of the nanocomposites is given in Table 4.8 and also shown in Figure 4.39, shows the variation of the ultimate tensile strength of MMNCs (AA 2014/ Al_2O_3 /150 nm) increases with the increase of weight percentage of nano Al_2O_3 reinforced particulates. Theoretically when hardness increases the UTS of the material also increases [Tom Chandler]. A relation existing between hardness(H) and UTS is H=(UTS)/k ; where "k" depends on material condition and type.

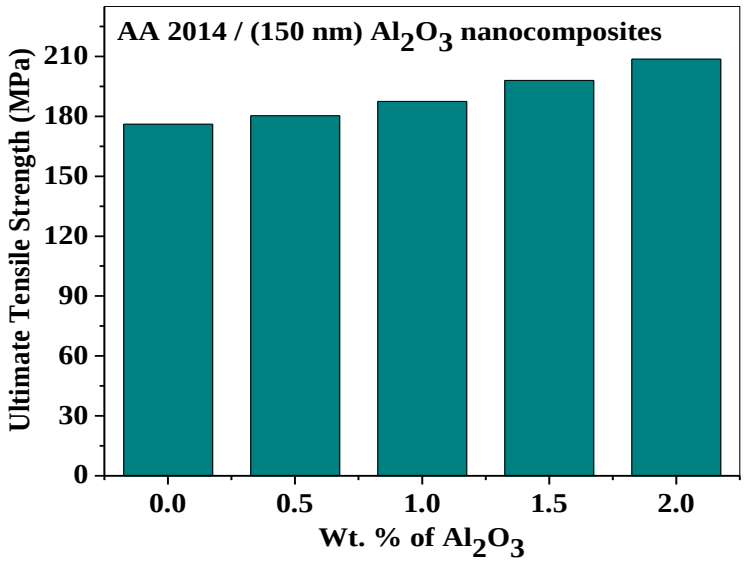

Figure 4.39 Variation in UTS of AA 2014 and its Nano Al_2O_3 reinforced Composites

The UTS of the MMNCs (AA 2014/ Al_2O_3 /150 nm) increased as the weight percentage of the nano ceramic Al_2O_3 particulate phase raised from 0 to 2wt% because of uniform distribution of the reinforced nano alumina particles as explained in the above section called microstructural studies. The UTS of the metal matrix nanocomposite increases by the quantity of 15.59% as the reinforcement content of nano Al_2O_3 particulates rises from 0 to 2 wt%.

4.8.5 Ductility or Percentage Elongation of AA 2014/ Al_2O_3 /150 nm Composites

The consequence of nano Al_2O_3 reinforced content on the ductility of MMNCs (AA 2014/ Al_2O_3 /150 nm) was calculated with respect to the percentage of elongation and the result is presented in Table 4.8 and also shown in Figure 4.40 of MMNCs.

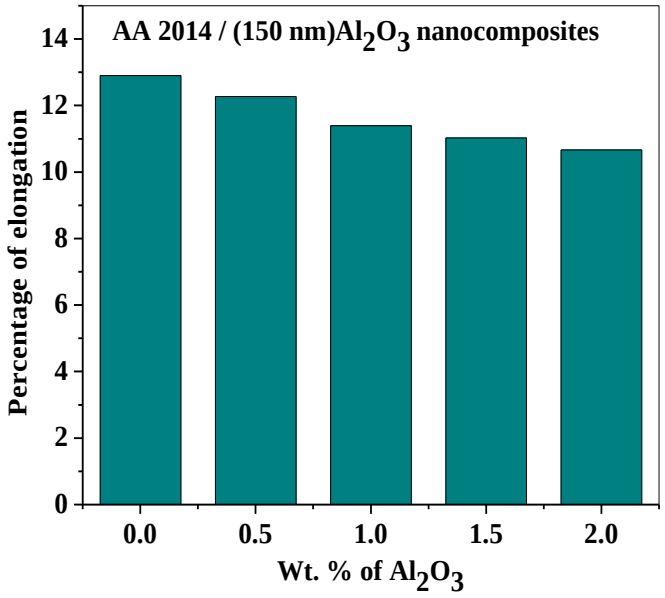

Figure 4.40 Variation in the Ductility of AA 2014 and its Nano Al_2O_3 reinforced Composites

The percentage of elongation of the metal matrix nanocomposites is established to be lesser value as compared with the base metal matrix material (AA 2014), and MMNCs containing highest reinforced content exhibits the lowest percentage of elongation than the other MMNCs of AA 2014/ Al_2O_3/150 nm premeditated. It can be seen from the Figure 4.40 ductility of the MMNCs decreases gradually with the increase of reinforced nano Al_2O_3 particulates. The ductility of MMNCs being decreased by an amount of 17.78% as the reinforced nano Al_2O_3 content is raised from 0 to 2 wt%.

4.9 XRD Analysis of MMNCs

4.9.1 XRD Patterns for AA 2014 with Al_2O_3 and SiC of size 50 nm and 150 nm

The structure and phase analysis of Al 2014 and Al 2219 alloy based nanocomposites were performed by X-Ray diffraction (XRD) using a Philips X-Ray diffract meter at 30mA, 40kV and (1/2˚/5sec) step size using Cuk_{α} radiation. The X-Ray diffraction results for the base Al 2014, and Al 2219 alloys are shown in Figure 4.41 and Figure 4.41. These results indicate the alloys purity and largest peaks of aluminium.

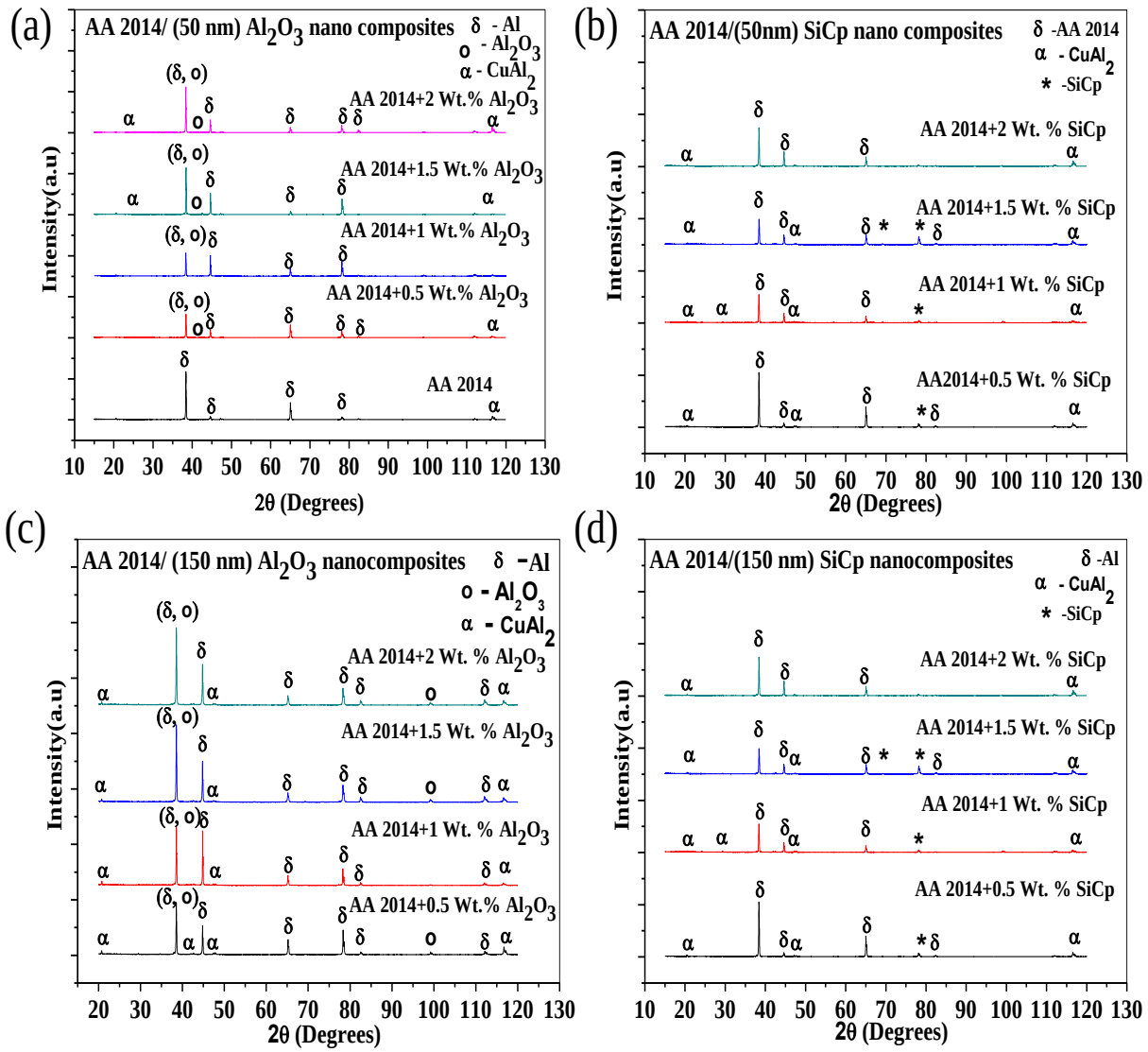

Figure 4.41 XRD analysis of AA 2014 nanocomposites (a) 50 nm Al_2O_3 (b) 50 nm SiC (c) 150 nm Al_2O_3 (d) 150 nm SiC

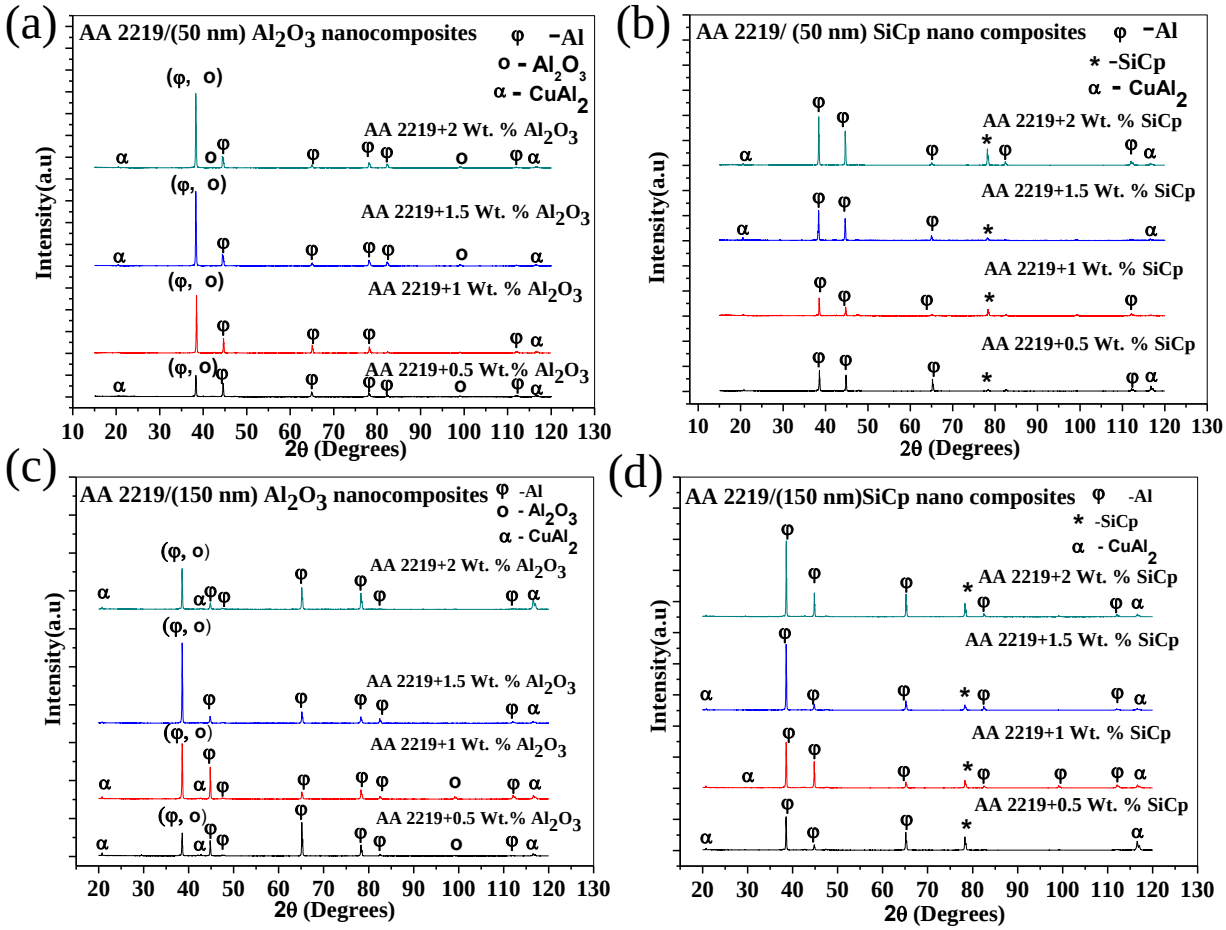

Figure 4.42 XRD analysis of AA 2219 nanocomposites (a) 50 nm Al_2O_3 (b) 50 nm SiC (c) 150 nm Al_2O_3 (d) 150 nm SiC

The X-ray diffraction result analysis of AA 2014/ (0.5, 1, 1.5 & 2) Wt. % (50 nm) Al_2O_3 nanocomposites are shown in Figure 4.41 (a) The results indicate the presence of aluminium in large peak, the presence of alumina (Al_2O_3) phase and intermetallic phase ($CuAl_2$) is indicated by minor peaks. A clearly visible Alumina (Al_2O_3) and $CuAl_2$ peak can be observed in the nanocomposites. The increase in the intensity of the alumina peaks with the increasing alumina content of the nanocomposite is also evident. The XRD pattern confirmed the presence of aluminium, alumina and $CuAl_2$ in the nanocomposites. The XRD results of AA 2014/ (0.5, 1, 1.5 &2) Wt. % (50 nm) SiC nanocomposites are shown in Figure 4.41. In the analysis aluminium as largest peak, the presence of silicon carbide phase and intermetallic phase ($CuAl_2$) is indicated by minor peaks. The increase of in the intensity of the silicon carbide peaks with the increasing silicon carbide content of the nanocomposite is also

evident. The X- ray pattern confirmed the presence of aluminium, silicon carbide and $CuAl_2$ in the nanocomposites.

The X-Ray diffraction analysis of AA 2219/ (0.5, 1, 1.5 & 2) Wt. % (50 nm) Al_2O_3 nanocomposites are shown in Figure 4.42. The large peaks result in aluminium, alumina and secondary peaks are intermetallic ($CuAl_2$). The increase of in the intensity of the alumina peaks with the increasing alumina content of the nanocomposite is also evident. The X- ray pattern confirmed the presence of aluminium, alumina and $CuAl_2$ in the nanocomposites.

The X-Ray diffraction analysis of AA 2219/ (0.5, 1, 1.5 & 2) Wt. % (50 nm) SiC nanocomposites are shown in Figure 4.42. The large peaks result in aluminium, and secondary peaks are intermetallic ($CuAl_2$) and silicon carbide. The increase of in the intensity of the silicon carbide peaks with the increasing silicon carbide content of the nanocomposite is also evident. The X- ray pattern confirmed the presence of aluminium, silicon carbide and $CuAl_2$ in the nanocomposites.

The X-Ray diffraction analysis of AA 2014/ (0.5, 1, 1.5 & 2) Wt. % (150 nm) Al_2O_3 nanocomposites are shown in Figure 4.41. The large peaks result in aluminium, alumina and secondary peaks are intermetallic ($CuAl_2$). The increase of in the intensity of the alumina peaks with the increasing alumina content of the nanocomposite is also evident. The X- ray pattern confirmed the presence of aluminium, alumina and $CuAl_2$ in the nanocomposites. The XRD analysis of AA 2014/ (0.5, 1, 1.5 & 2) Wt. % (150 nm) SiC nanocomposites are shown in Figure 4.41. The large peaks result in aluminium; minor peaks are silicon carbide and intermetallic ($CuAl_2$). The increase of in the intensity of the silicon carbide peaks with the increasing silicon carbide content of the nanocomposite is also evident. The X- ray pattern confirmed the presence of aluminium, alumina and $CuAl_2$ in the nanocomposites. The X-Ray diffraction analysis of AA 2219/ (0.5, 1, 1.5 & 2) Wt. % (150 nm) Al_2O_3 nanocomposites are shown in Figure 4.42. The large peaks result in aluminium, alumina and secondary peaks are intermetallic ($CuAl_2$). The increase of in the intensity of the alumina peaks with the increasing alumina content of the nanocomposite is also evident. The X- ray pattern confirmed the presence of aluminium, alumina and $CuAl_2$ in the nanocomposites. The XRD analysis of AA 2219/ (0.5, 1, 1.5 & 2) Wt. % (150 nm) SiC nanocomposites are shown in Figure 4.42. The large peaks result in aluminium; minor peaks are silicon carbide and intermetallic ($CuAl_2$).

The increase of in the intensity of the silicon carbide peaks with the increasing silicon carbide content of the nanocomposite is also evident. The X- ray pattern confirmed the presence of aluminium, alumina and $CuAl_2$ in the nanocomposites.

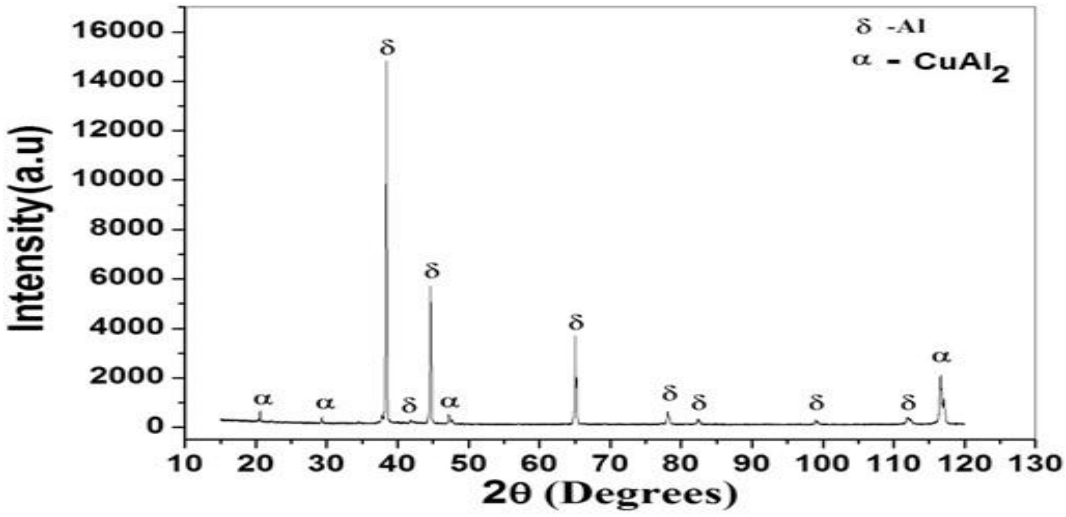

Figure 4.43 XRD of Al 2014 alloy

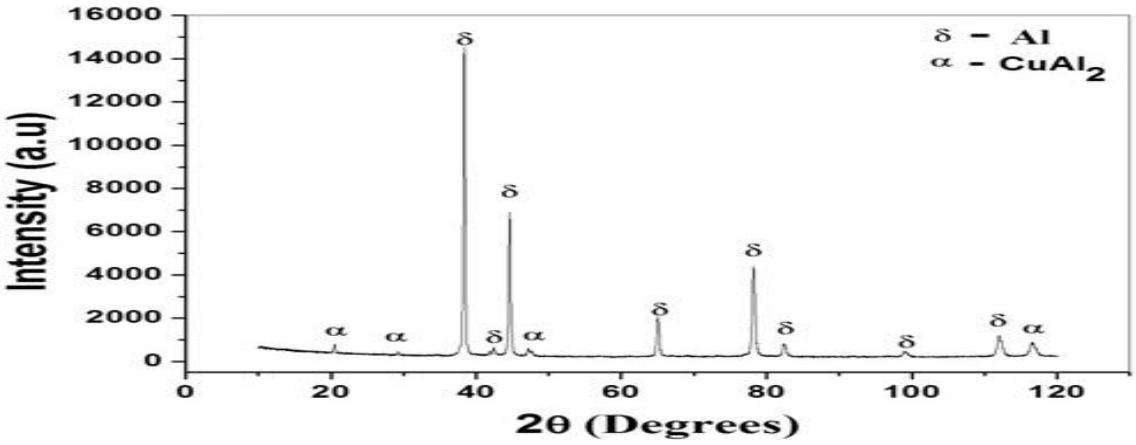

Figure 4.44 XRD of Al 2219 alloy

4.10 Effects of Reinforcements on the Metal Matrix Nano Composite

A comparison is made between AA2219/SiC/50 nm and AA2219/Al2O3/50 nm at 2 wt.% reinforcement presented in Tables (4.9 ,4.10, 4.11 & 4.12).

Table 4.9 Effects of nano SiC (50 nm) and nano Al_2O_3 (50 nm) Reinforcements @2wt.% on the MMNC (AA 2219).

Property	AA 2219/SiC 50 nm	AA 2219/Al2O3 50 nm
Density (g/cc)	2.8465	2.8551
Hardness (VHN)	162.88	159.32
Tensile Strength in (MPa)	222.85	219.28
Increase in brittleness	4.08	4.65

Table 4.10 Effects of nano SiC (150 nm) and nano Al_2O_3 (150 nm) Reinforcements @2wt.% on the MMNC (AA2219).

Property	AA 2219/SiC 150 nm	AA 2219/Al_2O_3 150 nm
Density (g/cc)	2.8465	2.8559
Hardness (BHN)	161.82	157.70
Tensile Strength in (MPa)	212.24	205.16
Increase in brittleness	4.05	4.45

Table 4.11 Effects of nano SiC (50 nm) and nano Al_2O_3 (50 nm) size Reinforcements @2wt.% on the MMNC (AA2014).

Property	AA2014/SiC 50 nm	AA2014/Al_2O_3 50 nm
Density (g/cc)	2.8071	2.8155
Hardness (BHN)	165.54	160.54
Tensile Strength in (Mpa)	244.07	219.31
Increase in brittleness	3.14	3.24

Table 4.12 Effects of nano SiC (150 nm) and nano Al_2O_3 150 nm size Reinforcements @2wt.% on the MMNC (AA2014).

Property	AA 2014/SiC 150 nm	AA2014/Al_2O_3 150 nm
Density (g/cc)	2.8071	2.8160
Hardness (BHN)	163.38	159.54
Tensile Strength in (MPa)	222.85	208.70
Increase in brittleness	3.05	3.19

It is also observed that for the same amount of reinforcement (2wt.%) of either SiC or Al_2O_3, the hardness and tensile strength are better for 50 nm reinforcements compared to 150 nm particle size. This may be due to surface to volume ratio of 50 nm particles is more than 150 nm particles. The hardness and strength of AA2219/SiC composite are better than AA2219/ Al_2O_3. Hence AA2219/SiC MMNC is recommended for structural components like aircraft and automobiles.

A further comparison is made between AA2014 and AA2219 SiC both 50 nm and 150 nm particle sizes and also AA2014& AA2219/ Al_2O_3 both 50 and 150 nm particles. It is observed that AA2014/SiC/50 nm and 150 nm composites are better than AA2219/SiC/50 nm and 150 nm and also AA2014/ Al_2O_3 /50 nm and 150 nm are meagerly better than AA2219/ Al_2O_3 /50 nm and 150 nm composites.

Hence from the above studies we could findout that AA2014/SiC/50 nm MMNCs are better with respect to strength and hardness among all other composites studied.

Tables 4.9 & 4.10 shows the effects of nano SiC and nano Al_2O_3 reinforcements on the MMC (AA 2219) material. It is observed that the percentage increase in density of AA 2219-nano Al_2O_3 is greater than that of AA 2219- nano SiC composites, which may be recognised for the reason that the density of Al_2O_3 is greater than SiC. Further, the percentage increase in hardness, ultimate tensile strength, and brittleness of AA 2219- nano SiC composites are greater than that of AA 2219-nano Al_2O_3 composites. This can be reasoned to the fact that the reduced porosity and better bonding between the nano reinforcement and the matrix material as evidenced by SEM images.

The percentage increase in hardness value and UTS value of MMNCs (AA 2219/SiC) is higher than that of AA 2219/Al_2O_3 based MMNCs, which is because the SiC particulates are harder than that of the Al_2O_3 particulates. The SiC reinforcement in the aluminium matrix composites is the most fracture resistant.

Table 4.11 & 4.12 shows the effects of nano SiC and nano Al_2O_3 reinforcements on the MMC (AA 2014) material. It is observed that the percentage increase in density of AA 2014-nano Al_2O_3 is greater than that of AA 2014- nano SiC composites, which may be recognised for the reason that the density of Al_2O_3 is greater than SiC. Further, the percentage increase in

hardness, ultimate tensile strength, and brittleness of AA 2014- nano SiC composites are greater than that of AA 2014-nano Al_2O_3 composites. This can be reasoned to the fact that the reduced porosity and better bonding between the nano reinforcement and the matrix material as evidenced by SEM images.

The percentage increase in hardness value and UTS value of MMNCs (AA 2014-SiC) is higher than that of AA 2014-Al_2O_3 based MMNCs, which is because the SiC particulates are harder than that of the Al_2O_3 particulates. The SiC reinforcement in the aluminium matrix composites is the most fracture resistant.

Summary

This chapter presents the physical and mechanical properties of

1.) AA2219/SiC/50 nm,

2.)AA2219/Al_2O_3/50 nm,

3.)AA2219/SiC/150 nm,

4.)AA2219/Al_2O_3/150 nm,

5.)AA2014/SiC/50 nm,

6.)AA2014/Al_2O_3/50 nm,

7.) AA2014/SiC/150 nm and

8.) AA2014/Al_2O_3/150 nm Metal Matrix Nano Composites Density, Hardness, Strength and Micrographs of each of MMNCs were measured and Results obtained were analyzed in detail.

Chapter 5

Analysis of Specific Wear Rate using Taguchi and Gray Level analysis

5.1 Specific Wear Rate of AA2219/SiC/50 nm composite:

The Taguchi's L_{16} orthogonal array (OA) has been used to conduct the experiments on wear studies of AA2219/SiC/50 nm as work material. The experimental results are shown in Table 5.1. The output of wear such as wear height(WH), volume of wear (VOW) and specific wear rate (SWR) are measured or caluculated. The purpose of this study is to know the influence of input process parameters on specific wear rate. As wear height , vlume of wear and specific wear rate are all the wear is measured by different authors as wear height,volume of wear and specific wear rate.All these terms representing wear are proportional to each other and have similar trend with respect to input parameters. Thus we studied specific wear rate in this chapter. Influence of input process parameters for both experimental and signal to noise ratio values was plotted. The output response characteristic curves (main effects) helped for investigation of the input process parameters influence on the output response characteristics. The average values of specific wear rate (SWR) for each of input (L, SD, SV, and Wt. %) parameters at level 1, 2, 3, and 4 for experimental and signal to noise ratio data was plotted. Figure 5.1 (a) and (b) shows that the SWR increased when the applied load and sliding distance were increased, and SWR is maximum at fourth level SWR decreases with increase in weight percentage of reinforced ceramic nanoparticles, Sliding velocity effect on specific wear rate is negligible, because all values are very close to the mean value reference line, it

clearly understand from the Figure 5.1 (a) and (b). Sliding distance has been most significant process parameter because it has greater inclination than other process parameters.

Table 5.1 Wear results for MMNCs AA 2219/SiC/50 nm

S. No	L	SD	SV	Wt. %	Response (Raw data)			Average WH (μm)	VOW (mm^3) 10e-3	SWR (mm^3/Nm)	S/N Ratio
					WH1 (μm)	WH2 (μm)	WH3 (μm)				
1	5	1000	0.733	0.5	27	29	28	28	791.28	0.0001582	76.0159
2	5	2000	1.0989	1	76	81	80	79	2232.54	0.0002233	73.0222
3	5	3000	1.465	1.5	116	119	116	117	3306.42	0.0002204	73.1358
4	5	4000	1.832	2	153	161	157	157	4436.82	0.0002218	73.0808
5	10	1000	1.0989	1.5	65	65	68	66	1865.16	0.0001865	74.5864
6	10	2000	0.733	2	139	141	125	135	3815.1	0.0001908	74.3884
7	10	3000	1.832	0.5	355	362	360	359	101.453	0.0003382	69.4165
8	10	4000	1.465	1	475	472	466	471	13310.46	0.0003328	69.5563
9	15	1000	1.465	2	83	86	89	86	2430.36	0.0001620	75.8097
10	15	2000	1.832	1.5	266	270	256	264	7460.64	0.0002487	72.0865
11	15	3000	0.733	1	465	459	456	460	12999.6	0.0002889	70.7850
12	15	4000	1.0989	0.5	910	898	901	903	25518.78	0.0004253	67.4261
13	20	1000	1.832	1	149	153	142	148	4182.48	0.0002091	73.5929
14	20	2000	1.465	0.5	506	515	512	511	14440.86	0.0003610	68.8499
15	20	3000	1.0989	2	559	560	549	556	15712.56	0.0002619	71.6373
16	20	4000	0.733	1.5	1010	1014	1000	1008	28486.08	0.0003561	68.9686

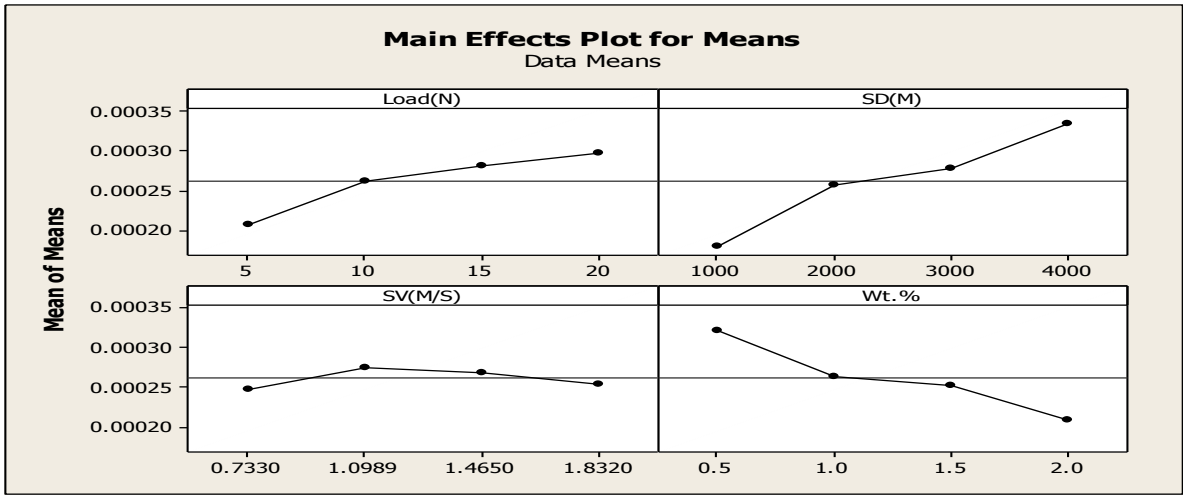

Figure 5.1 (a) Influence of Process Parameters on SWR (Experimental Data)

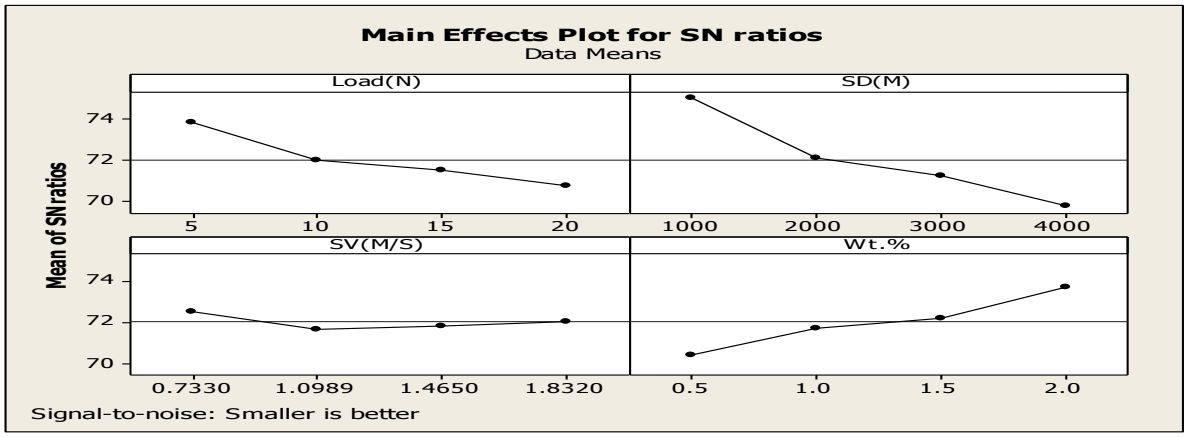

Figure 5.1(b) Influence of Process Parameters on SWR (S/N Data)

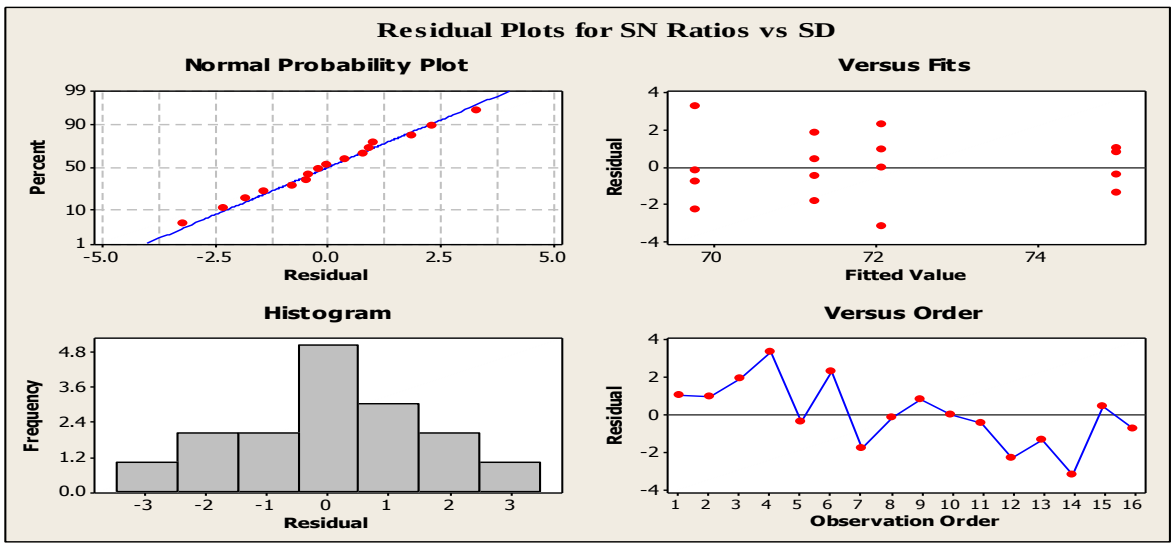

Figure 5.2(a) Residual plots for SN Ratios Vs SD

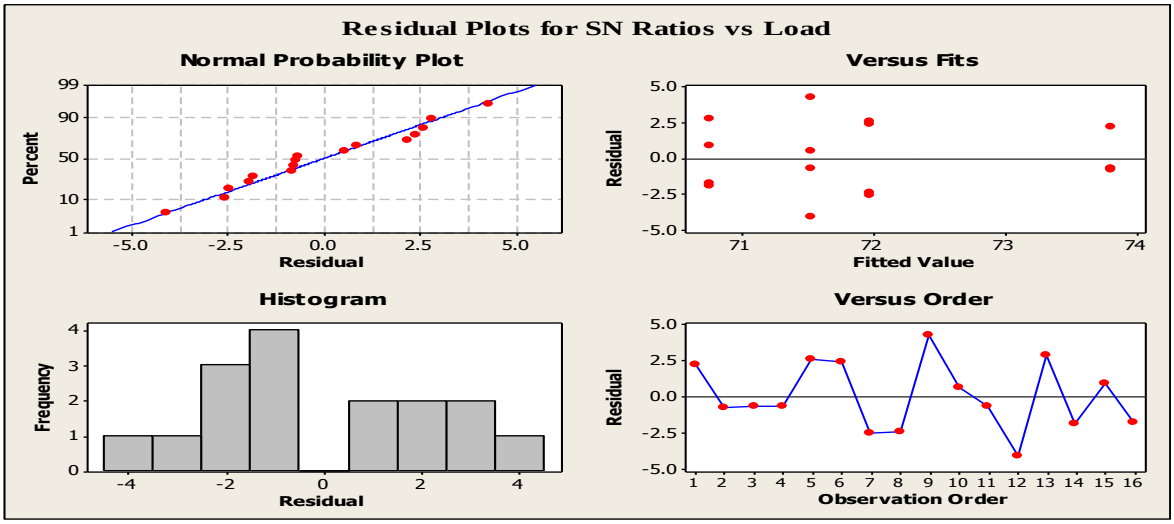

Figure 5.2(b) Residual plots for SN Ratios Vs Load

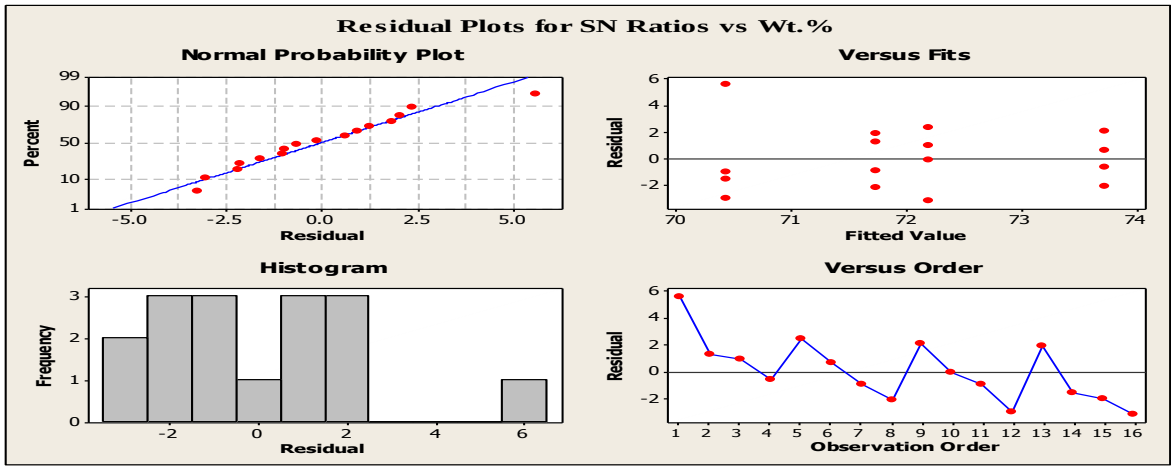

Figure 5.2(c) Residual plots for SN Ratios Vs Wt. %

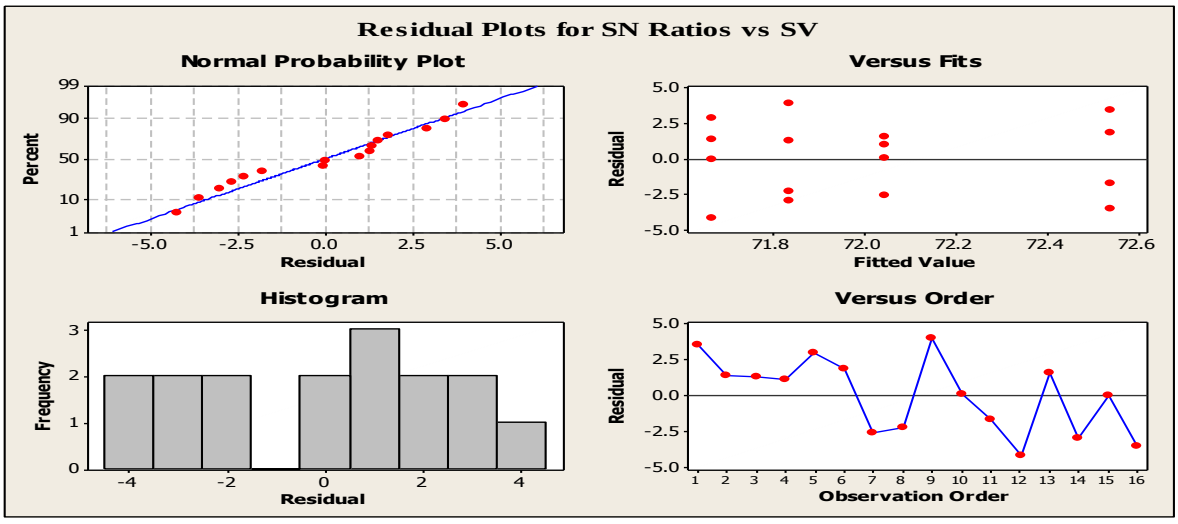

Figure 5.2(d) Residual plots for SN Ratios Vs SV

The residual graphs are used to observe the experimental data towards the solution of the problems like non-normality problems, non-random variation of the data problems, data non-constant variance problems, the relationship between the higher order problems and techniques related to outliers. The above mentioned problems can be found from the Figure 5.2(a), (b), (c), & (d). From the Fig. 5.2(a) is depicting residuals of S/N ratio Vs SD, the residuals are distributed along the straight line in normal probability graph and also very nearer symmetric nature of the histogram show that the residuals are normally distributed and then finally concluded that the experimental data was normal. From the plot of residual verses observation order, the residual does not exhibit any clear pattern; it means that there is no error because of time and data collection order.

Similar explanation may be applied to Figure 5.2(b) depicting residuals of S/N verses load, Figure 5.2(c) for residuals of S/N verses Wt.% and 5.2(d) for residuals verses sliding velocity.

5.1.1 Selection of optimal levels for SWR of MMNCs AA2219/SiC /50 nm

ANOVA results are presented in Table 5.2(a) for SWR(S/N data) and Table 5.2(b) for SWR (experimental data).

Based on the ANOVA, the significance of the input process parameters on output response SWR. It is found that input process parameter such as sliding velocity is least significant. From these tables, it is also clear that the input process parameters such as sliding distance (SD), load (L) and weight percentage (Wt. %) have considerable influence on the output response SWR. The contents in Table 5.3 present the table of reply for means, which means that the average value of each output response characteristic (means) for each level of each input process parameter.

The table shows the delta value calculated based on mathematical statistics and ranks of each input process parameter as it is decided by delta value, which contrasts the virtual magnitude of influence. The delta value is calculated based on the process parameter column, in which the difference of the highest value to the lowest value of each input process parameter. From Minitab software, ranks were assigned by using delta statistical values; highest delta statistical value indicates rank 1, second largest delta statistical value indicates rank2 and so on.

S = 0.503544 R-Sq = 99.26% R-Sq (adj) = 96.32%

Table 5.2 (a) Analysis of Variance for SWR (S/N Data)

ANOVA Table for S/N Ratios							
Source	DF	Seq SS	Adj SS	Adj MS	F	p	% of Contribution
Load(N)	3	20.1747	20.1747	6.7249	26.52	0.012	19.52
SD(M)	3	58.4471	58.4471	19.4824	76.84	0.002	56.55
SV(M/S)	3	1.7099	1.7099	0.57	2.25	0.262	1.65
Wt.%	3	22.2699	22.2699	7.4233	29.28	0.01	21.55
Error	3	0.7607	0.7607	0.2536			
Total	15	103.3622					

S = 0.0000164547 R-Sq = 99.16% R-Sq (adj) = 95.78%

Table 5.2(b) Analysis of Variance for SWR (Experimental Data)

ANOVA Table for Means						
Source	DF	Seq SS	Adj SS	Adj MS	F	P
Load(N)	3	0.01896*10e-6	0.01896*10e-6	0.00632*10e-6	23.34	0.014
SD(M)	3	0.049411*10e-6	0.049411*10e-6	0.0164703*10e-6	60.83	0.003
SV(M/S)	3	0.001753*10e-6	0.001753*10e-6	0.0005843*10e-6	2.16	0.272
Wt.%	3	0.0252897*10e-6	0.0252897*10e-6	0.0084299*10e-6	31.13	0.009
Residual Error	3	0.0008123*10e-6	0.0008123*10e-6	0.0002708*10e-6		
Total	15	0.0962261*10e-6				

DF - degrees of freedom, SS - sum of squares, MS - mean squares(Variance), F-ratio of variance of a source to variance of error, $P < 0.05$ - determines significance of a parameter at 95% confidence level

The ranks clearly explain the practical importance of each input process parameter to the output response (SWR). The ranks of process parameters show that input process parameter sliding distance have the maximum influence on specific wear rate (SWR) and then followed by weight percentage (Wt. %), load (L), sliding velocity (SV) in that order. The SWR is "lower is the better" type quality characteristic, Table 5.3 indicate that the 4^{th} level of

input process parameter load (L4), 4th level of sliding distance (SD4), 2nd level of sliding velocity (SV2), and 1st level of weight percentage (Wt. %1) provide maximum value of specific wear rate using MMNC's of aluminium alloy (AA2219/SiC/50 nm).

Table 5.3 Response Table for SWR (Experimental Data)

Response table for Means				
Level	Load	SD	SV	Wt.%
1	0.000206	0.000179	0.000249	**0.000321**
2	0.000262	0.000256	**0.000274**	0.000264
3	0.000281	0.000277	0.000269	0.000253
4	**0.000297**	**0.000334**	0.000254	0.000209
Delta	0.000091	0.000155	0.000026	0.000112
Rank	3	1	4	2

5.1.2 The Optimal and Predicted Values for AA 2219/SiC /50 nm

In this segment, the optimal results of the output response characteristic specific wear rate (SWR) all along with their individual confidence intervals have been estimated. The optimal levels of the input process parameters for the selected output response characteristic have been recognized and are reported in the previous section. The optimal result of the output response characteristic is estimated by considering the influence of the significant input process parameters only. However, the mean values of quality characteristics being obtained from the experiments may lie within 95% confidence interval (CI). The Taguchi approach for predicting the mean of the output response characteristic and determination of CI for the estimated means has been presented.

$\eta = (T + (Y_1 - T) + (Y_2 - T) + (Z_3 - T) \dots\dots\dots\dots + (Y_n - T) = Y_1 + Y_2 + Y_3 + \cdots - (n-1)T$ ..... (Eq.1)

Where η= Predicted mean of the output response at optimum condition.

T=overall mean of the response.

Y_1, Y_2, Y_3 are the significant process parameters of similar levels at optimum condition**.**

5.1.3 Specific Wear Rate using MMNCs AA2219/SiC/50 nm

The optimum value of specific wear rate (SWR) is predicted at optimal solution the levels of the significant input process parameters which have been chosen as fourth level of load (L4),

fourth level of sliding distance (SD4), second level of sliding velocity (SV2), and first level of weight percentage (Wt. %1).The predictable mean of the output response characteristic SWR can be determined (Kumar, 1993 and Roy, 1990) as

η_{SWR}=T+ (L4-T) + (SD4-T) + (SV2-T) + (Wt. %1-T) in mm^3/N-m ..... (Eq.2)

Where,

T=overall mean of SWR=0.0002616 mm^3/N-m.

The values of L4, SD4, SV2 and Wt. % are taken from the Table 5.3.

L4 = Average value of SWR at the 4^{th} level of load =0.000297 mm^3/N-m

SD4 = Average value of SWR at the 4^{th} level of sliding distance = 0.000334 mm^3/N-m

SV2 = Average value of SWR at the 2^{nd} level of sliding velocity= 0.000274 mm^3/N-m

Wt. % = Average value of SWR at the 1^{st} level of weight percentage = 0.000321 mm^3/N-m

Substituting the values of various terms in the given above (Eq.2).

η_{SWR}=0.0002616 + (0.000297-0.0002616) + (0.000334-0.0002616) + (0.000274-0.0002616) + (0.000321-0.0002616) in mm^3/N-m = 0.0004412 mm^3/N-m

The 95 % CI of the population (CI_{POP}) is calculated by using the following equation 3.as shown below:

$$CI_{POP} = \sqrt{\frac{F_{\propto}(1,f_e)V_e}{n_{eff}}} \quad \text{..... (Eq.3)}$$

$$n_{eff} = \frac{N}{1+[DOF\ associated\ \ in\ the\ estimate\ \ of\ mean\ \ response\ ]} \quad \text{..... (Eq.4)}$$

N= Number of results=16*3=48

V_e =Error variance =0.0002708*10e-6 (from Table 5.2 (b))

f_e =Error DOF=3 (from Table 5.2 (b))

$F_{0.05}(1,3)$=10.13 (Tabulated F value; Roy, 1990)

$F_{cr} < F_{cal}$ (significant process parameter) (Fisher's Test)

$F_{cr} > F_{cal}$ (non significant process parameter) (Fisher's Test)

F_{cr} =Critical F value =10.13 (Tabulated F value; Roy, 1990)

F_{cal} = Calculated F value (From ANOVA Table: 5.2 (b))

DOF associated in the estimate of mean response=12

n_{eff} =3.6923

So, CI_{POP} =± 2.7257*10e-5=±0.000027257

Therefore, the predicted 95% CI of the population is:

Mean $\eta_{SWR} - CI_{POP} < \eta_{SWR>} Mean\ \eta_{SWR} + CI_{POP}$

$0.0004412 - 0.000027257 < \eta_{SWR>} 0.0004412 + 0.000027257$

$0.0004139 < \eta_{SWR} > 0.0004685$

The optimum process parameters for wear test of AA 2219/SiC/50 nm MMNC and the influence of four process parameters namely load, sliding distance, sliding velocity, weight percentage have been investigated on SWR. Optimal set of process parameters has been predicted and verified experimentally on the work material. According to Fisher's test (F-Test), $F_{cr} < F_{cal}$ and then concluded that, Load, Sliding distance and Wt. % are significant. Sliding velocity is the non significant process parameter. The optimum results are shown in the Table 5.4 for minimum specific wear rate.

Regression Equation

SWR = 0.000148717 + 5.849e-006 Load (N) + 4.8655e-008 SD (M) + 3.43794e-006 SV (M/S) - 6.905e-005 Wt. %

Table 5.4 The optimal and predicted values for AA2219/SiC/50 nm using Taguchi analysis

Output response characteristics	Optimal Set of Input Process Parameters	Predicted optimal result in the optimal condition.	At Predicted Confidence Interval at 95% confidence Level	Experimental Value (average of three results)
SWR	L4-SD4-SV2-Wt. % 1	0.0004296	$0.0004139 < \eta_{SWR} > 0.0004685$	0.0004268

Further error between predicted model and experiments were calculated and the result is presented in Table 5.5. From this table it is observed that maximum error is about "3%".

Table 5.5 Error between experimental and predicted SWR for MMNC AA2219/SiC /50 nm

S. No	L	SD	SV	Wt. %	Average WH (μm)	Experimental SWR (mm^3/Nm)	Predicted SWR (mm3/Nm)	% of Error
1	5	1000	0.733	0.5	28	0.0001582	0.0001601	1.19
2	5	2000	1.0989	1	79	0.0002233	0.0002296	2.74
3	5	3000	1.465	1.5	117	0.0002204	0.0002252	2.13
4	5	4000	1.832	2	157	0.0002218	0.0002245	1.20
5	10	1000	1.0989	1.5	66	0.0001865	0.0001903	1.99
6	10	2000	0.733	2	135	0.0001908	0.0001956	2.45
7	10	3000	1.832	0.5	359	0.0003382	0.0003473	2.62
8	10	4000	1.465	1	471	0.0003328	0.0003387	1.74
9	15	1000	1.465	2	86	0.0001620	0.0001649	1.76
10	15	2000	1.832	1.5	264	0.0002487	0.0002503	0.63
11	15	3000	0.733	1	460	0.0002889	0.0002932	1.47
12	15	4000	1.0989	0.5	903	0.0004253	0.0004356	2.36
13	20	1000	1.832	1	148	0.0002091	0.0002122	1.46
14	20	2000	1.465	0.5	511	0.0003610	0.0003689	2.14
15	20	3000	1.0989	2	556	0.0002619	0.0002699	2.96
16	20	4000	0.733	1.5	1008	0.0003561	0.0003603	1.17

5.1.4 Optimization by using GRA for MMNC AA2219/SiC /50 nm

The author had conducted Gray Relational Analysis on the wear test results of AA2219/SiC/50 nm MMNC for further performance evaluation and regression modal for SWR, the GRA is presented below:

Step I: According to step one, the experimental output response results are converted into a signal to noise ratio (S/N). Moreover, then remaining analysis of data is a workout by using S/N ratios. In this analysis mainly our concentration is to minimize the output characteristic response i.e specific wear rate so that consider lower value of SWR as better (Lower is Better) result and the respective S/N ratio can be expressed as

$$\frac{S}{N} Ratio = -10 \log_{10} \left(\frac{1}{n} \sum_{i=1}^{n} y_{ij}^2 \right) \quad \text{..... (Eq. 1)}$$

Where n= Replications number and

y_{ij} =observed response value

i= 1, 2, 3, …..n;

j=1, 2, 3…….k.

Table 5.6 Orthogonal Array and Experimental Results Using MMNC AA 2219/SiC /50 nm

S. No	L	SD	SV	Wt. %	Response (Raw data)			Average WH (μm)	VOW (mm^3) 10e-3	SWR (mm^3/Nm)	S/N Ratio
					WH1 (μm)	WH2 (μm)	WH3 (μm)				
1	5	1000	0.733	0.5	27	29	28	28	791.28	0.0001582	76.0159
2	5	2000	1.0989	1	76	81	80	79	2232.54	0.0002233	73.0222
3	5	3000	1.465	1.5	116	119	116	117	3306.42	0.0002204	73.1358
4	5	4000	1.832	2	153	161	157	157	4436.82	0.0002218	73.0808
5	10	1000	1.0989	1.5	65	65	68	66	1865.16	0.0001865	74.5864
6	10	2000	0.733	2	139	141	125	135	3815.1	0.0001908	74.3884
7	10	3000	1.832	0.5	355	362	360	359	101.453	0.0003382	69.4165
8	10	4000	1.465	1	475	472	466	471	13310.46	0.0003328	69.5563
9	15	1000	1.465	2	83	86	89	86	2430.36	0.0001620	75.8097
10	15	2000	1.832	1.5	266	270	256	264	7460.64	0.0002487	72.0865
11	15	3000	0.733	1	465	459	456	460	12999.6	0.0002889	70.7850
12	15	4000	1.0989	0.5	910	898	901	903	25518.78	0.0004253	67.4261
13	20	1000	1.832	1	149	153	142	148	4182.48	0.0002091	73.5929
14	20	2000	1.465	0.5	506	515	512	511	14440.86	0.0003610	68.8499
15	20	3000	1.0989	2	559	560	549	556	15712.56	0.0002619	71.6373
16	20	4000	0.733	1.5	1010	1014	1000	1008	28486.08	0.0003561	68.9686

Signal to Noise ratio values for the output response characteristic SWR for AA2219/SiC /50 nm was calculated and presented in Table 5.6

Step II: To normalize the given output data for analysis, the first step in GRA is to perform data pre-processing. Transformation of the raw data to share consistently and measure it into considerable limits for conducting further analysis is nothing but normalization. Specifically, in our analysis, a linear normalization of the signal to noise ratio is developed within limits 0 and 1, this procedure called as grey relational generating. By using following formula (Eq.2) to develop the normalized S/N data. (y_{ij} is normalized as $Z_{ij}(0 \leq Z_{ij} \leq 1)$. The normalized specific wear rate corresponding to the smaller the best condition was expressed (Muthu Kumar et al., 2010) and as shown in Table 5.7.

$$Z_{ij} = \frac{\max\ (y_{ij}, i=1,2,.....n) - y_{ij}}{\max\ (y_{ij}, i=1,2,.....n) - \min\ (y_{ij}, i=1,2,.....n)} \quad \text{..... (Eq.2)}$$

The normalized output response related to the "larger is better" condition was expressed (Muthu Kumar et al., 2010)

$$Z_{ij} = \frac{y_{ij} - \min\ (y_{ij}, i=1,2,.....n)}{\max\ (y_{ij}, i=1,2,.....n) - \min\ (y_{ij}, i=1,2,.....n)} \quad \text{..... (Eq.3)}$$

Table 5.7 Normalized S/N ratio values for MMNC's AA 2219/SiC/50 nm

S.No	L	SD	SV	Wt.%	SWR (mm^3/Nm)	S/N Ratio	Normalized S/N Ratio
1	5	1000	0.733	0.5	0.0001582	76.0159	76.0159
2	5	2000	1.0989	1	0.0002233	73.0222	73.0222
3	5	3000	1.465	1.5	0.0002204	73.1358	73.1358
4	5	4000	1.832	2	0.0002218	73.0808	73.0808
5	10	1000	1.0989	1.5	0.0001865	74.5864	74.5864
6	10	2000	0.733	2	0.0001908	74.3884	74.3884
7	10	3000	1.832	0.5	0.0003382	69.4165	69.4165
8	10	4000	1.465	1	0.0003328	69.5563	69.5563
9	15	1000	1.465	2	0.0001620	75.8097	75.8097
10	15	2000	1.832	1.5	0.0002487	72.0865	72.0865
11	15	3000	0.733	1	0.0002889	70.7850	70.7850
12	15	4000	1.0989	0.5	0.0004253	67.4261	67.4261
13	20	1000	1.832	1	0.0002091	73.5929	73.5929
14	20	2000	1.465	0.5	0.0003610	68.8499	68.8499
15	20	3000	1.0989	2	0.0002619	71.6373	71.6373
16	20	4000	0.733	1.5	0.0003561	68.9686	68.9686

Step III: The Grey relational coefficient (shown in Table 5.8) was considered to explain the connection among the raw data and normalized data. Grey relational coefficient was expressed as (Muthu Kumar et al., 2010)

$$\gamma\left(y_o(k), y_i(k)\right) = \frac{\Delta\min + \xi\Delta\max}{\Delta_{oj}(k) + \xi\Delta\max} \quad \text{..... (Eq. 4)}$$

Where,

$y_o(k)$ = reference sequence and $y_j(k)$ = specific assessment sequence.

$\Delta_{oj} = \|y_o(k) - y_j(k)\|$ = difference between $y_o(k)$ and $y_j(k)$

$\Delta\min = \underset{\forall j \in i}{\Delta\min} \underset{\forall k}{\min} \|y_o(k) - y_j(k)\|$ = smallest data value of $y_j(k)$

$\Delta\max = \underset{\forall j \in i}{\Delta\max} \underset{\forall k}{\max} \|y_o(k) - y_j(k)\|$ = largest data value of $y_j(k)$

Where, ξ is the characteristic coefficient, and it is in the range $0 \leq \xi \leq 1$. Specific wear test input process variables are evenly distributed in this analysis so that the value of ξ is 0.5.

Table 5.8 Grey relational coefficient

S. No	L	SD	SV	Wt. %	SWR (mm^3/Nm)	S/N Ratio	Normalized S/N	Δ_{oj}	$\overset{\gamma}{}$ GRC
1	5	1000	0.733	0.5	0.0001582	76.0159	76.0159	1	0.3333
2	5	2000	1.0989	1	0.0002233	73.0222	73.0222	0.6515	0.4342
3	5	3000	1.465	1.5	0.0002204	73.1358	73.1358	0.6647	0.4293
4	5	4000	1.832	2	0.0002218	73.0808	73.0808	0.6583	0.4317
5	10	1000	1.0989	1.5	0.0001865	74.5864	74.5864	0.8336	0.3749
6	10	2000	0.733	2	0.0001908	74.3884	74.3884	0.8105	0.3815
7	10	3000	1.832	0.5	0.0003382	69.4165	69.4165	0.2317	0.6833
8	10	4000	1.465	1	0.0003328	69.5563	69.5563	0.2480	0.6684
9	15	1000	1.465	2	0.0001620	75.8097	75.8097	0.9760	0.3388
10	15	2000	1.832	1.5	0.0002487	72.0865	72.0865	0.5426	0.4796
11	15	3000	0.733	1	0.0002889	70.7850	70.7850	0.3910	0.5612
12	15	4000	1.0989	0.5	0.0004253	67.4261	67.4261	0	1
13	20	1000	1.832	1	0.0002091	73.5929	73.5929	0.7179	0.4105
14	20	2000	1.465	0.5	0.0003610	68.8499	68.8499	0.1658	0.7510
15	20	3000	1.0989	2	0.0002619	71.6373	71.6373	0.4903	0.5049
16	20	4000	0.733	1.5	0.0003561	68.9686	68.9686	0.1796	0.7357

Step IV: By considering the mean of the grey relational coefficient related to every output performance characteristic is called Grey relational grade value. In this situation has only one performance characteristic i.e. SWR. Final output performance characteristic of the more than one output response characteristic depends on the Grey relational grade. The Grey relational grade was expressed as (Muthu Kumar, 2010)

$$\overline{\gamma_j} = \frac{1}{k} \sum_{i=1}^{m} \gamma_{ij} \quad \text{..... (Eq.5)}$$

This method converts a multiple output response processes into a single output response optimization condition with the final Grey relational grade. Table 5.9 indicates the grey relation coefficient and Grey relational grade for every experimental result using Taguchi L16 orthogonal array. The Greater value of GRG tells the similar real result is very nearer to the perfectly normalized data value. In our analysis experiment, no 12 for MMNC AA 2219/SiC/50 nm has shown the greater GRG and then concluded that finest output performance response had been demonstrated out of 16 experimental results. The greater GRG gives, the nearer optimal solution. Greater the GRG gives the excellent product quality. A higher Grey relational grade implies better product quality; based on this the GRG, investigate the input process parameters influence on the output response (SWR) and also determine the optimal solution at each level for every controllable process parameter.

Table 5.9 Gray relational grade

S.No	L	SD	SV	Wt. %	SWR (mm^3/Nm)	S/N Ratio	Normalized S/N Ratio	Δ_{oj}	γ(GRC)	$\overline{\gamma_j}$
1	5	1000	0.733	0.5	0.0001582	76.0159	76.0159	1	0.3333	0.3333
2	5	2000	1.0989	1	0.0002233	73.0222	73.0222	0.6515	0.4342	0.4342
3	5	3000	1.465	1.5	0.0002204	73.1358	73.1358	0.6647	0.4293	0.4293
4	5	4000	1.832	2	0.0002218	73.0808	73.0808	0.6583	0.4317	0.4317
5	10	1000	1.0989	1.5	0.0001865	74.5864	74.5864	0.8336	0.3749	0.3749
6	10	2000	0.733	2	0.0001908	74.3884	74.3884	0.8105	0.3815	0.3815
7	10	3000	1.832	0.5	0.0003382	69.4165	69.4165	0.2317	0.6833	0.6833
8	10	4000	1.465	1	0.0003328	69.5563	69.5563	0.2480	0.6684	0.6684
9	15	1000	1.465	2	0.0001620	75.8097	75.8097	0.9760	0.3388	0.3388
10	15	2000	1.832	1.5	0.0002487	72.0865	72.0865	0.5426	0.4796	0.4796
11	15	3000	0.733	1	0.0002889	70.7850	70.7850	0.3910	0.5612	0.5612
12	**15**	**4000**	**1.0989**	**0.5**	**0.0004253**	**67.4261**	**67.4261**	**0**	**1**	**1**
13	20	1000	1.832	1	0.0002091	73.5929	73.5929	0.7179	0.4105	0.4105
14	20	2000	1.465	0.5	0.0003610	68.8499	68.8499	0.1658	0.7510	0.7510
15	20	3000	1.0989	2	0.0002619	71.6373	71.6373	0.4903	0.5049	0.5049
16	20	4000	0.733	1.5	0.0003561	68.9686	68.9686	0.1796	0.7357	0.7357

The mean of the GRG for every level of the other input process parameters of SWR can be calculated in a particular procedure. The mean of the GRG also called as average GRG for every level of the input process parameters is briefly summarized in Table 5.10.

Table 5.10 Average GRG

Input factors	Level 1	Level 2	Level 3	Level 4	Max-Min	rank
Load	0.4071	0.5270	0.5949	**0.6005**	0.1934	3
SD	0.3644	0.5116	0.5447	**0.7090**	0.3446	1
SV	0.5029	**0.5785**	0.5469	0.5013	0.0772	4
Wt%	**0.6919**	0.5186	0.5049	0.4142	0.2777	2

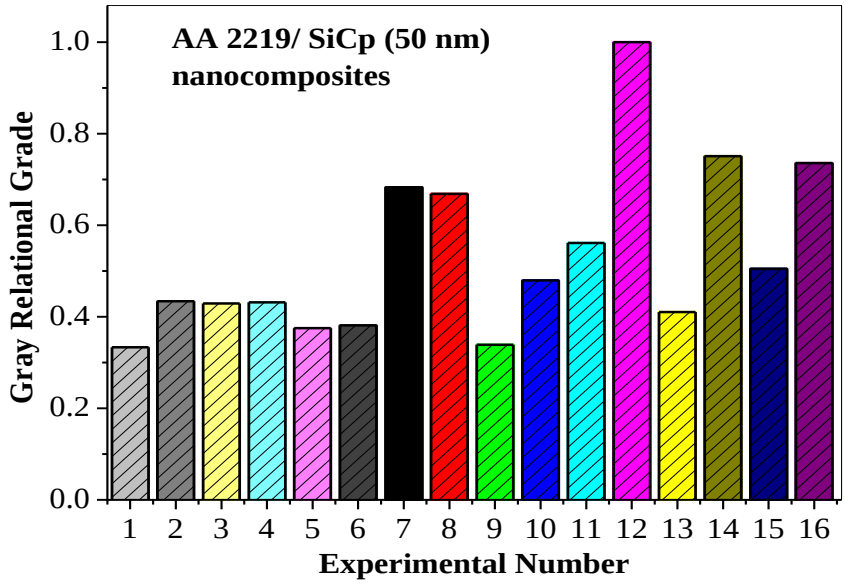

Figure 5.3 Gray relational grade plot of AA 2219 /SiC/50 nm composites

Step V: To investigate the optimal solution related to input process parameters and its level at different stages (Muthu Kumar, 2010), higher the GRG, gives the best output performance characteristic. Anyway, it is paramount to know the relative importance of input process parameters over the output response (SWR), so the optimal solution of the input process parameter levels can be found accurately. The optimal input parametric combinations are shown in Table 5.10. It is also bolded in the tables. The optimal process parameter setting

becomes L4 (Load, 20N), SD (sliding distance, 4000m), SV (sliding velocity, 1.0989m/s), and Wt. % (Weight percentage, 0.5%) for MMNC AA2219/SiC/50 nm.

[Therefore optimal solution for MMNC AA2219/SiC/50 nm is "L4 –SD4-SV2-Wt. %1"]

5.1.5 Conformation Test

The predicted grey relational analysis using optimal process parameters is given as:

$$\gamma = \gamma_{m+\sum(\gamma_n-\gamma_m)}$$

γ_n = Average GRG at optimal solution (L4-SD4-SV2-Wt%1) factor level wise

γ_m =Total mean average GRG =0.5324 (factor level wise)

γ=0.5324+ (0.6005-0.5324) + (0.7090-0.5324) + (0.5785-0.5324) + (0.6919-0.5324)

=0.9827

Optimal Gray relational grade = 1 (**RANK 1)**

% of grey relational grade= [(1-0.9827)/1]*100=1.73

5.1.6 General Regression Analysis

From the general regression analysis specific wear rate has been predicted and is presented in Table 5.11.

Regression Equation

SWR = 0.000148717 + 5.849e-006 Load (N) + 4.8655e-008 SD (M) + 3.43794e-006 SV (M/S) - 6.905e-005 Wt. %

Table 5.11 The optimal and predicted values for MMNC AA 2219/SiC/50 nm using Gray relational analysis

Response	Optimal Solution of process parameters	Experimental value	Predicted value	% Error
Specific Wear Rate	L4-SD4-SV2-Wt. %1	0.0004268 mm^3/N-m	0.0004296 mm^3/N-m	0.6517

Further the error between predicted model by GRA and experimental values was calculated and presented in Table 5.12. It is found that the error is "3%". Hence it is further concluded that the predicted model by GRA is good and it is in line with Taguchi model of prediction of SWR.

Table 5.12 Error between experimental and predicted SWR for MMNC AA2219/SiC /50 nm

S.No	L	SD	SV	Wt.%	Average WH (μm)	ExperimentalSWR (mm^3/Nm)	Predicted SWR (mm3/Nm)	% of Error
1	5	1000	0.733	0.5	28	0.0001582	0.0001601	1.19
2	5	2000	1.0989	1	79	0.0002233	0.0002296	2.74
3	5	3000	1.465	1.5	117	0.0002204	0.0002252	2.13
4	5	4000	1.832	2	157	0.0002218	0.0002245	1.20
5	10	1000	1.0989	1.5	66	0.0001865	0.0001903	1.99
6	10	2000	0.733	2	135	0.0001908	0.0001956	2.45
7	10	3000	1.832	0.5	359	0.0003382	0.0003473	2.62
8	10	4000	1.465	1	471	0.0003328	0.0003387	1.74
9	15	1000	1.465	2	86	0.0001620	0.0001649	1.76
10	15	2000	1.832	1.5	264	0.0002487	0.0002503	0.63
11	15	3000	0.733	1	460	0.0002889	0.0002932	1.47
12	15	4000	1.0989	0.5	903	0.0004253	0.0004356	2.36
13	20	1000	1.832	1	148	0.0002091	0.0002122	1.46
14	20	2000	1.465	0.5	511	0.0003610	0.0003689	2.14
15	20	3000	1.0989	2	556	0.0002619	0.0002699	2.96
16	20	4000	0.733	1.5	1008	0.0003561	0.0003603	1.17

5.1.7 Validation of the Experimental Results

The confirmation test was performed at the optimal solution with its chosen levels to calculate the quality response characteristics related to Wear test on MMNC AA 2219/SiC/50 nm work material. (Muthu Kumar et al., 2010) Experiment 12 shows the greater GRG for

MMNC AA2219/SiC/50 nm, signifying the optimal solution process parameter combination of L4-SD4-SV2-Wt. %1 has the best performance characteristic among all experiments, for validation of results to compare results with confirmation test results Table 5.9. Shows the comparison of the actual results of wear test on wear process parameters on MMNC AA 2219/SiC/50 nm work material. The output specific response results were obtained from the confirmation test are SWR = 0.0004268 mm^3/N-m, predicted SWR=0.0004296 mm^3/N-m, and percentage of error between predicted and experimental is 0.6517 as shown in Table 5.11. Gray relational grade has been improved by 1.73.

Similar tests were conducted and Taguchi and Gray relational Analysis was done on the remaining aluminium MMNCs shown in Table 5.13. Similar effects were observed in these tests also. Hence the results of these MMNCs were kept in Appendix-I for further reference. This chapter deals with analysis of specific wear rate using Taguchi and Gray level analysis of aluminium MMNCs fabricated by Ultrasonic assisted stir casting method.

Table 5.13 Metal Matrix Nano Composite(MMNC)

S.No	Metal Matrix Nano Composite(MMNC)
2.	AA2219/Al_2O_3/50 nm
3.	AA2219/SiC/150 nm
4.	AA2219/Al_2O_3/150 nm
5.	AA2014/SiC/50 nm
6.	AA2014/Al_2O_3/50 nm
7.	AA2014/SiC/150 nm
8.	AA2014/Al_2O_3/150 nm

Chapter 6

Wear studies on Aluminium-SiC and Al_2O_3 reinforced MMNCs

Friction and wear characteristics of the fabricated aluminium based nanocomposites were presented in this chapter. Wear of the test specimens is measured in three modes namely volume of wear in mm^3, height of wear in mm and specific wear rate in mm^3/Nm are measured. Though all the modes are proportional to each other, several authors (G.B.Veeresh Kumar, 2012) have dealt them independently in their works. Hence we also made an attempt to present all these forms of wear independently for each aluminium MMNC material.

6.1 Wear Resistance Properties of AA2219/SiC/50 nm Nanocomposites

6.1.1 Volume of Wear AA2219/SiC/50 nm Nanocomposites

The variation in the volume of wear with sliding distance under different loads are shown in Figure 6.1 a,b,c&d . The cast AA 2219/SiC/50 nm MMNC undergo higher volume of wear with an increase in sliding distance. The volume of wear of AA2219/SiC/50 nm the metal matrix nanocomposites was observed at all the sliding distances and concluded that the volume of wear of MMNC was less when compared with base MMC. The volume of wear was reduced while increasing the weight percentage of nano SiC in the base alloy. The variation in the volume of wear with an applied load is shown in Figure 6.2 a,b,c&d at sliding distances of

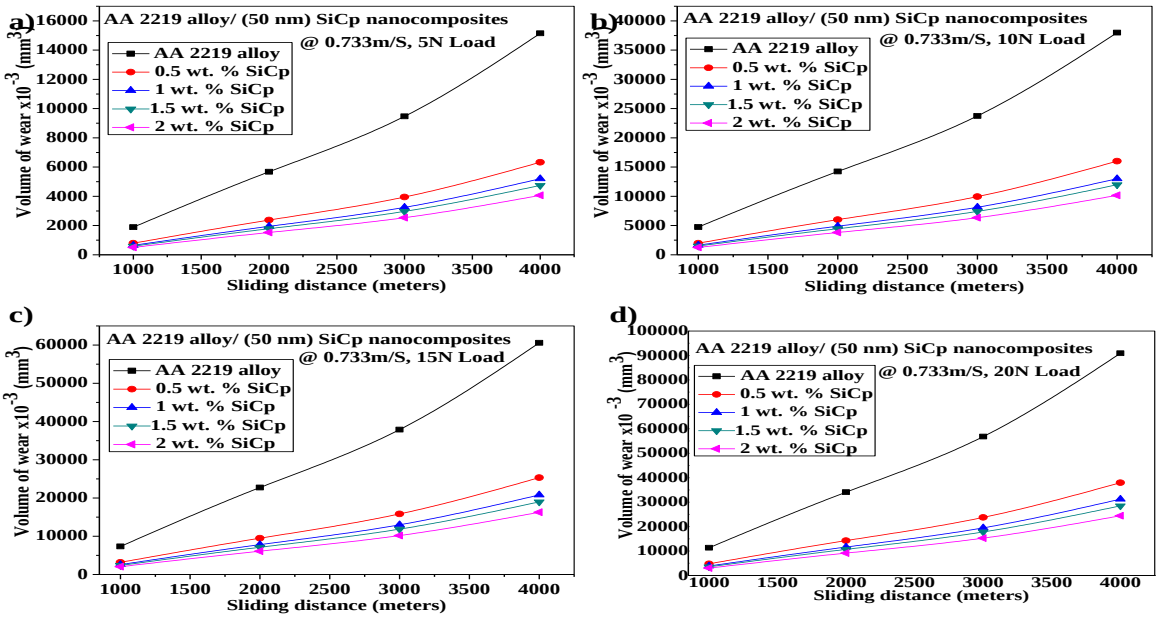

Figure 6.1 Variation of the volume of wear AA 2219 alloy and its nano SiC based MMNCs a) at 5 N load b) at 10 N load c) at 15 N load d) at 20 N load, with sliding distance of 1000 to 4000 m, at a constant sliding velocity of 0.733 m/s.

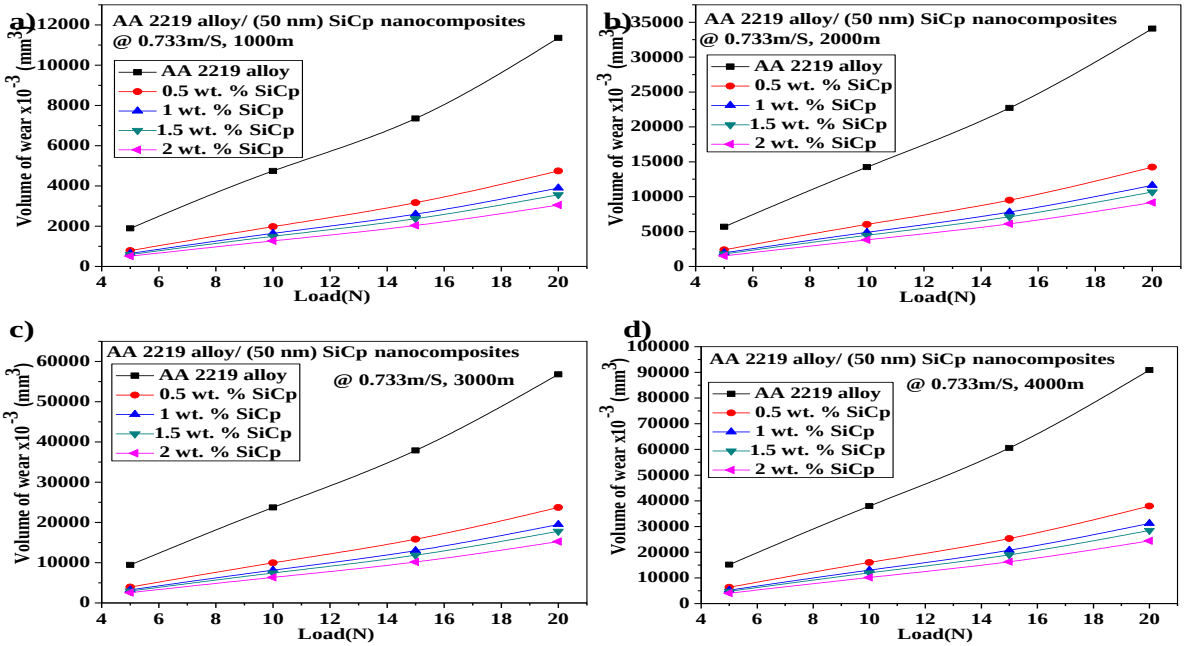

Figure 6.2 Variation of the volume of wear AA 2219 alloy and its nano SiC based MMNCs a) at 1000 m sliding distance b) at 2000 m sliding distance c) at 3000 m sliding distance d) at 4000 m sliding distance, with an applied load of 5 N to 20 N, at constant sliding velocity 0.733 m/s.

1 km, 2 km, 3 km & 4 km respectively. The cast AA2219 and its nano SiC reinforced metal matrix nanocomposites undergo higher volume of wear with an increase in applied load. The volume of wear of the metal matrix nanocomposites was observed at all the applied loads and concluded that the volume of wear of AA2219/SiC/50 nm composite was less when compared with base MMC. The volume of wear was reduced while increasing the weight percentage of nano SiC in the base alloy and it is shown in Figures 6.2. In all these results sliding velocity kept constant (SV=0.733m/s). The reasons for all these works are well known fact established in literature. As the wt.% of particulate SiC increase in AA2219 the hardness and strength were increasing hence resistance to wear is also increases.

6.1.2 Wear Height AA2219/SiC/50 nm Nano Composite

The variation in the wear height with sliding distance under different loads are shown in Figure 6.3 a,b,c&d . The cast AA2219/SiC/50 nm MMNC undergo higher loss in wear height with an increase in sliding distance. The wear height of AA2219/SiC/50 nm the metal matrix nanocomposites was observed at all the sliding distances and concluded that the wear height of MMNC was less when compared with base MMC.

The loss of wear height was reduced while increasing the weight percentage of nano SiC in the base alloy. The variation in the wear height with an applied load is shown in Figure 6.4 a,b,c&d at sliding distances of 1km,2km,3km&4km respectively. The cast AA2219and its nano SiC reinforced metal matrix nanocomposites undergo higher loss of wear height with an increase in applied load.

The wear height of the metal matrix nanocomposites was observed at all the applied loads and concluded that the loss of wear height of AA2219/SiC/50 nm composite was less when compared with base MMC. The loss of wear height was reduced while increasing the weight percentage of nano SiC in the base alloy and it is shown in Figures 6.4. In all these results sliding velocity kept constant (SV=0.733m/s).

The reasons for all these works are well known fact established in literature. As the wt.% of particulate SiC increase in AA2219 the hardness and strength were increasing hence resistance to wear is also increases.

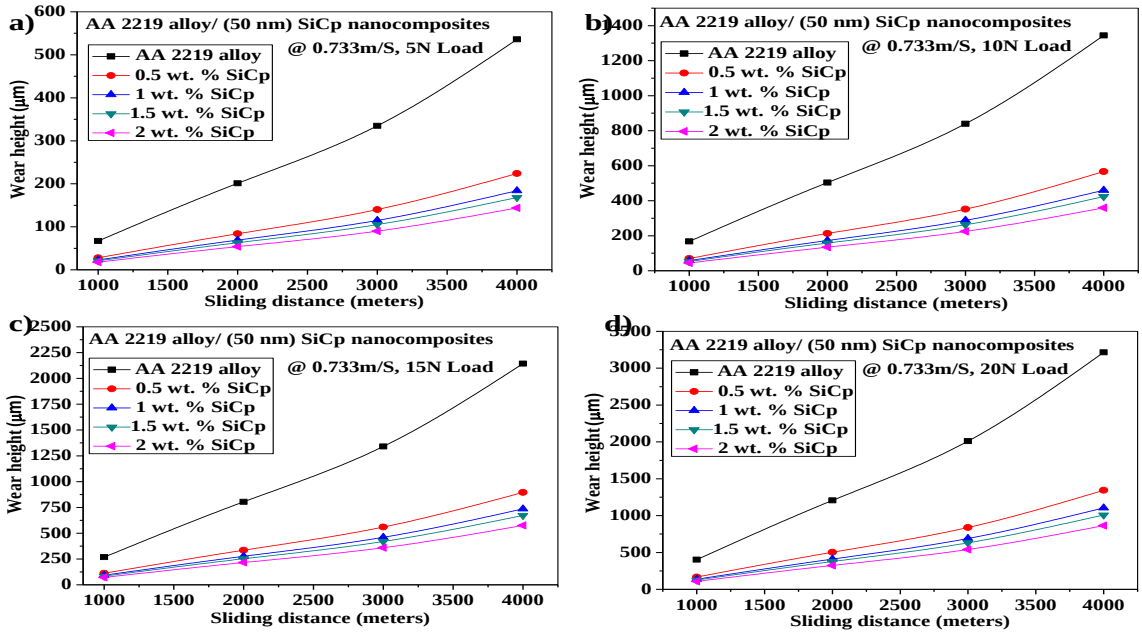

Figure 6.3 Variation of wear height AA 2219 alloy and its nano SiC based MMNCs a) at 5 N load b) at 10 N load c) at 15 N load d) at 20 N load, with sliding distance of 1000 m to 4000 m, at constant sliding velocity of 0.733 m/S.

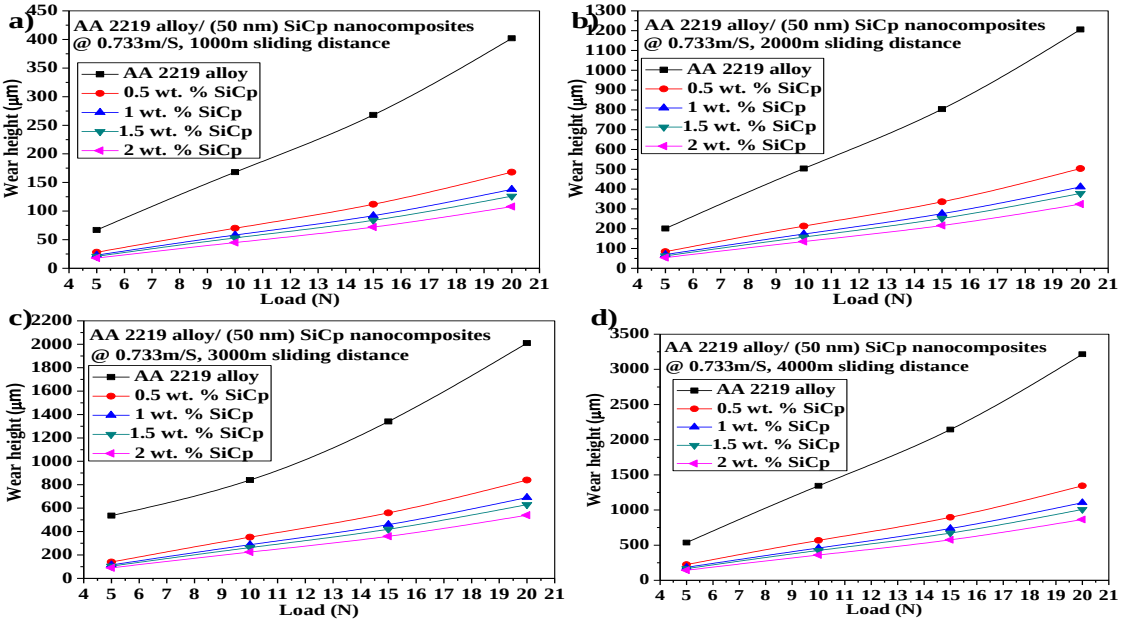

Figure 6.4 Variation of wear height of AA 2219 alloy and its nano SiC based MMNCs a) at 1000 m sliding distance b) at 2000 m sliding distance c) at 3000 m sliding distance d) at 4000 m sliding distance, with an Applied load of 5 N to 20 N & at constant Sliding Velocity 0.733 m/s.

6.1.3 Wear Weight Loss AA2219/SiC /50 nm Nanocomposites

The variation in the wear weight loss with sliding distance under different loads are shown in Figure 6.5 a,b,c&d . The cast AA2219/SiC/50 nm MMNC undergo higher wear weight loss with an increase in sliding distance. The wear weight loss of AA2219/SiC/50 nm the metal matrix nanocomposites was observed at all the sliding distances and concluded that the wear weight loss of MMNC was less when compared with base MMC. The wear weight loss was reduced while increasing the weight percentage of nano SiC in the base alloy. The variation in the wear weight loss with an applied load is shown in Figure 6.6 a,b,c&d at sliding distances of 1km,2km,3km&4km respectively.

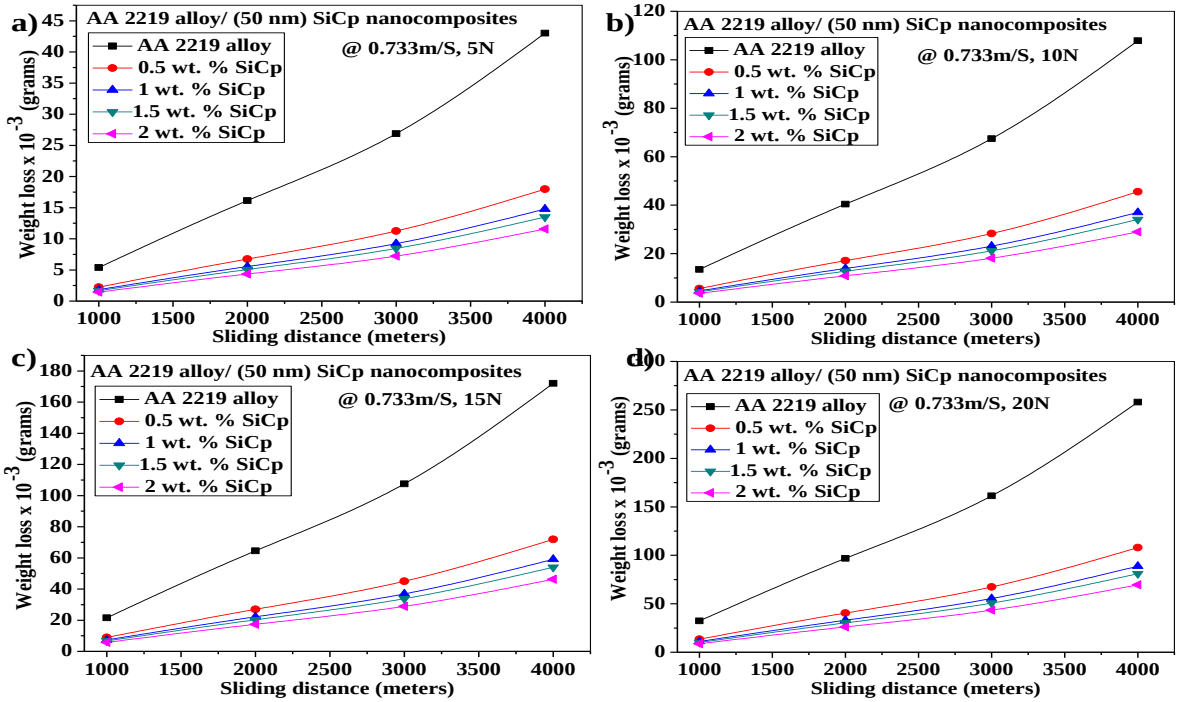

Figure 6.5 Variation of wear weight loss AA2219 alloy and its nano SiC based MMNCs a) at 5 N load b) at 10 N load c) at 15 N load d) at 20 N load, with sliding distance of 1000 m to 4000 m and at constant sliding velocity of 0.733 m/S.

The cast AA2219and its nano SiC reinforced metal matrix nanocomposites undergo higher wear weight loss with an increase in applied load. The wear weight loss of the metal matrix nanocomposites was observed at all the applied loads and concluded that the wear weight loss of AA2219/SiC/50 nm composite was less when compared with base MMC. The wear weight loss was reduced while increasing the weight percentage of nano SiC in the base alloy and it

is shown in Figures 6.6. In all these results sliding velocity kept constant (SV=0.733m/s). The reasons for all these works are well known fact established in literature. As the wt.% of particulate SiC increase in AA2219 the hardness and strength were increasing hence resistance to wear is also increases.

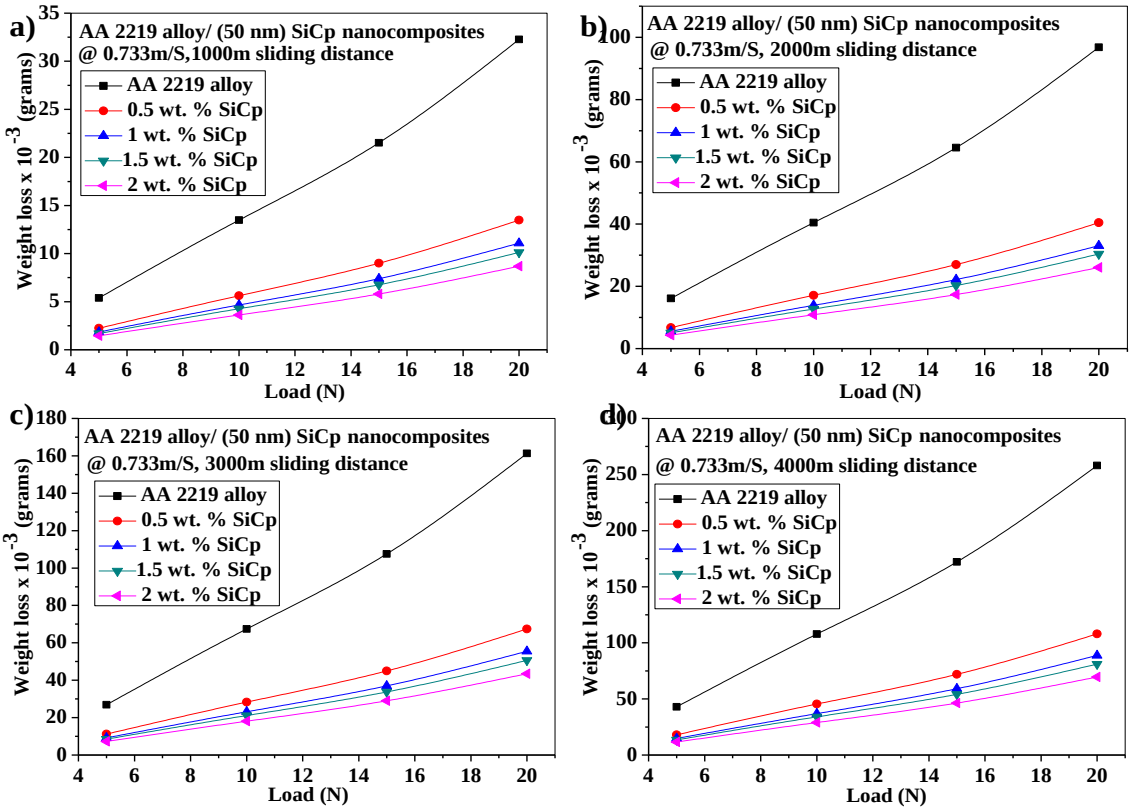

Figure 6.6 Variation of wear weight loss of AA2219 alloy and its nano SiC MMNCs a) at 1000 m sliding distance b) at 2000 m sliding distance c) at 3000 m sliding distance d) at 4000 m sliding distance, with an applied load of 5 N to 20 N, and constant sliding velocity 0.733 m/s.

6.1.4 Specific Wear Rate AA2219/SiC /50 nm Nanocomposite

The variation in the specific wear rate with sliding distance under different loads are shown in Figure 6.7 a,b,c&d . The cast AA2219/SiC/50 nm MMNC undergo higher specific wear rate with an increase in sliding distance. The specific wear rate of AA2219/SiC/50 nm the metal matrix nanocomposites was observed at all the sliding distances and concluded that the specific wear rate of MMNC was less when compared with base MMC. The specific wear rate was reduced while increasing the weight percentage of nano SiC in the base alloy. The variation in the specific wear rate with an applied

load is shown in Figure 6.8 a,b,c&d at sliding distances of 1km,2km,3km&4km respectively. The cast AA2219 and its nano SiC reinforced metal matrix nanocomposites undergo higher specific wear rate with an increase in applied load. The specific wear rate of the metal matrix nanocomposites was observed at all the applied loads and concluded that the specific wear rate of AA2219/SiC/50 nm composite was less when compared with base MMC. The specific wear rate was reduced while increasing the weight percentage of nano SiC in the base alloy and it is shown in Figures 6.8. In all these results sliding velocity kept constant (SV=0.733m/s). The reasons for all these works are well known fact established in literature. As the wt.% of particulate SiC increase in AA2219 the hardness and strength were increasing hence resistance to wear is also increases.

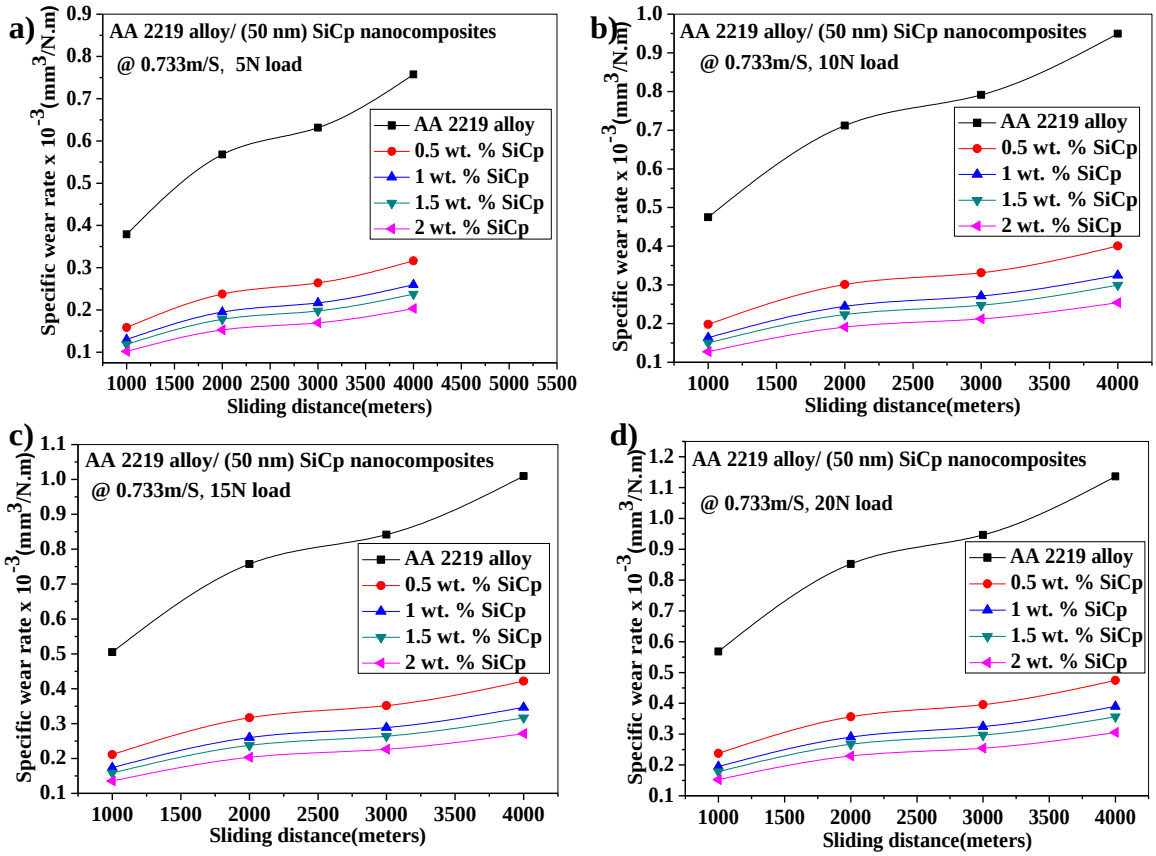

Figure 6.7 Variation of specific wear rate AA2219 alloy and its nano SiC based MMNCs a) at 5 N load b) at 10 N load c) at 15 N load d) at 20 N load, with sliding distance of 1000 m to 4000 m and at constant sliding velocity of 0.733 m/S.

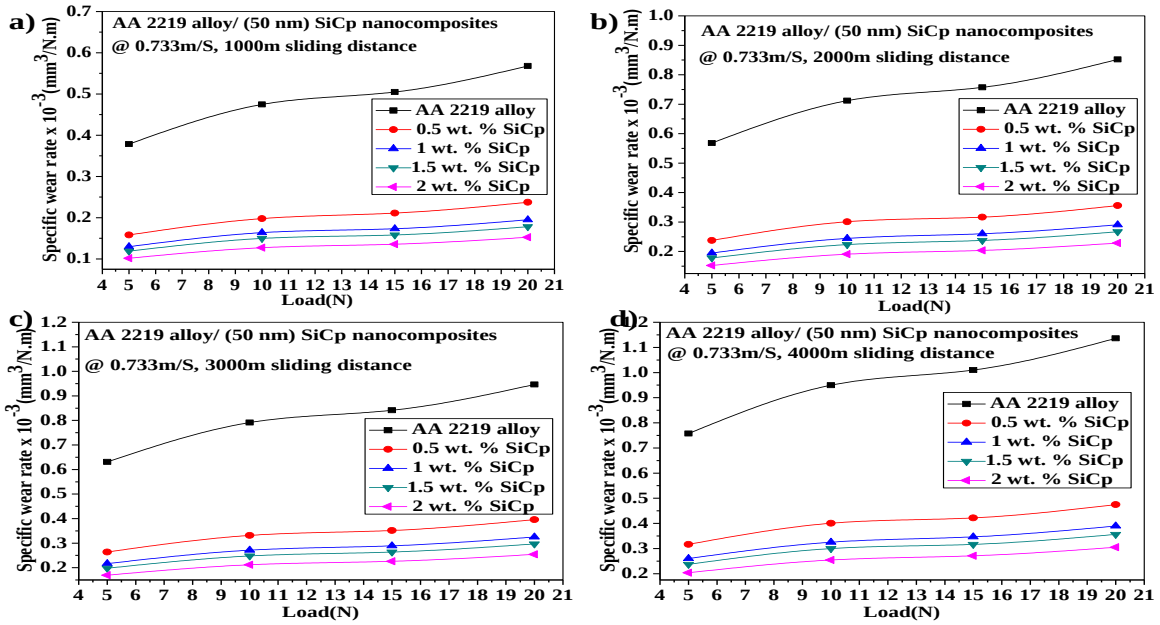

Figure 6.8 Variation of specific wear rate of AA2219 alloy and its nano SiC based MMNCs a) at 1000 m sliding distance b) at 2000 m sliding distance c) at 3000 m sliding distance d) at 4000 m sliding distance, with an applied load of 5 N to 20 N and constant sliding velocity 0.733 m/s.

6.1.5 Coefficient of Friction of AA2219/SiC /50 nm/ Nanocomposite

The variation in coefficient of friction of AA2219/SiC/50 nm nanocomposites with sliding distance is shown in Figure 6.9 a,b,c&d for sliding distance 1km,2km,3km&4km AA2219/SiC/50 nm MMNC obeys the law of static and dynamic friction as friction coefficient is observed to be decreases with increase in sliding distance. The coefficient of friction of the metal matrix nanocomposites was observed at all the sliding distances and concluded that the coefficient of friction is more when compared with base material.

The variation in coefficient of friction with load is shown in Figure 6.10 a,b,c&d for 5 N,10 N,15 N&20 N respectively. As shown in Figure 6.10 a,b,c&d the coefficient of friction of the AA2219/SiC/50 nm metal matrix nanocomposites was observed at all the applied loads and concluded that the coefficient of friction of MMNCs increases with load. The coefficient of friction was increased while increasing the weight percentage of nano SiC in the base alloy. This obeys the law of friction.

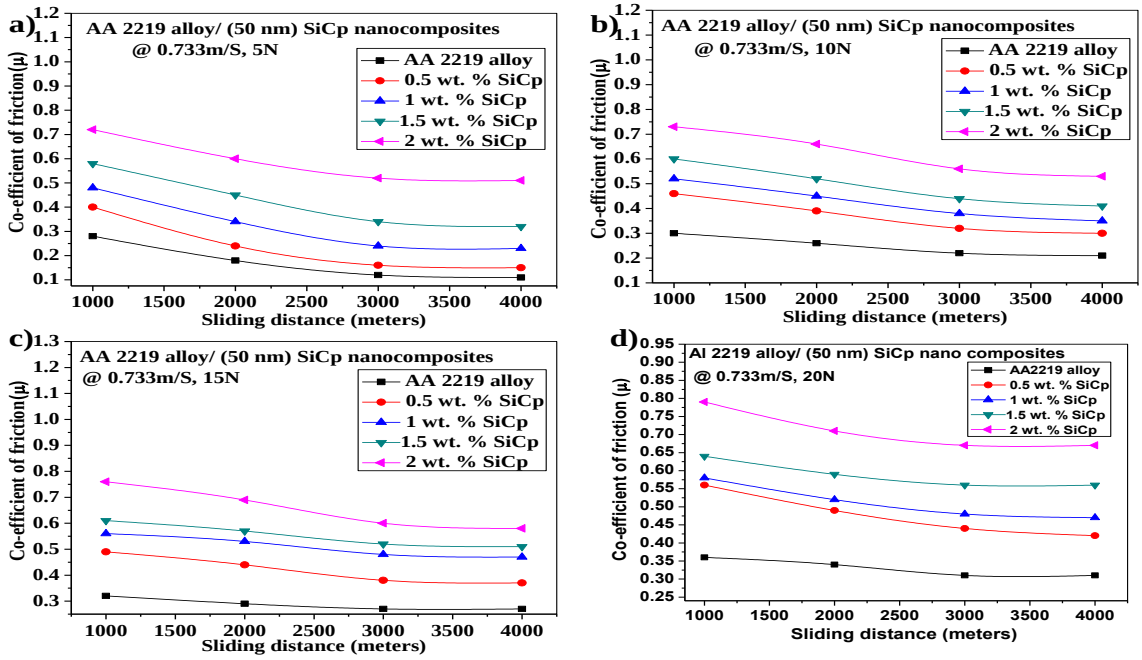

Figure 6.9 Variation of COF AA2219 alloy and its SiC Nano Composites a) at 5 N load b) at 10 N load c) at 15 N load d) at 20 N load, with sliding distance of 1000 m to 4000 m and at constant sliding velocity of 0.733 m/S.

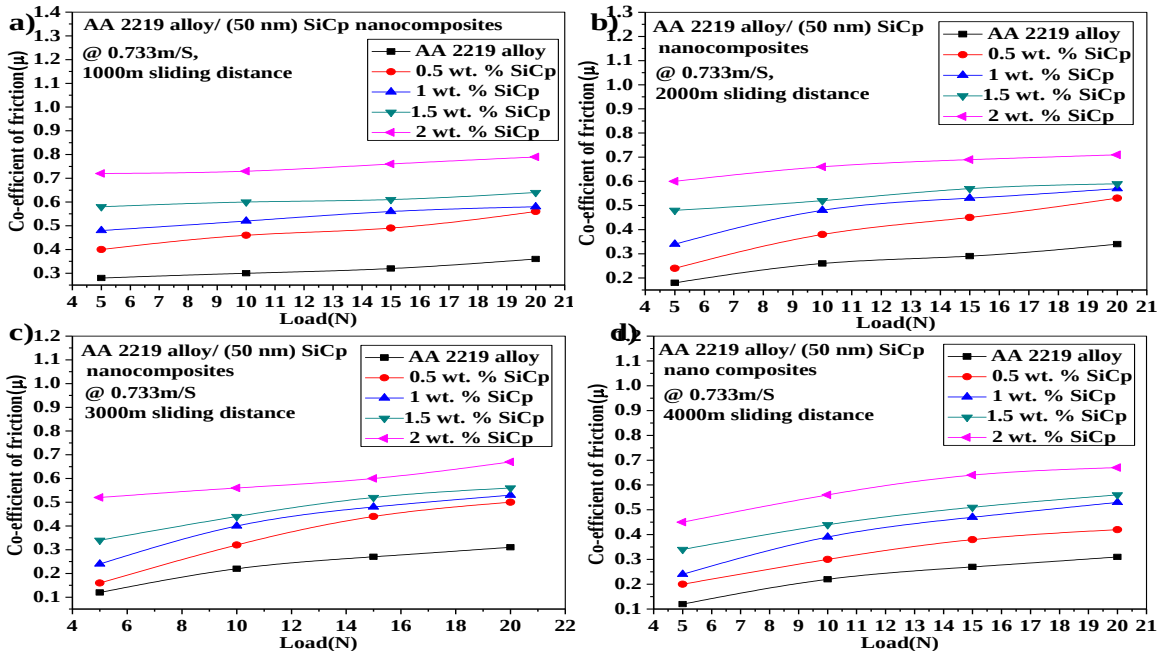

Figure 6.10 Variation of COF of AA2219 alloy and its SiC Nano Composites a) at 1000 m sliding distance b) at 2000 m sliding distance c) at 3000 m sliding distance d) at 4000 m sliding distance, with an applied load of 5 N to 20 N, and at constant sliding velocity 0.733 m/s.

6.2 Wear Resistance Properties of AA2219/Al_2O_3/50 nm Nanocomposites

6.2.1 Volume of Wear AA 2219/Al_2O_3 /50 nm Nano Composite

The variation in the volume of wear with sliding distance under different loads are shown in Figure 6.11 a,b,c&d . The cast AA 2219/Al_2O_3/50 nm MMNC undergo higher volume of wear with an increase in sliding distance. The volume of wear of AA2219/Al_2O_3/50 nm the metal matrix nanocomposites was observed at all the sliding distances and concluded that the volume of wear of MMNC was less when compared with base MMC. The volume of wear was reduced while increasing the weight percentage of nano Al_2O_3 in the base alloy. The variation in the volume of wear with an applied load is shown in Figure 6.12 a,b,c&d at sliding distances of 1km,2km,3km&4km respectively. The cast AA2219 and its nano Al_2O_3 reinforced metal matrix nanocomposites undergo higher volume of wear with an increase in applied load.

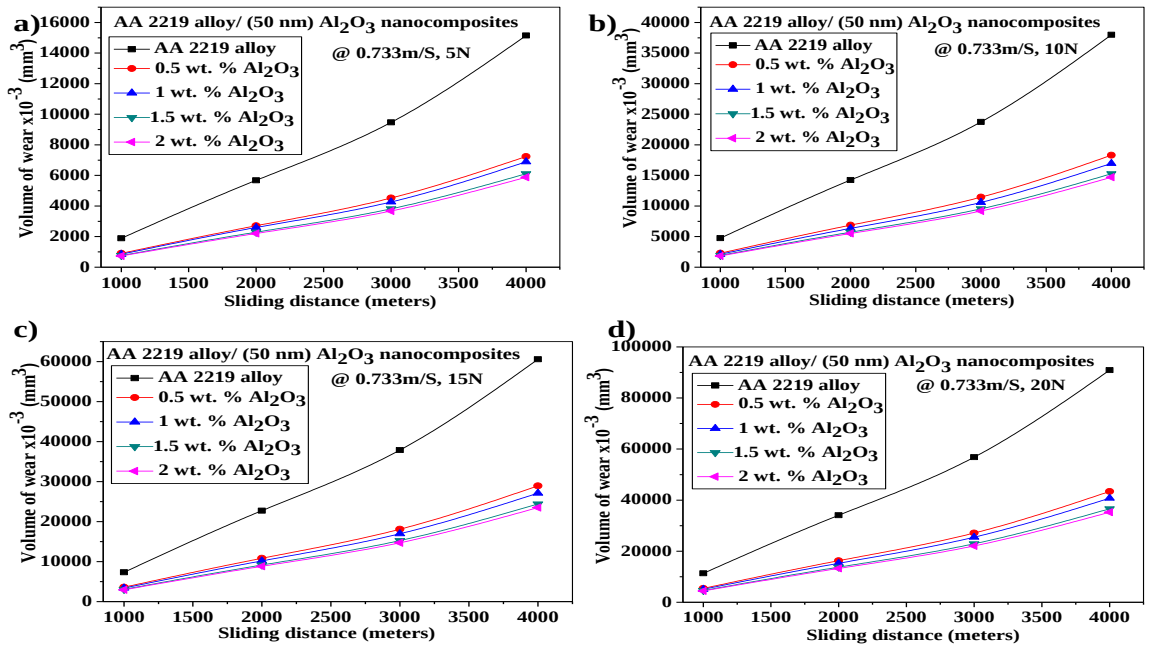

Figure 6.11 Variation of the volume of wear AA2219 alloy and its nano Al_2O_3 based MMNCs a) at 5 N load b) at 10 N load c) at 15 N load d) at 20 N load, with sliding distance of 1000 to 4000 m, at a constant sliding velocity of 0.733 m/s

The volume of wear of the metal matrix nanocomposites was observed at all the applied loads and concluded that the volume of wear of AA2219/ Al_2O_3/50 nm composite was less when compared with base MMC. The volume of wear was reduced while increasing the weight percentage of nano Al_2O_3 in the base alloy and it is shown in Figures

6.12. In all these results sliding velocity kept constant (SV=0.733m/s). The reasons for all these works are well known fact established in literature. As the wt.% of particulate Al_2O_3 increase in AA2219 the hardness and strength were increasing hence resistance to wear is also increases.

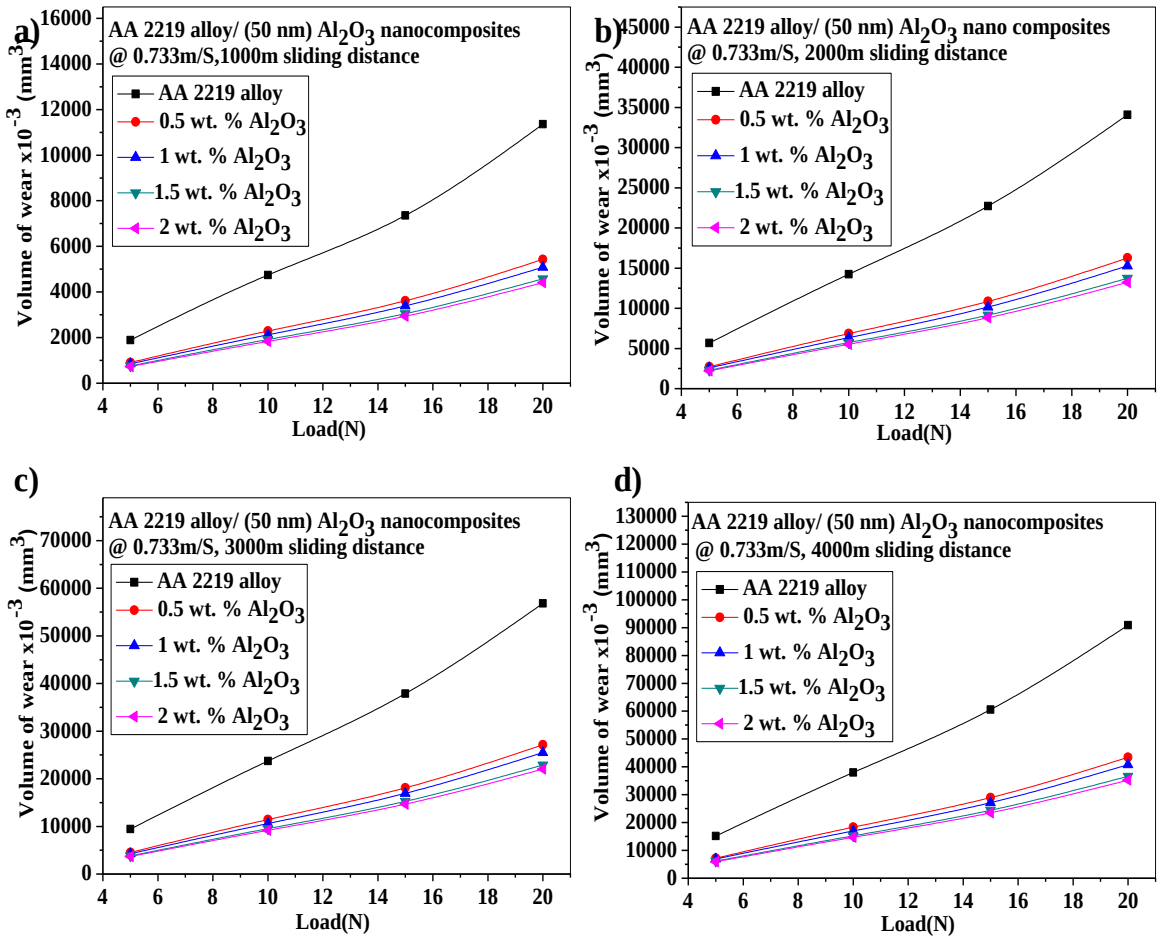

Figure 6.12 Variation of the volume of wear AA 2219 alloy and its nano Al_2O_3 based MMNCs a) at 1000 m sliding distance b) at 2000 m sliding distance c) at 3000 m sliding distance d) at 4000 m sliding distance, with an applied load of 5 N to 20 N, at constant sliding velocity 0.733 m/s.

6.2.2 Wear Height AA 2219/Al_2O_3 /50 nm Nanocomposite

The variation in the wear height with sliding distance under different loads are shown in Figure 6.13 a,b,c&d . The cast AA2219/Al_2O_3/50 nm MMNC undergo higher loss in wear height with an increase in sliding distance. The wear height of AA2219/Al_2O_3/50 nm the metal matrix nanocomposites was observed at all the sliding distances and concluded that the wear height of MMNC was less when compared with base MMC. The loss of wear height was reduced while increasing the weight

percentage of nano Al_2O_3 in the base alloy. The variation in the wear height with an applied load is shown in Figure 6.14 a,b,c&d at sliding distances of 1km,2km,3km&4km respectively. The cast AA2219and its nano Al_2O_3 reinforced metal matrix nanocomposites undergo higher loss of wear height with an increase in applied load. The wear height of the metal matrix nanocomposites was observed at all the applied loads and concluded that the loss of wear height of AA2219/ Al_2O_3/50 nm composite was less when compared with base MMC. The loss of wear height was reduced while increasing the weight percentage of nano Al_2O_3 in the base alloy and it is shown in Figures 6.14. In all these results sliding velocity kept constant (SV=0.733m/s). The reasons for all these works are well known fact established in literature. As the wt.% of particulate Al_2O_3 increase in AA2219 the hardness and strength were increasing hence resistance to wear is also increases.

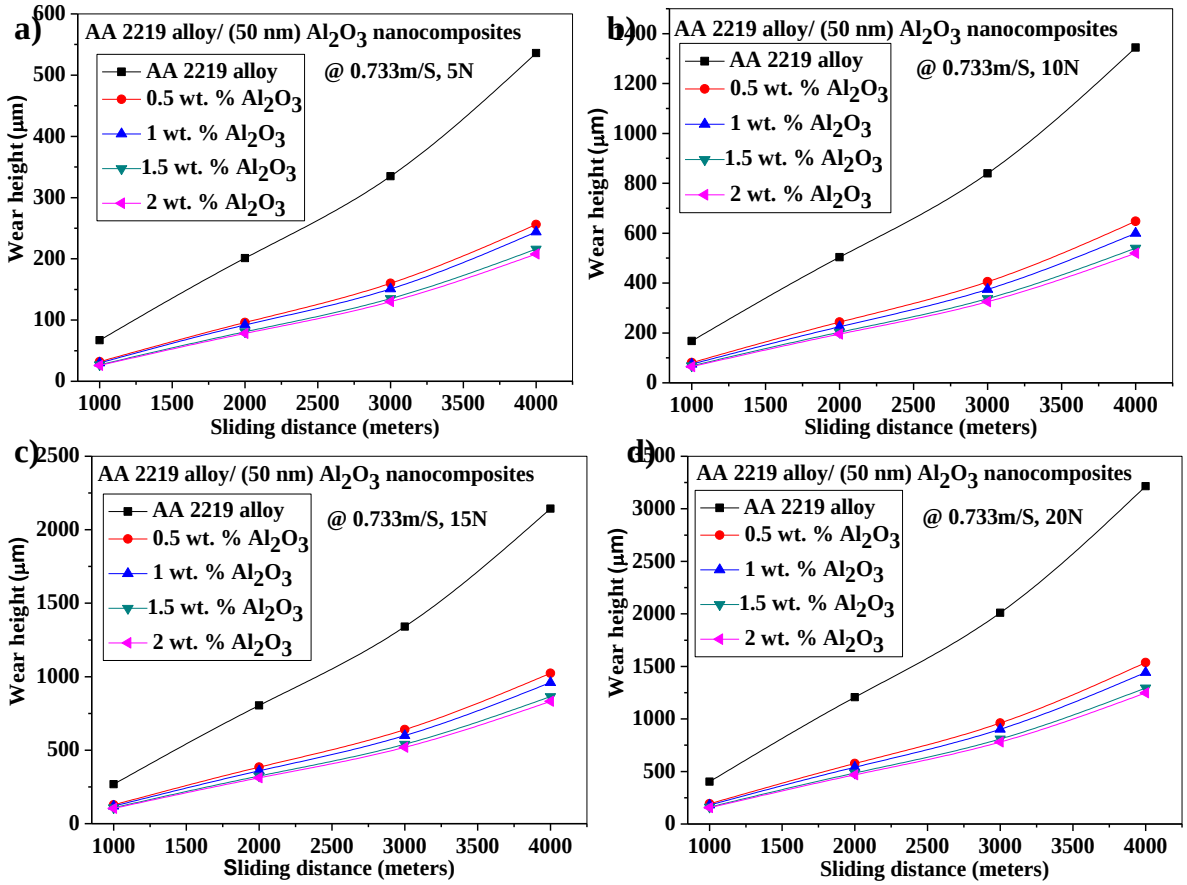

Figure 6.13 Variation of wear height AA 2219 alloy and its nano Al_2O_3 based MMNCs a) at 5 N load b) at 10 N load c) at 15 N load d) at 20 N load, with sliding distance of 1000 m to 4000 m, at constant sliding velocity of 0.733 m/s.

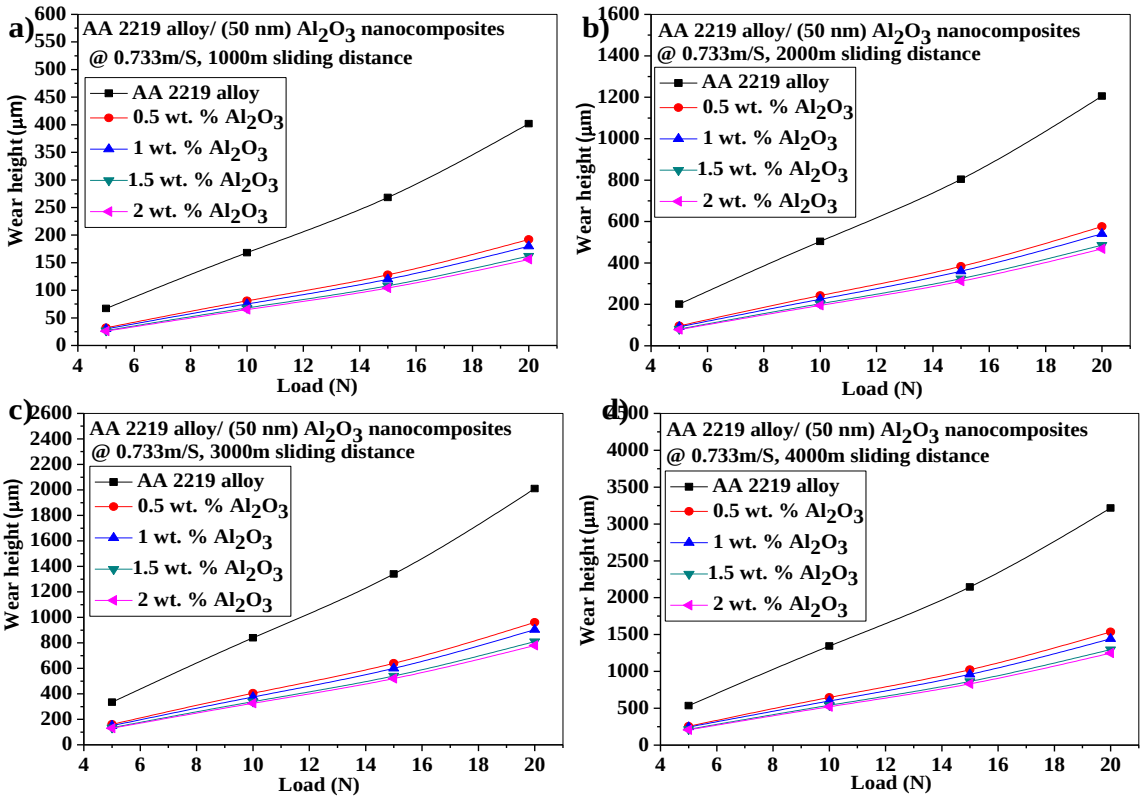

Figure 6.14 Variation of wear height of AA 2219 alloy and its nano Al_2O_3 based MMNCs a) at 1000 m sliding distance b) at 2000 m sliding distance c) at 3000 m sliding distance d) at 4000 m sliding distance, with an Applied load of 5 N to 20 N & at constant Sliding Velocity 0.733 m/s.

6.2.3 Wear Weight Loss AA2219/Al_2O_3 /50 nm Nanocomposite

The variation in the wear weight loss with sliding distance under different loads are shown in Figure 6.15 a,b,c&d . The cast AA2219/Al_2O_3/50 nm MMNC undergo higher wear weight loss with an increase in sliding distance. The wear weight loss of AA2219/ Al_2O_3/50 nm the metal matrix nanocomposites was observed at all the sliding distances and concluded that the wear weight loss of MMNC was less when compared with base MMC. The wear weight loss was reduced while increasing the weight percentage of nano Al_2O_3 in the base alloy. The variation in the wear weight loss with an applied load is shown in Figure 6.16 a,b,c&d at sliding distances of 1Km,2Km,3Km&4Km respectively. The cast AA2219and its nano Al_2O_3 reinforced metal matrix nanocomposites undergo higher wear weight loss with an increase in applied load. The wear weight loss of the metal matrix nanocomposites was observed at all the applied loads and concluded that the wear weight loss of AA2219/ Al_2O_3/50 nm composite was less when compared with base

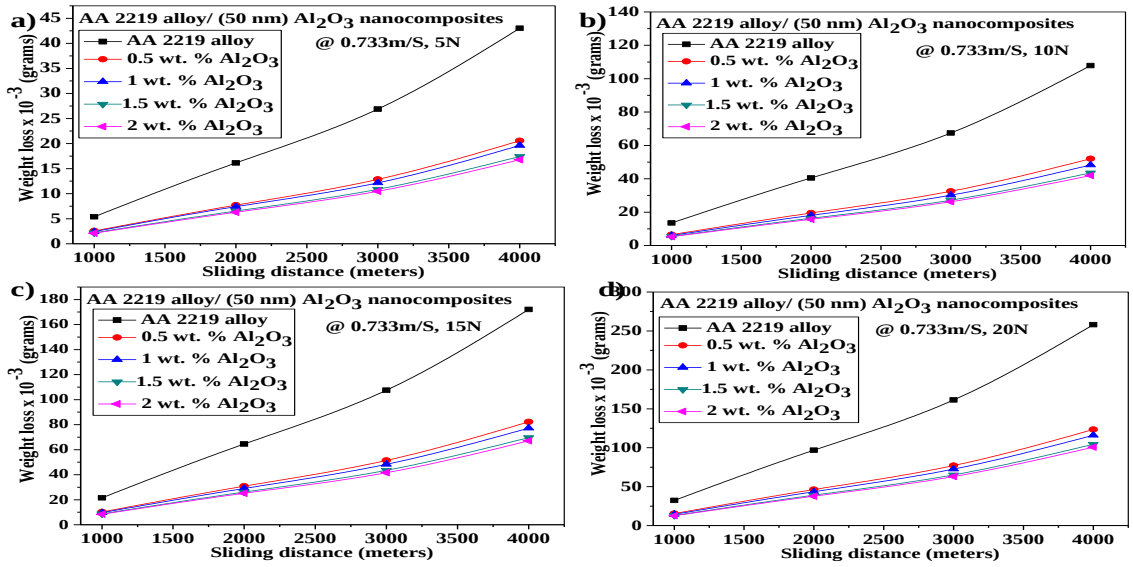

Figure 6.15 Variation of wear weight loss AA2219 alloy and its nano Al_2O_3 based MMNCs a) at 5 N load b) at 10 N load c) at 15 N load d) at 20 N load, with sliding distance of 1000 m to 4000 m and at constant sliding velocity of 0.733 m/s.

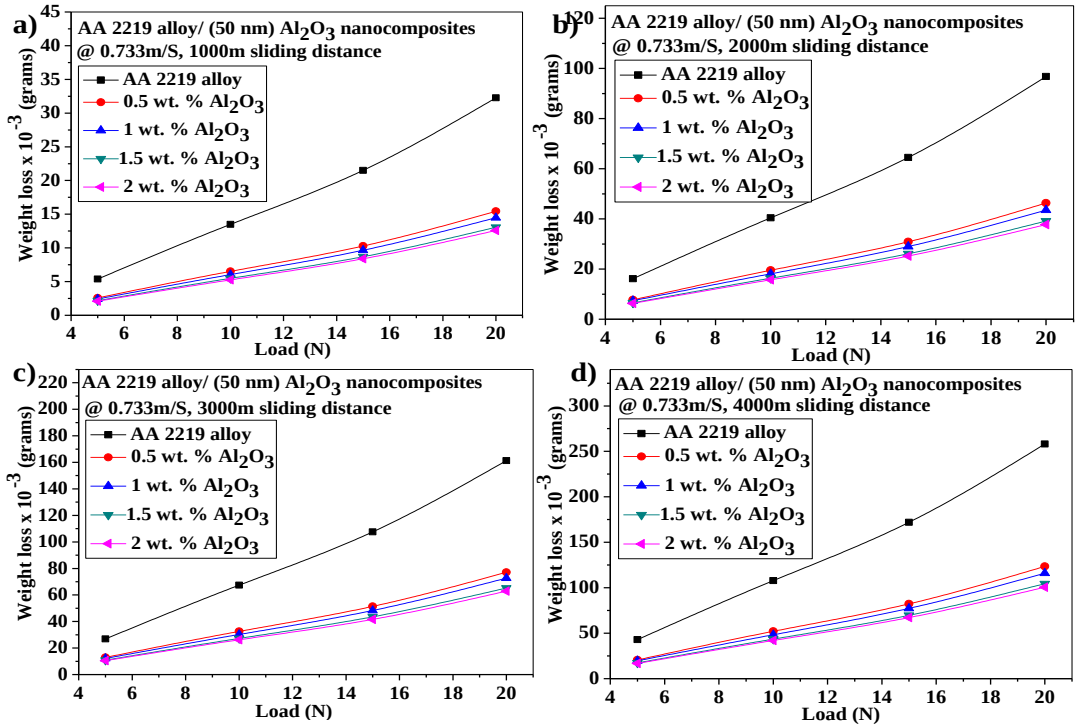

Figure 6.16 Variation of wear weight loss of AA2219 alloy and its nano Al_2O_3 MMNCs a) at 1000 m sliding distance b) at 2000 m sliding distance c) at 3000 m sliding distance d) at 4000 m sliding distance, with an applied load of 5 N to 20 N, and constant sliding velocity 0.733 m/s.

MMC. The wear weight loss was reduced while increasing the weight percentage of nano Al_2O_3 in the base alloy and it is shown in Figures 6.16. In all these results sliding velocity kept constant (SV=0.733m/s). The reasons for all these works are well known fact established in literature. As the wt.% of particulate Al_2O_3 increase in AA2219 the hardness and strength were increasing hence resistance to wear is also increases.

6.2.4 Specific Wear Rate AA 2219/Al_2O_3/50 nm Nanocomposites

The variation in the specific wear rate with sliding distance under different loads are shown in Figure 6.17 a,b,c&d . The cast AA2219/Al_2O_3/50 nm MMNC undergo higher specific wear rate with an increase in sliding distance. The specific wear rate of AA2219/ Al_2O_3/50 nm the metal matrix nanocomposites was observed at all the sliding distances and concluded that the specific wear rate of MMNC was less when compared with base MMC.

The specific wear rate was reduced while increasing the weight percentage of nano Al_2O_3 in the base alloy. The variation in the specific wear rate with an applied load is shown in Figure 6.18 a,b,c&d at sliding distances of 1Km,2Km,3Km&4Km respectively. The cast AA2219 and its nano Al_2O_3 reinforced metal matrix nanocomposites undergo higher specific wear rate with an increase in applied load. The specific wear rate of the metal matrix nanocomposites was observed at all the applied loads and concluded that the specific wear rate of AA2219/ Al_2O_3/50 nm composite was less when compared with base MMC.

The specific wear rate was reduced while increasing the weight percentage of nano Al_2O_3 in the base alloy and it is shown in Figures 6.18. In all these results sliding velocity kept constant (SV=0.733m/s).

The reasons for all these works are well known fact established in literature. As the wt.% of particulate Al_2O_3 increase in AA2219 the hardness and strength were increasing hence resistance to wear is also increases.

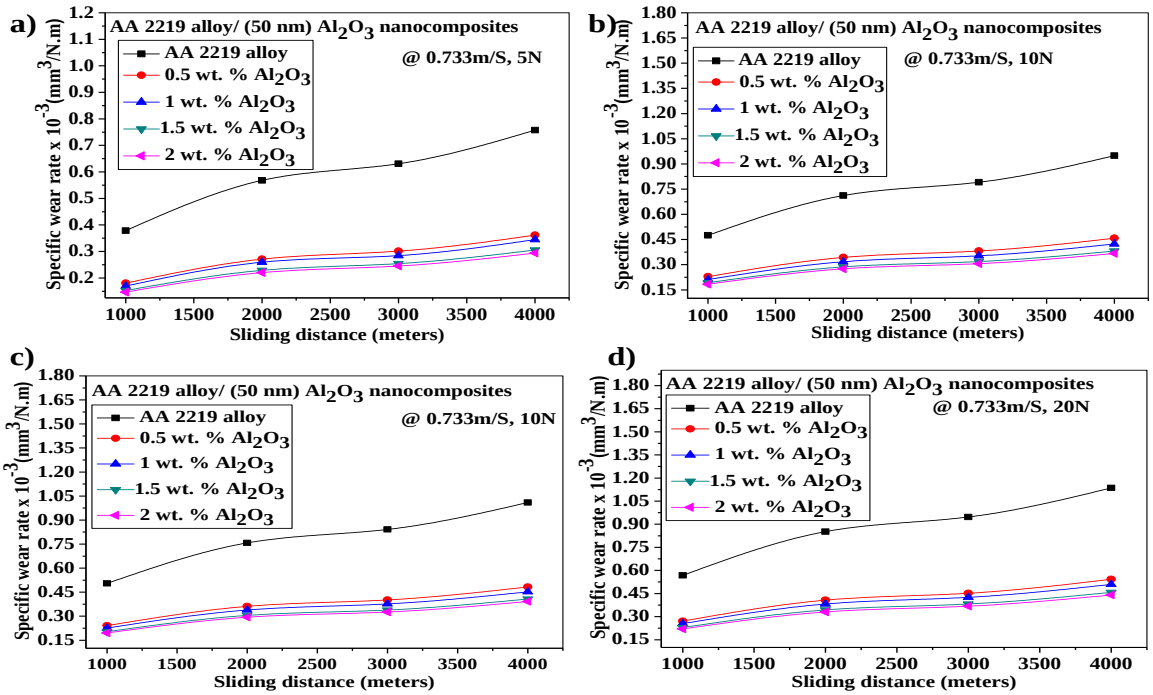

Figure 6.17 Variation of specific wear rate AA2219 alloy and its nano Al_2O_3 based MMNCs a) at 5 N load b) at 10 N load c) at 15 N load d) at 20 N load, with sliding distance of 1000 m to 4000 m and at constant sliding velocity of 0.733 m/s.

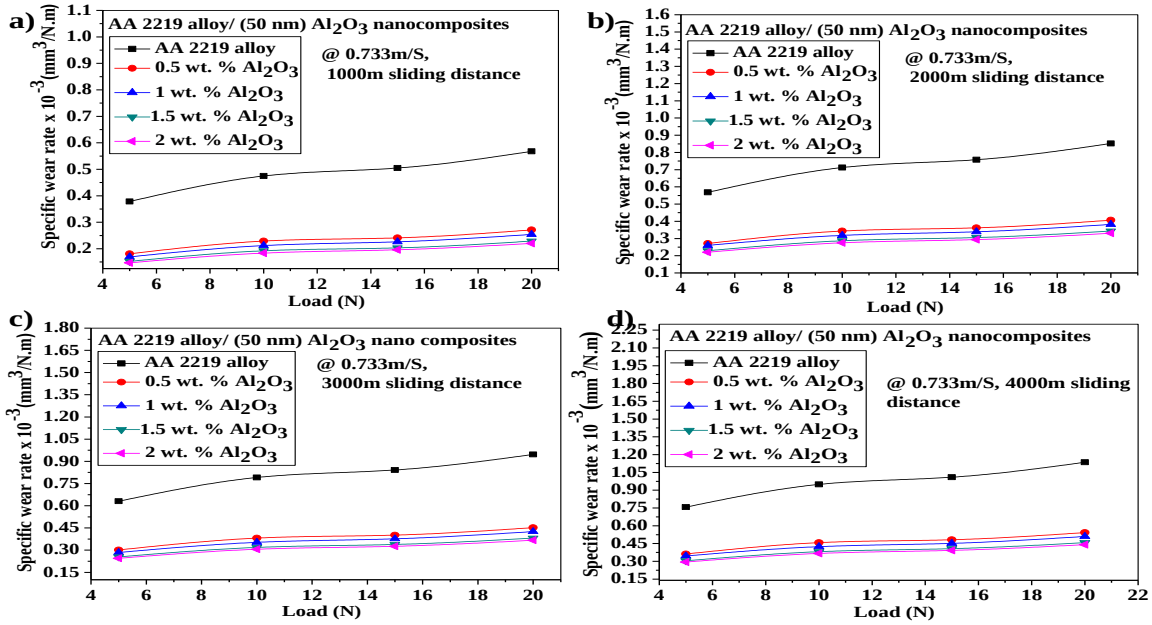

Figure 6.18 Variation of specific wear rate of AA2219 alloy and its nano Al_2O_3 based MMNCs a) at 1000 m sliding distance b) at 2000 m sliding distance c) at 3000 m sliding distance d) at 4000 m sliding distance, with an applied load of 5 N to 20 N and constant sliding velocity 0.733 m/s.

6.2.5 Coefficient of Friction of AA 2219/Al_2O_3/50 nm Nanocomposites

The variation in coefficient of friction of AA2219/Al_2O_3/50 nm nanocomposites with sliding distance is shown in Figure 6.19 a,b,c&d for sliding distance 1Km,2Km,3Km and 4Km AA2219/ Al_2O_3/50 nm MMNC obeys the law of static and dynamic friction as friction coefficient is observed to be decreases with increase in sliding distance. The coefficient of friction of the metal matrix nanocomposites was observed at all the sliding distances and concluded that the coefficient of friction is more when compared with base material. The variation in coefficient of friction with load is shown in Figure 6.20 a,b,c&d for 5 N,10 N,15 N&20 N respectively. As shown in Figure 6.20 a,b,c&d the coefficient of friction of the AA2219/Al_2O_3/50 nm metal matrix nanocomposites was observed at all the applied loads and concluded that the coefficient of friction of MMNCs increases with load. The coefficient of friction was increased while increasing the weight percentage of nano Al_2O_3 in the base alloy. This obeys the law of friction.

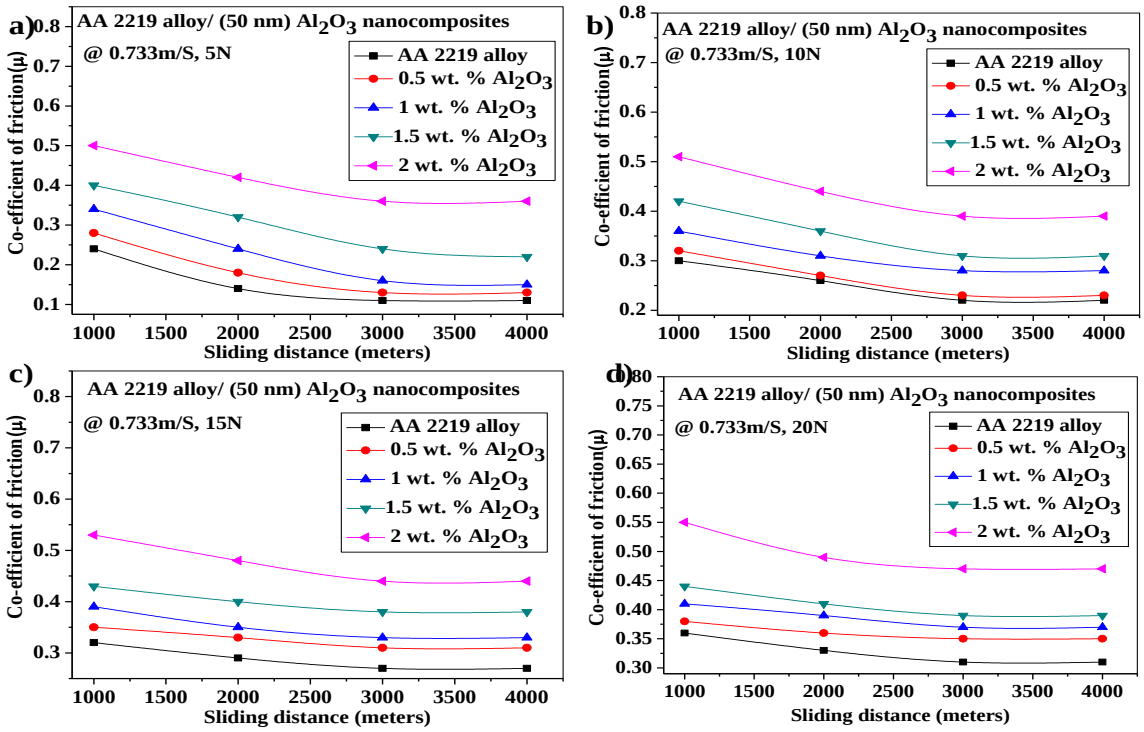

Figure 6.19 Variation of COF AA2219 alloy and its Al_2O_3 Nano Composites a) at 5 N load b) at 10 N load c) at 15 N load d) at 20 N load, with sliding distance of 1000 m to 4000 m and at constant sliding velocity of 0.733 m/s.

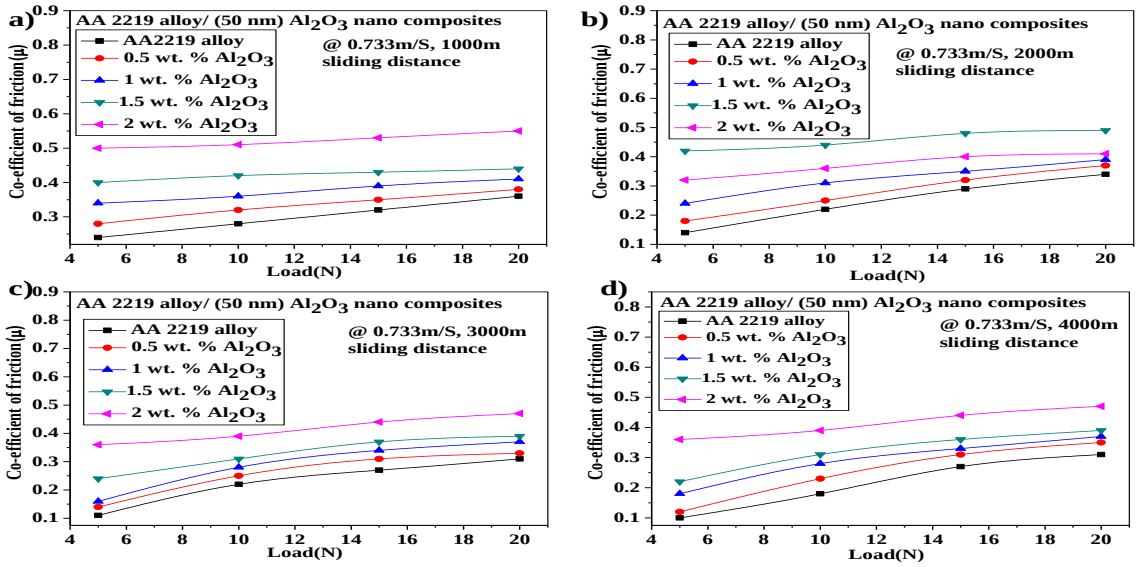

Figure 6.20 Variation of COF of AA2219 alloy and its Al_2O_3 Nano Composites a) at 1000 m sliding distance b) at 2000 m sliding distance c) at 3000 m sliding distance d) at 4000 m sliding distance, with an applied load of 5 N to 20 N, and at constant sliding velocity 0.733 m/s.

6.3 Wear Resistance Properties of AA2219/SiC/150 nm Nanocomposites

6.3.1 Volume of Wear AA 2219/SiC/150 nm Nanocomposites

The variation in the volume of wear with sliding distance under different loads are shown in Figure 6.21 a,b,c&d . The cast AA 2219/SiC/150 nm MMNC undergo higher volume of wear with an increase in sliding distance. The volume of wear of AA2219/SiC/150 nm the metal matrix nanocomposites was observed at all the sliding distances and concluded that the volume of wear of MMNC was less when compared with base MMC. The volume of wear was reduced while increasing the weight percentage of nano SiC in the base alloy. The variation in the volume of wear with an applied load is shown in Figure 6.22 a,b,c&d at sliding distances of 1Km,2Km,3Km&4Km respectively. The cast AA2219 and its nano SiC reinforced metal matrix nanocomposites undergo higher volume of wear with an increase in applied load. The volume of wear of the metal matrix nanocomposites was observed at all the applied loads and concluded that the volume of wear of AA2219/SiC/150 nm composite was less when compared with base MMC. The volume of wear was reduced while increasing the weight percentage of nano SiC in the base alloy and it is shown in Figures 6.22. In all these results sliding velocity kept constant (SV=0.733m/s). The reasons for all these works are well known fact established in literature.

As the wt.% of particulate SiC increase in AA2219 the hardness and strength were increasing hence resistance to wear is also increases.

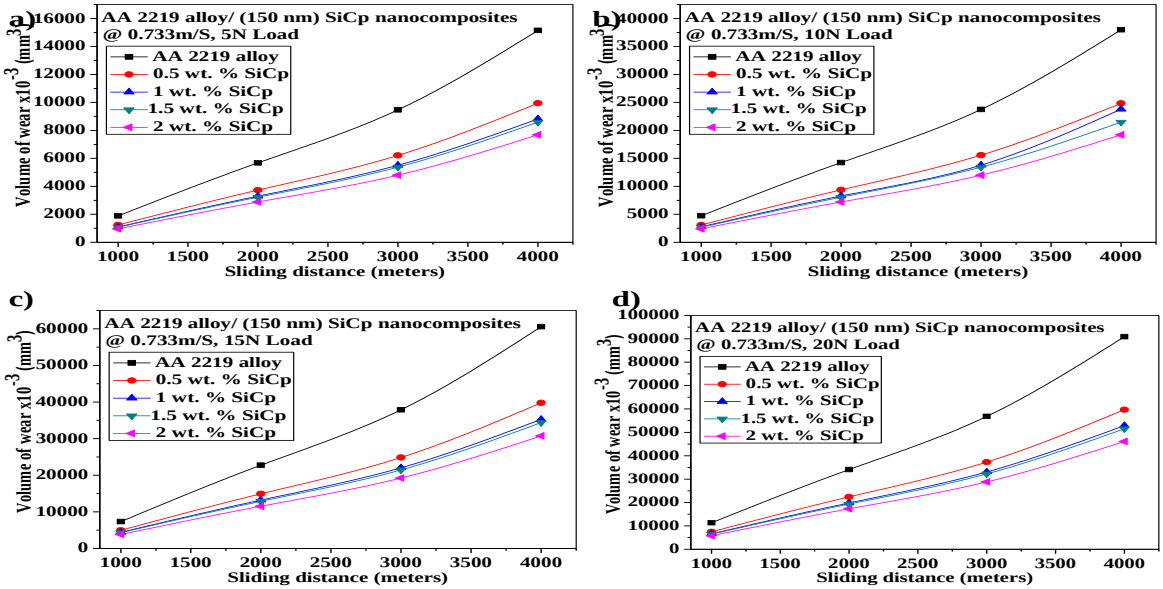

Figure 6.21 Variation of the volume of wear AA 2219 alloy and its nano SiC based MMNCs a) at 5 N load b) at 10 N load c) at 15 N load d) at 20 N load, with sliding distance of 1000 to 4000 m, at a constant sliding velocity of 0.733 m/s.

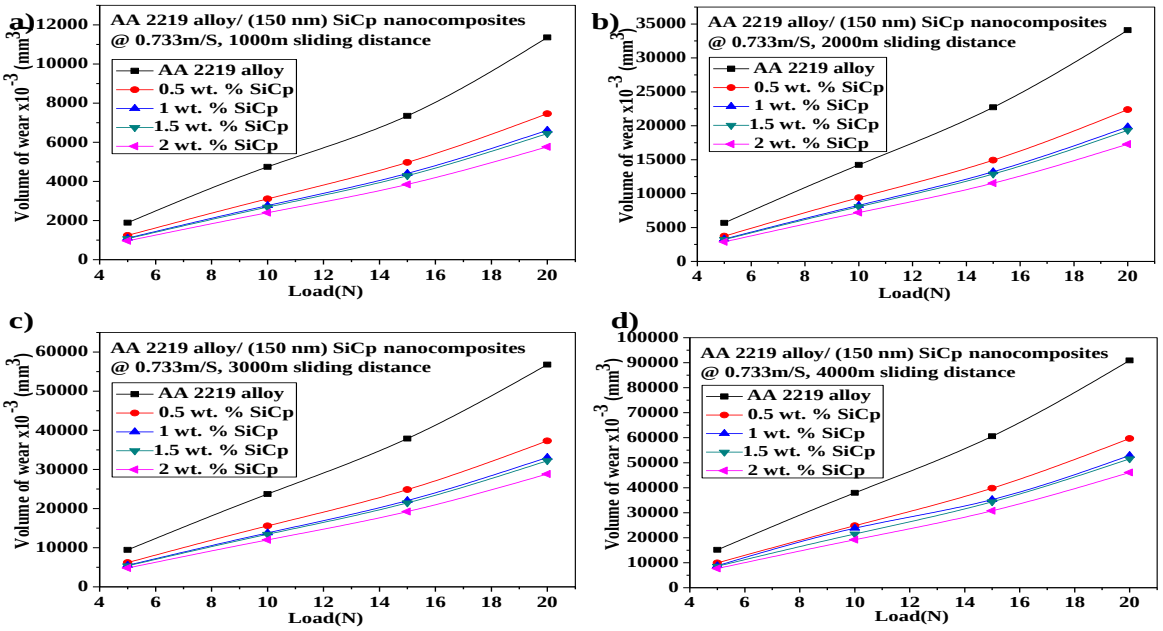

Figure 6.22 Variation of the volume of wear AA 2219 alloy and its nano SiC based MMNCs a) at 1000 m sliding distance b) at 2000 m sliding distance c) at 3000 m sliding distance d) at 4000 m sliding distance, with an applied load of 5 N to 20 N, at constant sliding velocity 0.733 m/s.

6.3.2 Wear Height AA 2219/SiC/150 nm Nanocomposites

The variation in the wear height with sliding distance under different loads are shown in Figure 6.23 a,b,c&d . The cast AA2219/SiC/150 nm MMNC undergo higher loss in wear height with an increase in sliding distance. The wear height of AA2219/SiC/150 nm the metal matrix nanocomposites was observed at all the sliding distances and concluded that the wear height of MMNC was less when compared with base MMC. The loss of wear height was reduced while increasing the weight percentage of nano SiC in the base alloy. The variation in the wear height with an applied load is shown in Figure 6.24 a,b,c&d at sliding distances of 1Km,2Km,3Km&4Km respectively. The cast AA2219and its nano SiC reinforced metal matrix nanocomposites undergo higher loss of wear height with an increase in applied load. The wear height of the metal matrix nanocomposites was observed at all the applied loads and concluded that the loss of wear height of AA2219/SiC/150 nm composite was less when compared with base MMC. The loss of wear height was reduced while increasing the weight percentage of nano SiC in the base alloy and it is shown in Figures 6.24. In all these results sliding velocity kept constant (SV=0.733m/s). The reasons for all these works are well known fact established in literature. As the wt.% of particulate SiC increase in AA2219 the hardness and strength were increasing hence resistance to wear is also increases.

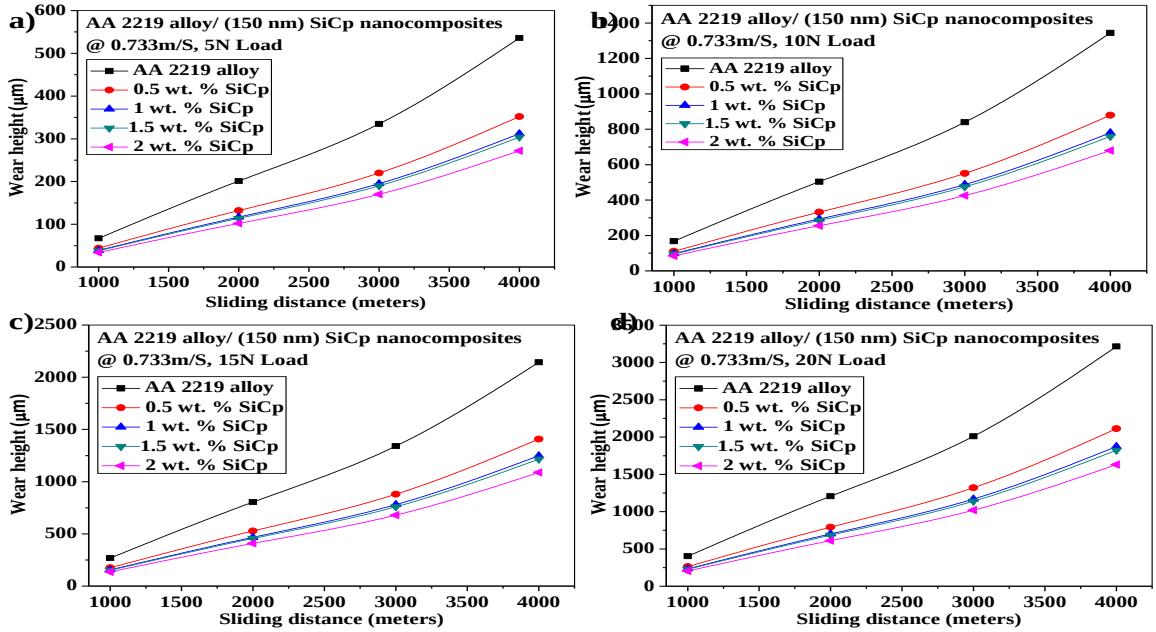

Figure 6.23 Variation of wear height AA 2219 alloy and its nano SiC based MMNCs a) at 5 N load b) at 10 N load c) at 15 N load d) at 20 N load, with sliding distance of 1000 m to 4000 m, at constant sliding velocity of 0.733 m/s.

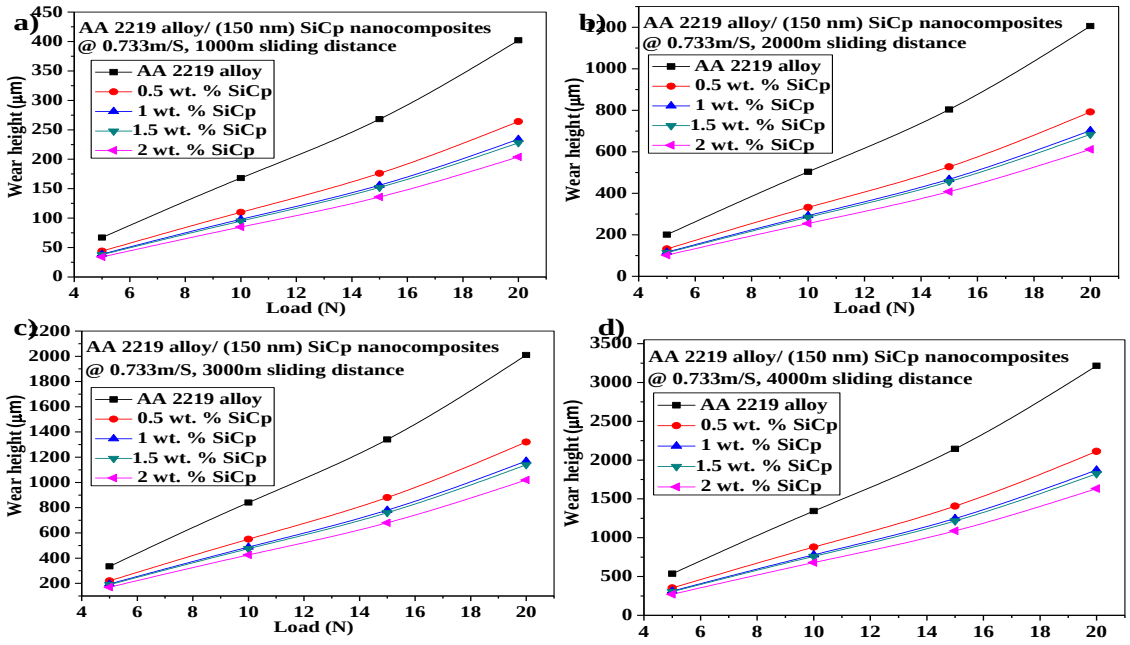

Figure 6.24 Variation of wear height of AA 2219 alloy and its nano SiC based MMNCs a) at 1000 m sliding distance b) at 2000 m sliding distance c) at 3000 m sliding distance d) at 4000 m sliding distance, with an Applied load of 5 N to 20 N & at constant Sliding Velocity 0.733 m/s.

6.3.3 Wear Weight Loss AA 2219/SiC /150 nm Nanocomposite

The variation in the wear weight loss with sliding distance under different loads are shown in Figure 6.25 a,b,c&d . The cast AA2219/SiC/150 nm MMNC undergo higher wear weight loss with an increase in sliding distance. The wear weight loss of AA2219/SiC/150 nm the metal matrix nanocomposites was observed at all the sliding distances and concluded that the wear weight loss of MMNC was less when compared with base MMC. The wear weight loss was reduced while increasing the weight percentage of nano SiC in the base alloy. The variation in the wear weight loss with an applied load is shown in Figure 6.26 a,b,c&d at sliding distances of 1Km,2Km,3Km&4Km respectively. The cast AA2219and its nano SiC reinforced metal matrix nanocomposites undergo higher wear weight loss with an increase in applied load. The wear weight loss of the metal matrix nanocomposites was observed at all the applied loads and concluded that the wear weight loss of AA2219/SiC/150 nm composite was less when compared with base MMC. The wear weight loss was reduced while increasing the weight percentage of nano SiC in the base alloy and it is shown in Figures 6.26. In all these results sliding velocity kept constant (SV=0.733m/s). The reasons for all these works are well known fact established in literature.

As the wt.% of particulate SiC increase in AA2219 the hardness and strength were increasing hence resistance to wear is also increases.

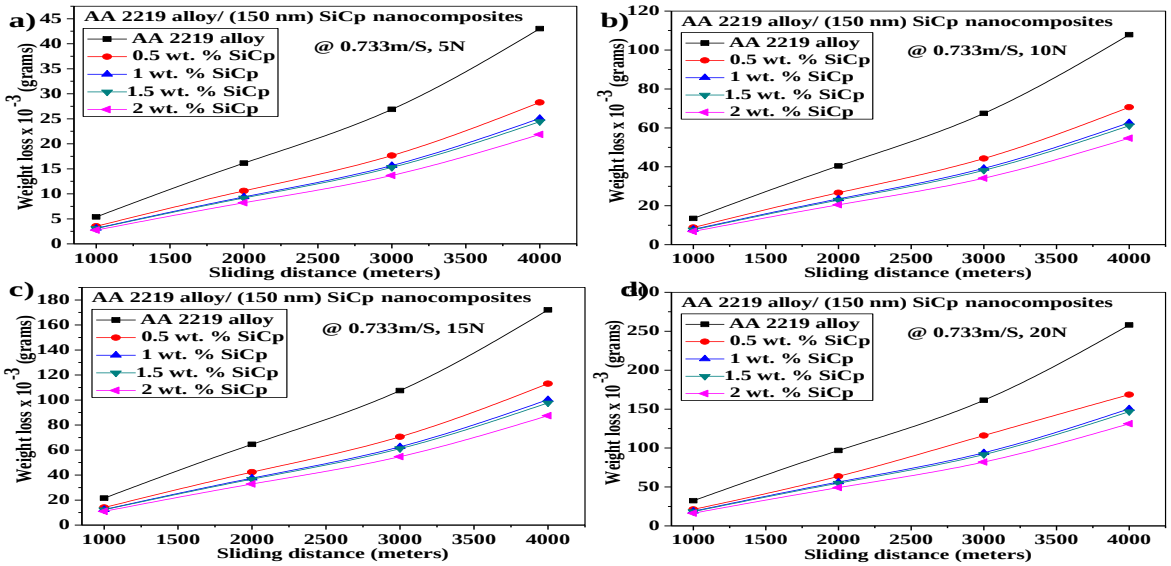

Figure 6.25 Variation of wear weight loss AA2219 alloy and its nano SiC based MMNCs a) at 5 N load b) at 10 N load c) at 15 N load d) at 20 N load, with sliding distance of 1000 m to 4000 m and at constant sliding velocity of 0.733 m/s.

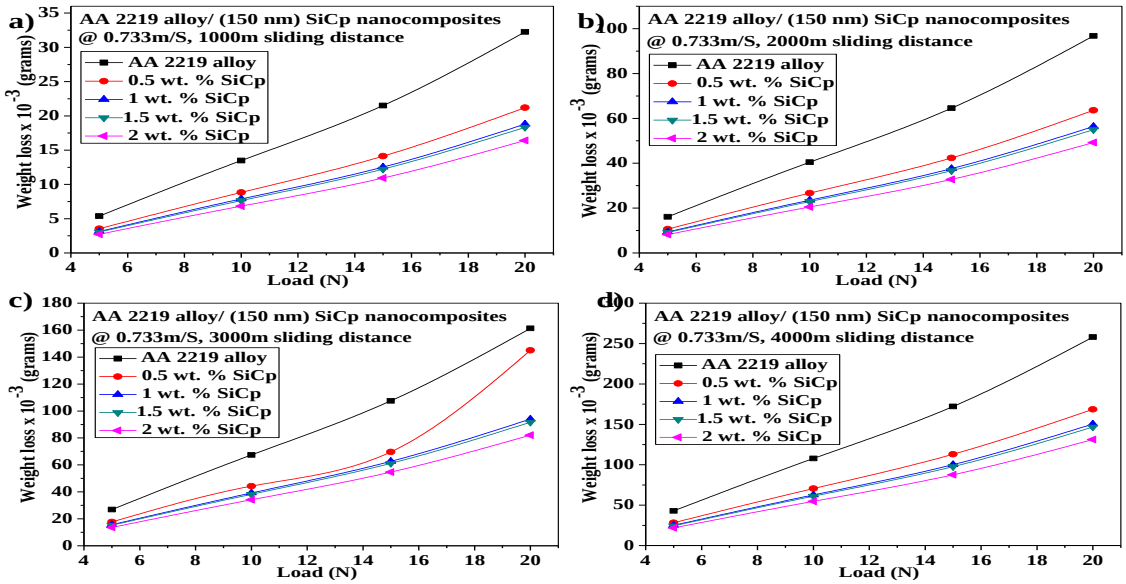

Figure 6.26 Variation of wear weight loss of AA2219 alloy and its nano SiC MMNCs a) at 1000 m sliding distance b) at 2000 m sliding distance c) at 3000 m sliding distance d) at 4000 m sliding distance, with an applied load of 5 N to 20 N, and constant sliding velocity 0.733 m/s.

6.3.4 Specific Wear Rate AA 2219/SiC/150 nm Nanocomposite

The variation in the specific wear rate with sliding distance under different loads are shown in Figure 6.27 a,b,c&d . The cast AA2219/SiC/150 nm MMNC undergo higher specific wear rate with an increase in sliding distance. The specific wear rate of AA2219/SiC/150 nm the metal matrix nanocomposites was observed at all the sliding distances and concluded that the specific wear rate of MMNC was less when compared with base MMC.

The specific wear rate was reduced while increasing the weight percentage of nano SiC in the base alloy. The variation in the specific wear rate with an applied load is shown in Figure 6.28 a,b,c&d at sliding distances of 1Km,2Km,3Km&4Km respectively. The cast AA2219 and its nano SiC reinforced metal matrix nanocomposites undergo higher specific wear rate with an increase in applied load.

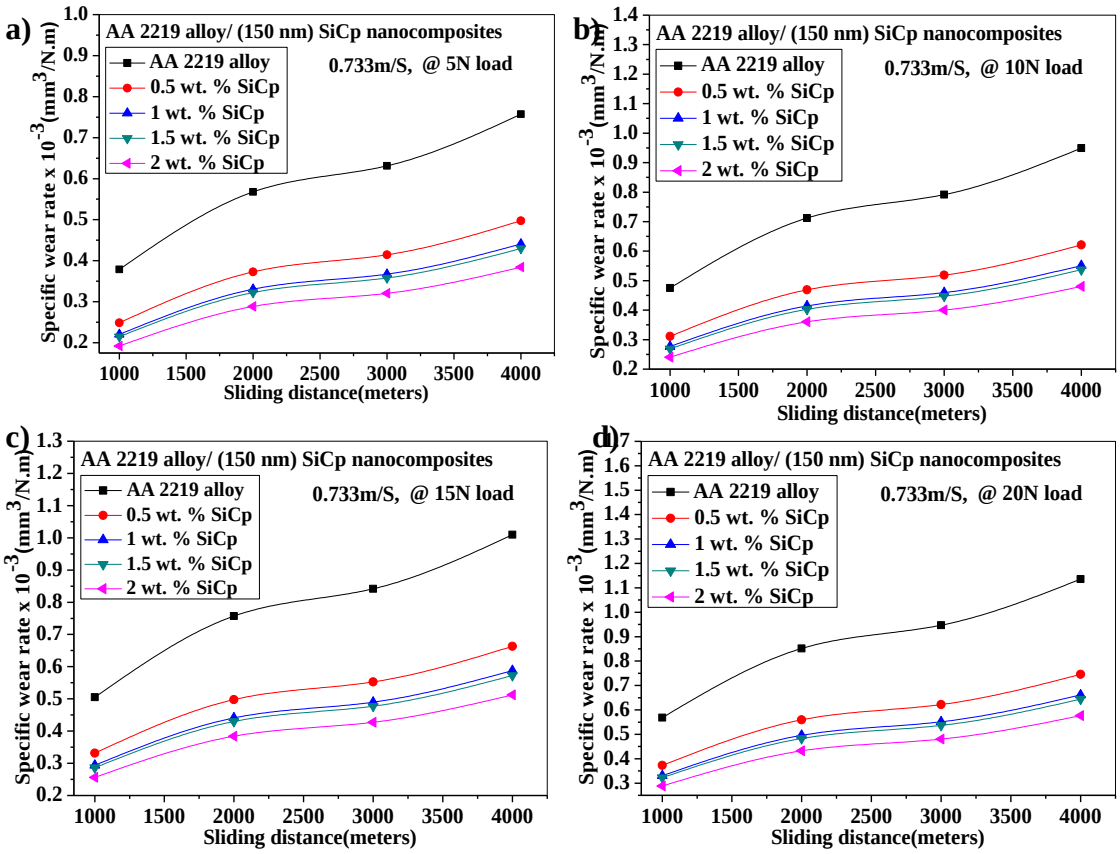

Figure 6.27 Variation of specific wear rate AA2219 alloy and its nano SiC based MMNCs a) at 5 N load b) at 10 N load c) at 15 N load d) at 20 N load, with sliding distance of 1000 m to 4000 m and at constant sliding velocity of 0.733 m/s.

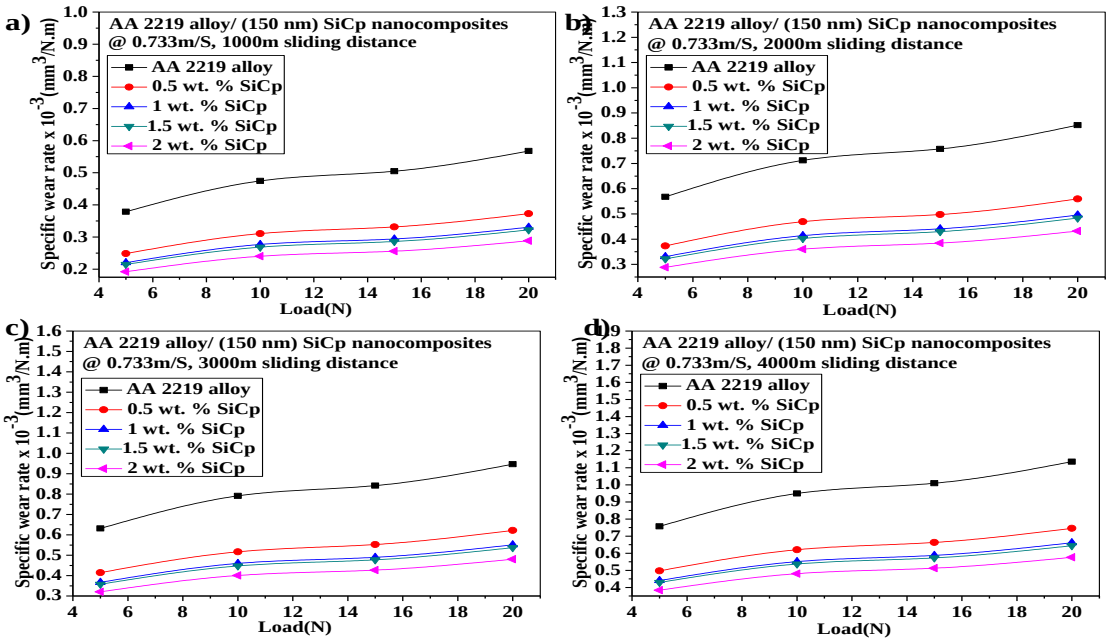

Figure 6.28 Variation of specific wear rate of AA2219 alloy and its nano SiC based MMNCs a) at 1000 m sliding distance b) at 2000 m sliding distance c) at 3000 m sliding distance d) at 4000 m sliding distance, with an applied load of 5 N to 20 N and constant sliding velocity 0.733 m/s.

The specific wear rate of the metal matrix nanocomposites was observed at all the applied loads and concluded that the specific wear rate of AA2219/SiC/150 nm composite was less when compared with base MMC. The specific wear rate was reduced while increasing the weight percentage of nano SiC in the base alloy and it is shown in Figures 6.28. In all these results sliding velocity kept constant (SV=0.733m/s). The reasons for all these works are well known fact established in literature. As the wt.% of particulate SiC increase in AA2219 the hardness and strength were increasing hence resistance to wear is also increases.

6.3.5 Coefficient of Friction of AA 2219/SiC/150 nm Nanocomposite

The variation in coefficient of friction of AA2219/SiC/150 nm nanocomposites with sliding distance is shown in Figure 6.29 a,b,c&d for sliding distance 1Km,2Km,3Km and 4Km AA2219/SiC/150 nm MMNC obeys the law of static and dynamic friction as friction coefficient is observed to be decreases with increase in sliding distance. The coefficient of friction of the metal matrix nanocomposites was observed at all the sliding distances and concluded that the coefficient of friction is more when compared with base material. The variation in coefficient of friction with load is shown in Figure 6.30 a,b,c&d for 5 N,10 N,15

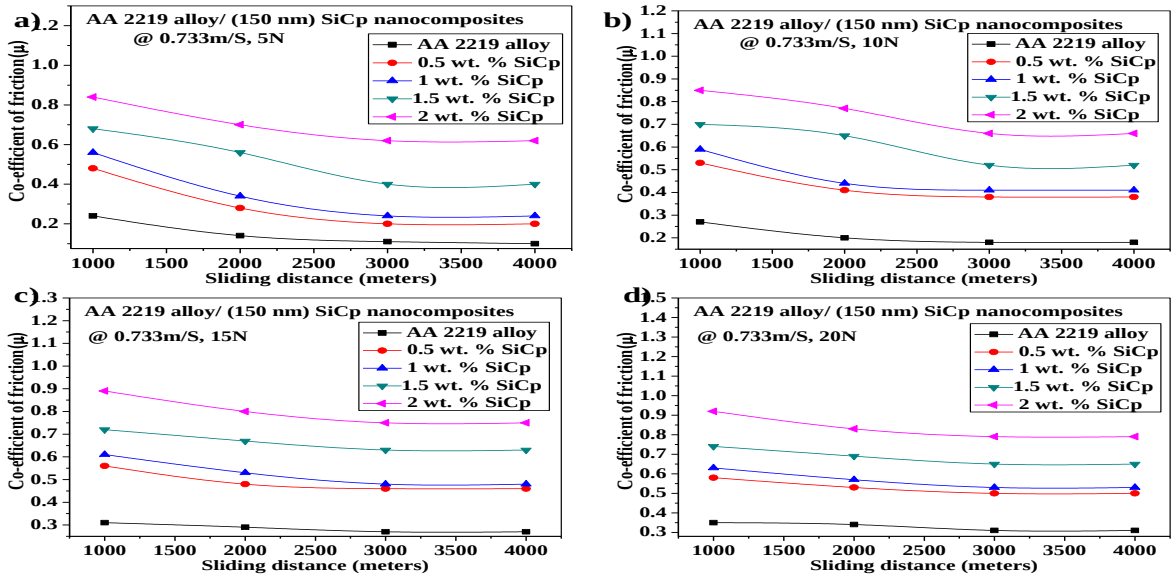

Figure 6.29 Variation of COF AA2219 alloy and its SiC Nano Composites a) at 5 N load b) at 10 N load c) at 15 N load d) at 20 N load, with sliding distance of 1000 m to 4000 m and at constant sliding velocity of 0.733 m/s.

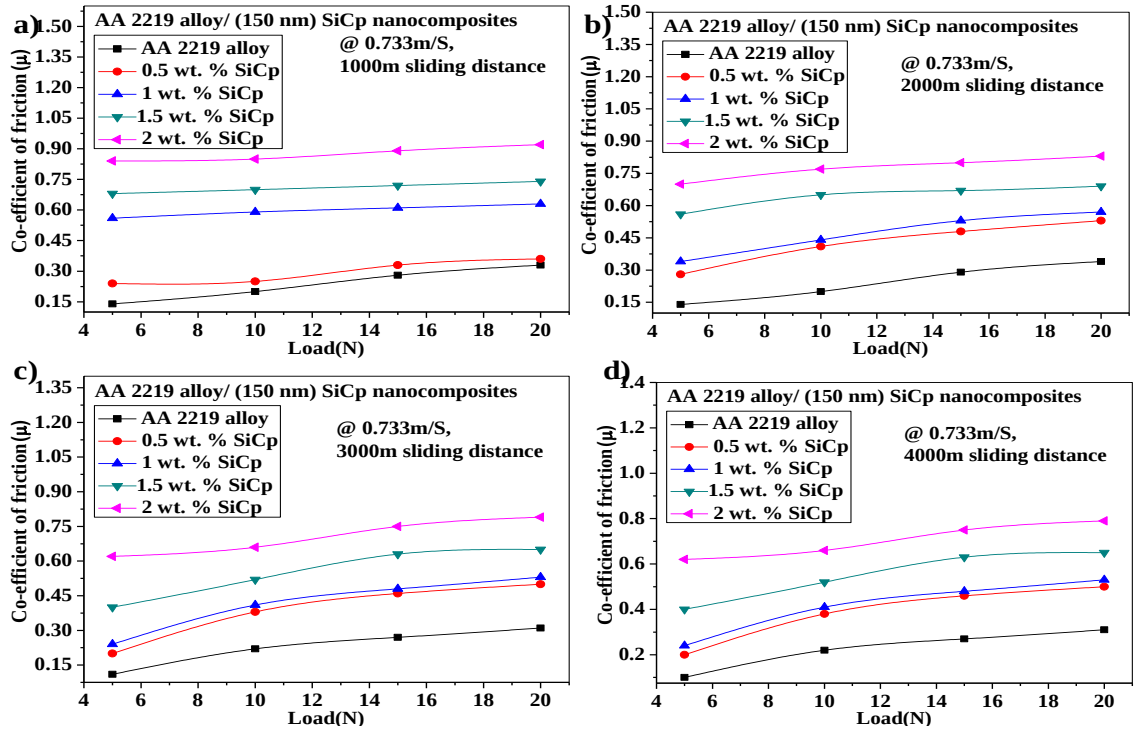

Figure 6.30 Variation of COF of AA2219 alloy and its SiC Nano Composites a) at 1000 m sliding distance b) at 2000 m sliding distance c) at 3000 m sliding distance d) at 4000 m sliding distance, with an applied load of 5 N to 20 N, and at constant sliding velocity 0.733 m/s.

N&20 N respectively. As shown in Figure 6.30 a,b,c&d the coefficient of friction of the AA2219/SiC/150 nm metal matrix nanocomposites was observed at all the applied loads and concluded that the coefficient of friction of MMNCs increases with load. The coefficient of friction was increased while increasing the weight percentage of nano SiC in the base alloy. This obeys the law of friction.

6.4 Wear Resistance Properties of AA2219/Al_2O_3/150 nm Nanocomposites

6.4.1 Volume of Wear AA 2219/Al_2O_3/150 nm Nanocomposite

The variation in the volume of wear with sliding distance under different loads are shown in Figure 6.31 a,b,c&d . The cast AA 2219/Al_2O_3/150 nm MMNC undergo higher volume of wear with an increase in sliding distance. The volume of wear of AA2219/Al_2O_3/150 nm the metal matrix nanocomposites was observed at all the sliding distances and concluded that the volume of wear of MMNC was less when compared with base MMC. The volume of wear was reduced while increasing the weight percentage of nano Al_2O_3 in the base alloy.

The variation in the volume of wear with an applied load is shown in Figure 6.32 a,b,c&d at sliding distances of 1Km,2Km,3Km&4Km respectively. The cast AA2219 and its nano Al_2O_3 reinforced metal matrix nanocomposites undergo higher volume of wear with an increase in applied load. The volume of wear of the metal matrix nanocomposites was observed at all the applied loads and concluded that the volume of wear of AA2219/ Al_2O_3/150 nm composite was less when compared with base MMC.

The volume of wear was reduced while increasing the weight percentage of nano Al_2O_3 in the base alloy and it is shown in Figures 6.32. In all these results sliding velocity kept constant (SV=0.733m/s).

The reasons for all these works are well known fact established in literature. As the wt.% of particulate Al_2O_3 increase in AA2219 the hardness and strength were increasing hence resistance to wear is also increases.

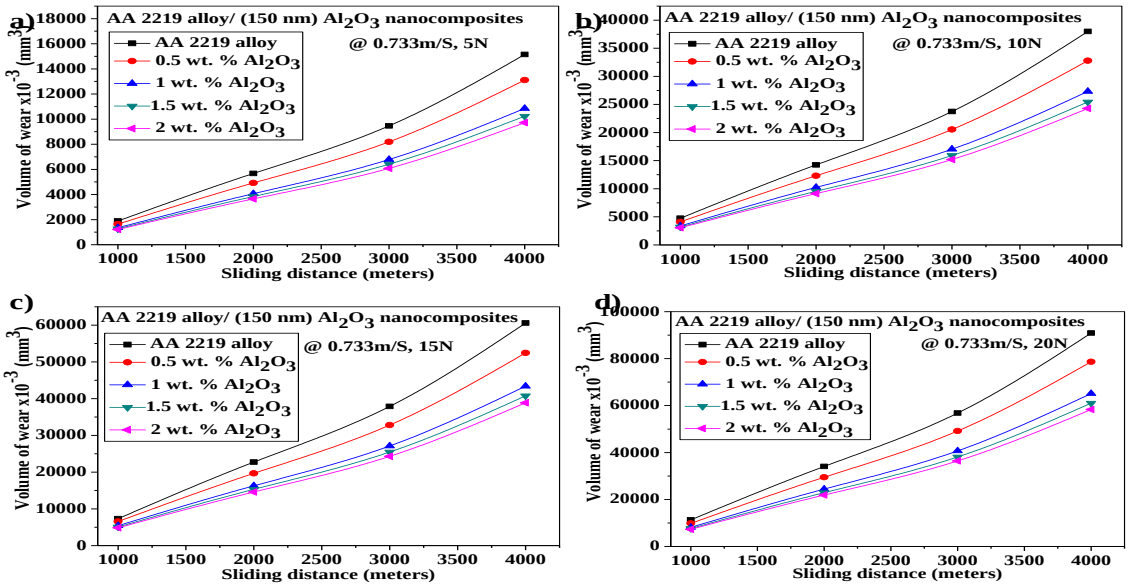

Figure 6.31 Variation of the volume of wear AA 2219 alloy and its nano Al_2O_3 based MMNCs a) at 5 N load b) at 10 N load c) at 15 N load d) at 20 N load, with sliding distance of 1000 to 4000 m, at a constant sliding velocity of 0.733 m/s.

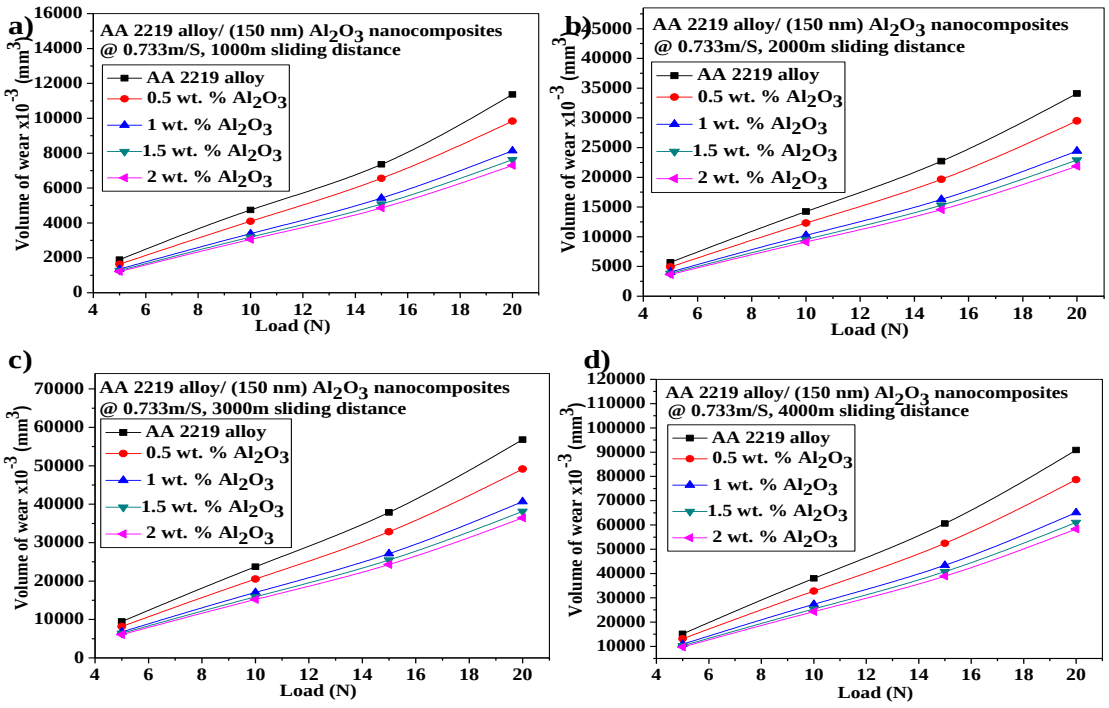

Figure 6.32 Variation of the volume of wear AA 2219 alloy and its nano Al_2O_3 based MMNCs a) at 1000 m sliding distance b) at 2000 m sliding distance c) at 3000 m sliding distance d) at 4000 m sliding distance, with an applied load of 5 N to 20 N, at constant sliding velocity 0.733 m/s.

6.4.2 Wear Height AA 2219/Al_2O_3/150 nm Nanocomposites

The variation in the wear height with sliding distance under different loads are shown in Figure 6.33 a,b,c&d . The cast AA2219/Al_2O_3/150 nm MMNC undergo higher loss in wear height with an increase in sliding distance. The wear height of AA2219/Al_2O_3/150 nm the metal matrix nanocomposites was observed at all the sliding distances and concluded that the wear height of MMNC was less when compared with base MMC. The loss of wear height was reduced while increasing the weight percentage of nano Al_2O_3 in the base alloy. The variation in the wear height with an applied load is shown in Figure 6.34 a,b,c&d at sliding distances of 1Km,2Km,3Km&4Km respectively. The cast AA2219and its nano Al_2O_3 reinforced metal matrix nanocomposites undergo higher loss of wear height with an increase in applied load. The wear height of the metal matrix nanocomposites was observed at all the applied loads and concluded that the loss of wear height of AA2219/ Al_2O_3/150 nm composite was less when compared with base MMC. The loss of wear height was reduced while increasing the weight percentage of nano Al_2O_3 in the base alloy and it is shown in Figures 6.34. In all these results sliding velocity kept constant (SV=0.733m/s). The reasons for all these works are well known fact established in literature. As the wt.% of particulate Al_2O_3 increase in AA2219 the hardness and strength were increasing hence resistance to wear is also increases.

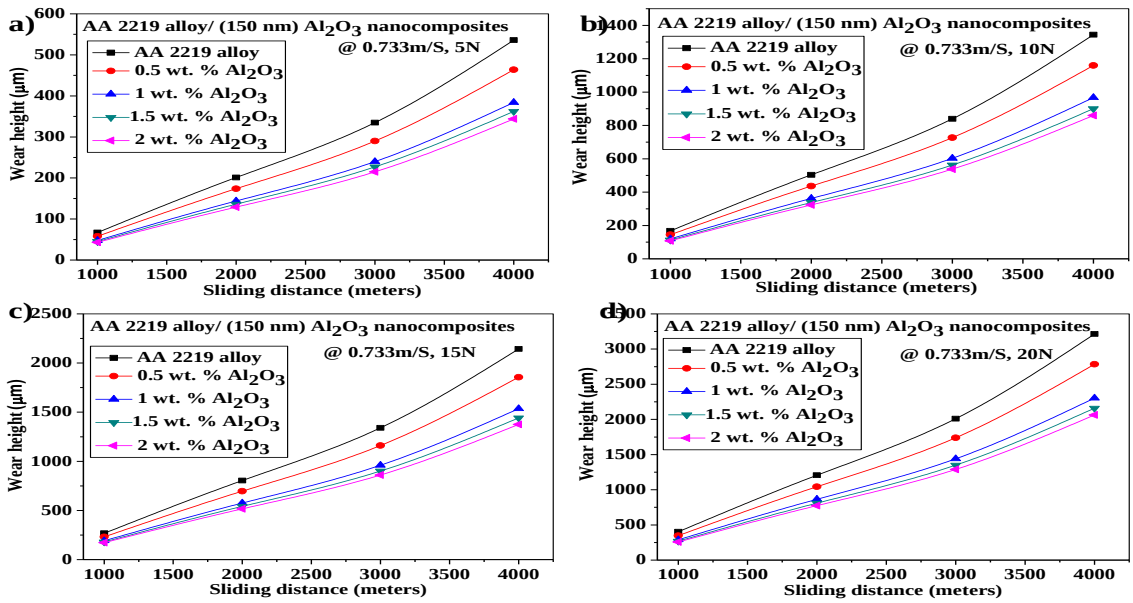

Figure 6.33 Variation of wear height AA 2219 alloy and its nano Al_2O_3 based MMNCs a) at 5 N load b) at 10 N load c) at 15 N load d) at 20 N load, with sliding distance of 1000 m to 4000 m, at constant sliding velocity of 0.733 m/s.

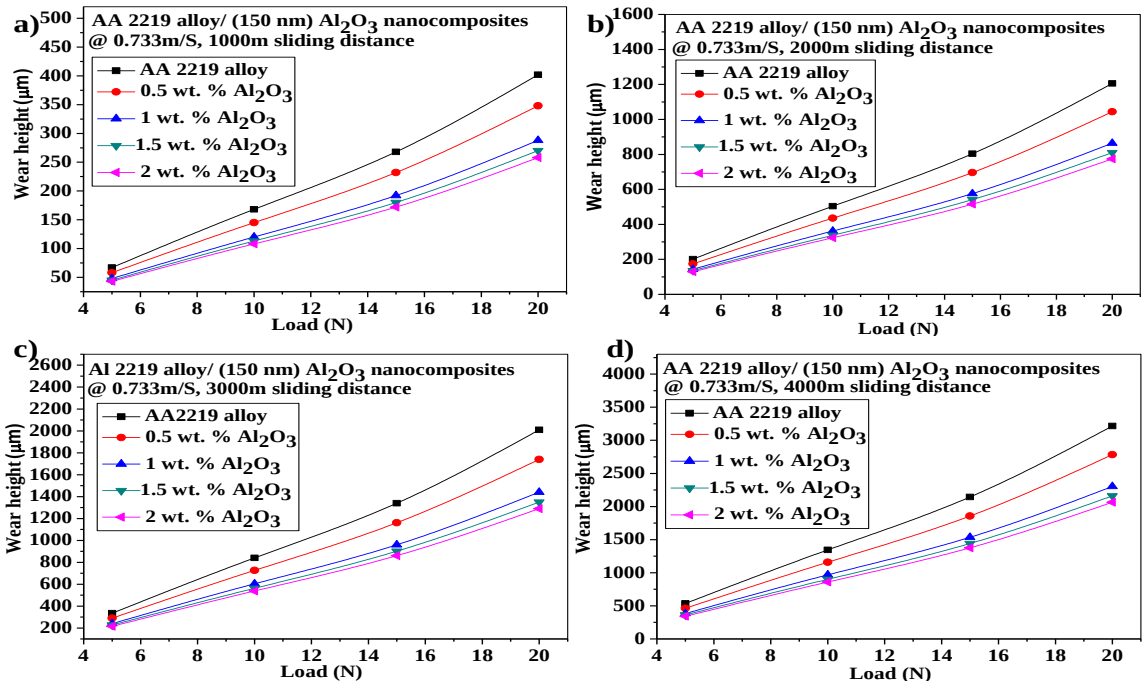

Figure 6.34 Variation of wear height of AA 2219 alloy and its nano Al_2O_3 based MMNCs a) at 1000 m sliding distance b) at 2000 m sliding distance c) at 3000 m sliding distance d) at 4000 m sliding distance, with an Applied load of 5 N to 20 N & at constant Sliding Velocity 0.733 m/s.

6.4.3 Wear Weight Loss AA 2219/Al_2O_3/150 nm Nanocomposite

The variation in the wear weight loss with sliding distance under different loads are shown in Figure 6.35 a,b,c&d . The cast AA2219/Al_2O_3/150 nm MMNC undergo higher wear weight loss with an increase in sliding distance. The wear weight loss of AA2219/ Al_2O_3/150 nm the metal matrix nanocomposites was observed at all the sliding distances and concluded that the wear weight loss of MMNC was less when compared with base MMC. The wear weight loss was reduced while increasing the weight percentage of nano Al_2O_3 in the base alloy. The variation in the wear weight loss with an applied load is shown in Figure 6.36 a,b,c&d at sliding distances of 1Km,2Km,3Km&4Km respectively. The cast AA2219and its nano Al_2O_3 reinforced metal matrix nanocomposites undergo higher wear weight loss with an increase in applied load. The wear weight loss of the metal matrix nanocomposites was observed at all the applied loads and concluded that the wear weight loss of AA2219/ Al_2O_3/150 nm composite was less when compared with base MMC. The wear weight loss was reduced while increasing the weight percentage of nano Al_2O_3 in the base alloy and it is shown in Figures 6.36. In all these results sliding velocity kept

constant (SV=0.733m/s). The reasons for all these works are well known fact established in literature. As the wt.% of particulate Al_2O_3 increase in AA2219 the hardness and strength were increasing hence resistance to wear is also increases.

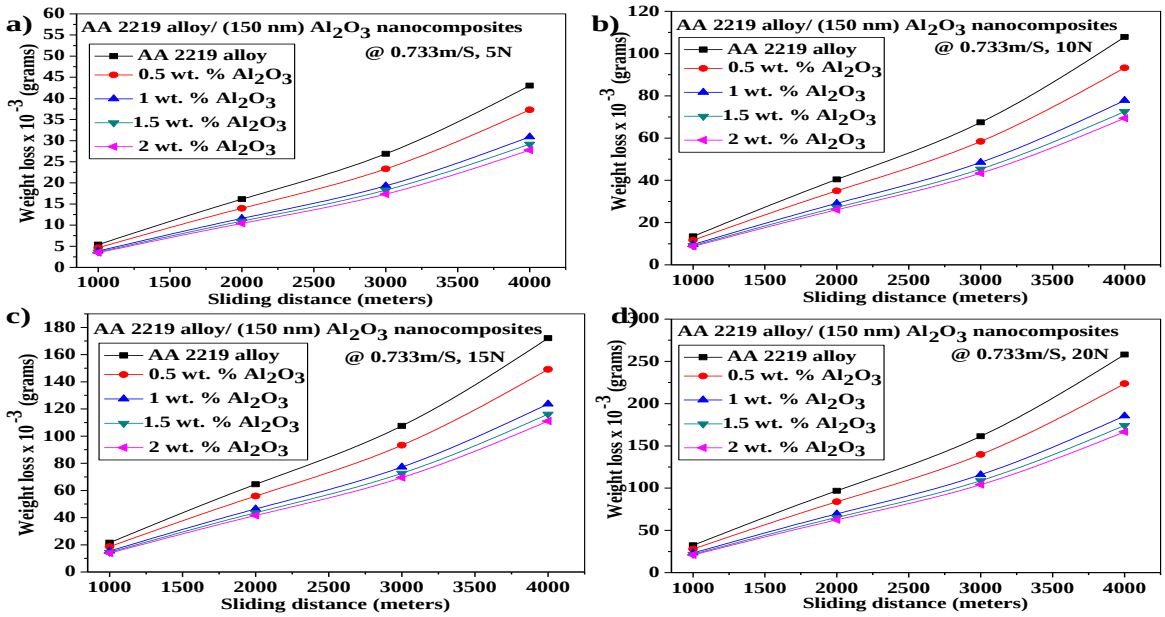

Figure 6.35 Variation of wear weight loss AA2219 alloy and its nano Al_2O_3 based MMNCs a) at 5 N load b) at 10 N load c) at 15 N load d) at 20 N load, with sliding distance of 1000 m to 4000 m and at constant sliding velocity of 0.733 m/s.

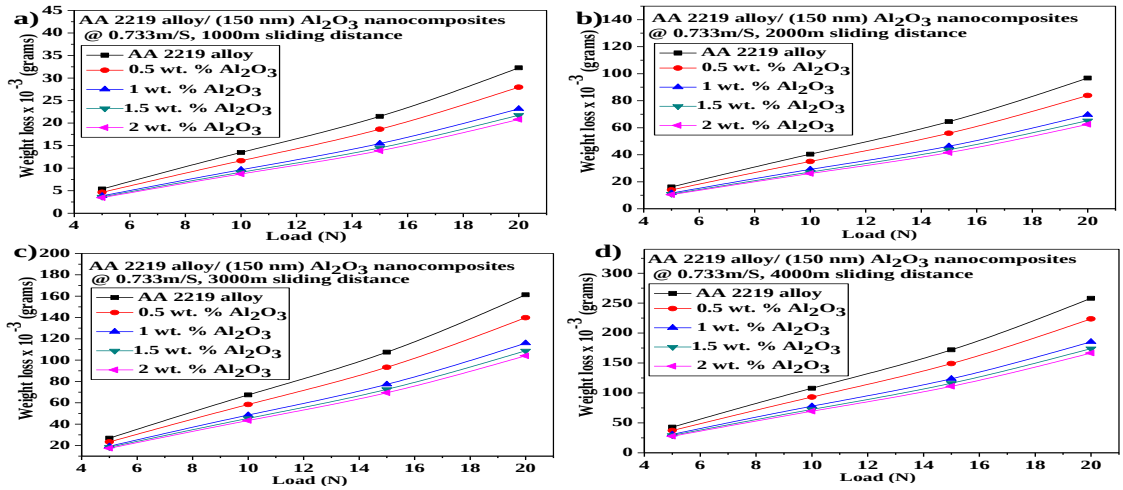

Figure 6.36 Variation of wear weight loss of AA2219 alloy and its nano Al_2O_3 MMNCs a) at 1000 m sliding distance b) at 2000 m sliding distance c) at 3000 m sliding distance d) at 4000 m sliding distance, with an applied load of 5 N to 20 N, and constant sliding velocity 0.733 m/s.

6.4.4 Specific Wear Rate AA 2219/Al2O3/150 nm Nanocomposite

The variation in the specific wear rate with sliding distance under different loads are shown in Figure 6.37 a,b,c&d . The cast AA2219/Al_2O_3/150 nm MMNC undergo higher specific wear rate with an increase in sliding distance. The specific wear rate of AA2219/ Al_2O_3/150 nm the metal matrix nanocomposites was observed at all the sliding distances and concluded that the specific wear rate of MMNC was less when compared with base MMC. The specific wear rate was reduced while increasing the weight percentage of nano Al_2O_3 in the base alloy. The variation in the specific wear rate with an applied load is shown in Figure 6.38 a,b,c&d at sliding distances of 1Km,2Km,3Km&4Km respectively. The cast AA2219 and its nano Al_2O_3 reinforced metal matrix nanocomposites undergo higher specific wear rate with an increase in applied load. The specific wear rate of the metal matrix nanocomposites was observed at all the applied loads and concluded that the specific wear rate of AA2219/ Al_2O_3/150 nm composite was less when compared with base MMC. The specific wear rate was reduced while increasing the weight percentage of nano Al_2O_3 in the base alloy and it is shown in Figures 6.38. In all these results sliding velocity kept constant (SV=0.733m/s). The reasons for all these works are well known fact established in literature. As the wt.% of particulate Al_2O_3 increase in AA2219 the hardness and strength were increasing hence resistance to wear is also increases.

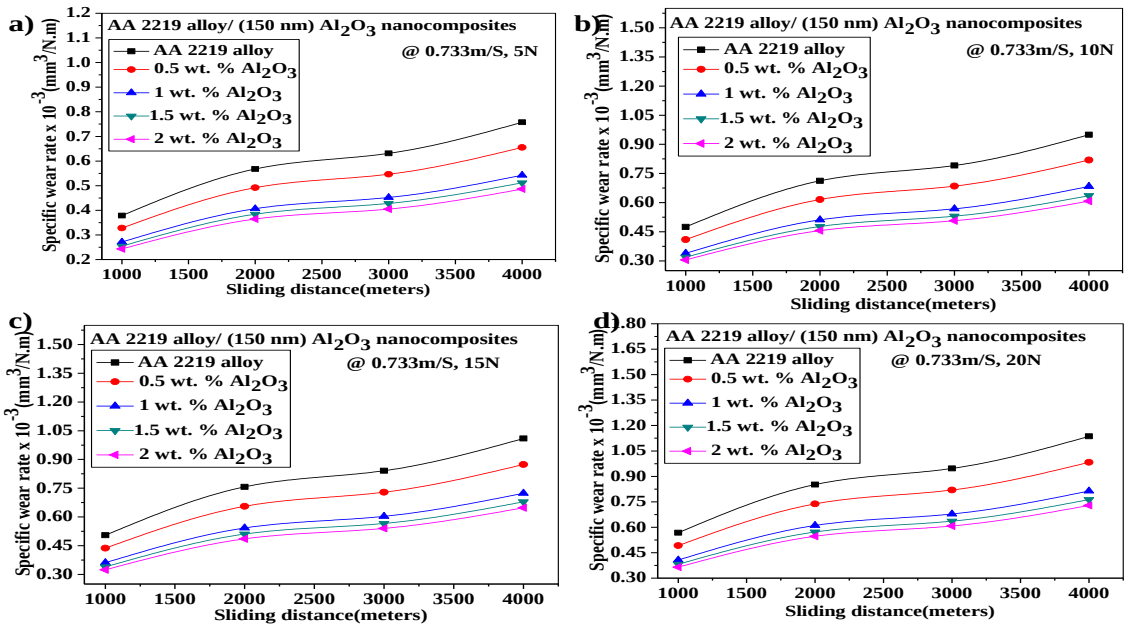

Figure 6.37 Variation of specific wear rate AA2219 alloy and its nano Al_2O_3 based MMNCs a) at 5 N load b) at 10 N load c) at 15 N load d) at 20 N load, with sliding distance of 1000 m to 4000 m and at constant sliding velocity of 0.733 m/s.

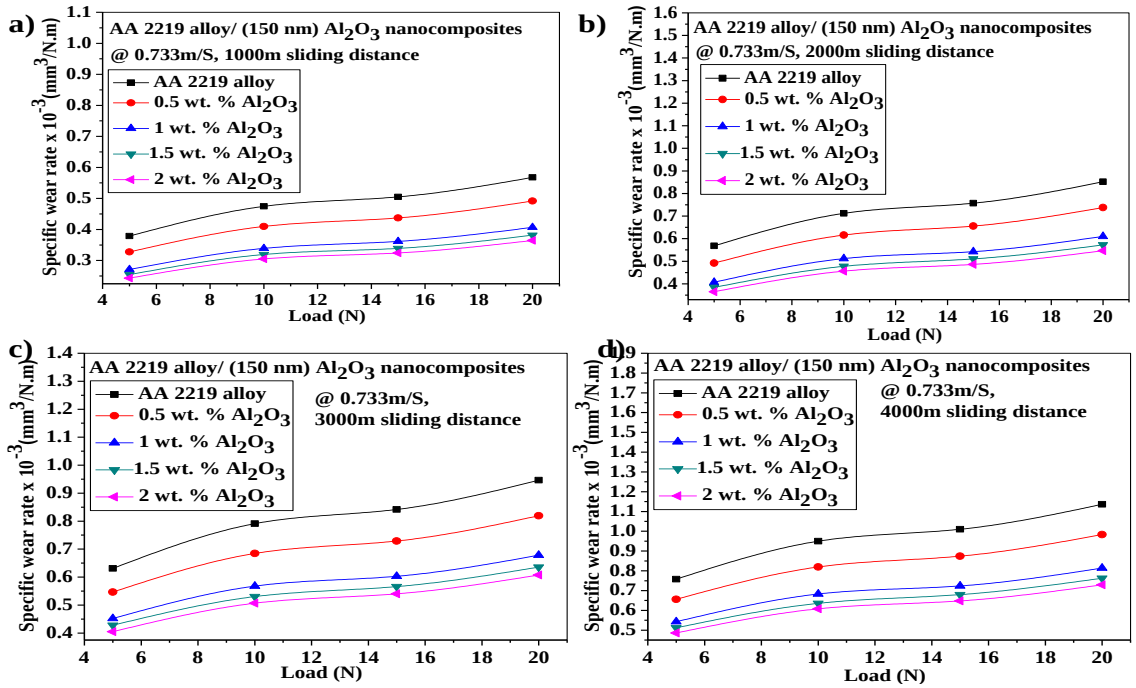

Figure 6.38 Variation of specific wear rate of AA2219 alloy and its nano Al_2O_3 based MMNCs a) at 1000 m sliding distance b) at 2000 m sliding distance c) at 3000 m sliding distance d) at 4000 m sliding distance, with an applied load of 5 N to 20 N and constant sliding velocity 0.733 m/s.

6.4.5 Coefficient of Friction of AA 2219/Al_2O_3/150 nm Nanocomposite

The variation in coefficient of friction of AA2219/Al_2O_3/150 nm nanocomposites with sliding distance is shown in Figure 6.39 a,b,c&d for sliding distance 1Km,2Km,3Km and 4Km AA2219/Al_2O_3/150 nm MMNC obeys the law of static and dynamic friction as friction coefficient is observed to be decreases with increase in sliding distance. The coefficient of friction of the metal matrix nanocomposites was observed at all the sliding distances and concluded that the coefficient of friction is more when compared with base material. The variation in coefficient of friction with load is shown in Figure 6.40 a,b,c&d for 5 N,10 N,15 N&20 N respectively. As shown in Figure 6.40 a,b,c&d the coefficient of friction of the AA2219/Al_2O_3/150 nm metal matrix nanocomposites was observed at all the applied loads and concluded that the coefficient of friction of MMNCs increases with load. The coefficient of friction was increased while increasing the weight percentage of nano Al_2O_3 in the base alloy. This obeys the law of friction.

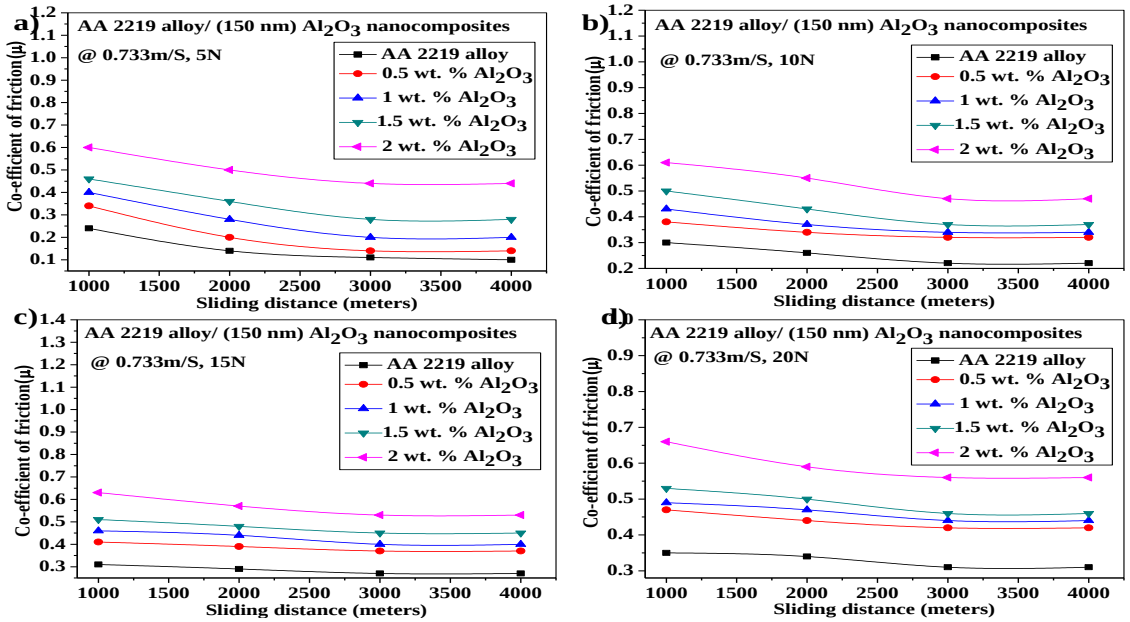

Figure 6.39 Variation of COF AA2219 alloy and its Al_2O_3 Nano Composites a) at 5 N load b) at 10 N load c) at 15 N load d) at 20 N load, with sliding distance of 1000 m to 4000 m and at constant sliding velocity of 0.733 m/s.

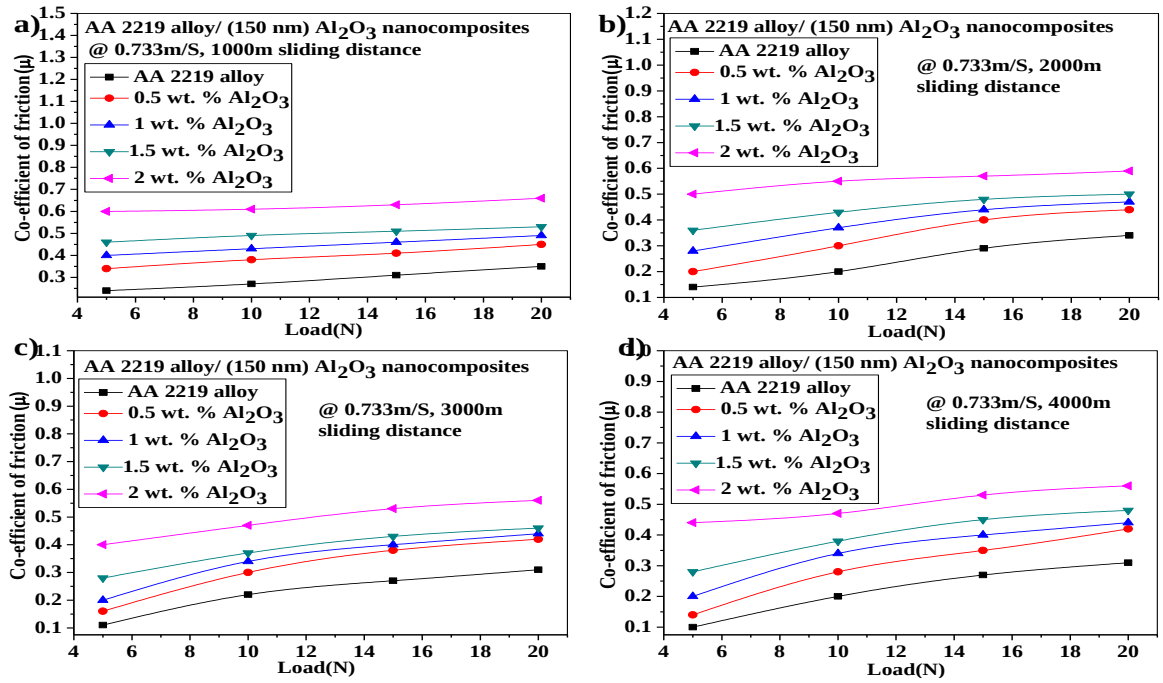

Figure 6.40 Variation of COF of AA2219 alloy and its Al_2O_3 Nano Composites a) at 1000 m sliding distance b) at 2000 m sliding distance c) at 3000 m sliding distance d) at 4000 m sliding distance, with an applied load of 5 N to 20 N, and at constant sliding velocity 0.733 m/s.

6.5 Wear Resistance Properties of AA2014/SiC/50 nm Nanocomposites

6.5.1 Volume of Wear AA2014/SiC/50 nm Nanocomposite

The variation in the volume of wear with sliding distance under different loads are shown in Figure 6.41 a,b,c&d . The cast AA2014/SiC/50 nm MMNC undergo higher volume of wear with an increase in sliding distance. The volume of wear of AA2014/SiC/50 nm the metal matrix nanocomposites was observed at all the sliding distances and concluded that the volume of wear of MMNC was less when compared with base MMC. The volume of wear was reduced while increasing the weight percentage of nano SiC in the base alloy. The variation in the volume of wear with an applied load is shown in Figure 6.42 a,b,c&d at sliding distances of 1Km,2Km,3Km&4Km respectively. The cast AA2014and its nano SiC reinforced metal matrix nanocomposites undergo higher volume of wear with an increase in applied load. The volume of wear of the metal matrix nanocomposites was observed at all the applied loads and concluded that the volume of wear of AA2014/SiC/50 nm composite was less when compared with base MMC. The volume of wear was reduced while increasing the weight percentage of nano SiC in the base alloy and it is shown in Figures 6.42. In all these results sliding velocity kept constant (SV=0.733m/s). The reasons for all these works are well known fact established in literature. As the wt.% of particulate SiC increase in AA2014 the hardness and strength were increasing hence resistance to wear is also increases.

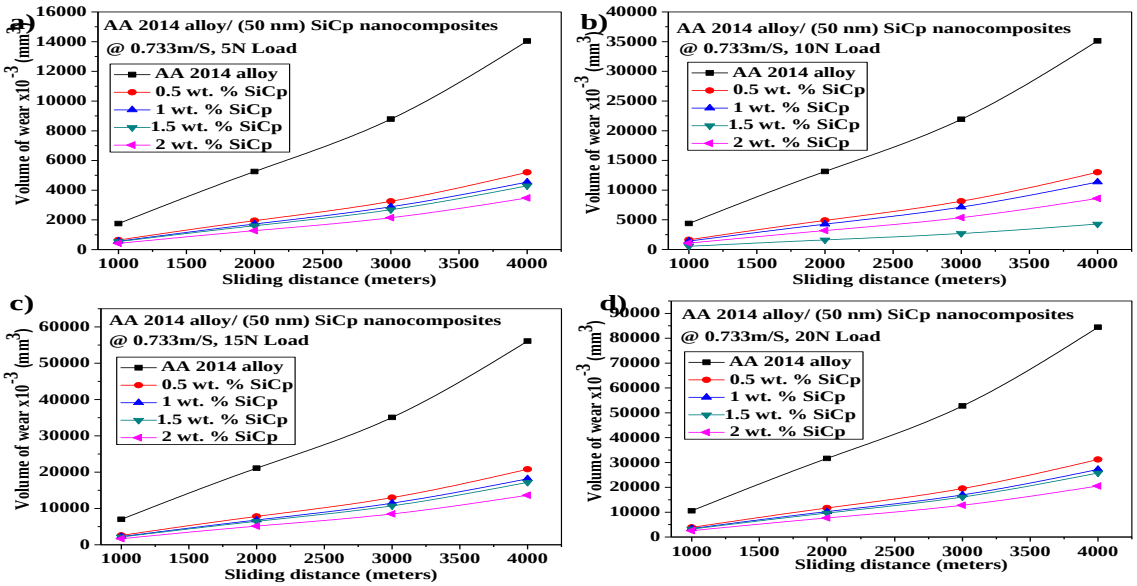

Figure 6.41 Variation of the volume of wear AA 2014 alloy and its nano SiC based MMNCs a) at 5 N load b) at 10 N load c) at 15 N load d) at 20 N load, with sliding distance of 1000 to 4000 m, at a constant sliding velocity of 0.733 m/s.

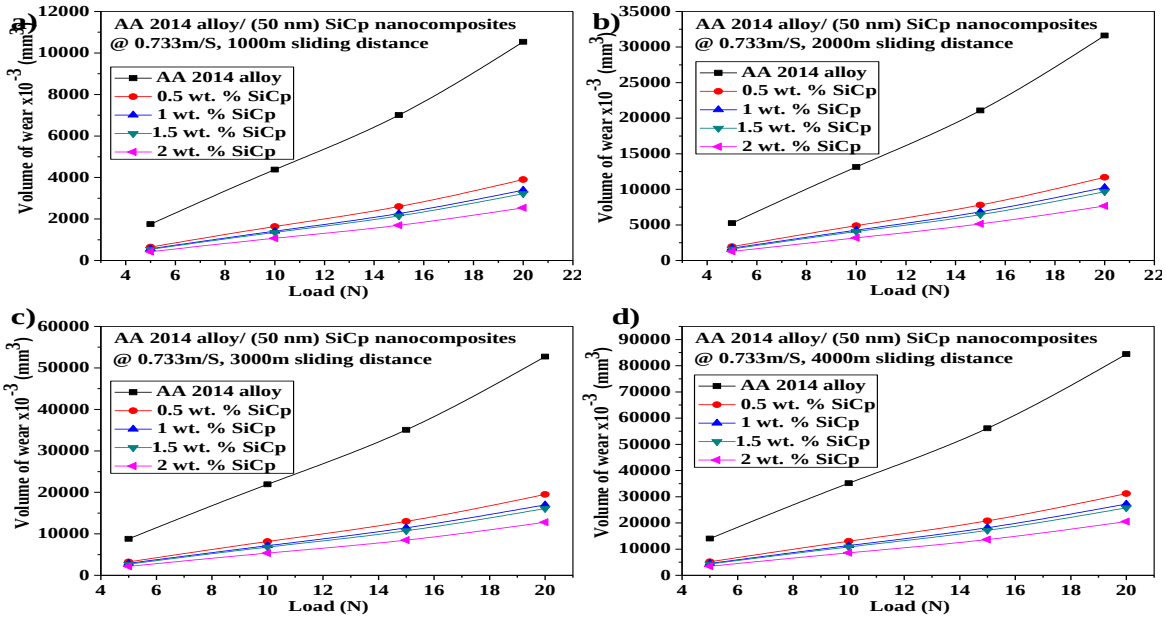

Figures 6.42 Variation of the volume of wear AA 2014 alloy and its nano SiC based MMNCs a) at 1000 m sliding distance b) at 2000 m sliding distance c) at 3000 m sliding distance d) at 4000 m sliding distance, with an applied load of 5 N to 20 N, at constant sliding velocity 0.733 m/s.

6.5.2 Wear Height AA 2014/SiC/50 nm Nanocomposites

The variation in the wear height with sliding distance under different loads are shown in Figure 6.43 a,b,c&d . The cast AA2014/SiC/50 nm MMNC undergo higher loss in wear height with an increase in sliding distance. The wear height of AA2014/SiC/50 nm the metal matrix nanocomposites was observed at all the sliding distances and concluded that the wear height of MMNC was less when compared with base MMC. The loss of wear height was reduced while increasing the weight percentage of nano SiC in the base alloy. The variation in the wear height with an applied load is shown in Figure 6.44 a,b,c&d at sliding distances of 1Km,2Km,3Km&4Km respectively. The cast AA2014and its nano SiC reinforced metal matrix nanocomposites undergo higher loss of wear height with an increase in applied load. The wear height of the metal matrix nanocomposites was observed at all the applied loads and concluded that the loss of wear height of AA2014/SiC/50 nm composite was less when compared with base MMC. The loss of wear height was reduced while increasing the weight percentage of nano SiC in the base alloy and it is shown in Figures 6.44. In all these results sliding velocity kept constant (SV=0.733m/s). The reasons for all these works are well known fact established in literature.

As the wt.% of particulate SiC increase in AA2014 the hardness and strength were increasing hence resistance to wear is also increases.

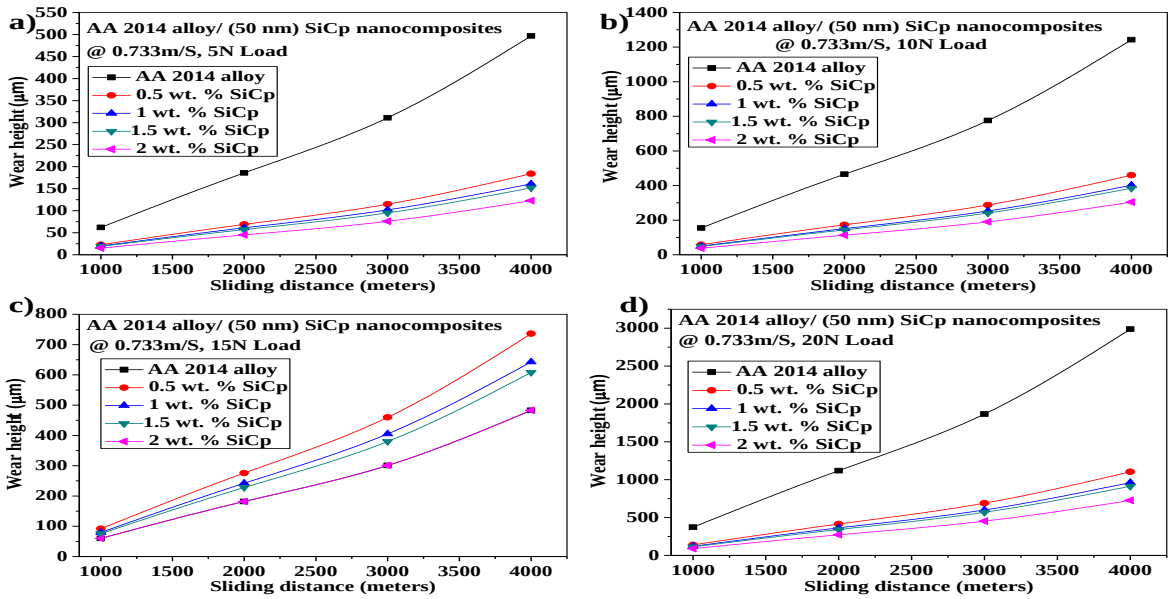

Figure 6.43 Variation of wear height AA 2014 alloy and its nano SiC based MMNCs a) at 5 N load b) at 10 N load c) at 15 N load d) at 20 N load, with sliding distance of 1000 m to 4000 m, at constant sliding velocity of 0.733 m/s.

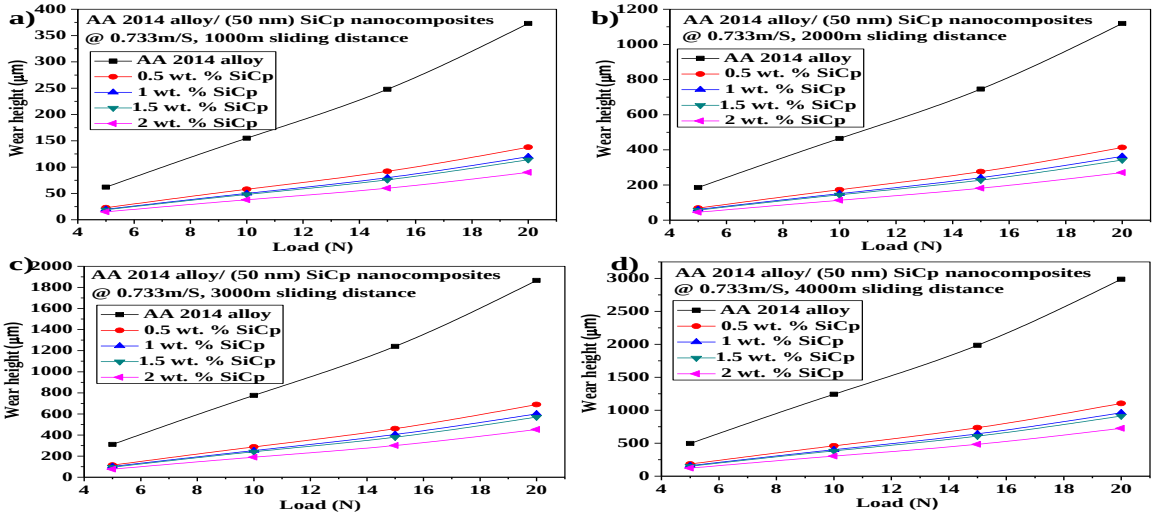

Figure 6.44 Variation of wear height of AA 2014 alloy and its nano SiC based MMNCs a) at 1000 m sliding distance b) at 2000 m sliding distance c) at 3000 m sliding distance d) at 4000 m sliding distance, with an Applied load of 5 N to 20 N & at constant Sliding Velocity 0.733 m/s.

6.5.3 Wear Weight Loss AA2014/SiC/50 nm Nanocomposites

The variation in the wear weight loss with sliding distance under different loads are shown in Figure 6.45 a,b,c&d . The cast AA2014/SiC/50 nm MMNC undergo higher wear weight loss with an increase in sliding distance. The wear weight loss of AA2014/SiC/50 nm the metal matrix nanocomposites was observed at all the sliding distances and concluded that the wear weight loss of MMNC was less when compared with base MMC. The wear weight loss was reduced while increasing the weight percentage of nano SiC in the base alloy. The variation in the wear weight loss with an applied load is shown in Figure 6.46 a,b,c&d at sliding distances of 1Km,2Km,3Km&4Km respectively. The cast AA2014and its nano SiC reinforced metal matrix nanocomposites undergo higher wear weight loss with an increase in applied load. The wear weight loss of the metal matrix nanocomposites was observed at all the applied loads and concluded that the wear weight loss of AA2014/SiC/50 nm composite was less when compared with base MMC. The wear weight loss was reduced while increasing the weight percentage of nano SiC in the base alloy and it is shown in Figures 6.46. In all these results sliding velocity kept constant (SV=0.733m/s). The reasons for all these works are well known fact established in literature. As the wt.% of particulate SiC increase in AA2014 the hardness and strength were increasing hence resistance to wear is also increases.

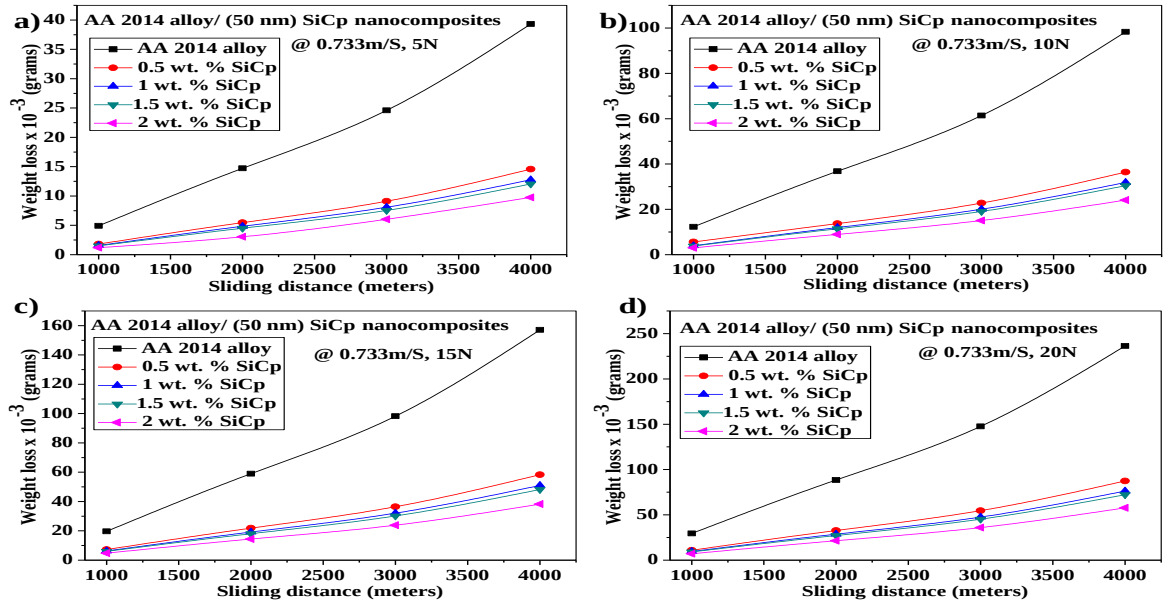

Figure 6.45 Variation of wear weight loss AA2014 alloy and its nano SiC based MMNCs a) at 5 N load b) at 10 N load c) at 15 N load d) at 20 N load, with sliding distance of 1000 m to 4000 m and at constant sliding velocity of 0.733 m/s.

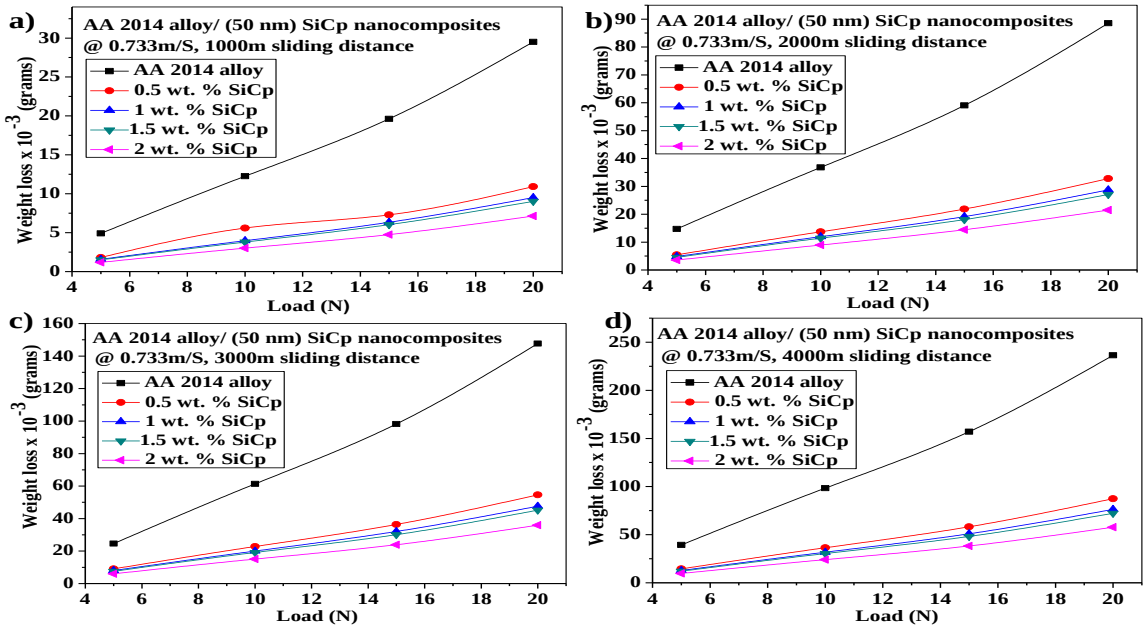

Figure 6.46 Variation of wear weight loss of AA2014 alloy and its nano SiC MMNCs a) at 1000 m sliding distance b) at 2000 m sliding distance c) at 3000 m sliding distance d) at 4000 m sliding distance, with an applied load of 5 N to 20 N, and constant sliding velocity 0.733 m/s.

6.5.4 Specific Wear Rate AA 2014/SiC/50 nm Nanocomposites

The variation in the specific wear rate with sliding distance under different loads are shown in Figure 6.47 a,b,c&d . The cast AA2014/SiC/50 nm MMNC undergo higher specific wear rate with an increase in sliding distance. The specific wear rate of AA2014/SiC/50 nm the metal matrix nanocomposites was observed at all the sliding distances and concluded that the specific wear rate of MMNC was less when compared with base MMC. The specific wear rate was reduced while increasing the weight percentage of nano SiC in the base alloy. The variation in the specific wear rate with an applied load is shown in Figure 6.48 a,b,c&d at sliding distances of 1Km,2Km,3Km&4Km respectively. The cast AA2014 and its nano SiC reinforced metal matrix nanocomposites undergo higher specific wear rate with an increase in applied load. The specific wear rate of the metal matrix nanocomposites was observed at all the applied loads and concluded that the specific wear rate of AA2014/SiC/50 nm composite was less when compared with base MMC. The specific wear rate was reduced while increasing the weight percentage of nano SiC in the base alloy and it is shown in Figures 6.48. In all these results sliding velocity kept constant (SV=0.733m/s). The reasons for all these works are well known

fact established in literature. As the wt.% of particulate SiC increase in AA2014 the hardness and strength were increasing hence resistance to wear is also increases.

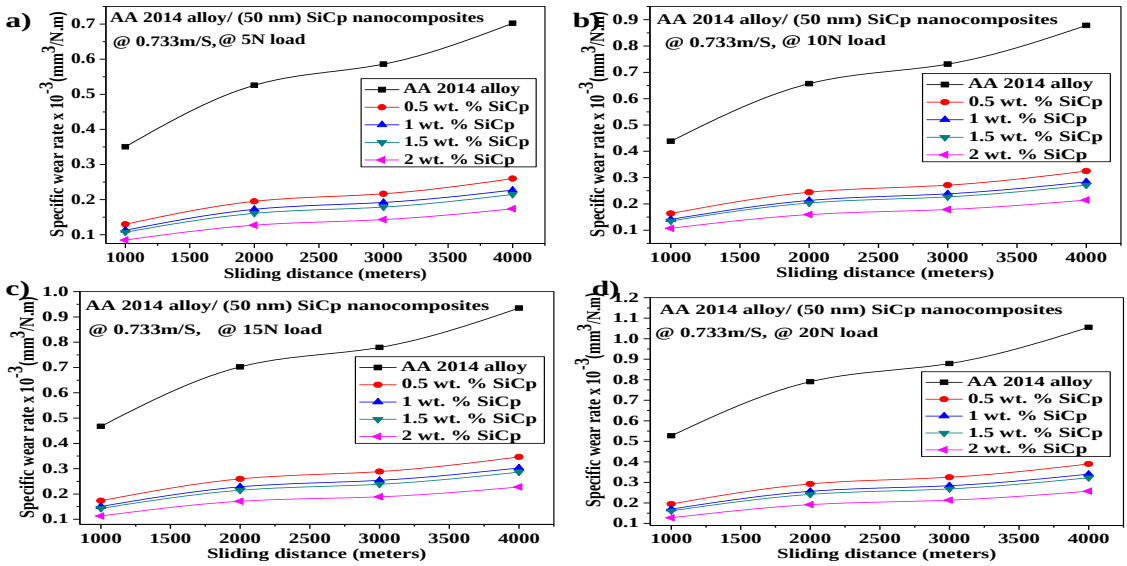

Figure 6.47 Variation of specific wear rate AA2014 alloy and its nano SiC based MMNCs a) at 5 N load b) at 10 N load c) at 15 N load d) at 20 N load, with sliding distance of 1000 m to 4000 m and at constant sliding velocity of 0.733 m/s.

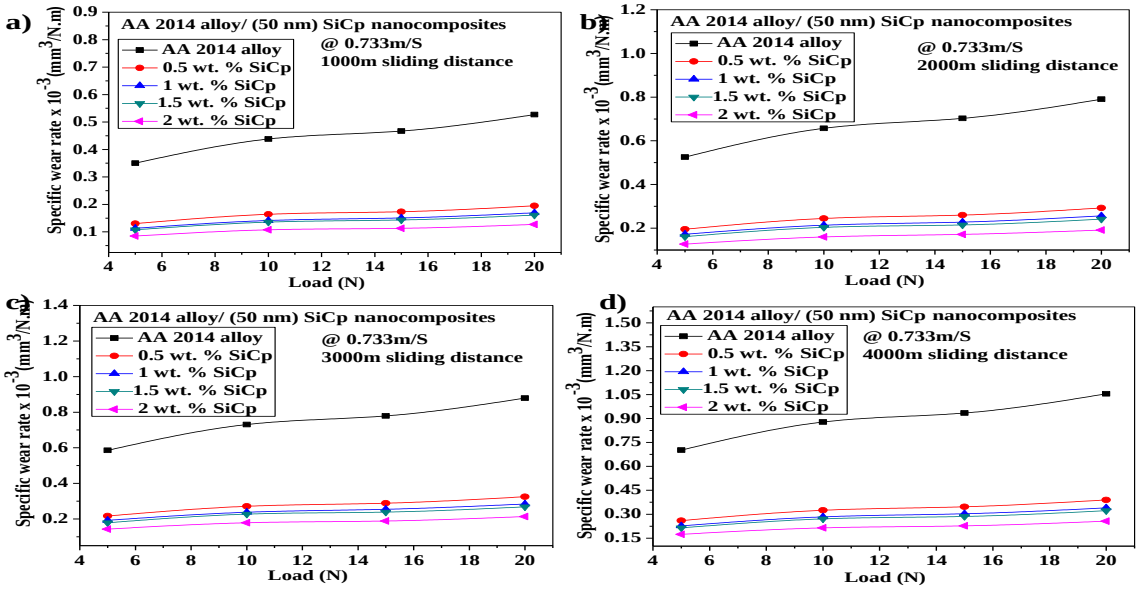

Figure 6.48 Variation of specific wear rate of AA2014 alloy and its nano SiC based MMNCs a) at 1000 m sliding distance b) at 2000 m sliding distance c) at 3000 m sliding distance d) at 4000 m sliding distance, with an applied load of 5 N to 20 N and constant sliding velocity 0.733 m/s.

6.5.5 Coefficient of Friction of AA 2014/SiC/50 nm Nanocomposites

The variation in coefficient of friction of AA2014/SiC/50 nm nanocomposites with sliding distance is shown in Figure 6.49 a,b,c&d for sliding distance 1Km,2Km,3Km and 4Km AA2014/SiC/50 nm MMNC obeys the law of static and dynamic friction as friction coefficient is observed to be decreases with increase in sliding distance. The coefficient of friction of the metal matrix nanocomposites was observed at all the sliding distances and concluded that the coefficient of friction is more when compared with base material. The variation in coefficient of friction with load is shown in Figure 6.50 a,b,c&d for 5 N,10 N,15 N&20 N respectively. As shown in Figure 6.50 a,b,c&d the coefficient of friction of the AA2014/SiC/50 nm metal matrix nanocomposites was observed at all the applied loads and concluded that the coefficient of friction of MMNCs increases with load. The coefficient of friction was increased while increasing the weight percentage of nano SiC in the base alloy. This obeys the law of friction.

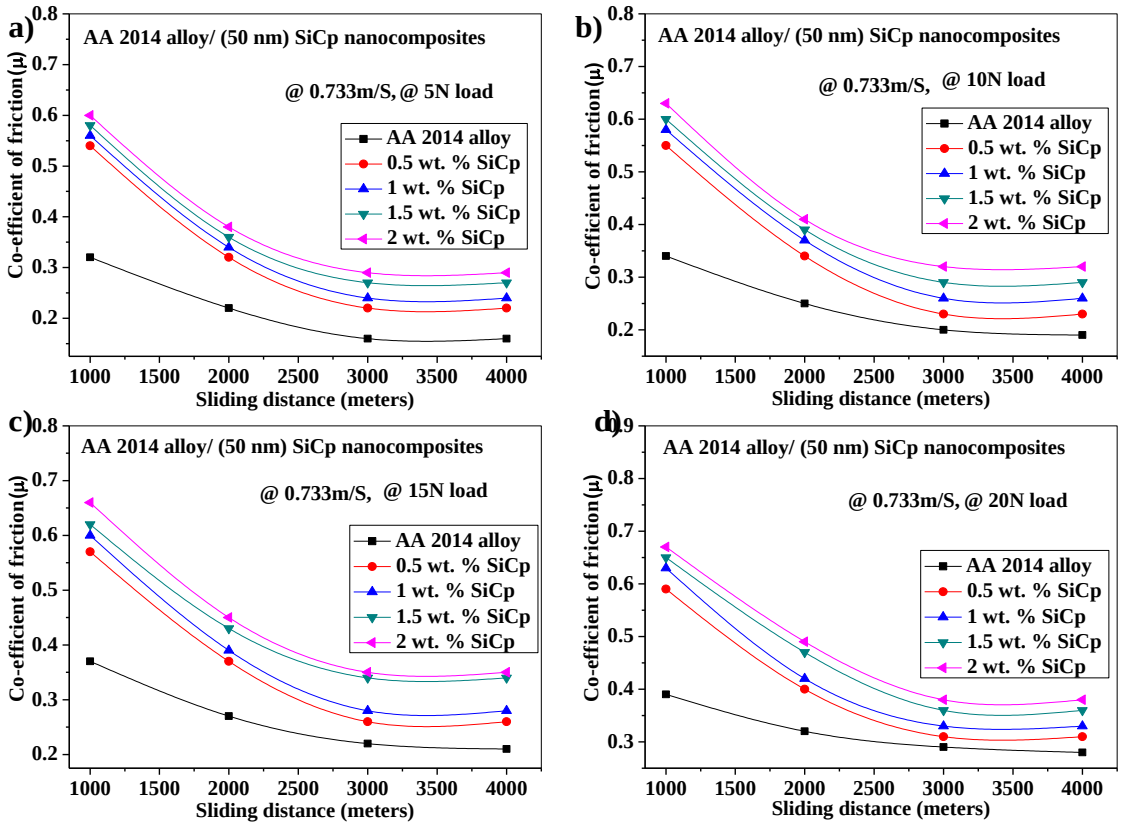

Figure 6.49 Variation of COF AA2014 alloy and its SiC Nano Composites a) at 5 N load b) at 10 N load c) at 15 N load d) at 20 N load, with sliding distance of 1000 m to 4000 m and at constant sliding velocity of 0.733 m/s.

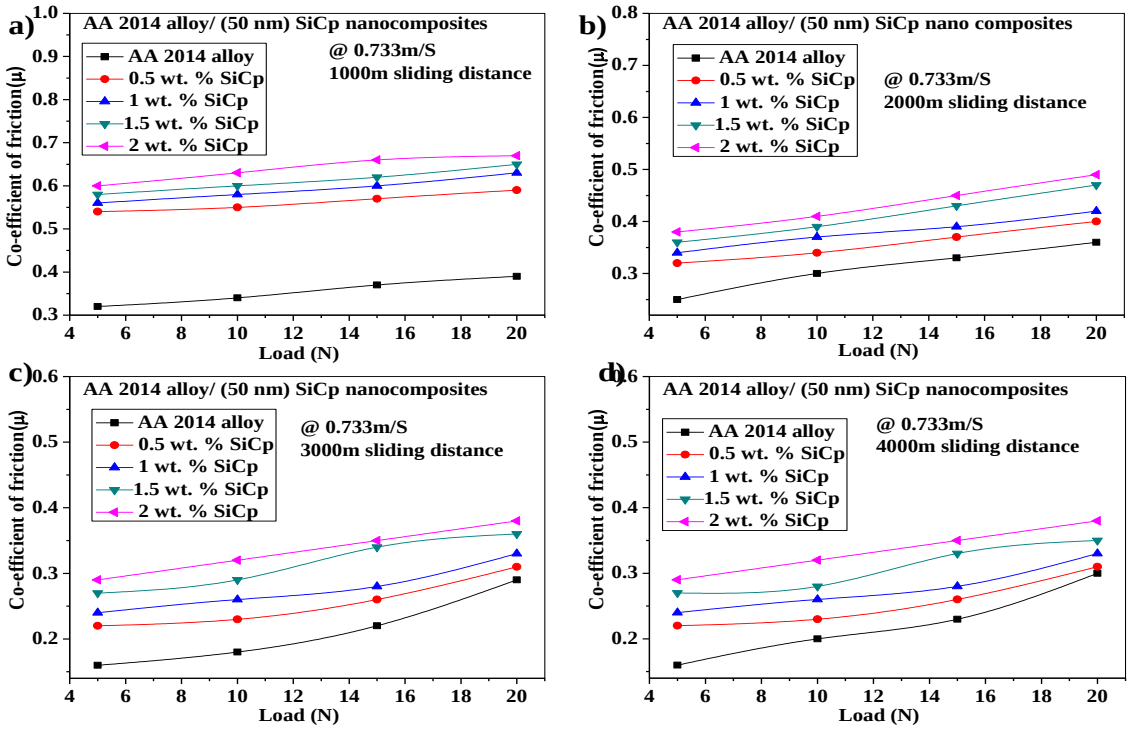

Figure 6.50 Variation of COF of AA2014 alloy and its SiC Nano Composites a) at 1000 m sliding distance b) at 2000 m sliding distance c) at 3000 m sliding distance d) at 4000 m sliding distance, with an applied load of 5 N to 20 N, and at constant sliding velocity 0.733 m/s.

The variation in coefficient of friction with load is shown in Figure 5.51 Cast AA 2014 and its nano SiC reinforced metal matrix nanocomposites undergo initially lower coefficient of friction at 0 to 1000 m and then gradually increased while the increase in load clearly MMNCs obey the law of friction. As shown in Figure 5.51, the coefficient of friction of the metal matrix nanocomposites was observed at all the sliding distances and concluded that the coefficient of friction of MMNCs was more when compared with base MMC. The coefficient of friction was increased while increasing the weight percentage of nano SiC in the base alloy and it was shown from Figure 5.51.

6.6 Wear Resistance Properties of AA2014/Al_2O_3/50 nm Nanocomposites

6.6.1 Volume of Wear AA2014/Al_2O_3 /50 nm Nanocomposites

The variation in the volume of wear with sliding distance under different loads are shown in Figure 6.51 a,b,c&d . The cast AA2014/Al_2O_3/50 nm MMNC undergo higher volume of wear with an

increase in sliding distance. The volume of wear of AA2014/Al_2O_3/50 nm the metal matrix nanocomposites was observed at all the sliding distances and concluded that the volume of wear of MMNC was less when compared with base MMC. The volume of wear was reduced while increasing the weight percentage of nano Al_2O_3 in the base alloy. The variation in the volume of wear with an applied load is shown in Figure 6.52 a,b,c&d at sliding distances of 1Km,2Km,3Km&4Km respectively. The cast AA2014 and its nano Al_2O_3 reinforced metal matrix nanocomposites undergo higher volume of wear with an increase in applied load. The volume of wear of the metal matrix nanocomposites was observed at all the applied loads and concluded that the volume of wear of AA2014/ Al_2O_3/50 nm composite was less when compared with base MMC. The volume of wear was reduced while increasing the weight percentage of nano Al_2O_3 in the base alloy and it is shown in Figures 6.52. In all these results sliding velocity kept constant (SV=0.733m/s). The reasons for all these works are well known fact established in literature. As the wt.% of particulate Al_2O_3 increase in AA2014 the hardness and strength were increasing hence resistance to wear is also increases.

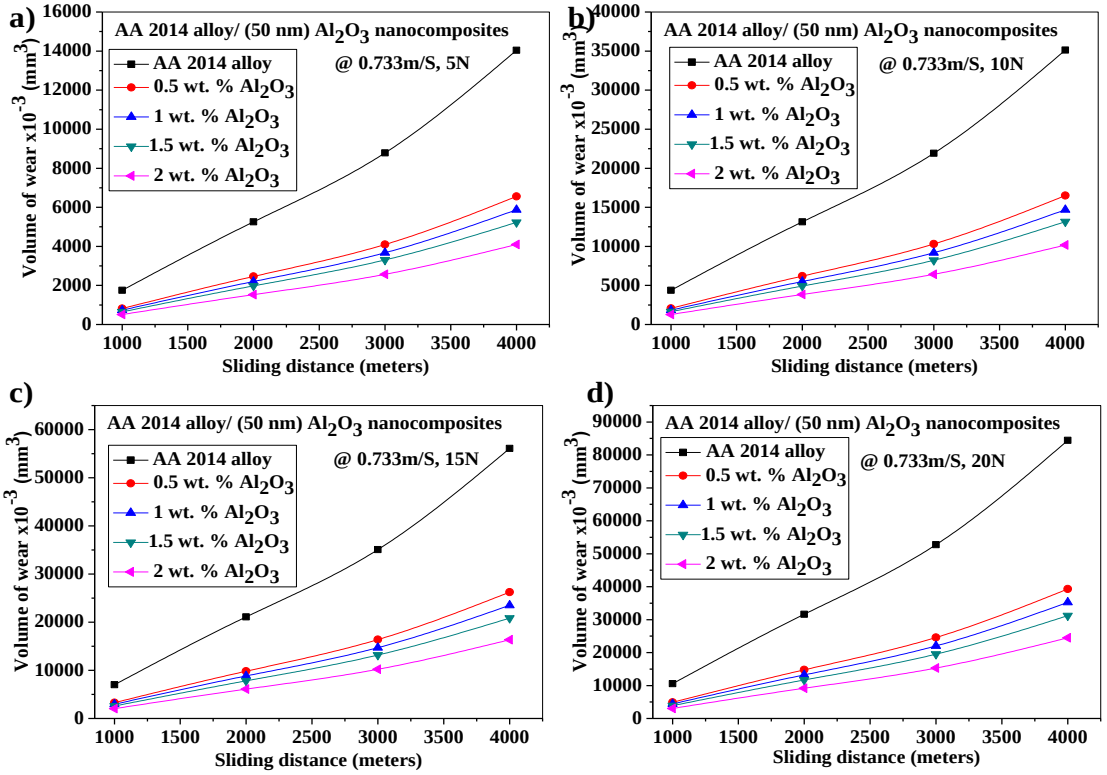

Figure 6.51 Variation of the volume of wear AA 2014 alloy and its nano Al_2O_3 based MMNCs a) at 5 N load b) at 10 N load c) at 15 N load d) at 20 N load, with sliding distance of 1000 to 4000 m, at a constant sliding velocity of 0.733 m/s.

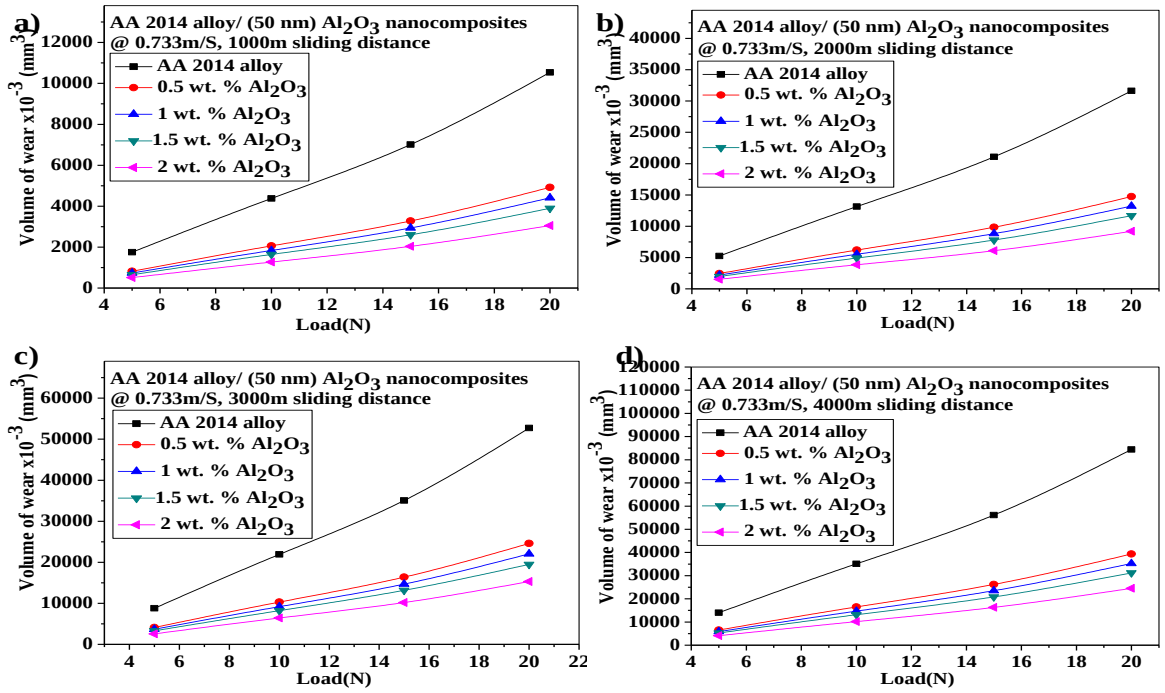

Figure 6.52 Variation of the volume of wear AA 2014 alloy and its nano Al_2O_3 based MMNCs a) at 1000 m sliding distance b) at 2000 m sliding distance c) at 3000 m sliding distance d) at 4000 m sliding distance, with an applied load of 5 N to 20 N, at constant sliding velocity 0.733 m/s.

6.6.2 Wear Height AA 2014/Al_2O_3/50 nm Nanocomposites

The variation in the wear height with sliding distance under different loads are shown in Figure 6.53 a,b,c&d . The cast AA2014/Al_2O_3/50 nm MMNC undergo higher loss in wear height with an increase in sliding distance. The wear height of AA2014/Al_2O_3/50 nm the metal matrix nanocomposites was observed at all the sliding distances and concluded that the wear height of MMNC was less when compared with base MMC. The loss of wear height was reduced while increasing the weight percentage of nano Al_2O_3 in the base alloy. The variation in the wear height with an applied load is shown in Figure 6.54 a,b,c&d at sliding distances of 1Km,2Km,3Km&4Km respectively. The cast AA2014and its nano Al_2O_3 reinforced metal matrix nanocomposites undergo higher loss of wear height with an increase in applied load. The wear height of the metal matrix nanocomposites was observed at all the applied loads and concluded that the loss of wear height of AA2014/ Al_2O_3/50 nm composite was less when compared with base MMC. The loss of wear height was reduced while increasing the weight percentage of nano Al_2O_3 in the base alloy and it is shown in Figures 6.54. In all these results sliding velocity kept constant

(SV=0.733m/s). The reasons for all these works are well known fact established in literature. As the wt.% of particulate Al_2O_3 increase in AA2014 the hardness and strength were increasing hence resistance to wear is also increases.

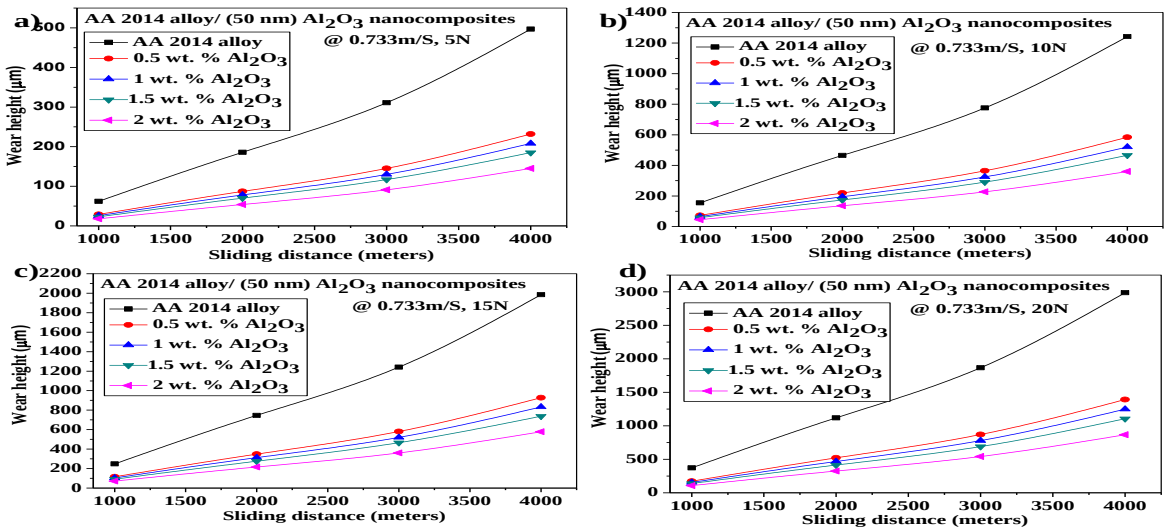

Figure 6.53 Variation of wear height AA 2014 alloy and its nano Al_2O_3 based MMNCs a) at 5 N load b) at 10 N load c) at 15 N load d) at 20 N load, with sliding distance of 1000 m to 4000 m, at constant sliding velocity of 0.733 m/s.

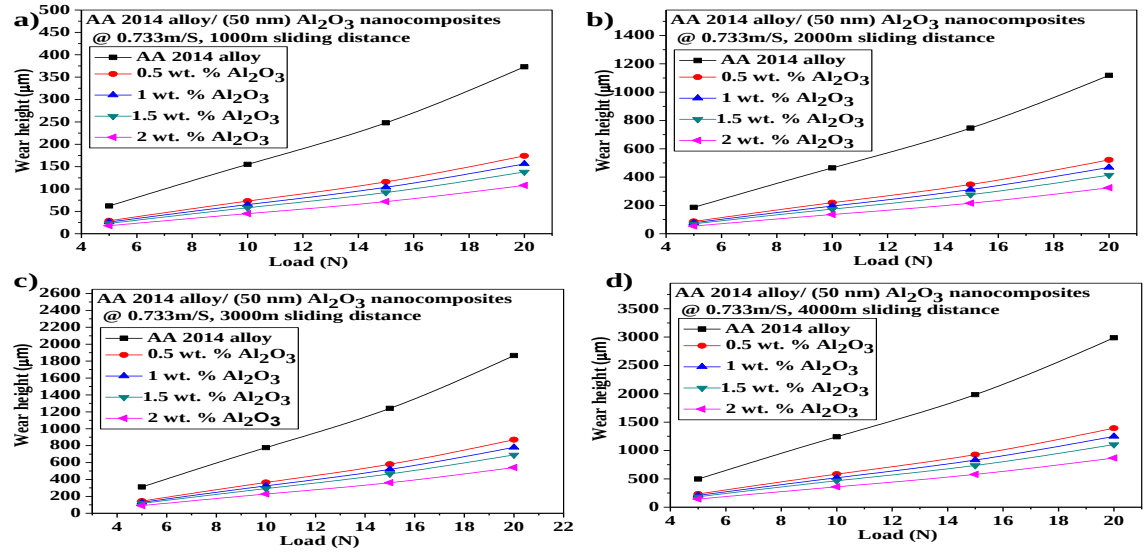

Figure 6.54 Variation of wear height of AA 2014 alloy and its nano Al_2O_3 based MMNCs a) at 1000 m sliding distance b) at 2000 m sliding distance c) at 3000 m sliding distance d) at 4000 m sliding distance, with an Applied load of 5 N to 20 N & at constant Sliding Velocity 0.733 m/s.

6.6.3 Wear Weight Loss AA 2014/Al_2O_3/50 nm Nanocomposites

The variation in the wear weight loss with sliding distance under different loads are shown in Figure 6.55 a,b,c&d . The cast AA2014/Al_2O_3/50 nm MMNC undergo higher wear weight loss with an increase in sliding distance. The wear weight loss of AA2014/ Al_2O_3/50 nm the metal matrix nanocomposites was observed at all the sliding distances and concluded that the wear weight loss of MMNC was less when compared with base MMC. The wear weight loss was reduced while increasing the weight percentage of nano Al_2O_3 in the base alloy. The variation in the wear weight loss with an applied load is shown in Figure 6.56 a,b,c&d at sliding distances of 1Km,2Km,3Km&4Km respectively. The cast AA2014and its nano Al_2O_3 reinforced metal matrix nanocomposites undergo higher wear weight loss with an increase in applied load. The wear weight loss of the metal matrix nanocomposites was observed at all the applied loads and concluded that the wear weight loss of AA2014/ Al_2O_3/50 nm composite was less when compared with base MMC. The wear weight loss was reduced while increasing the weight percentage of nano Al_2O_3 in the base alloy and it is shown in Figures 6.56. In all these results sliding velocity kept constant (SV=0.733m/s). The reasons for all these works are well known fact established in literature. As the wt.% of particulate Al_2O_3 increase in AA2014 the hardness and strength were increasing hence resistance to wear is also increases.

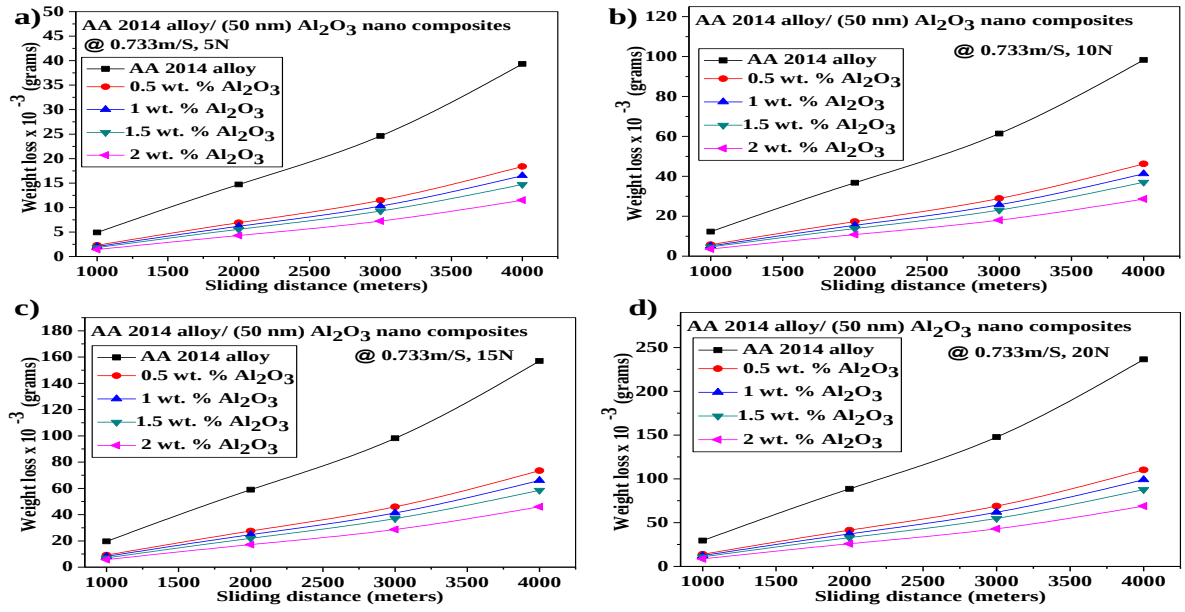

Figure 6.55 Variation of wear weight loss AA2014 alloy and its nano Al_2O_3 based MMNCs a) at 5 N load b) at 10 N load c) at 15 N load d) at 20 N load, with sliding distance of 1000 m to 4000 m and at constant sliding velocity of 0.733 m/s.

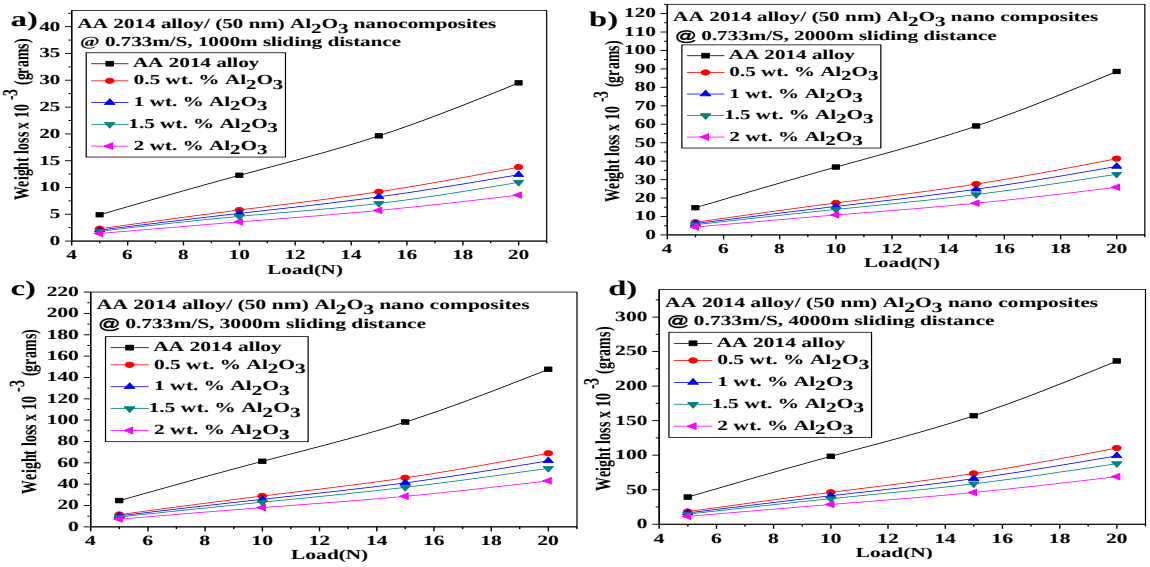

Figure 6.56 Variation of wear weight loss of AA2014 alloy and its nano Al_2O_3 MMNCs a) at 1000 m sliding distance b) at 2000 m sliding distance c) at 3000 m sliding distance d) at 4000 m sliding distance, with an applied load of 5 N to 20 N, and constant sliding velocity 0.733 m/s.

6.6.4 Specific Wear Rate AA2014/Al2O3/50 nm Nanocomposites

The variation in the specific wear rate with sliding distance under different loads are shown in Figure 6.57 a,b,c&d . The cast AA2014/Al_2O_3/50 nm MMNC undergo higher specific wear rate with an increase in sliding distance. The specific wear rate of AA2014/ Al_2O_3/50 nm the metal matrix nanocomposites was observed at all the sliding distances and concluded that the specific wear rate of MMNC was less when compared with base MMC. The specific wear rate was reduced while increasing the weight percentage of nano Al_2O_3 in the base alloy. The variation in the specific wear rate with an applied load is shown in Figure 6.58 a,b,c&d at sliding distances of 1Km,2Km,3Km&4Km respectively. The cast AA2014 and its nano Al_2O_3 reinforced metal matrix nanocomposites undergo higher specific wear rate with an increase in applied load. The specific wear rate of the metal matrix nanocomposites was observed at all the applied loads and concluded that the specific wear rate of AA2014/ Al_2O_3/50 nm composite was less when compared with base MMC. The specific wear rate was reduced while increasing the weight percentage of nano Al_2O_3 in the base alloy and it is shown in Figures 6.58. In all these results sliding velocity kept constant (SV=0.733m/s). The reasons for all these works are well known

fact established in literature. As the wt.% of particulate Al_2O_3 increase in AA2014 the hardness and strength were increasing hence resistance to wear is also increases.

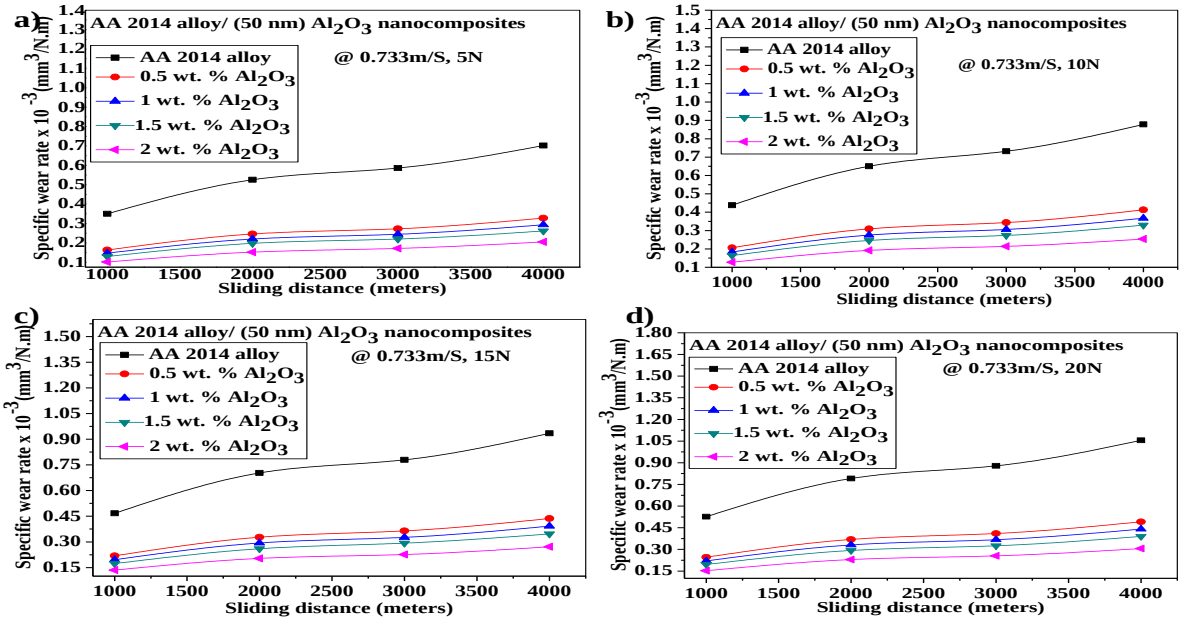

Figure 6.57 Variation of specific wear rate AA2014 alloy and its nano Al_2O_3 based MMNCs a) at 5 N load b) at 10 N load c) at 15 N load d) at 20 N load, with sliding distance of 1000 m to 4000 m and at constant sliding velocity of 0.733 m/s.

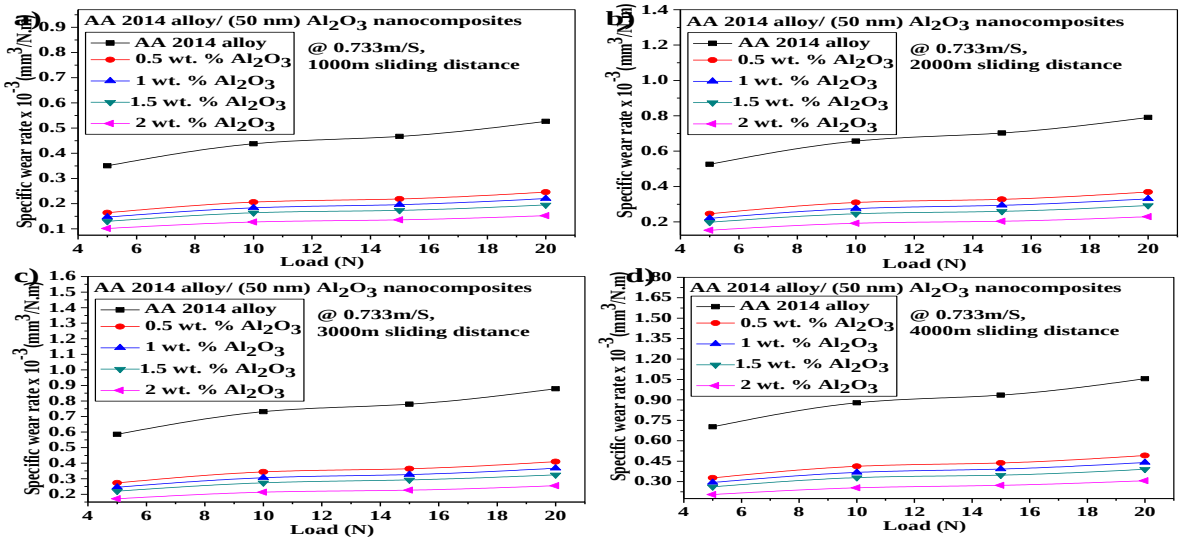

Figure 6.58 Variation of specific wear rate of AA2014 alloy and its nano Al_2O_3 based MMNCs a) at 1000 m sliding distance b) at 2000 m sliding distance c) at 3000 m sliding distance d) at 4000 m sliding distance, with an applied load of 5 N to 20 N and constant sliding velocity 0.733 m/s.

6.6.5 Coefficient of Friction of AA2014/Al_2O_3/50 nm Nanocomposites

The variation in coefficient of friction of AA2014/Al_2O_3/50 nm nanocomposites with sliding distance is shown in Figure 6.59 a,b,c&d for sliding distance 1Km,2Km,3Km and 4Km AA2014/ Al_2O_3/50 nm MMNC obeys the law of static and dynamic friction as friction coefficient is observed to be decreases with increase in sliding distance. The coefficient of friction of the metal matrix nanocomposites was observed at all the sliding distances and concluded that the coefficient of friction is more when compared with base material. The variation in coefficient of friction with load is shown in Figure 6.60 a,b,c&d for 5 N,10 N,15 N&20 N respectively. As shown in Figure 6.60 a,b,c&d the coefficient of friction of the AA2014/Al_2O_3/50 nm metal matrix nanocomposites was observed at all the applied loads and concluded that the coefficient of friction of MMNCs increases with load. The coefficient of friction was increased while increasing the weight percentage of nano Al_2O_3 in the base alloy. This obeys the law of friction.

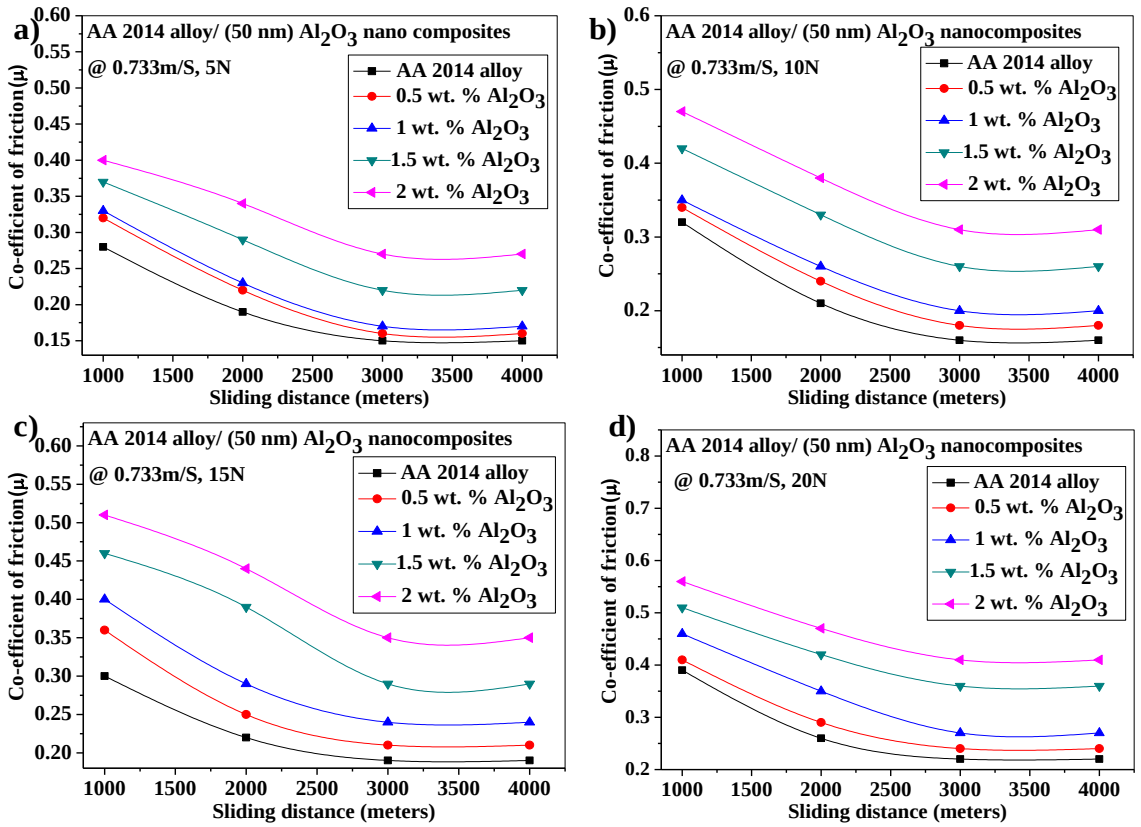

Figure 6.59 Variation of COF AA2014 alloy and its Al_2O_3 Nano Composites a) at 5 N load b) at 10 N load c) at 15 N load d) at 20 N load, with sliding distance of 1000 m to 4000 m and at constant sliding velocity of 0.733 m/s.

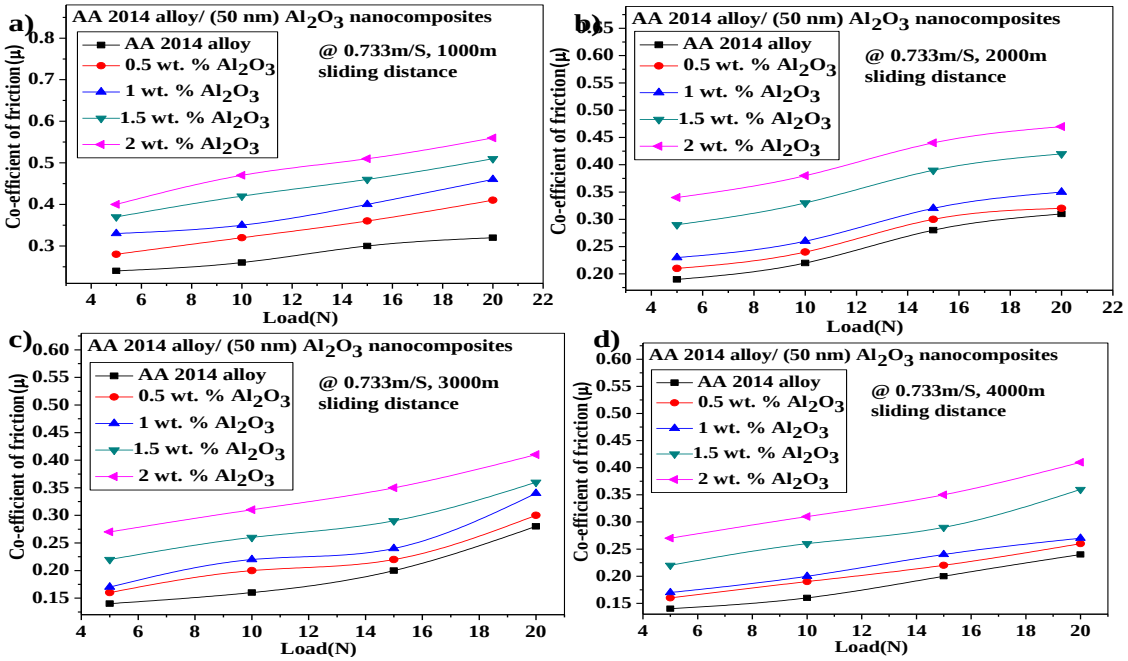

Figure 6.60 Variation of COF of AA2014 alloy and its Al_2O_3 Nano Composites a) at 1000 m sliding distance b) at 2000 m sliding distance c) at 3000 m sliding distance d) at 4000 m sliding distance, with an applied load of 5 N to 20 N, and at constant sliding velocity 0.733 m/s.

6.7 Wear Resistance Properties of AA2014/SiC/150 nm Nanocomposites

6.7.1 Volume of Wear AA2014/SiC/150 nm Nanocomposites

The variation in the volume of wear with sliding distance under different loads are shown in Figure 6.61 a,b,c&d . The cast AA2014/SiC/150 nm MMNC undergo higher volume of wear with an increase in sliding distance. The volume of wear of AA2014/SiC/150 nm the metal matrix nanocomposites was observed at all the sliding distances and concluded that the volume of wear of MMNC was less when compared with base MMC. The volume of wear was reduced while increasing the weight percentage of nano SiC in the base alloy. The variation in the volume of wear with an applied load is shown in Figure 6.62 a,b,c&d at sliding distances of 1Km,2Km,3Km&4Km respectively. The cast AA2014and its nano SiC reinforced metal matrix nanocomposites undergo higher volume of wear with an increase in applied load. The volume of wear of the metal matrix nanocomposites was observed at all the applied loads and concluded that the volume of wear of AA2014/SiC/150 nm composite was less when compared with base MMC. The volume of

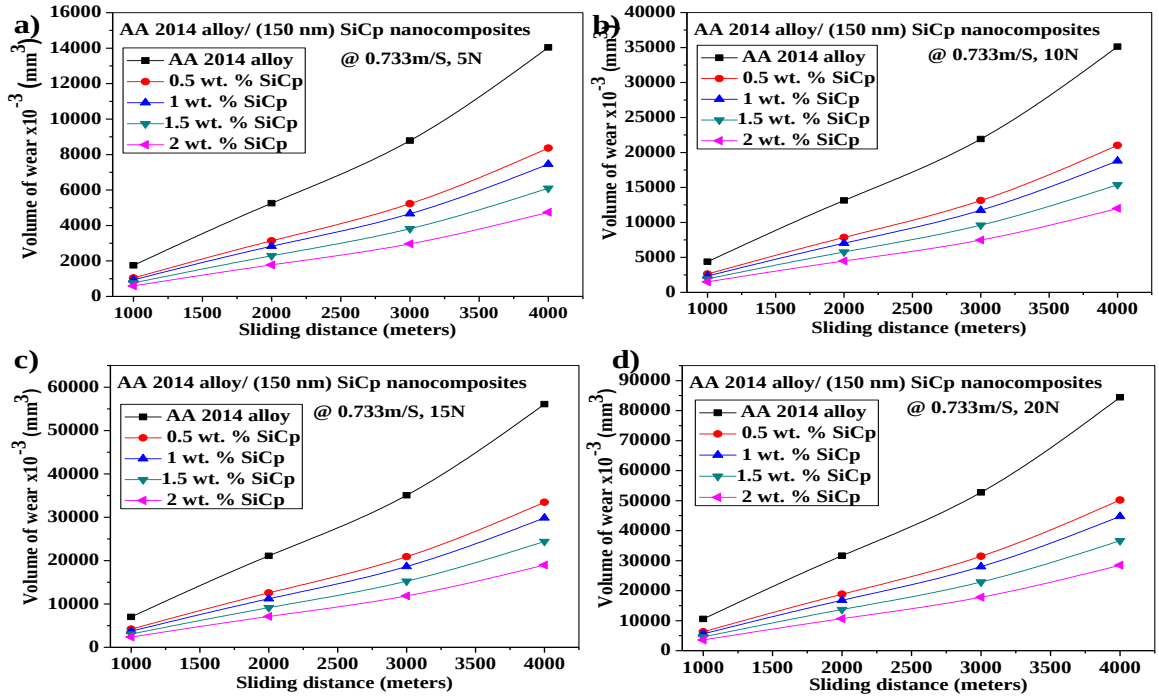

Figure 6.61 Variation of the volume of wear AA 2014 alloy and its nano SiC based MMNCs a) at 5 N load b) at 10 N load c) at 15 N load d) at 20 N load, with sliding distance of 1000 to 4000 m, at a constant sliding velocity of 0.733 m/s.

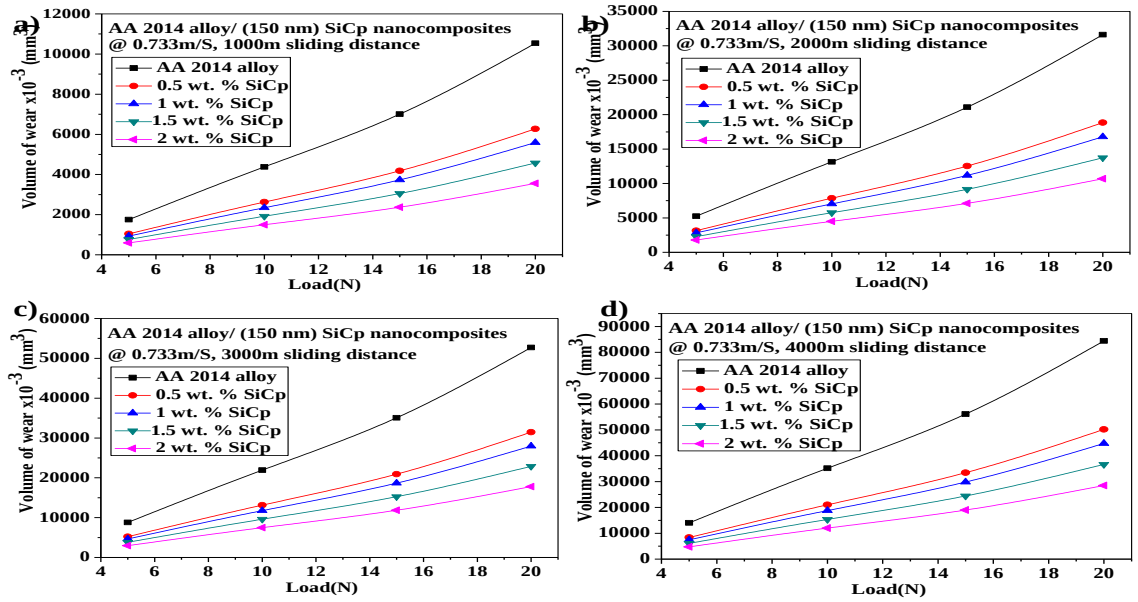

Figure 6.62 Variation of the volume of wear AA 2014 alloy and its nano SiC based MMNCs a) at 1000 m sliding distance b) at 2000 m sliding distance c) at 3000 m sliding distance d) at 4000 m sliding distance, with an applied load of 5 N to 20 N, at constant sliding velocity 0.733 m/s.

wear was reduced while increasing the weight percentage of nano SiC in the base alloy and it is shown in Figures 6.62. In all these results sliding velocity kept constant (SV=0.733m/s). The reasons for all these works are well known fact established in literature. As the wt.% of particulate SiC increase in AA2014 the hardness and strength were increasing hence resistance to wear is also increases.

6.7.2 Wear Height AA 2014/SiC/150 nm Nanocomposites

The variation in the wear height with sliding distance under different loads are shown in Figure 6.63 a,b,c&d . The cast AA2014/SiC/150 nm MMNC undergo higher loss in wear height with an increase in sliding distance. The wear height of AA2014/SiC/150 nm the metal matrix nanocomposites was observed at all the sliding distances and concluded that the wear height of MMNC was less when compared with base MMC.

The loss of wear height was reduced while increasing the weight percentage of nano SiC in the base alloy. The variation in the wear height with an applied load is shown in Figure 6.64 a,b,c&d at sliding distances of 1Km,2Km,3Km&4Km respectively.

The cast AA2014and its nano SiC reinforced metal matrix nanocomposites undergo higher loss of wear height with an increase in applied load. The wear height of the metal matrix nanocomposites was observed at all the applied loads and concluded that the loss of wear height of AA2014/SiC/150 nm composite was less when compared with base MMC.

The loss of wear height was reduced while increasing the weight percentage of nano SiC in the base alloy and it is shown in Figures 6.64. In all these results sliding velocity kept constant (SV=0.733m/s). The reasons for all these works are well known fact established in literature. As the wt.% of particulate SiC increase in AA2014 the hardness and strength were increasing hence resistance to wear is also increases.

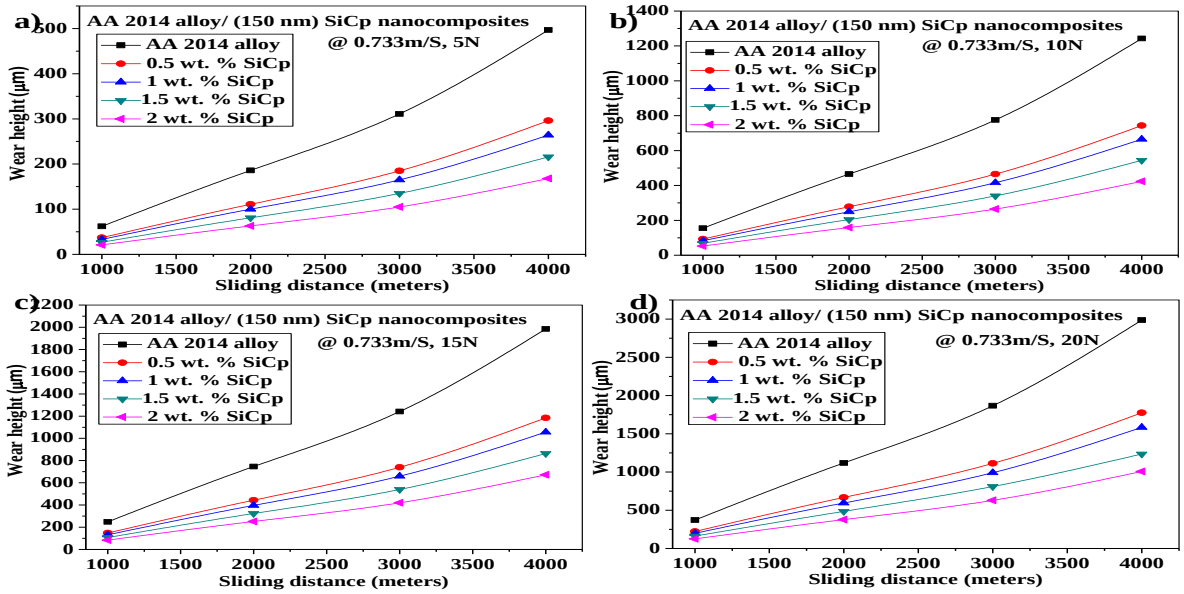

Figure 6.63 Variation of wear height AA 2014 alloy and its nano SiC based MMNCs a) at 5 N load b) at 10 N load c) at 15 N load d) at 20 N load, with sliding distance of 1000 m to 4000 m, at constant sliding velocity of 0.733 m/s.

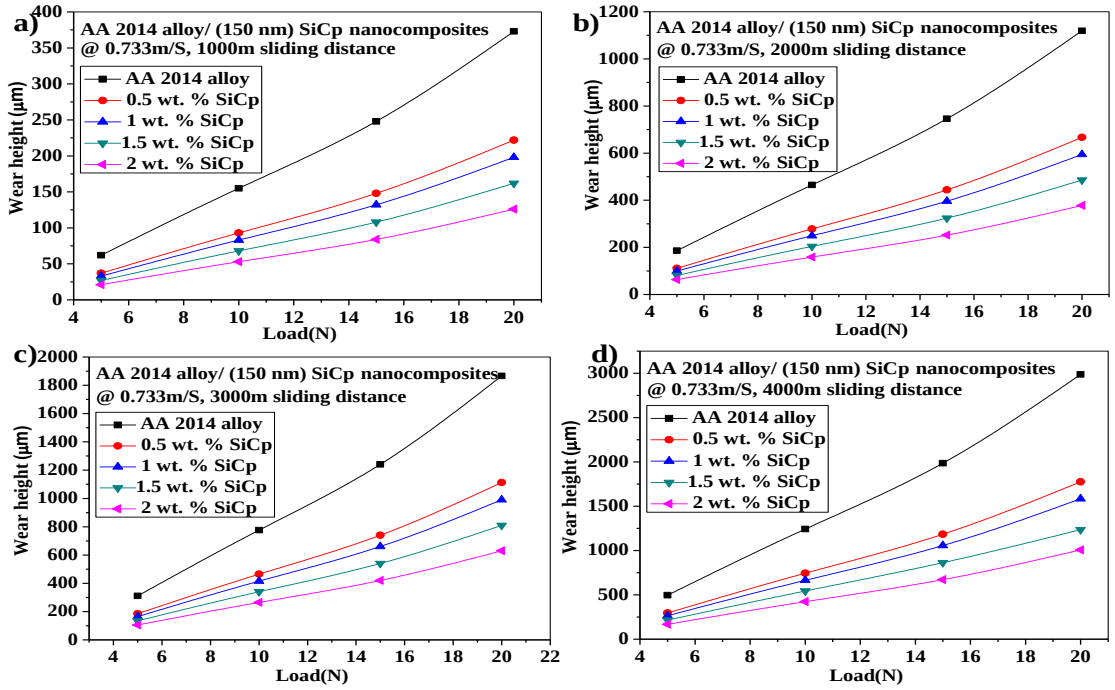

Figure 6.64 Variation of wear height of AA 2014 alloy and its nano SiC based MMNCs a) at 1000 m sliding distance b) at 2000 m sliding distance c) at 3000 m sliding distance d) at 4000 m sliding distance, with an Applied load of 5 N to 20 N & at constant Sliding Velocity 0.733 m/s.

6.7.3 Wear Weight Loss AA 2014/SiC/150 nm Nanocomposites

The variation in the wear weight loss with sliding distance under different loads are shown in Figure 6.65 a,b,c&d . The cast AA2014/SiC/150 nm MMNC undergo higher wear weight loss with an increase in sliding distance. The wear weight loss of AA2014/SiC/150 nm the metal matrix nanocomposites was observed at all the sliding distances and concluded that the wear weight loss of MMNC was less when compared with base MMC. The wear weight loss was reduced while increasing the weight percentage of nano SiC in the base alloy. The variation in the wear weight loss with an applied load is shown in Figure 6.66 a,b,c&d at sliding distances of 1Km,2Km,3Km&4Km respectively. The cast AA2014and its nano SiC reinforced metal matrix nanocomposites undergo higher wear weight loss with an increase in applied load. The wear weight loss of the metal matrix nanocomposites was observed at all the applied loads and concluded that the wear weight loss of AA2014/SiC/150 nm composite was less when compared with base MMC.

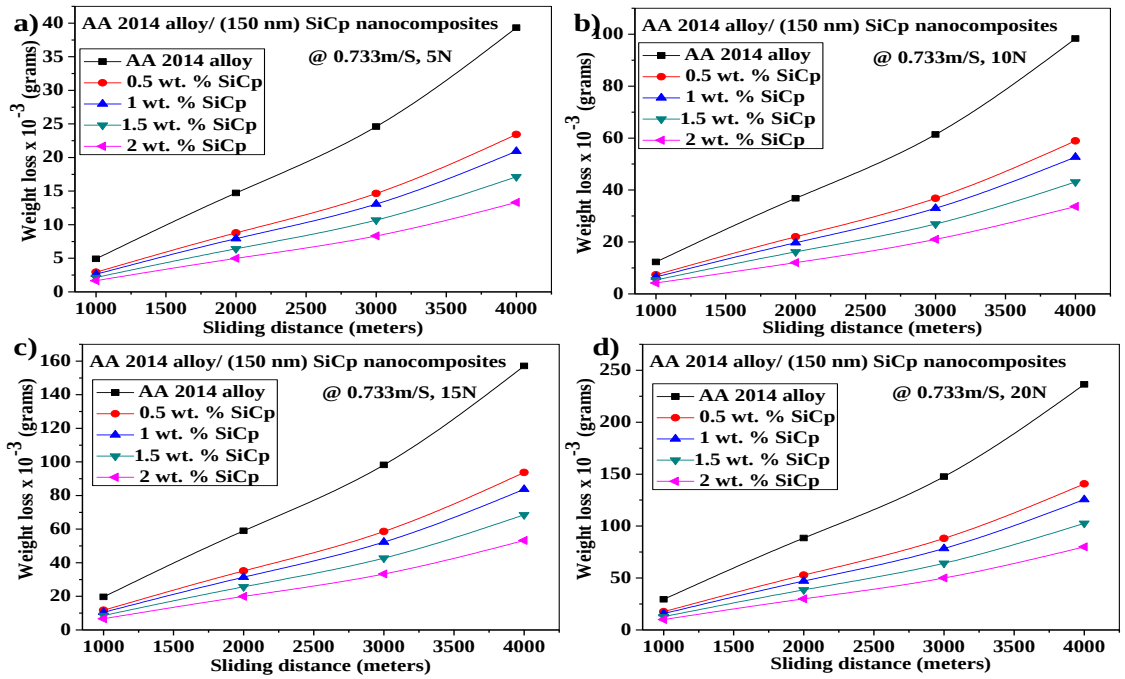

Figure 6.65 Variation of wear weight loss AA2014 alloy and its nano SiC based MMNCs a) at 5 N load b) at 10 N load c) at 15 N load d) at 20 N load, with sliding distance of 1000 m to 4000 m and at constant sliding velocity of 0.733 m/s.

The wear weight loss was reduced while increasing the weight percentage of nano SiC in the base alloy and it is shown in Figures 6.66. In all these results sliding velocity kept constant (SV=0.733m/s). The reasons for all these works are well known fact established in literature. As the wt.% of particulate SiC increase in AA2014 the hardness and strength were increasing hence resistance to wear is also increases.

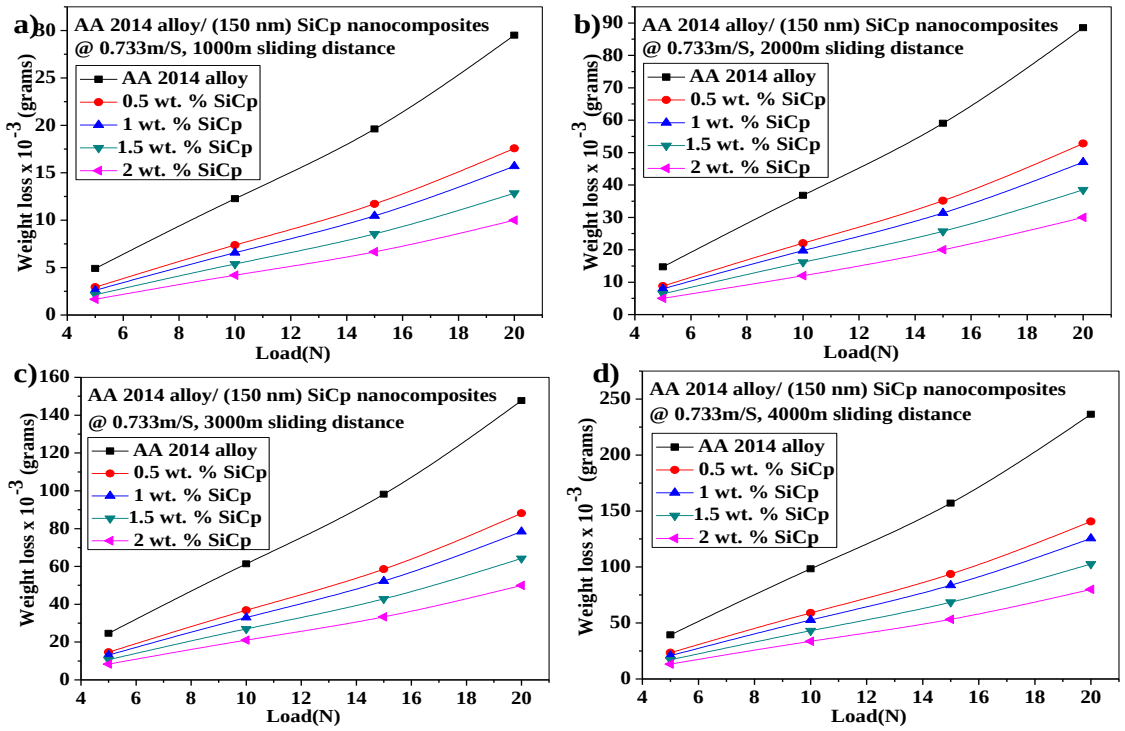

Figure 6.66 Variation of wear weight loss of AA2014 alloy and its nano SiC MMNCs a) at 1000 m sliding distance b) at 2000 m sliding distance c) at 3000 m sliding distance d) at 4000 m sliding distance, with an applied load of 5 N to 20 N, and constant sliding velocity 0.733 m/s.

6.7.4 Specific Wear Rate AA 2014/SiC/150 nm Nanocomposites

The variation in the specific wear rate with sliding distance under different loads are shown in Figure 6.67 a,b,c&d . The cast AA2014/SiC/150 nm MMNC undergo higher specific wear rate with an increase in sliding distance. The specific wear rate of AA2014/SiC/150 nm the metal matrix nanocomposites was observed at all the sliding distances and concluded that the specific wear rate of MMNC was less when compared with base MMC. The specific wear rate was reduced while increasing the weight percentage of nano SiC in the base alloy. The variation in the specific wear rate with an applied load is shown in Figure 6.68 a,b,c&d at sliding distances of 1Km,2Km,3Km&4Km respectively. The cast AA2014 and its nano SiC reinforced metal matrix nanocomposites undergo higher specific wear rate with an increase in applied load. The specific wear rate of the metal matrix nanocomposites was observed at all the applied loads and concluded that the specific wear rate of AA2014/SiC/150 nm composite was less when compared with base MMC. The specific wear rate was reduced while increasing the weight

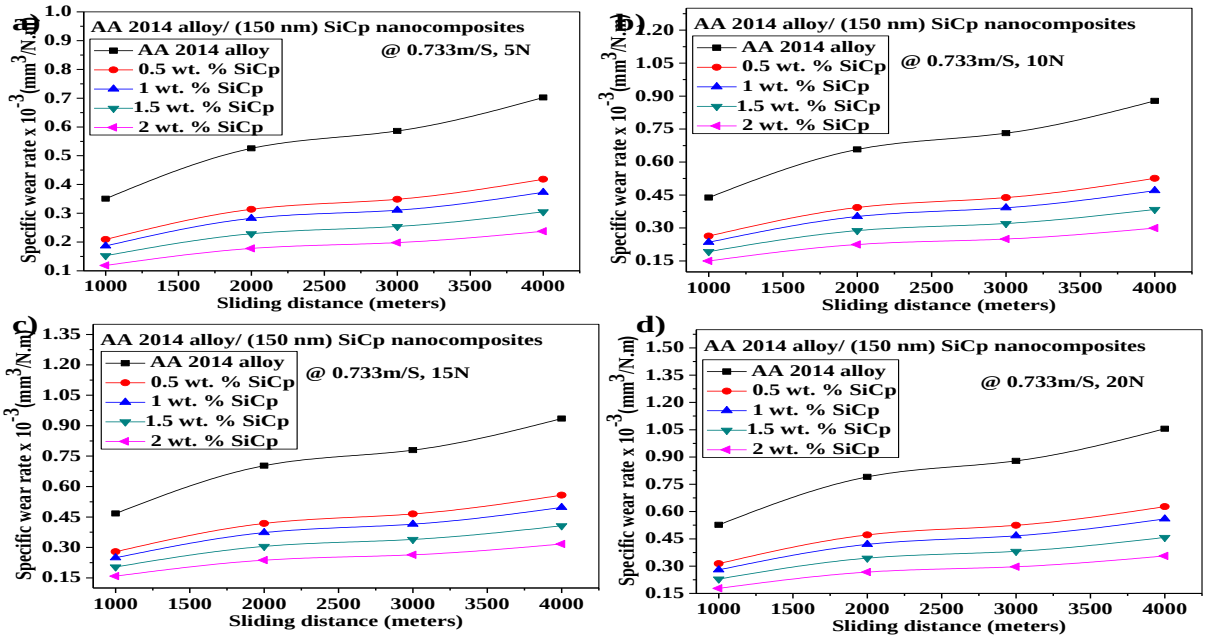

Figure 6.67 Variation of specific wear rate AA2014 alloy and its nano SiC based MMNCs a) at 5 N load b) at 10 N load c) at 15 N load d) at 20 N load, with sliding distance of 1000 m to 4000 m and at constant sliding velocity of 0.733 m/s.

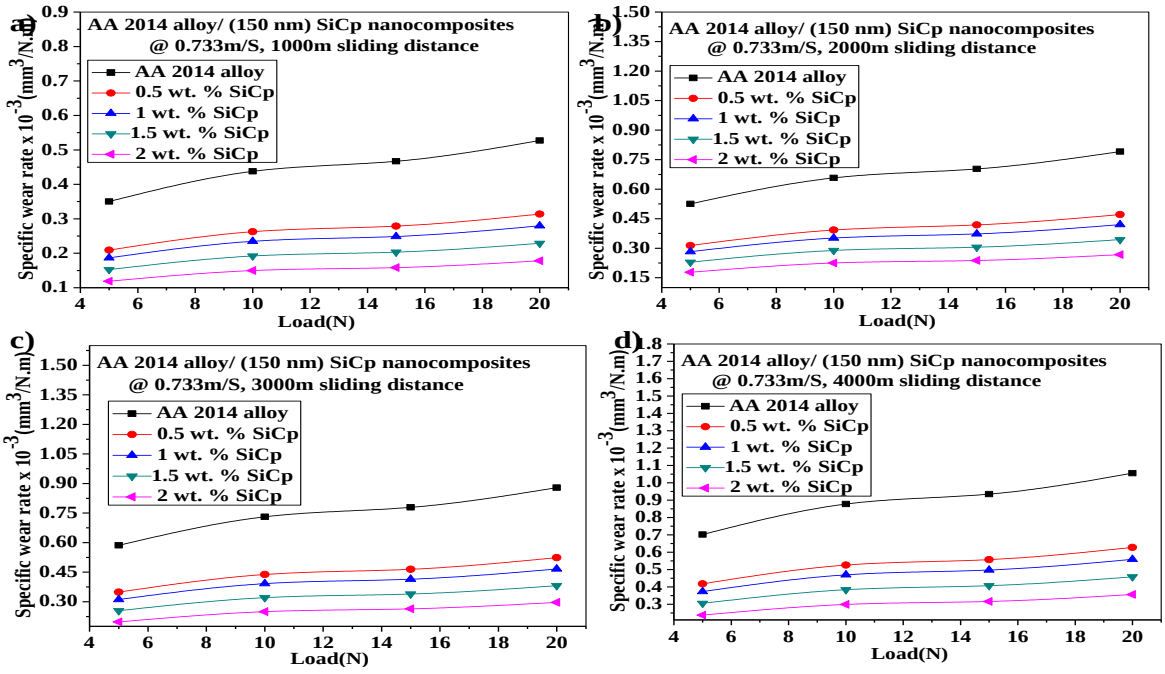

Figure 6.68 Variation of specific wear rate of AA2014 alloy and its nano SiC based MMNCs a) at 1000 m sliding distance b) at 2000 m sliding distance c) at 3000 m sliding distance d) at 4000 m sliding distance, with an applied load of 5 N to 20 N and constant sliding velocity 0.733 m/s.

percentage of nano SiC in the base alloy and it is shown in Figures 6.68. In all these results sliding velocity kept constant (SV=0.733m/s). The reasons for all these works are well known fact established in literature. As the wt.% of particulate SiC increase in AA2014 the hardness and strength were increasing hence resistance to wear is also increases.

6.7.5 Coefficient of Friction of AA 2014/SiC/150 nm Nanocomposites

The variation in coefficient of friction of AA2014/SiC/150 nm nanocomposites with sliding distance is shown in Figure 6.69 a,b,c&d for sliding distance 1Km,2Km,3Km and 4Km AA2014/SiC/150 nm MMNC obeys the law of static and dynamic friction as friction coefficient is observed to be decreases with increase in sliding distance. The coefficient of friction of the metal matrix nanocomposites was observed at all the sliding distances and concluded that the coefficient of friction is more when compared with base material. The variation in coefficient of friction with load is shown in Figure 6.70 a,b,c&d for 5 N,10 N,15 N&20 N respectively. As shown in Figure 6.70 a,b,c&d the coefficient of friction of the AA2014/SiC/150 nm metal matrix nanocomposites was observed at all the applied loads and concluded that the coefficient of friction of MMNCs increases with load. The coefficient of friction was increased while increasing the weight percentage of nano SiC in the base alloy. This obeys the law of friction.

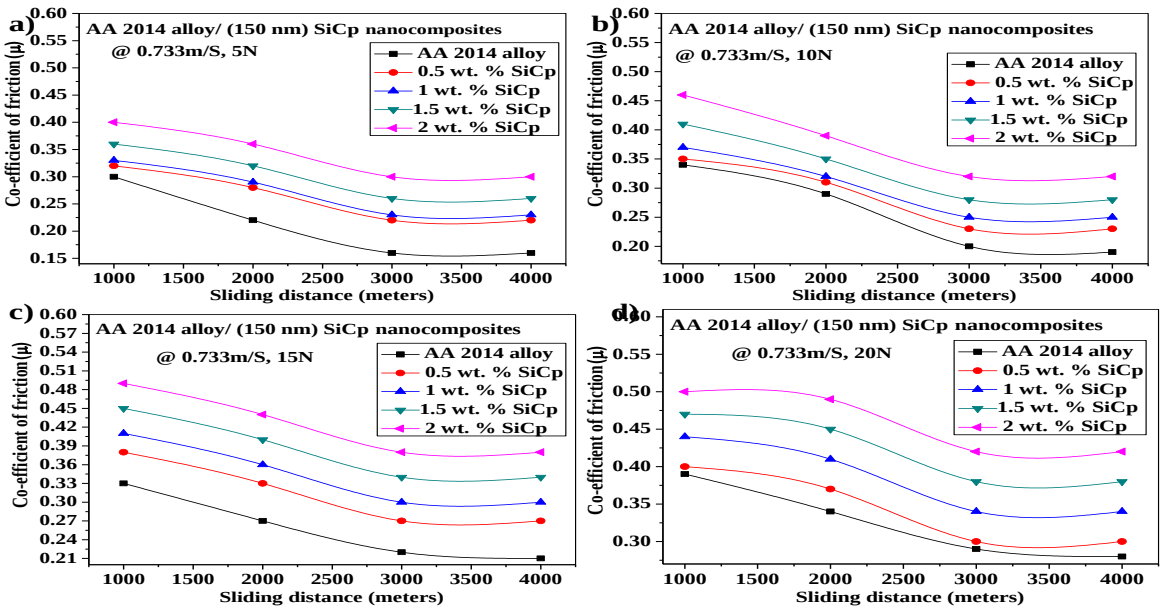

Figure 6.69 Variation of COF AA2014 alloy and its SiC Nano Composites a) at 5 N load b) at 10 N load c) at 15 N load d) at 20 N load, with sliding distance of 1000 m to 4000 m and at constant sliding velocity of 0.733 m/s.

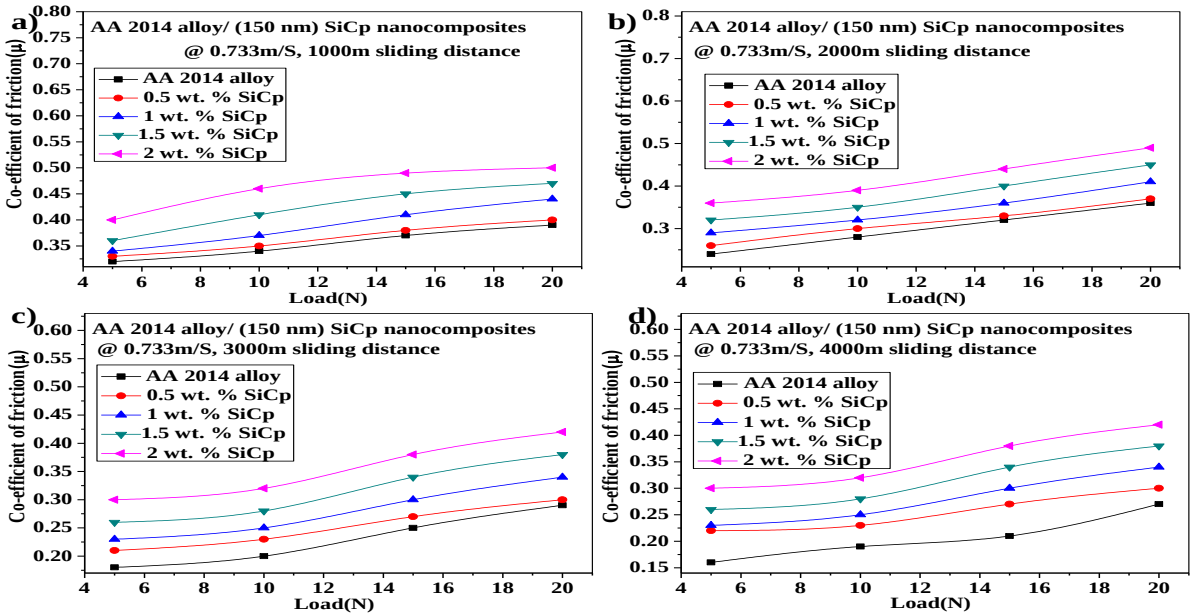

Figure 6.70 Variation of COF of AA2014 alloy and its SiC Nano Composites a) at 1000 m sliding distance b) at 2000 m sliding distance c) at 3000 m sliding distance d) at 4000 m sliding distance, with an applied load of 5 N to 20 N, and at constant sliding velocity 0.733 m/s.

6.8 Wear Resistance Properties of AA2014/Al_2O_3/150 nm Nanocomposites

6.8.1 Volume of Wear AA2014/Al_2O_3/150 nm Nanocomposites

The variation in the volume of wear with sliding distance under different loads are shown in Figure 6.71 a,b,c&d . The cast AA2014/Al_2O_3/150 nm MMNC undergo higher volume of wear with an increase in sliding distance. The volume of wear of AA2014/Al_2O_3/150 nm the metal matrix nanocomposites was observed at all the sliding distances and concluded that the volume of wear of MMNC was less when compared with base MMC. The volume of wear was reduced while increasing the weight percentage of nano Al_2O_3 in the base alloy. The variation in the volume of wear with an applied load is shown in Figure 6.72 a,b,c&d at sliding distances of 1Km,2Km,3Km&4Km respectively. The cast AA2014 and its nano Al_2O_3 reinforced metal matrix nanocomposites undergo higher volume of wear with an increase in applied load. The volume of wear of the metal matrix nanocomposites was observed at all the applied loads and concluded that the volume of wear of AA2014/ Al_2O_3/150 nm composite was less when compared with base MMC. The volume of wear was reduced while increasing the weight percentage of nano Al_2O_3

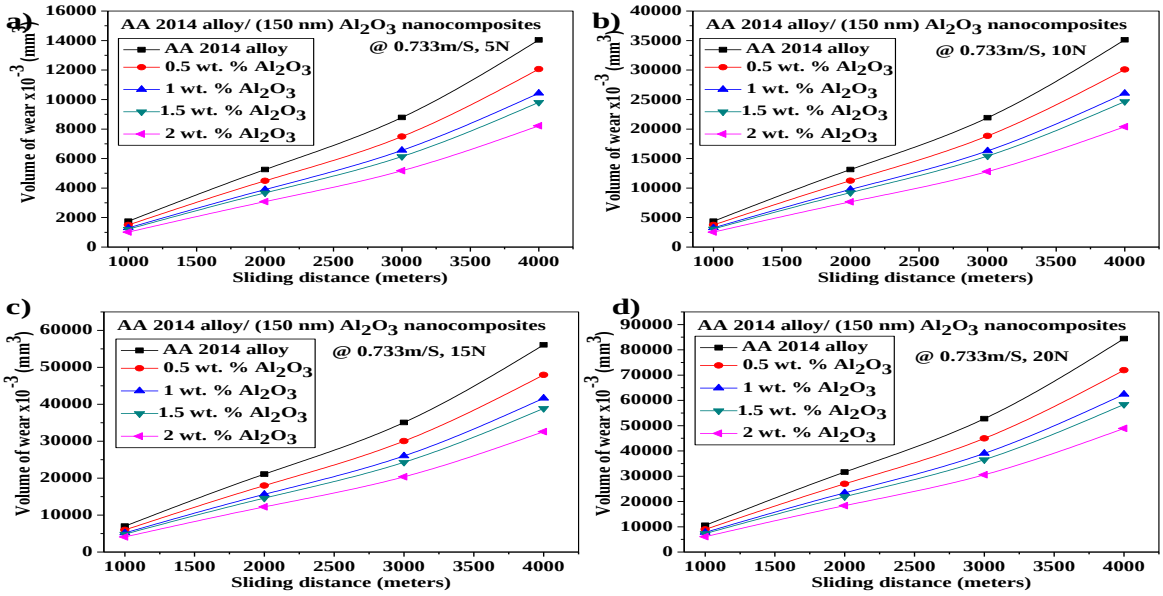

Figure 6.71 Variation of the volume of wear AA 2014 alloy and its nano Al_2O_3 based MMNCs a) at 5 N load b) at 10 N load c) at 15 N load d) at 20 N load, with sliding distance of 1000 to 4000 m, at a constant sliding velocity of 0.733 m/s.

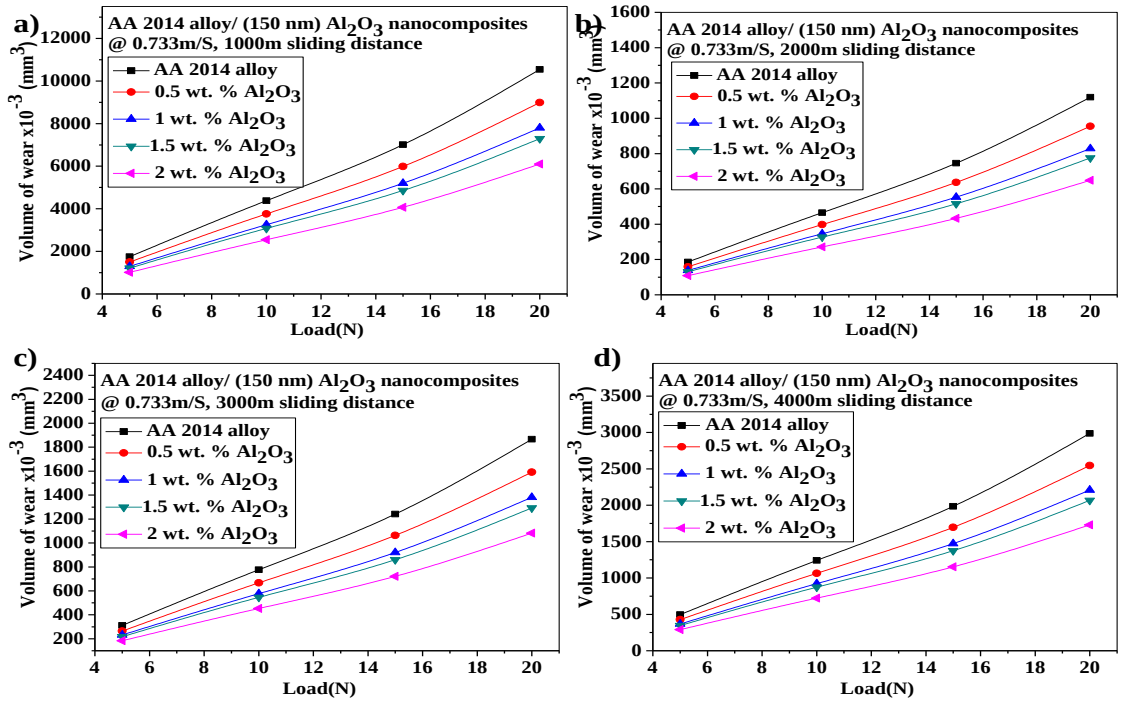

Figure 6.72 Variation of the volume of wear AA 2014 alloy and its nano Al_2O_3 based MMNCs a) at 1000 m sliding distance b) at 2000 m sliding distance c) at 3000 m sliding distance d) at 4000 m sliding distance, with an applied load of 5 N to 20 N, at constant sliding velocity 0.733 m/s.

in the base alloy and it is shown in Figures 6.72. In all these results sliding velocity kept constant (SV=0.733m/s). The reasons for all these works are well known fact established in literature. As the wt.% of particulate Al_2O_3 increase in AA2014 the hardness and strength were increasing hence resistance to wear is also increases.

6.8.2 Wear Height AA 2014/Al_2O_3/150 nm Nanocomposites

The variation in the wear height with sliding distance under different loads are shown in Figure 6.73 a,b,c&d . The cast AA2014/Al_2O_3/150 nm MMNC undergo higher loss in wear height with an increase in sliding distance. The wear height of AA2014/Al_2O_3/150 nm the metal matrix nanocomposites was observed at all the sliding distances and concluded that the wear height of MMNC was less when compared with base MMC.

The loss of wear height was reduced while increasing the weight percentage of nano Al_2O_3 in the base alloy. The variation in the wear height with an applied load is shown in Figure 6.74 a,b,c&d at sliding distances of 1Km,2Km,3Km&4Km respectively. The cast AA2014and its nano Al_2O_3 reinforced metal matrix nanocomposites undergo higher loss of wear height with an increase in applied load.

The wear height of the metal matrix nanocomposites was observed at all the applied loads and concluded that the loss of wear height of AA2014/ Al_2O_3/150 nm composite was less when compared with base MMC. The loss of wear height was reduced while increasing the weight percentage of nano Al_2O_3 in the base alloy and it is shown in Figures 6.74. In all these results sliding velocity kept constant (SV=0.733m/s).

The reasons for all these works are well known fact established in literature. As the wt.% of particulate Al_2O_3 increase in AA2014 the hardness and strength were increasing hence resistance to wear is also increases.

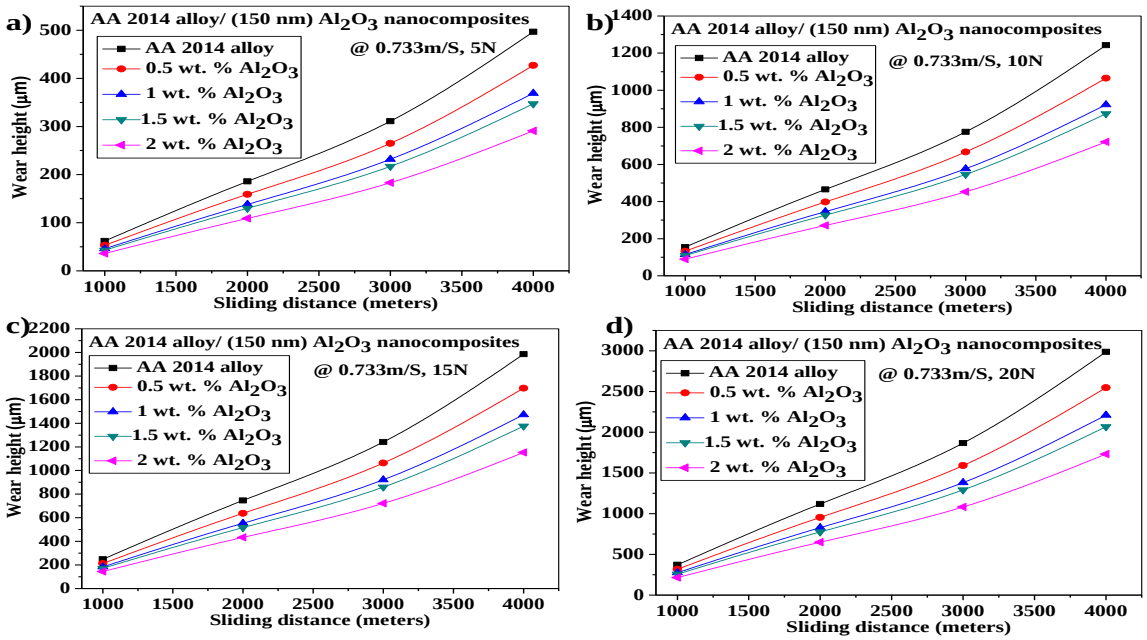

Figure 6.73 Variation of wear height AA 2014 alloy and its nano Al_2O_3 based MMNCs a) at 5 N load b) at 10 N load c) at 15 N load d) at 20 N load, with sliding distance of 1000 m to 4000 m, at constant sliding velocity of 0.733 m/s.

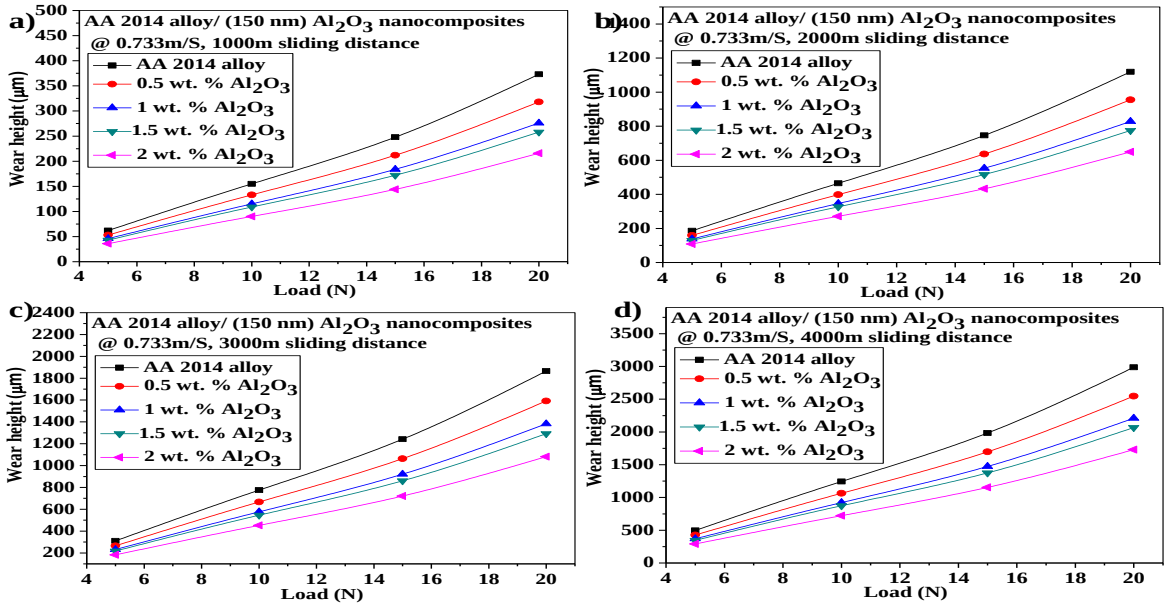

Figure 6.74 Variation of wear height of AA 2014 alloy and its nano Al_2O_3 based MMNCs a) at 1000 m sliding distance b) at 2000 m sliding distance c) at 3000 m sliding distance d) at 4000 m sliding distance, with an Applied load of 5 N to 20 N & at constant Sliding Velocity 0.733 m/s.

6.8.3 Wear Weight Loss AA 2014/Al_2O_3/150 nm Nanocomposites

The variation in the wear weight loss with sliding distance under different loads are shown in Figure 6.75 a,b,c&d . The cast AA2014/Al_2O_3/150 nm MMNC undergo higher wear weight loss with an increase in sliding distance. The wear weight loss of AA2014/ Al_2O_3/150 nm the metal matrix nanocomposites was observed at all the sliding distances and concluded that the wear weight loss of MMNC was less when compared with base MMC. The wear weight loss was reduced while increasing the weight percentage of nano Al_2O_3 in the base alloy. The variation in the wear weight loss with an applied load is shown in Figure 6.76 a,b,c&d at sliding distances of 1Km,2Km,3Km&4Km respectively. The cast AA2014and its nano Al_2O_3 reinforced metal matrix nanocomposites undergo higher wear weight loss with an increase in applied load. The wear weight loss of the metal matrix nanocomposites was observed at all the applied loads and concluded that the wear weight loss of AA2014/ Al_2O_3/150 nm composite was less when compared with base MMC. The wear weight loss was reduced while increasing the weight percentage of nano Al_2O_3 in the base alloy and it is shown in Figures 6.76. In all these results sliding velocity kept constant (SV=0.733m/s). The reasons for all these works are well known fact established in literature. As the wt.% of particulate Al_2O_3 increase in AA2014 the hardness and strength were increasing hence resistance to wear is also increases.

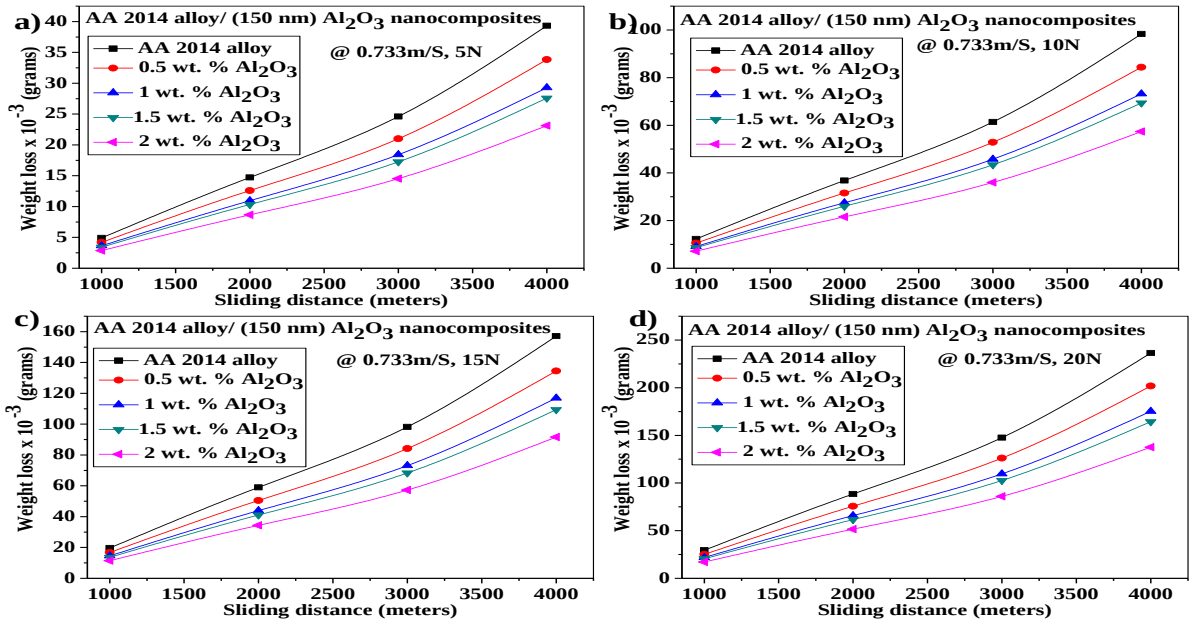

Figure 6.75 Variation of wear weight loss AA2014 alloy and its nano Al_2O_3 based MMNCs a) at 5 N load b) at 10 N load c) at 15 N load d) at 20 N load, with sliding distance of 1000 m to 4000 m and at constant sliding velocity of 0.733 m/s.

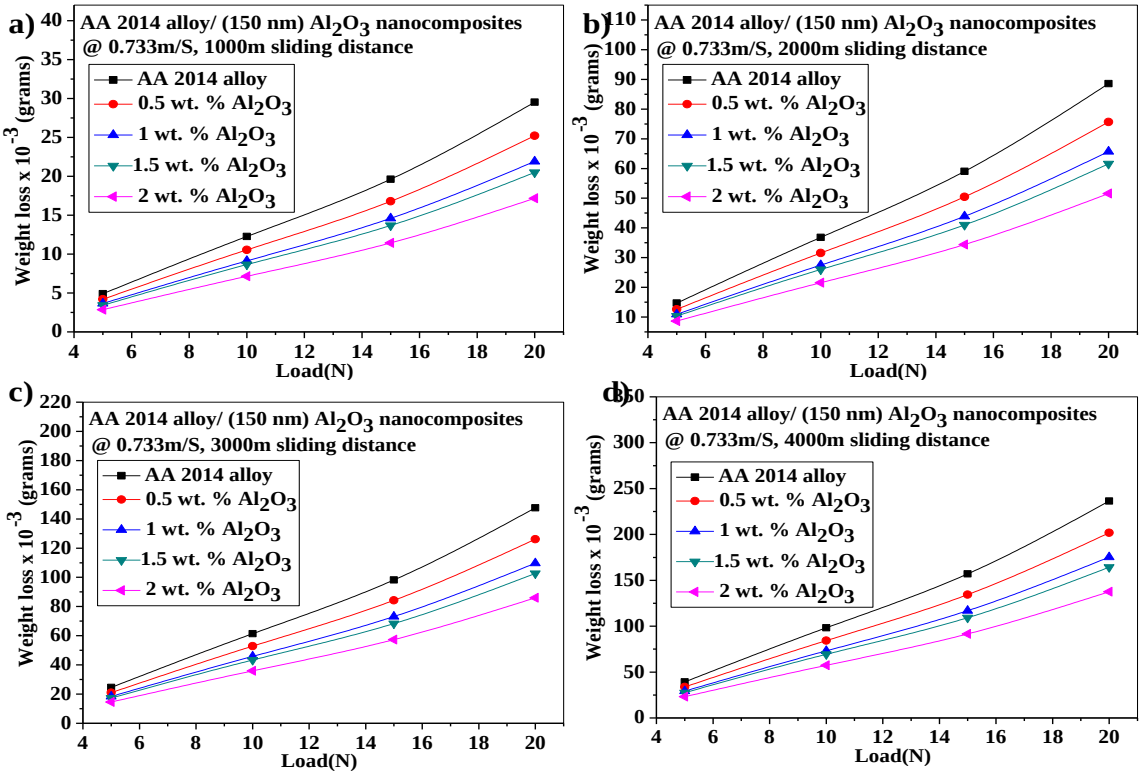

Figure 6.76 Variation of wear weight loss of AA2014 alloy and its nano Al_2O_3 MMNCs a) at 1000 m sliding distance b) at 2000 m sliding distance c) at 3000 m sliding distance d) at 4000 m sliding distance, with an applied load of 5 N to 20 N, and constant sliding velocity 0.733 m/s.

6.8.4 Specific Wear Rate AA2014/Al_2O_3/150 nm Nanocomposites

The variation in the specific wear rate with sliding distance under different loads are shown in Figure 6.77 a,b,c&d . The cast AA2014/Al_2O_3/150 nm MMNC undergo higher specific wear rate with an increase in sliding distance. The specific wear rate of AA2014/ Al_2O_3/150 nm the metal matrix nanocomposites was observed at all the sliding distances and concluded that the specific wear rate of MMNC was less when compared with base MMC. The specific wear rate was reduced while increasing the weight percentage of nano Al_2O_3 in the base alloy. The variation in the specific wear rate with an applied load is shown in Figure 6.78 a,b,c&d at sliding distances of 1km,2km,3km&4km respectively. The cast AA2014 and its nano Al_2O_3 reinforced metal matrix nanocomposites undergo higher specific wear rate with an increase in applied load. The specific wear rate of the metal matrix nanocomposites was observed at all the applied loads and concluded that the specific wear rate of AA2014/ Al_2O_3/150 nm composite was less when

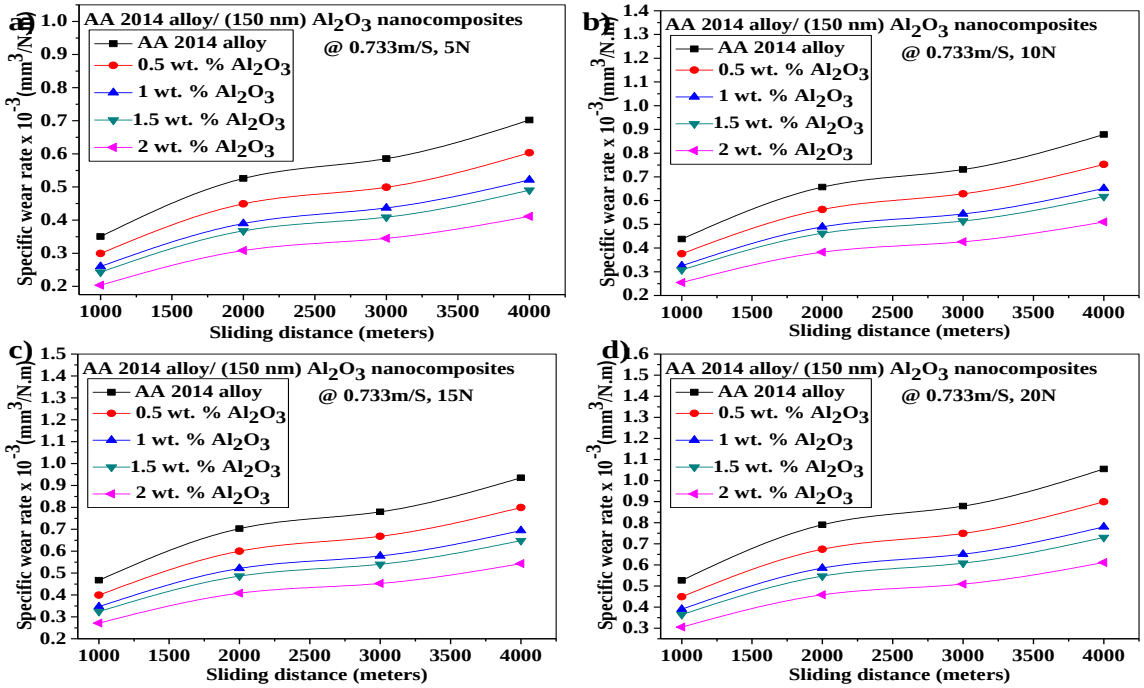

Figure 6.77 Variation of specific wear rate AA2014 alloy and its nano Al_2O_3 based MMNCs a) at 5 N load b) at 10 N load c) at 15 N load d) at 20 N load, with sliding distance of 1000 m to 4000 m and at constant sliding velocity of 0.733 m/s.

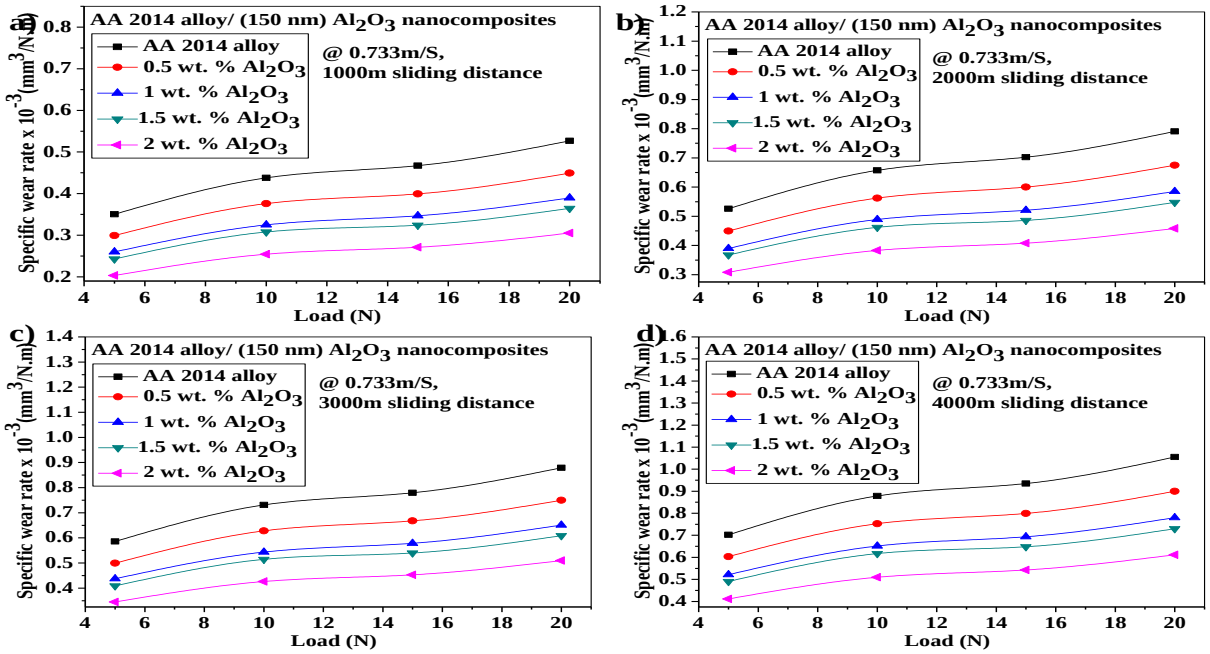

Figure 6.78 Variation of specific wear rate of AA2014 alloy and its nano Al_2O_3 based MMNCs a) at 1000 m sliding distance b) at 2000 m sliding distance c) at 3000 m sliding distance d) at 4000 m sliding distance, with an applied load of 5 N to 20 N and constant sliding velocity 0.733 m/s.

compared with base MMC. The specific wear rate was reduced while increasing the weight percentage of nano Al_2O_3 in the base alloy and it is shown in Figures 6.78. In all these results sliding velocity kept constant (SV=0.733m/s). The reasons for all these works are well known fact established in literature. As the wt.% of particulate Al_2O_3 increase in AA2014 the hardness and strength were increasing hence resistance to wear is also increases.

6.8.5 Coefficient of Friction of AA2014/ Al_2O_3/150 nm Nanocomposites

The variation in coefficient of friction of AA2014/Al_2O_3/150 nm nanocomposites with sliding distance is shown in Figure 6.79 a,b,c&d for sliding distance 1Km,2Km,3Km and 4Km AA2014/ Al_2O_3/150 nm MMNC obeys the law of static and dynamic friction as friction coefficient is observed to be decreases with increase in sliding distance. The coefficient of friction of the metal matrix nanocomposites was observed at all the sliding distances and concluded that the coefficient of friction is more when compared with base material. The variation in coefficient of friction with load is shown in Figure 6.80 a,b,c&d for 5 N,10 N,15 N&20 N respectively.

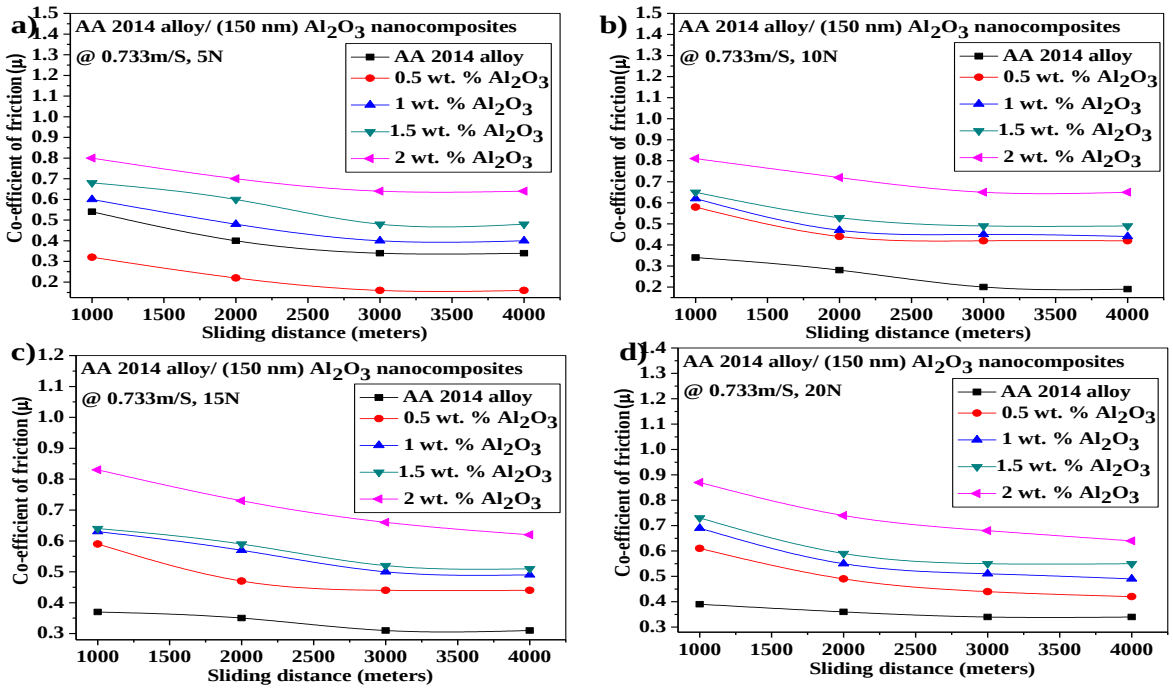

Figure 6.79 Variation of COF AA2014 alloy and its Al_2O_3 Nano Composites a) at 5 N load b) at 10 N load c) at 15 N load d) at 20 N load, with sliding distance of 1000 m to 4000 m and at constant sliding velocity of 0.733 m/s.

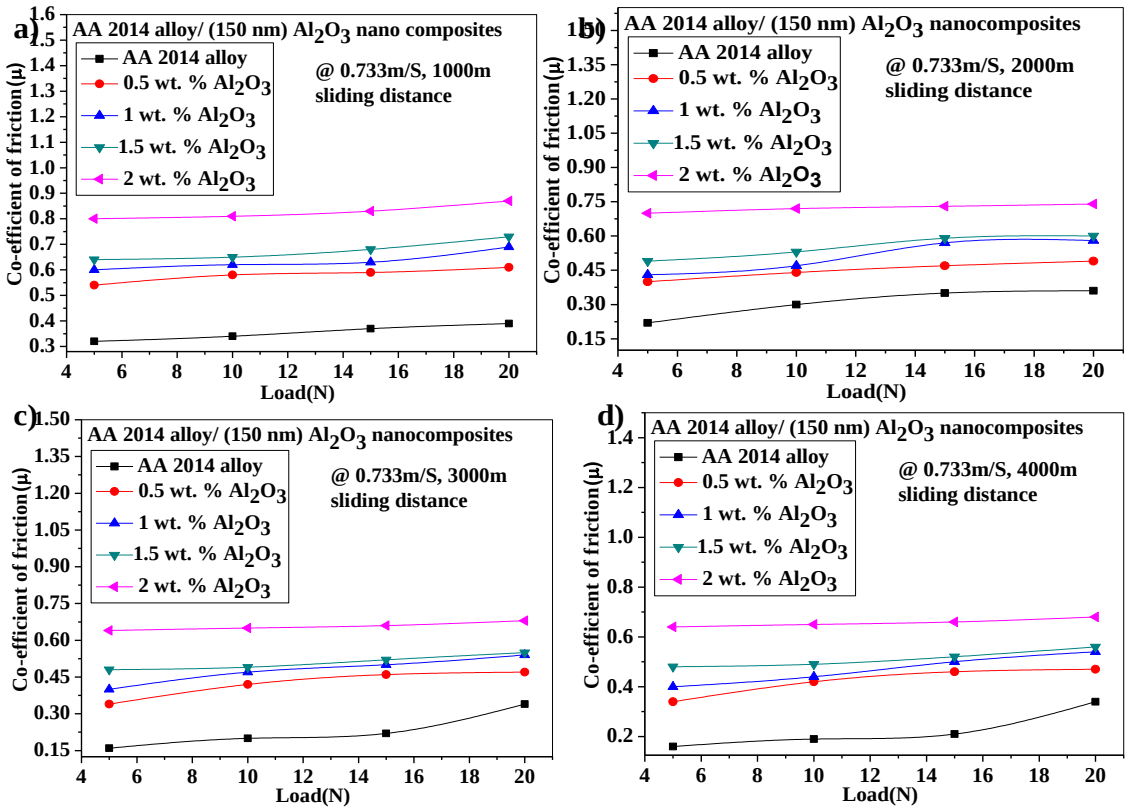

Figure 6.80 Variation of COF of AA2014 alloy and its Al_2O_3 Nano Composites a) at 1000 m sliding distance b) at 2000 m sliding distance c) at 3000 m sliding distance d) at 4000 m sliding distance, with an applied load of 5 N to 20 N, and at constant sliding velocity 0.733 m/s.

As shown in Figure 6.80 a,b,c&d the coefficient of friction of the AA2014/Al_2O_3/150 nm metal matrix nanocomposites was observed at all the applied loads and concluded that the coefficient of friction of MMNCs increases with load. The coefficient of friction was increased while increasing the weight percentage of nano Al_2O_3 in the base alloy. This obeys the law of friction.

6.9 Scanning Electron Micrograph

Teskon Scanning Electron Microscope (SEM) (Model 840) at National Institute of Technology, Warangal was used to study the worn surfaces of AA 2219-2 wt% SiC (50 nm&150 nm)/Al_2O_3 (50 nm,150 nm) and AA 2014-2 wt% SiC (50 nm&150 nm)/Al_2O_3 (50 nm,150 nm) specimens at maximum applied load of 20 N and maximum sliding distance of 4 km.

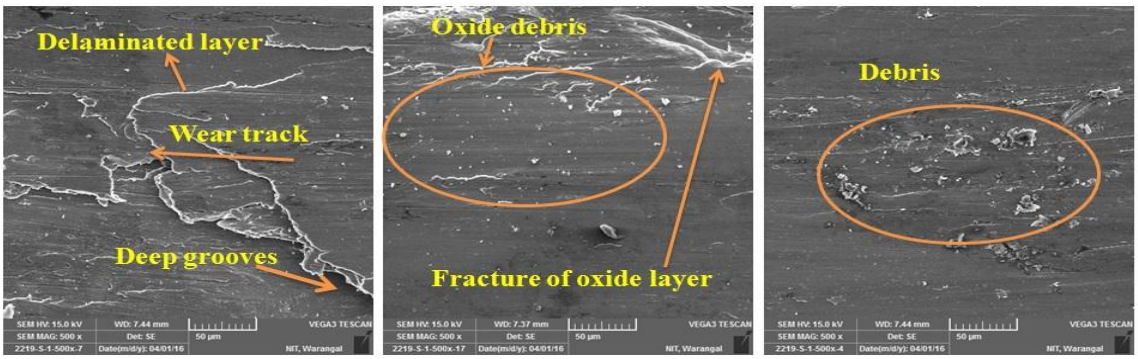

Figure 6.81 shows the worn surfaces of AA 2219/2 wt% /SiC /50 nm MMNC

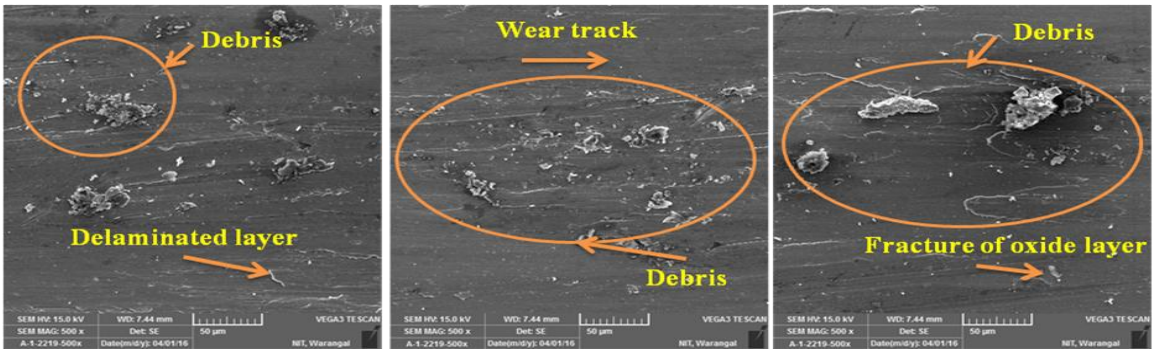

Figure 6.82 shows the worn surfaces of AA 2219/2 wt%/ Al_2O_3 /50 nm MMNC

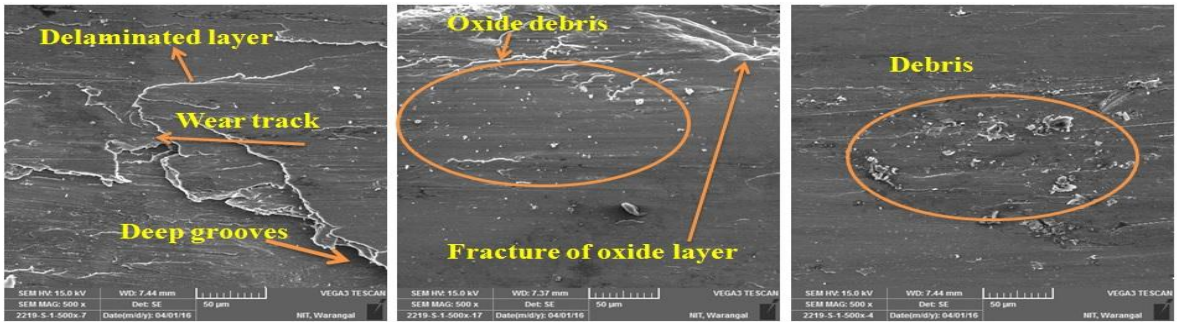

Figure 6.83 shows the worn surfaces of AA 2219/2 wt% /SiC/150 nm MMNC

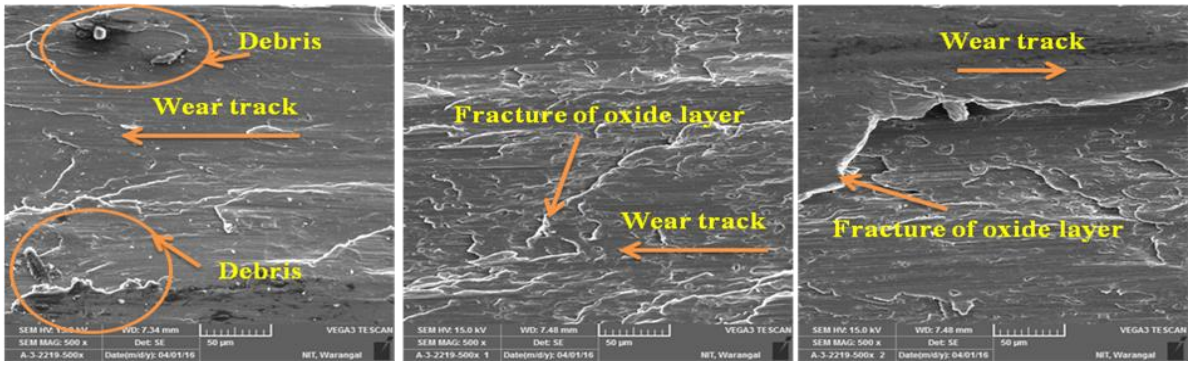

Figure 6.84 shows the worn surfaces of AA 2219/2 wt% /Al_2O_3 / 150 nm MMNC

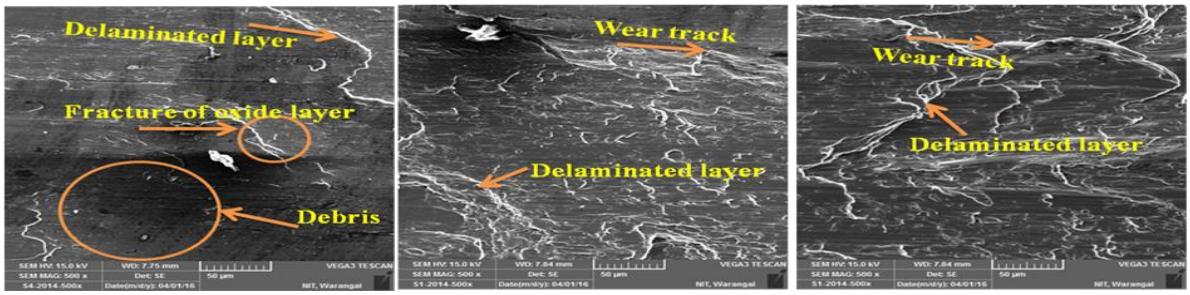

Figure 6.85 shows the worn surfaces of AA 2014/2 wt% /SiC/50 nm MMNC

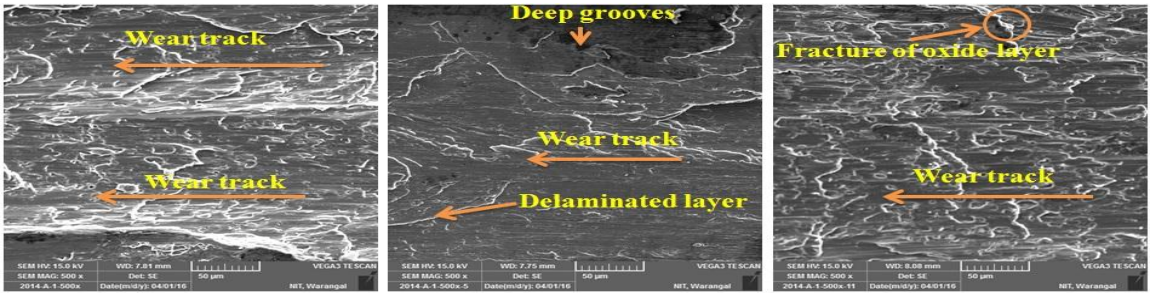

Figure 6.86 shows the worn surfaces of AA 2014/2 wt% /Al_2O_3 /50 nm MMNC

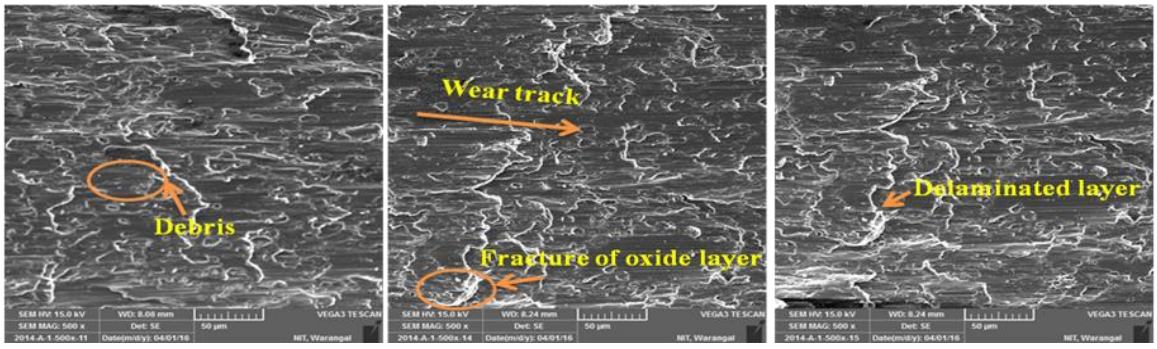

Figure 6.87 shows the worn surfaces of AA 2014/2 wt% /SiC /150 nm MMNC

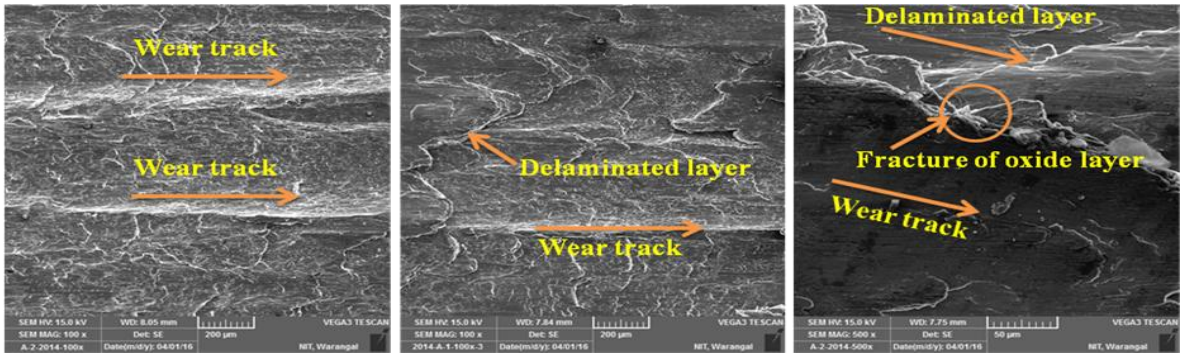

Figure 6.88 shows the worn surfaces of AA 2014/2 wt% /Al_2O_3 /150 nm MMNC

Chapter 7

Discussion and Analysis

This chapter deals with relationship between all the properties of aluminium MMNCs fabricated by Ultrasonic assisted stir casting method. The properties such as density, ultimate tensile strength, hardness and tribological properties were evaluated for the following composites.

1.) AA2219/SiC/50nm

2.)AA2219/Al_2O_3/50nm

3.)AA2219/SiCp/150nm

4.)AA2219/Al_2O_3/150nm

5.)AA2014/SiCp/50nm

6.)AA2014/Al_2O_3/50nm

7.) AA2014/SiCp/150nm

8.) AA2014/Al_2O_3/150nm

7.1 Nano aluminium alloys property results

7.1.1 Density

Table 7.1: Results of Density

S.No	Alloy Name By Wt.% of nano particles	Theoretical Density by rule of mixture	Experimental Density by weight to volume ratio.	% of error.
1. AA2219/SiCp/50nm				
1	0	2.8400	2.8400	0
2	0.5	2.8416	2.8405	0.038
3	1	2.8433	2.8427	0.021
4	1.5	2.8448	2.8439	0.032
5	2	2.8465	2.8455	0.035

2.AA2219/Al_2O_3/50nm				
1.	0	2.8400	2.8400	0
2.	0.5	2.8438	2.8429	0.032
3.	1	2.8476	2.8463	0.046
4.	1.5	2.8513	2.8501	0.042
5.	2	2.8551	2.8539	0.042
3.AA2219/SiCp/150nm				
1.	0	2.8400	2.8400	0
2.	0.5	2.8416	2.8404	0.042
3.	1	2.8433	2.8422	0.038
4.	1.5	2.8448	2.8437	0.039
5.	2	2.8465	2.8452	0.046
4.AA2219/Al_2O_3/150nm				
1.	0	2.8400	2.8400	0
2.	0.5	2.8440	2.8432	0.028
3.	1	2.8480	2.8473	0.025
4.	1.5	2.8520	2.8502	0.063
5.	2	2.8559	2.8543	0.056
5.AA2014/SiC/50nm				
1.	0	2.8000	2.8000	0
2.	0.5	2.8041	2.8032	0.032
3.	1	2.8082	2.8074	0.028
4.	1.5	2.8120	2.8102	0.064
5.	2	2.8160	2.8151	0.032
6.AA2014/Al_2O_3/50nm				
1.	0	2.8000	2.8000	0
2.	0.5	2.8039	2.8032	0.025
3.	1	2.8078	2.8071	0.025
4.	1.5	2.8117	2.8103	0.050
5.	2	2.8155	2.8144	0.039
7.AA2014/SiC/150nm				
1.	0	2.8000	2.8000	0
2.	0.5	2.8018	2.8007	0.039
3.	1	2.8036	2.8024	0.043
4.	1.5	2.8053	2.8042	0.039
5.	2	2.8071	2.8063	0.028
8.AA2014/Al_2O_3/150nm				
1.	0	2.8000	2.8000	0
2.	0.5	2.8018	2.8004	0.050
3.	1	2.8036	2.8022	0.049

4	1.5	2.8053	2.8044	0.032
5.	2	2.8071	2.8065	0.021

7.1.2 Hardness

Table 7.2: Results of Hardness

S.No	Wt.% of nano particles	Average Hardness Value
1. AA2219/SiCp/50nm		
1	0	149.38
2	0.5	156.70
3	1	160.48
4	1.5	160.26
5	2	162.88
2.AA2219/Al_2O_3/50nm		
1.	0	149.38
2.	0.5	156.70
3.	1	160.48
4.	1.5	160.26
5.	2	162.88
3.AA2219/SiCp/150nm		
1.	0	149.38
2.	0.5	154.96
3.	1	159.04
4.	1.5	159.10
5.	2	161.82
4.AA2219/Al_2O_3/150nm		
1.	0	149.38
2.	0.5	152.26
3.	1	155.62
4.	1.5	155.50
5.	2	157.70
5.AA2014/SiC/50nm		
1.	0	154.32
2.	0.5	159.32
3.	1	164.24
4.	1.5	166.3
5.	2	165.54
6.AA2014/Al_2O_3/50nm		
1.	0	154.32
2.	0.5	155.32
3.	1	156.62
4.	1.5	157.94
5.	2	160.54
7.AA2014/SiC/150nm		

1.	0	154.32
2.	0.5	158.24
3.	1	162.9
4.	1.5	165.22
5.	2	163.38
8.AA2014/Al_2O_3/150nm		
1.	0	154.32
2.	0.5	154.72
3.	1	155.66
4	1.5	156.72
5.	2	159.54

7.1.3 Ultimate tensile strength (UTS)

Table 7.3: Results of UTS

S.No	Wt.% of nano particles	Ultimate tensile strength (UTS)
1. AA2219/SiCp/50nm		
1	0	169.79
2	0.5	222.85
3	1	233.46
4	1.5	240.54
5	2	261.76
2.AA2219/Al_2O_3/50nm		
1.	0	169.79
2.	0.5	219.28
3.	1	229.89
4.	1.5	236.96
5.	2	251.11
3.AA2219/SiCp/150nm		
1.	0	169.79
2.	0.5	212.24
3.	1	222.85
4.	1.5	229.92
5.	2	254.69
4.AA2219/Al_2O_3/150nm		
1.	0	176.16
2.	0.5	205.16
3.	1	215.77
4.	1.5	226.39
5.	2	233.46
5.AA2014/SiC/50nm		
1.	0	176.16
2.	0.5	198.09
3.	1	208.70

4.	1.5	226.39
5.	2	244.07
6.AA2014/Al_2O_3/50nm		
1.	0	176.16
2.	0.5	183.94
3.	1	198.08
4.	1.5	208.70
5.	2	219.31
7.AA2014/SiC/150nm		
1.	0	176.16
2.	0.5	191.01
3.	1	198.09
4.	1.5	208.70
5.	2	222.85
8.AA2014/Al_2O_3/150nm		
1.	0	176.16
2.	0.5	180.40
3.	1	187.48
4	1.5	198.08
5.	2	208.70

7.2 Tribological Properties

Table 7.4: Results of Tribological Properties

S.No	Load	SD	WH (μm)	VOW 10e-3	SWR 10e-3	Weight Loss(10e-3)	Frictional Force(N)	COF
Base Alloy AA2219								
1.	5	1000	67	1893.42	0.3787	5.3773	1.4	0.28
2.	5	2000	201	5680.26	0.5680	16.1319	0.9	0.18
3.	5	3000	335	9467.1	0.6311	26.8866	0.6	0.12
4.	5	4000	536	15147.36	0.7574	43.0185	0.6	0.12
1.	10	1000	168	4747.68	0.4748	13.4834	3.0	0.30
2.	10	2000	504	14243.04	0.7122	40.4502	2.6	0.26
3.	10	3000	840	23738.4	0.7913	67.4171	2.2	0.22
4.	10	4000	1344	37981.44	0.9495	107.8673	2.2	0.22
1.	15	1000	268	7353.68	0.5049	21.5093	4.8	0.32
2.	15	2000	804	22721.04	0.7574	64.5278	4.4	0.29
3.	15	3000	1340	37868.4	0.8415	107.5463	4.0	0.27
4.	15	4000	2144	60589.44	1.0098	172.0740	4.0	0.27

1.	20	1000	402	11360.52	0.5680	32.2639	7.2	0.36
2.	20	2000	1206	34081.56	0.8520	96.7916	6.7	0.34
3.	20	3000	2010	56802.6	0.9467	161.3194	6.1	0.31
4.	20	4000	3216	90884.16	1.1361	258.1110	6.1	0.31
1.AA2219/SiCp/50nm @ 0.5 Wt.%								
1.	5	1000	28	791.26	0.1583	2.248	2.0	0.4
2.	5	2000	84	2373.84	0.2374	6.746	1.2	0.24
3.	5	3000	140	3956.4	0.2638	11.243	0.8	0.16
4.	5	4000	224	6330.24	0.3165	17.988	0.8	0.16
1.	10	1000	70	1978.2	0.1978	5.621	4.6	0.46
2.	10	2000	213	6019.38	0.3010	17.105	4.5	0.45
3.	10	3000	352	9947.52	0.3316	28.267	3.8	0.38
4.	10	4000	567	16023.42	0.4006	45.532	3.8	0.38
1.	15	1000	112	3165.12	0.2110	8.994	7.4	0.49
2.	15	2000	336	9495.36	0.3165	26.982	7.2	0.48
3.	15	3000	560	15825.60	0.3517	44.970	7.1	0.47
4.	15	4000	896	25320.96	0.4220	71.9520	7.1	0.47
1.	20	1000	168	4747.68	0.2374	13.491	11.2	0.56
2.	20	2000	504	14243.04	0.3561	40.473	10.6	0.53
3.	20	3000	840	23738.4	0.3956	67.455	10.0	0.50
4.	20	4000	1344	37981.44	0.4748	107.928	10.0	0.50
1 Wt.%								
1.	5	1000	23	649.98	0.1299	1.848	2.4	0.48
2.	5	2000	69	1949.94	0.1949	5.544	1.7	0.34
3.	5	3000	115	3249.90	0.2167	9.240	1.2	0.24
4.	5	4000	184	5199.84	0.2599	14.785	1.2	0.24
1.	10	1000	58	1639.84	0.1639	4.6576	5.2	0.52
2.	10	2000	173	4888.98	0.2444	13.9008	4.8	0.48
3.	10	3000	288	8138.88	0.2713	23.1413	4.5	0.45
4.	10	4000	460	12999.60	0.3250	36.9618	4.5	0.45
1.	15	1000	92	2599.92	0.1733	7.3924	8.4	0.56

2.	15	2000	276	7799.76	0.2599	22.1770	7.9	0.53
3.	15	3000	460	12999.60	0.2889	36.9618	7.2	0.48
4.	15	4000	736	20799.36	0.3466	59.1388	7.2	0.48
1.	20	1000	138	3899.88	0.1950	11.0885	11.6	0.58
2.	20	2000	411	11614.86	0.2904	33.0245	11.3	0.57
3.	20	3000	690	19499.40	0.3250	55.4426	10.6	0.53
4.	20	4000	1104	31199.04	0.3899	88.7082	10.6	0.53
1.5 Wt.%								
1.	5	1000	21	593.46	0.1187	1.6883	2.9	0.58
2.	5	2000	63	1780.38	0.1780	5.0648	2.4	0.48
3.	5	3000	105	2967.30	0.1978	8.4414	1.7	0.34
4.	5	4000	168	4747.68	0.2374	13.5062	1.7	0.34
1.	10	1000	53	1497.78	0.1498	4.2609	6.0	0.60
2.	10	2000	158	4465.08	0.2232	12.7023	5.2	0.52
3.	10	3000	263	7432.38	0.2477	21.1436	4.4	0.44
4.	10	4000	424	11982.24	0.2996	34.0871	4.4	0.44
1.	15	1000	84	2373.84	0.1583	6.7531	9.2	0.61
2.	15	2000	252	7121.52	0.2374	20.2593	8.6	0.57
3.	15	3000	420	11869.20	0.2638	33.7655	8.2	0.55
4.	15	4000	672	18990.72	0.3165	54.0248	8.2	0.55
1.	20	1000	126	3560.76	0.1780	10.1297	12.7	0.64
2.	20	2000	378	10682.28	0.2671	30.3890	11.8	0.59
3.	20	3000	630	17803.80	0.2967	50.6482	11.2	0.56
4.	20	4000	1008	28486.08	0.3561	81.0372	11.2	0.56
2 Wt.%								
1.	5	1000	18	508.68	0.1017	1.4480	3.6	0.72
2.	5	2000	54	1526.04	0.1526	4.3439	3.0	0.60
3.	5	3000	90	2543.4	0.1696	7.2398	2.6	0.52
4.	5	4000	144	4069.44	0.2035	11.5837	2.6	0.52
1.	10	1000	45	1271.7	0.1272	3.6199	7.3	0.73
2.	10	2000	135	3815.1	0.1908	10.8597	6.6	0.66

3.	10	3000	225	6358.5	0.2120	18.0995	5.6	0.56
4.	10	4000	360	10173.6	0.2543	28.9592	5.6	0.56
1.	15	1000	72	2034.72	0.1356	5.7918	11.40	0.76
2.	15	2000	216	6104.16	0.2035	17.3755	10.3	0.69
3.	15	3000	360	10173.6	0.2261	28.9592	9.6	0.64
4.	15	4000	576	16277.76	0.2713	46.3346	9.6	0.64
1.	20	1000	108	3052.08	0.1526	8.6877	15.7	0.79
2.	20	2000	324	9156.24	0.2289	26.0632	14.2	0.71
3.	20	3000	540	15260.4	0.2543	43.4387	13.4	0.67
4.	20	4000	864	24416.64	0.3052	69.5019	13.4	0.67
2. AA2219/Al_2O_3/50 nm @0.5Wt.%								
1.	5	1000	32	904.32	0.1808	2.5707	1.4	0.28
2.	5	2000	96	2712.96	0.2713	7.7151	0.8	0.16
3.	5	3000	160	4521.60	0.3014	12.8585	0.6	0.12
4.	5	4000	256	7234.56	0.3617	20.5736	0.6	0.12
1.	10	1000	81	2289.06	0.2289	6.5096	3.2	0.32
2.	10	2000	243	6867.18	0.3433	19.5289	2.8	0.28
3.	10	3000	405	11445.3	0.3815	32.5481	2.7	0.27
4.	10	4000	648	18312.48	0.4578	52.0770	2.7	0.27
1.	15	1000	128	3617.28	0.2412	10.2868	5.2	0.35
2.	15	2000	384	10851.84	0.3617	30.8605	5.0	0.33
3.	15	3000	640	18086.4	0.4020	51.434	4.9	0.32
4.	15	4000	1024	28938.24	0.4824	82.2946	4.9	0.32
1.	20	1000	192	5425.92	0.2713	15.4302	7.6	0.38
2.	20	2000	576	16277.76	0.4069	46.2906	7.3	0.37
3.	20	3000	960	27129.6	0.4522	77.1512	6.9	0.35
4.	20	4000	1536	43407.36	0.5426	123.442	6.9	0.35
1 Wt.%								
1.	5	1000	30	847.8	0.1696	2.414	1.7	0.34
2.	5	2000	92	2599.92	0.2599	7.403	1.2	0.24
3.	5	3000	151	4267.26	0.2845	12.151	0.8	0.16

4.	5	4000	244	6895.44	0.3448	19.635	0.8	0.16
1.	10	1000	75	2119.5	0.2120	6.0355	3.6	0.36
2.	10	2000	225	6358.5	0.3179	18.106	3.1	0.31
3.	10	3000	375	10597.5	0.3533	30.177	2.8	0.28
4.	10	4000	600	16956	0.4239	48.284	2.8	0.28
1.	15	1000	120	3391.2	0.2261	9.656	5.8	0.39
2.	15	2000	360	10173.6	0.3391	28.970	5.5	0.37
3.	15	3000	600	16956	0.3768	48.2839	5.0	0.33
4.	15	4000	960	27129.6	0.4522	77.254	5.0	0.33
1.	20	1000	180	5086.8	0.2543	14.485	8.1	0.41
2.	20	2000	541	15288.66	0.3822	43.536	7.8	0.39
3.	20	3000	903	25518.78	0.4253	72.667	7.3	0.37
4.	20	4000	1442	40750.92	0.5094	116.042	7.3	0.37
1.5 Wt.%								
1.	5	1000	27	763.02	0.1526	2.176	2.0	0.40
2.	5	2000	81	2289.06	0.2289	6.527	1.7	0.34
3.	5	3000	135	3815.10	0.2543	10.878	1.2	0.24
4.	5	4000	216	6104.16	0.3052	17.405	1.2	0.24
1.	10	1000	68	1921.68	0.1922	5.479	4.2	0.42
2.	10	2000	203	5736.78	0.2868	16.357	3.6	0.36
3.	10	3000	338	9551.88	0.3184	27.235	3.1	0.31
4.	10	4000	540	15260.4	0.3815	43.512	3.1	0.31
1.	15	1000	108	3052.08	0.2035	8.702	6.4	0.43
2.	15	2000	324	9156.24	0.3052	26.107	6.0	0.40
3.	15	3000	540	15260.4	0.3391	43.512	5.7	0.38
4.	15	4000	864	24416.64	0.4069	69.619	5.7	0.38
1.	20	1000	162	4578.12	0.2289	13.054	8.8	0.44
2.	20	2000	486	13734.36	0.3434	39.161	8.2	0.41
3.	20	3000	810	22890.6	0.3815	65.268	7.7	0.39
4.	20	4000	1296	36624.96	0.4578	104.429	7.7	0.39
2 Wt.%								

1.	5	1000	26	734.76	0.1469	2.098	2.5	0.50
2.	5	2000	78	2204.28	0.2204	6.293	2.1	0.42
3.	5	3000	130	3673.8	0.2449	10.489	1.8	0.36
4.	5	4000	208	5878.08	0.2939	16.783	1.8	0.36
1.	10	1000	65	1836.90	0.1837	5.245	5.1	0.51
2.	10	2000	195	5510.7	0.2755	15.734	4.6	0.46
3.	10	3000	325	9184.5	0.3062	26.223	3.9	0.39
4.	10	4000	520	14695.2	0.3674	41.956	3.9	0.39
1.	15	1000	104	2939.04	0.1959	8.391	7.9	0.53
2.	15	2000	312	8817.12	0.2939	25.174	7.2	0.48
3.	15	3000	520	14695.2	0.3266	41.556	6.7	0.44
4.	15	4000	832	23512.32	0.3919	67.130	6.7	0.44
1.	20	1000	156	4408.56	0.2204	12.587	10.9	0.55
2.	20	2000	468	13225.68	0.3306	37.761	9.8	0.49
3.	20	3000	780	22042.8	0.3674	62.934	9.3	0.47
4.	20	4000	1248	35268.48	0.4409	100.695	9.3	0.47
3.AA2219/SiCp/150 nm @ 0.5 Wt.%								
1.	5	1000	44	1243.44	0.2487	3.5334	2.4	0.48
2.	5	2000	132	3730.32	0.3730	10.6001	1.4	0.28
3.	5	3000	220	6217.20	0.4145	17.6668	1.0	0.20
4.	5	4000	352	9947.52	0.4974	28.2669	1.0	0.20
1.	10	1000	110	3108.6	0.3109	8.8334	5.3	0.53
2.	10	2000	332	9382.32	0.4691	26.6601	4.1	0.41
3.	10	3000	551	15571.26	0.5190	44.2473	3.8	0.38
4.	10	4000	879	24840.54	0.6210	70.5869	3.8	0.38
1.	15	1000	176	4973.76	0.3316	14.1334	8.4	0.56
2.	15	2000	528	14921.28	0.4974	42.4003	7.2	0.48
3.	15	3000	880	24868.8	0.5526	70.6672	6.9	0.46
4.	15	4000	1408	39790.08	0.6632	113.0675	6.9	0.46
1.	20	1000	264	7460.64	0.3730	21.2002	11.5	0.58
2.	20	2000	792	22381.92	0.5595	63.6005	10.6	0.53

3.	20	3000	1320	37303.20	0.6217	166.001	10.0	0.50
4.	20	4000	2112	59685.12	0.7461	168.6012	10.0	0.50
1 Wt.%								
1.	5	1000	39	1102.14	0.2204	3.1337	2.8	0.56
2.	5	2000	117	3306.42	0.3306	9.4011	1.7	0.34
3.	5	3000	195	5510.70	0.3674	15.6686	1.2	0.24
4.	5	4000	312	8817.12	0.4409	25.0697	1.2	0.24
1.	10	1000	98	2769.48	0.2769	7.8745	5.9	0.59
2.	10	2000	293	8280.18	0.4140	23.5430	4.4	0.44
3.	10	3000	488	13790.18	0.4597	39.2116	4.1	0.41
4.	10	4000	780	13790.88	0.5511	62.6743	4.1	0.41
1.	15	1000	156	4408.56	0.2939	12.5348	9.1	0.61
2.	15	2000	468	13225.68	0.4409	37.6046	7.9	0.53
3.	15	3000	780	22042.80	0.4898	62.6743	7.2	0.48
4.	15	4000	1248	35268.48	0.5878	100.2789	7.2	0.48
1.	20	1000	234	6612.84	0.3306	18.8023	12.6	0.63
2.	20	2000	702	19838.52	0.4960	56.4069	11.3	0.57
3.	20	3000	1170	33064.20	0.5511	94.0114	10.6	0.53
4.	20	4000	1872	52902.72	0.6613	150.4183	10.6	0.53
1.5 Wt.%								
1.	5	1000	38	1073.88	0.2148	3.0549	3.4	0.68
2.	5	2000	114	3221.64	0.3222	9.1649	2.8	0.56
3.	5	3000	190	5369.4	0.3580	15.2749	2.0	0.40
4.	5	4000	304	8591.04	0.4296	24.4398	2.0	0.40
1.	10	1000	95	2684.7	0.2685	7.6374	7	0.70
2.	10	2000	285	8054.1	0.4027	22.9123	6.5	0.65
3.	10	3000	475	13423.5	0.4475	38.1872	5.2	0.52
4.	10	4000	760	21477.6	0.5369	61.0995	5.2	0.52
1.	15	1000	152	4295.52	0.2864	12.2199	10.8	0.72
2.	15	2000	456	12886.56	0.4296	36.6597	10.1	0.67
3.	15	3000	760	21477.60	0.4773	61.0995	9.5	0.63

4.	15	4000	1216	34364.16	0.5727	97.7592	9.5	0.63
1.	20	1000	228	6443.28	0.3221	18.3298	14.8	0.74
2.	20	2000	684	19329.84	0.4832	54.9895	13.7	0.69
3.	20	3000	1140	32216.4	0.5369	91.6492	12.9	0.65
4.	20	4000	1824	51546.24	0.6443	146.6387	12.9	0.65
2 Wt.%								
1	5	1000	34	960.84	0.1922	2.7350	4.2	0.84
2.	5	2000	102	2882.52	0.2883	8.2051	3.5	0.70
3.	5	3000	170	4804.2	0.3203	13.6752	3.1	0.62
4.	5	4000	272	7686.72	0.3843	21.8802	3.1	0.62
1.	10	1000	85	2402.1	0.2402	6.8376	8.5	0.85
2.	10	2000	255	7203.3	0.3603	20.5127	7.7	0.77
3.	10	3000	425	12010.5	0.4004	34.1879	6.6	0.66
4.	10	4000	680	19216.8	0.4804	54.7006	6.6	0.66
1.	15	1000	136	3843.23	0.2562	10.9401	13.3	0.89
2.	15	2000	408	11530.08	0.3843	32.8204	12.0	0.80
3.	15	3000	680	19216.80	0.4270	54.7006	11.2	0.75
4.	15	4000	1088	30746.88	0.5124	87.5210	11.2	0.75
1.	20	1000	204	5765.04	0.2883	16.4102	18.3	0.92
2.	20	2000	612	17295.12	0.4324	49.2301	16.5	0.83
3.	20	3000	1020	28825.2	0.4804	82.0509	15.7	0.79
4.	20	4000	1632	46120.32	0.5765	131.2815	15.7	0.79
4. AA2219/Al_2O_3/150 nm @0.5Wt.%								
1.	5	1000	58	1639.08	0.3278	4.6615	1.7	0.34
2.	5	2000	174	4917.24	0.4917	13.9846	1.0	0.2
3.	5	3000	290	8195.4	0.5464	23.3077	0.7	0.14
4.	5	4000	464	13112.64	0.6556	37.2923	0.7	0.14
1.	10	1000	145	4097.7	0.4098	11.6539	3.8	0.38
2.	10	2000	436	12321.36	0.6161	35.0419	3.4	0.34
3.	10	3000	727	20545.02	0.6848	58.4300	3.2	0.32
4.	10	4000	1160	32781.60	0.8195	93.2309	3.2	0.32

1.	15	1000	232	6556.32	0.4371	18.6462	6.2	0.41
2.	15	2000	696	19668.96	0.6556	55.9385	6.0	0.40
3.	15	3000	1161	32809.86	0.7291	93.3112	5.9	0.39
4.	15	4000	1856	52450.56	0.8742	149.1693	5.9	0.39
1.	20	1000	348	9834.48	0.4917	27.9693	9.3	0.47
2.	20	2000	1044	29503.44	0.7376	83.9078	8.8	0.44
3.	20	3000	1740	49172.4	0.8195	139.8463	8.3	0.42
4.	20	4000	2784	78675.84	0.9834	223.7541	8.3	0.42
1 Wt.%								
1.	5	1000	48	1356.48	0.2713	3.8633	2.0	0.40
2.	5	2000	144	4069.44	0.4069	11.5898	1.4	0.28
3.	5	3000	240	6782.4	0.4522	19.3163	1.0	0.20
4.	5	4000	384	10851.84	0.5426	30.9060	1.0	0.20
1.	10	1000	120	3391.2	0.3391	9.6581	4.3	0.43
2.	10	2000	362	10230.12	0.5115	29.1354	3.7	0.37
3.	10	3000	603	17040.78	0.5680	48.5321	3.4	0.34
4.	10	4000	967	27327.42	0.6832	77.8285	3.4	0.34
1.	15	1000	192	5425.92	0.3617	15.4530	7.0	0.47
2.	15	2000	576	16277.76	0.5426	46.3590	6.6	0.44
3.	15	3000	960	27129.60	0.6029	77.2651	6.0	0.40
4.	15	4000	1536	43407.36	0.7235	123.6241	6.0	0.40
1.	20	1000	288	8138.88	0.4069	23.1795	9.7	0.49
2.	20	2000	864	24416.64	0.6104	69.5386	9.4	0.47
3.	20	3000	1440	40694.40	0.6782	115.8977	8.8	0.44
4.	20	4000	2304	65111.04	0.8139	185.4362	8.8	0.44
1.5 Wt.%								
1.	5	1000	45	1271.7	0.2543	3.6269	2.4	0.48
2.	5	2000	136	3843.36	0.3843	10.9613	2.0	0.40
3.	5	3000	227	6415.02	0.4277	18.2956	1.4	0.28
4.	5	4000	362	10230.12	0.5115	29.1763	1.4	0.28
1.	10	1000	113	3193.38	0.3193	9.1075	5	0.50

2.	10	2000	338	9551.88	0.4776	27.2419	4.3	0.43
3.	10	3000	563	15910.38	0.5303	45.3764	3.7	0.37
4.	10	4000	900	25434	0.6359	72.5378	3.7	0.37
1.	15	1000	180	5086.8	0.3391	14.5076	7.7	0.51
2.	15	2000	542	15316.92	0.5106	43.6839	7.2	0.48
3.	15	3000	901	25462.26	0.5658	72.6184	6.8	0.45
4.	15	4000	1442	40750.92	0.6792	116.2216	6.8	0.45
1.	20	1000	270	7630.2	0.3815	21.7613	10.6	0.53
2.	20	2000	810	22890.6	0.5723	65.2839	9.8	0.49
3.	20	3000	1350	38151.0	0.6359	108.8066	9.2	0.46
4.	20	4000	2160	61041.6	0.7630	174.0906	9.2	0.46
2 Wt.%								
1.	5	1000	43	1215.18	0.2430	3.4704	3.0	0.60
2.	5	2000	129	3645.54	0.3646	10.4113	2.5	0.50
3.	5	3000	215	6075.90	0.4051	17.3522	2.2	0.44
4.	5	4000	344	9721.44	0.4861	27.7635	2.2	0.44
1.	10	1000	108	3052.08	0.3052	8.7164	6.1	0.61
2.	10	2000	323	9127.98	0.4564	26.0686	5.5	0.55
3.	10	3000	538	15203.88	0.5068	43.4208	4.7	0.47
4.	10	4000	860	24303.60	0.6076	69.4087	4.7	0.47
1.	15	1000	172	4860.42	0.3241	13.8817	9.5	0.63
2.	15	2000	516	14582.16	0.4861	41.6452	8.6	0.57
3.	15	3000	860	24303.60	0.5401	69.4087	8.0	0.53
4.	15	4000	1376	38885.76	0.6481	111.0538	8.0	0.53
1.	20	1000	258	7291.08	0.3646	20.8226	13.1	0.66
2.	20	2000	774	21873.24	0.5468	62.4678	11.8	0.59
3.	20	3000	1290	36455.4	0.6076	104.1129	11.2	0.56
4.	20	4000	2064	58328.64	0.7291	166.5808	11.2	0.56
Base Alloy AA2014								
1.	5	1000	62	1752.12	0.3504	4.9059	1.6	0.32
2.	5	2000	186	5256.36	0.5256	14.7178	1.1	0.22

3.	5	3000	311	8788.86	0.5859	24.6088	0.8	0.16
4.	5	4000	497	14045.22	0.7023	39.3266	0.8	0.16
1.	10	1000	155	4380.3	0.4380	12.2648	3.4	0.34
2.	10	2000	465	13140.9	0.6570	36.7945	3.0	0.30
3.	10	3000	776	21929.76	0.7310	61.4033	2.7	0.27
4.	10	4000	1243	35127.18	0.8782	98.3561	2.7	0.27
1.	15	1000	248	7008.48	0.4672	19.6237	5.6	0.37
2.	15	2000	746	21081.96	0.7027	59.0295	5.2	0.35
3.	15	3000	1241	35070.66	0.7793	98.1978	4.6	0.31
4.	15	4000	1985	56096.1	0.9349	157.069	4.6	0.31
1.	20	1000	373	10540.98	0.5270	29.5147	7.8	0.39
2.	20	2000	1119	31622.94	0.7906	88.5442	7.3	0.36
3.	20	3000	1866	52733.16	0.8789	147.6528	6.9	0.34
4.	20	4000	2987	84412.62	1.0552	236.3553	6.9	0.34
5.AA2014/SiCp/50nm @ 0.5 Wt.%								
1.	5	1000	23	649.98	0.1299	1.8211	2.7	0.54
2.	5	2000	69	1949.94	0.1950	5.4633	1.6	0.32
3.	5	3000	115	3249.9	0.2167	9.1056	1.1	0.22
4.	5	4000	184	5199.84	0.2599	14.5689	1.1	0.22
1.	10	1000	58	1639.08	0.1639	5.5924	5.5	0.55
2.	10	2000	173	4888.98	0.2444	13.6979	3.4	0.34
3.	10	3000	288	8138.88	0.2713	22.8035	2.3	0.23
4.	10	4000	460	12999.60	0.3250	36.4223	2.3	0.23
1.	15	1000	92	2599.92	0.1733	7.2845	8.5	0.57
2.	15	2000	276	7799.76	0.2599	21.8534	5.6	0.37
3.	15	3000	460	12999.60	0.2889	36.4223	3.9	0.26
4.	15	4000	736	20799.36	0.3467	58.2756	3.9	0.26
1.	20	1000	138	3899.88	0.1950	10.9267	11.8	0.59
2.	20	2000	414	11699.64	0.2925	32.7801	8.0	0.40
3.	20	3000	690	19499.4	0.3250	54.633	6.2	0.31
4.	20	4000	1104	31199.04	0.3899	87.4135	6.2	0.31

1 Wt.%								
1.	5	1000	20	565.20	0.1130	1.5846	2.8	0.56
2.	5	2000	61	1723.86	0.1724	4.8330	1.7	0.34
3.	5	3000	102	2882.52	0.1922	8.0814	1.2	0.24
4.	5	4000	161	4549.86	0.227	12.7559	1.2	0.24
1.	10	1000	50	1413	0.1413	3.9615	5.8	0.58
2.	10	2000	151	4267.26	0.2134	11.9637	3.7	0.37
3.	10	3000	253	7149.78	0.2383	20.0451	2.6	0.26
4.	10	4000	402	11360.52	0.2840	31.8504	2.6	0.26
1.	15	1000	80	2260.8	0.1507	6.3384	9	0.60
2.	15	2000	242	6838.92	0.2280	19.1736	5.9	0.39
3.	15	3000	405	11445.3	0.2543	32.0880	4.2	0.28
4.	15	4000	643	18171.18	0.3029	50.9447	4.2	0.28
1.	20	1000	120	3391.2	0.1696	9.5026	12.6	0.63
2.	20	2000	363	10258.38	0.2565	28.7604	8.4	0.42
3.	20	3000	601	16984.26	0.2839	47.6171	6.6	0.33
4.	20	4000	962	27186.12	0.3398	76.2190	6.6	0.33
1.5 Wt.%								
1.	5	1000	19	536.94	0.1074	1.5063	2.9	0.58
2.	5	2000	57	1610.82	0.1611	4.5188	1.8	0.36
3.	5	3000	95	2684.70	0.1789	7.5314	1.4	0.27
4.	5	4000	152	4295.52	0.2148	12.0502	1.4	0.27
1.	10	1000	48	1356.48	0.1356	3.8053	6.0	0.60
2.	10	2000	144	4069.44	0.2035	11.4160	3.9	0.39
3.	10	3000	241	6810.66	0.2270	19.1059	2.9	0.29
4.	10	4000	384	10851.84	0.2713	30.4427	2.9	0.29
1.	15	1000	76	2147.76	0.1432	6.0251	9.3	0.62
2.	15	2000	228	6443.28	0.2148	18.0753	6.5	0.43
3.	15	3000	380	10738.8	0.2386	30.1256	5.1	0.34
4.	15	4000	608	17182.08	0.2864	48.2009	5.1	0.34
1.	20	1000	114	3221.64	0.1611	9.0377	13	0.65

2.	20	2000	342	9664.92	0.2416	27.1130	9.4	0.47
3.	20	3000	570	16108.2	0.2685	45.1883	7.2	0.36
4.	20	4000	912	25773.12	0.3222	72.3013	7.2	0.36
2 Wt.%								
1.	5	1000	15	423.9	0.0848	1.1899	3.0	0.60
2.	5	2000	45	1271.7	0.1272	305698	1.9	0.38
3.	5	3000	76	2147.76	0.1432	6.0289	1.5	0.29
4.	5	4000	123	3475.98	0.1738	9.7574	1.5	0.29
1.	10	1000	38	1073.88	0.1074	3.0145	6.3	0.63
2.	10	2000	113	3193.38	0.1597	8.9641	4.1	0.41
3.	10	3000	190	5369.4	0.1790	15.0724	3.2	0.32
4.	10	4000	304	8591.04	0.2148	24.1159	3.2	0.32
1.	15	1000	60	1695.60	0.1130	4.7597	9.9	0.66
2.	15	2000	182	5143.32	0.1714	14.4378	6.8	0.45
3.	15	3000	301	8506.26	0.1890	23.8779	5.3	0.35
4.	15	4000	483	13649.58	0.2275	38.3157	5.3	0.35
1.	20	1000	90	2543.4	0.1272	7.1396	13.4	0.67
2.	20	2000	271	7658.46	0.1915	21.4981	9.8	0.49
3.	20	3000	453	12801.78	0.2134	35.9359	7.6	0.38
4.	20	4000	727	20545.02	0.2568	57.6719	7.6	0.38
6. AA2014/Al_2O_3/50 nm @0.5Wt.%								
1.	5	1000	29	819.54	0.1639	2.2979	1.4	0.28
2.	5	2000	87	2458.62	0.2459	6.8937	1.0	0.19
3.	5	3000	145	4097.70	0.2732	11.4895	0.7	0.14
4.	5	4000	232	6556.32	0.3278	18.3833	0.7	0.14
1.	10	1000	73	2062.98	0.2063	5.7844	3.2	0.32
2.	10	2000	219	6188.94	0.3094	17.3532	2.1	0.21
3.	10	3000	365	10314.9	0.3438	28.9219	1.6	0.16
4.	10	4000	584	16503.84	0.4126	46.2751	1.6	0.16
1.	15	1000	116	3278.16	0.2185	9.1916	5.4	0.36
2.	15	2000	348	9834.48	0.3278	27.5749	3.8	0.25

3.	15	3000	580	16390.80	0.3642	45.9582	3.0	0.20
4.	15	4000	928	26225.28	0.4371	73.5331	3.0	0.20
1.	20	1000	174	4917.24	0.2457	13.7874	8.2	0.41
2.	20	2000	522	14751.72	0.3688	41.3623	5.8	0.29
3.	20	3000	870	24586.20	0.4098	68.9372	4.8	0.24
4.	20	4000	1392	39337.92	0.4917	110.2996	4.8	0.24
1Wt.%								
1.	5	1000	33	932.58	0.1865	2.6146	1.7	0.33
2.	5	2000	100	2826	0.2826	7.9229	1.5	0.29
3.	5	3000	165	4662.9	0.3109	13.0729	1.2	0.23
4.	5	4000	264	7460.64	0.3730	20.9167	1.2	0.23
1.	10	1000	83	2345.58	0.2346	6.5761	3.7	0.37
2.	10	2000	249	7036.74	0.3518	19.7282	3.2	0.32
3.	10	3000	416	11756.16	0.3919	32.9596	2.5	0.25
4.	10	4000	665	18792.9	0.4698	52.6878	2.5	0.25
1.	15	1000	132	3730.32	0.2487	10.4583	6.2	0.41
2.	15	2000	396	11190.96	0.3730	31.3749	5.4	0.36
3.	15	3000	660	18651.60	0.4145	52.2916	4.5	0.30
4.	15	4000	1056	29842.56	0.4974	83.6666	4.5	0.30
1.	20	1000	198	5595.48	0.2798	15.6875	8.8	0.44
2.	20	2000	594	16786.44	0.4197	47.0625	8.2	0.41
3.	20	3000	990	27977.40	0.4663	78.4374	6.8	0.34
4.	20	4000	1584	44763.84	0.5595	125.4999	6.8	0.34
1.5 Wt.%								
1.	5	1000	27	763.02	0.1526	2.1405	1.8	0.36
2.	5	2000	81	2289.06	0.2289	6.4215	1.6	0.32
3.	5	3000	135	3815.10	0.2543	10.7025	1.3	0.26
4.	5	4000	216	6104.16	0.3052	17.1240	1.3	0.26
1.	10	1000	68	1921.68	0.1922	5.3909	4.1	0.41
2.	10	2000	204	5765.04	0.2883	16.1727	3.5	0.35
3.	10	3000	340	9608.4	0.3203	26.9544	2.8	0.28

4.	10	4000	544	15373.44	0.3843	43.1271	2.8	0.28
1.	15	1000	108	3052.08	0.2035	8.5620	6.8	0.45
2.	15	2000	324	9156.24	0.3052	25.6860	6.0	0.40
3.	15	3000	540	15260.4	0.3391	42.8100	5.1	0.34
4.	15	4000	864	24416.64	0.4069	68.4960	5.1	0.34
1.	20	1000	162	4578.12	0.2289	12.8430	9.4	0.47
2.	20	2000	486	13734.36	0.3434	38.5290	9	0.45
3.	20	3000	810	22890.6	0.3815	64.2150	7.6	0.38
4.	20	4000	1236	36624.96	0.4578	102.7440	7.6	0.38
2 Wt.%								
1.	5	1000	21	593.46	0.1187	1.6659	2.0	0.40
2.	5	2000	63	1780.38	0.1780	4.9977	1.8	0.36
3.	5	3000	105	2967.30	0.1978	8.3295	1.5	0.30
4.	5	4000	168	4747.68	0.2374	13.3272	1.5	0.30
1.	10	1000	53	1497.78	0.1498	4.2044	4.6	0.46
2.	10	2000	159	4493.34	0.2247	12.0221	3.9	0.39
3.	10	3000	265	7488.9	0.2496	21.0221	3.2	0.32
4.	10	4000	424	11982.24	0.2996	33.6353	3.2	0.32
1.	15	1000	84	2373.84	0.1583	6.6636	7.4	0.49
2.	15	2000	252	7121.52	0.2374	19.9908	6.6	0.44
3.	15	3000	420	11869.20	0.2638	33.3180	5.7	0.38
4.	15	4000	672	18990.72	0.3165	53.3089	5.7	0.38
1.	20	1000	126	3560.76	0.1780	9.9954	10.0	0.50
2.	20	2000	378	10682.28	0.2671	29.9862	9.8	0.49
3.	20	3000	630	17803.80	0.2967	49.9770	8.4	0.42
4.	20	4000	1008	28486.08	0.3561	79.9633	8.4	0.42
7.AA2014/SiCp/150 nm @ 0.5 Wt.%								
1.	5	1000	29	819.54	0.1639	2.2979	1.4	0.28
2.	5	2000	87	2458.62	0.2459	6.8937	1.0	0.19
3.	5	3000	145	4097.70	0.2732	11.4895	0.7	0.14
4.	5	4000	232	6556.32	0.3278	18.3833	0.7	0.14

1.	10	1000	73	2062.98	0.2063	5.7844	3.2	0.32
2.	10	2000	219	6188.94	0.3094	17.3532	2.1	0.21
3.	10	3000	365	10314.9	0.3438	28.9219	1.6	0.16
4.	10	4000	584	16503.84	0.4126	46.2751	1.6	0.16
1.	15	1000	116	3278.16	0.2185	9.1916	5.4	0.36
2.	15	2000	348	9834.48	0.3278	27.5749	3.8	0.25
3.	15	3000	580	16390.80	0.3642	45.9582	3.0	0.20
4.	15	4000	928	26225.28	0.4371	73.5331	3.0	0.20
1.	20	1000	174	4917.24	0.2457	13.7874	8.2	0.41
2.	20	2000	522	14751.72	0.3688	41.3623	5.8	0.29
3.	20	3000	870	24586.20	0.4098	68.9372	4.8	0.24
4.	20	4000	1392	39337.92	0.4917	110.2996	4.8	0.24
1Wt.%								
1.	5	1000	26	734.76	0.1469	2.0631	1.7	0.33
2.	5	2000	78	2204.28	0.2204	6.1892	1.2	0.23
3.	5	3000	130	3673.80	0.2449	10.3153	0.9	0.17
4.	5	4000	208	5878.08	0.2939	16.5045	0.9	0.17
1.	10	1000	65	1836.90	0.1837	5.1576	3.5	0.35
2.	10	2000	195	5510.7	0.2755	15.4729	2.6	0.26
3.	10	3000	325	9184.5	0.3062	25.7882	2.0	0.20
4.	10	4000	520	14695.20	0.3674	41.2612	2.0	0.20
1.	15	1000	104	2939.04	0.1959	8.2522	6.0	0.40
2.	15	2000	312	8817.12	0.2939	24.7567	4.4	0.29
3.	15	3000	520	14695.20	0.3266	41.2612	3.6	0.24
4.	15	4000	832	23512.32	0.3919	66.0179	3.6	0.24
1.	20	1000	156	4408.56	0.2204	12.3784	9.2	0.46
2.	20	2000	468	13225.68	0.3306	37.1351	7.0	0.35
3.	20	3000	780	22042.80	0.3674	61.8918	5.4	0.27
4.	20	4000	1248	35268.48	0.4409	99.0268	5.4	0.27
1.5 Wt.%								
1.	5	1000	23	649.98	0.1299	1.8275	1.9	0.37

2.	5	2000	70	1978.2	0.1978	5.5621	1.5	0.29
3.	5	3000	117	3306.42	0.2204	9.2967	1.1	0.22
4.	5	4000	185	5228.1	0.2614	14.6998	1.1	0.22
1.	10	1000	58	1639.08	0.1639	4.6086	4.2	0.42
2.	10	2000	174	4917.24	0.2459	13.8258	3.3	0.33
3.	10	3000	291	8223.66	0.2741	23.1225	2.6	0.26
4.	10	4000	466	13169.16	0.3292	37.0277	2.6	0.26
1.	15	1000	92	2599.92	0.1733	7.0277	6.9	0.46
2.	15	2000	276	7799.76	0.2599	21.9306	5.9	0.39
3.	15	3000	466	13169.16	0.2926	37.0277	4.4	0.29
4.	15	4000	737	20827.62	0.3471	58.5610	4.4	0.29
1.	20	1000	138	3899.88	0.1950	10.9652	10.2	0.51
2.	20	2000	414	11699.64	0.2925	32.8959	8.4	0.42
3.	20	3000	690	19499.4	0.3250	54.8265	7.2	0.36
4.	20	4000	1105	31227.30	0.3903	87.8018	7.2	0.36
2 Wt.%								
1.	5	1000	18	508.68	0.1017	1.4303	2.0	0.40
2.	5	2000	54	1526.04	0.1526	4.2908	1.7	0.34
3.	5	3000	91	2571.66	0.1714	7.2307	1.4	0.27
4.	5	4000	145	4097.7	0.2049	11.5215	1.4	0.27
1.	10	1000	45	1271.7	0.1272	3.5756	4.7	0.47
2.	10	2000	136	3843.36	0.1922	10.8064	3.8	0.38
3.	10	3000	227	6415.02	0.2138	18.0371	3.1	0.31
4.	10	4000	360	10173.6	0.2543	28.6051	3.1	0.31
1.	15	1000	72	2034.72	0.1356	5.7210	7.7	0.51
2.	15	2000	216	6104.16	0.2035	17.1631	6.6	0.44
3.	15	3000	361	10201.86	0.2267	28.6846	5.3	0.35
4.	15	4000	578	16334.28	0.2722	45.9271	5.3	0.35
1.	20	1000	108	3052.08	0.1526	8.5815	11.2	0.56
2.	20	2000	325	9184.5	0.2296	25.8241	9.4	0.47
3.	20	3000	542	15316.92	0.2553	43.066	8.2	0.41

4.	20	4000	867	24501.42	0.3063	68.8906	8.2	0.41
8. AA2014/Al_2O_3/150nm@0.5Wt.%								
1.	5	1000	53	1497.78	0.2995	4.1999	2.7	0.54
2.	5	2000	159	4493.34	0.4493	12.5998	2.0	0.40
3.	5	3000	265	7488.9	0.4993	20.9996	1.7	0.34
4.	5	4000	427	12067.02	0.6034	33.8371	1.7	0.34
1.	10	1000	133	3758.58	0.3759	10.5394	5.8	0.58
2.	10	2000	398	11247.48	0.5624	31.5391	4.4	0.44
3.	10	3000	667	18848.42	0.6283	52.8557	4.2	0.42
4.	10	4000	1065	30096.9	0.7524	84.3947	4.2	0.42
1.	15	1000	212	5991.12	0.3994	16.7997	8.9	0.59
2.	15	2000	637	18001.62	0.6001	50.4783	7.0	0.47
3.	15	3000	1063	30040.38	0.6676	84.2362	6.9	0.46
4.	15	4000	1697	47957.22	0.7992	134.4768	6.9	0.46
1.	20	1000	318	8986.68	0.4493	25.1995	12.2	0.61
2.	20	2000	955	26988.3	0.6747	75.6779	9.8	0.49
3.	20	3000	1592	44989.92	0.7498	126.1562	9.3	0.47
4.	20	4000	2547	71978.22	0.8997	201.8341	9.3	0.47
1 Wt.%								
1.	5	1000	46	1299.96	0.2599	3.6505	3.0	0.6
2.	5	2000	138	3899.88	0.3899	10.9516	2.4	0.48
3.	5	3000	232	6556.32	0.4371	18.4115	2.0	0.40
4.	5	4000	369	10427.94	0.5214	29.2837	2.0	0.40
1.	10	1000	115	3249.9	0.3250	9.1264	6.2	0.62
2.	10	2000	346	9777.96	0.4889	27.4585	4.7	0.47
3.	10	3000	577	16306.02	0.5435	45.7906	4.4	0.47
4.	10	4000	922	26055.72	0.6514	73.1697	4.4	0.44
1.	15	1000	184	5199.84	0.3467	14.6022	9.5	0.63
2.	15	2000	553	15627.78	0.5209	43.8859	8.6	0.57
3.	15	3000	921	26027.46	0.5784	73.0903	7.5	0.5
4.	15	4000	1473	41626.98	0.6938	116.8968	7.5	0.5

1.	20	1000	276	7799.76	0.3899	21.9033	13.7	0.69
2.	20	2000	828	23399.28	0.5849	65.7099	11.6	0.58
3.	20	3000	1382	39055.32	0.6509	109.6751	10.8	0.54
4.	20	4000	2209	62426.34	0.7803	175.3056	10.8	0.44
1.5 Wt.%								
1.	5	1000	43	1215.18	0.2430	3.4171	3.4	0.68
2.	5	2000	130	3673.8	0.3674	10.3307	3.0	0.60
3.	5	3000	217	6132.42	0.4088	17.2444	2.4	0.48
4.	5	4000	347	9806.22	0.4903	27.5751	2.4	0.48
1.	10	1000	109	3080.34	0.3080	8.6619	6.5	0.65
2.	10	2000	327	9241.02	0.4621	25.9857	5.3	0.53
3.	10	3000	546	15429.96	0.5143	43.3890	4.9	0.49
4.	10	4000	873	24670.98	0.6168	69.3748	4.9	0.49
1.	15	1000	172	4860.72	0.3240	13.6683	9.7	0.64
2.	15	2000	516	14582.16	0.4861	41.0050	8.8	0.59
3.	15	3000	860	24303.60	0.5401	68.3417	7.8	0.52
4.	15	4000	1376	38885.76	0.6481	109.3468	7.8	0.52
1.	20	1000	258	7291.08	0.3646	20.5025	14.6	0.73
2.	20	2000	775	21901.5	0.5475	61.5870	11.8	0.59
3.	20	3000	1292	36511.92	0.6085	102.6715	11.0	0.55
4.	20	4000	2067	58413.42	0.7302	164.2585	11.0	0.55
2 Wt.%								
1.	5	1000	36	1017.36	0.2035	2.8608	4.0	0.80
2.	5	2000	109	3080.34	0.3080	8.6619	3.5	0.70
3.	5	3000	183	5171.58	0.3448	14.5425	3.2	0.64
4.	5	4000	291	8223.66	0.4112	23.1249	3.2	0.64
1.	10	1000	90	2543.4	0.2543	7.1520	8.1	0.81
2.	10	2000	271	7658.46	0.3829	21.5356	7.2	0.72
3.	10	3000	453	12801.78	0.4267	35.9986	6.5	0.65
4.	10	4000	722	20403.72	0.5101	57.3753	6.5	0.65
1.	15	1000	144	4069.44	0.2713	11.4433	12.5	0.83

2.	15	2000	433	12236.58	0.4079	34.4093	10.9	0.73
3.	15	3000	721	20375.46	0.4528	57.2958	9.9	0.66
4.	15	4000	1153	32583.78	0.5431	91.6256	9.9	0.66
1.	20	1000	216	6104.16	0.3052	17.1649	17.4	0.87
2.	20	2000	649	18340.74	0.4585	51.5742	14.8	0.74
3.	20	3000	1082	30577.32	0.5096	85.9834	13.5	0.68
4.	20	4000	1731	48918.06	0.6115	137.5576	13.5	0.68

7.3 Analysis of Results

The base metal matrix aluminium alloys (AA2219&AA2014) reinforced with silicon carbide & Alumina Nanocomposites are casted using the ultrasonic assisted stir casting process and these various samples of Aluminium MMNCs were prepared. The samples were prepared for various tribological and mechanical tests according to ASTM standards. The morphology, topography, phases and chemical composition of the various nanocomposites are analyzed using SEM and XRD. The mechanical properties were measured by the ultimate tensile strength, hardness, and yield strength tests on the tensile testing machine and Vickers microhardness tester. The wear tests were conducted on a pin on disc setup against the counter body material. The wear surface of the nanocomposites was examined using SEM.

Metal Matrix Nano Composites(1 to 8) Density, Hardness, Strength and Micrographs of each of MMNCs were measured and Results obtained were analyzed in detail. The confirmation test was performed at the optimal solution with its chosen levels to calculate the quality response characteristics related to Wear test on MMNC AA 2219/SiC/50 nm work material. (Muthu Kumar et al., 2010) Experiment 12 shows the greater GRG for MMNC AA2219/SiC/50 nm, signifying the optimal solution process parameter combination of L4-SD4-SV2-Wt. %1 has the best performance characteristic among all experiments, for validation of results to compare results with confirmation test results Table 5.9. Shows the comparison of the actual results of wear test on wear process parameters on MMNC AA 2219/SiC/50 nm work material. The output specific response results were obtained from the confirmation test are SWR = 0.0004268 mm^3/N-m, predicted SWR=0.0004296 mm^3/N-m,

and percentage of error between predicted and experimental is 0.6517 as shown in Table 5.11. Gray relational grade has been improved by 1.73.

Similar tests were conducted and Taguchi and Gray relational Analysis was done on the remaining aluminium MMNCs shown in Table 5.13. Similar effects were observed in these tests also. Hence the results of these MMNCs were kept in Appendix-I for further reference. This chapter deals with analysis of specific wear rate using Taguchi and Gray level analysis of aluminium MMNCs fabricated by Ultrasonic assisted stir casting method.

Density of all above (1 to 8) metal matrix nanocomposites has been increased with respect to the %NPs(wt).This phenomena was happened because of intermolecular forces of base matrix material and reinforcement material. The relative error of density indicates porosity and it is very low from chapter 4. Clearly it concluded that porosity is very less. The porosity is low in 50 nm MMNCs when compared to the 150 nm, it means size of the reinforcement increases porosity also increases because the surface area decreases.

Hardness of metal matrix nanocomposites has been increased with increase of %NPs(wt) because dendrite structures was formed at the grain boundary this was shown in chapter 4, and also another reason porosity is low. The width of the dendrite is increased with the increase of %NPs(wt).This phenomena was happened more likely uniform distribution of ceramic NPs

Ultimate tensile strength of the metal matrix nanocomposites has been increased with the increase of %NPs(wt) because this phenomena was happened more likely uniform distribution of ceramic NPs and also porosity is low and hardness is more.

Specific wear rate has been decreased with increase of %NPs(wt) because the contacting surface area of NPs was increased and also hardness is increased.so that it has given better specific wear rate. Size of NPs increases the specific wear rate also increases.

Chapter 8

Conclusions

The significant conclusions of the studies carried out on AA 2219/AA 2014/(SiC &Al_2O_3) MMNC's are as follows.

- The liquid metallurgy route (Ultrasonic assisted stir casting) was successfully adopted in the preparation of AA 2219/AA 2014 (SiC & Al_2O_3) MMNCs containing the filler contents up to 2wt. % with average grain size 50nm and 150nm. The particulates diffusion in the liquid AA 2219/AA 2014 during Ultrasonic assisted stir casting process while fabrication of MMNC's was observed. The microstructural studies reveal the uniform distribution of the particles in the metal matrix system and the minimal amount of porosity.

- The densities of the composites are found to be improved than that of their base matrix and the experimental and theoretical density values are in line with each other. The density of the AA 2219/SiC/50nm composite material increases by an amount of 0.6% as the SiC content increases from 0 to 2Wt. % and in case of AA2219/Al_2O_3/50nm , AA 2219/SiC 150nm, AA 2219/Al_2O_3/150 nm, AA 2014/SiC/50nm AA2014/Al2O3/50 nm , AA 2014/SiC/150 nm and AA2014/Al2O3/50 nm, nanocomposites, the increase in density was found to be 0.53%, 0.23%,0.56%,0.25%,0.55,0.25%, and 0.57% respectively.

- The hardness of the composites found to be increased with increase in filler content and the composites containing higher filler content exhibit higher hardness. The hardness of the AA 2219/SiC/ 50 nm composite material increases by an amount of 9.39% as the content of SiC increases from 0 to 2Wt. % and in case of AA2219/Al_2O_3/50nm, AA2219/SiC/150nm, AA2219/Al_2O_3/150 nm, AA2014/SiC/50 nm, AA2014/Al_2O_3/50nm ,AA2014/SiC/150nm and AA2014/Al_2O_3/150nm, nanocomposites, the increase in hardness was found to be 5.9%, 7.45%, 5.09%, 8.28%, 3.1%, 6.6% and 1.9% respectively.
- The ultimate tensile strength of the composites are found to be higher than that of base matrix and composites containing higher filler content exhibits superior tensile strength properties than other composites studied. The ultimate tensile strength of the AA 2219/SiC/50nm composite material increases by an amount of 35.14% as the content of SiC increases from 0 to 2wt.% and in case of AA2219/Al_2O_3/50nm, AA2219/SiC/150nm,AA2219/Al_2O_3/150nm,AA2014/SiC/50nm, AA2014/Al_2O_3/50nm ,AA2014/SiC/150nm and AA2014/Al_2O_3/150nm, nanocomposites, the increase in ultimate tensile strength was found to be 32.38%, 33.35%, 27.27%, 19.68%, 27.82%, 20.95% and 15.59% respectively.
- Taguchi L16 orthogonal array is used to conduct experiments for varying Input parameters namely applied a load, sliding distance, sliding velocity and weight % of nano ceramic particulates. The output parameter of the study is specific wear rate. The results of the experimentation were analyzed using Taguchi and Grey Relation Analysis techniques. ANOVA, GRA analysis on specific wear rate has been performed. Sliding distance, load and Wt.% of reinforcement parameters are having more influence on specific wear rate. Whereas sliding velocity influence is minimum. We found same regression models in both the cases. We also found that there is maximum error of 3% between experimental and regression values on the entire set of experimentation. Hence regression models can be used as an accurate model to predict specific wear rate of Aluminium MMNCs.
- The optimum wear test input parameters for minimum specific wear rate have been observed (a). According to Taguchi analysis the optimal process parameters for AA 2219 based metal matrix nanocomposites are “L4-SD4-SV2-Wt.%1”, and for AA 2014 based metal matrix nanocomposites are “L4-SD4-SV3-Wt.%1”. Grey relational analysis (GRA)

was also performed i.e. Minimization of the specific wear rate of all the eight metal matrix nanocomposites. According to Grey relational analysis the optimal process parameters for AA 2219 based metal matrix nanocomposites are "L4-SD4-SV2-Wt.%1", and for AA 2014 based metal matrix nanocomposites are "L4-SD4-SV3-Wt.%1". Hence both analysis techniques are in concurrence.

- The wear resistance of the composites is found higher than that of base alloy. Increased applied loads and sliding distances resulted in a higher volumetric loss and weight height loss.The wear height loss of nanocomposites decreases significantly with the increase in nano ceramic particulates content is increased from 0 to 2 it. %. The same is shown clearly in wear graphs.
- The specific wear rate, for a given composition at a given sliding distance with increased load, the specific wear rate increases and a given composition with increased sliding distance, the specific wear rate decreases. Further, as the filler content increases in the composite for a given sliding distance, the specific wear rate reduces. Therefore, it can be concluded that the material parameter (Reinforcement content) and the test parameter, i.e., applied load and sliding distance effects the wear factor.
- The scanning electron micrograph (SEM) images and XRD analysis for all eight metal matrix nanocomposites were studied. The SEM image clearly shows the uniform distribution of the ceramic nanoparticles and no porosity. XRD shows the different phases and elements of the metal matrix nanocomposites.

Future Work

There is a good scope for study of dispersion of nano particles and stirring effect on the formation of aluminium MMNC structures using CFD or any other similar technique. This area is not yet explored by any researchers.

Aluminium based nanocomposites certainly better in mechanical and tribological properties. However their other properties such as electrical and electronic properties need to be explored. Aluminium based hybrid nanocomposites like AAxxxx/SiC/Al2O3/xx fabrication and related properties evaluation is a very good scope for future work.

Appendix I

A) Specific Wear Rate of AA2219/Al_2O_3/50 nm composite:

Table A1 Wear results for MMNC AA 2219/Al_2O_3/50 nm

S. No	L	SD	SV	Wt. %	Response (Raw data)			Average WH (μm)	VOW (mm^3) 10e-3	SWR (mm^3/Nm)	S/N Ratio
					WH1 (μm)	WH2 (μm)	WH3 (μm)				
1	5	1000	0.733	0.5	28	33	35	32	0.9043	0.0001809	71.2102
2	5	2000	1.0989	1	101	94	99	98	2.7695	0.0002770	70.2290
3	5	3000	1.465	1.5	153	150	135	146	4.1260	0.0002751	73.0222
4	5	4000	1.832	2	209	225	220	218	6.1607	0.0003080	71.1976
5	10	1000	1.0989	1.5	82	78	77	79	2.2325	0.0002233	68.1365
6	10	2000	0.733	2	184	202	199	195	5.5107	0.0002755	67.2964
7	10	3000	1.832	0.5	420	413	415	416	11.7562	0.0003919	73.3593
8	10	4000	1.465	1	616	608	609	611	17.2669	0.0004317	70.0697
9	15	1000	1.465	2	117	105	120	114	3.2216	0.0002148	68.4778
10	15	2000	1.832	1.5	329	338	332	333	9.4106	0.0003137	66.2494
11	15	3000	0.733	1	595	608	597	600	16.956	0.0003768	71.2863
12	15	4000	1.0989	0.5	1028	1036	1038	1034	29.2208	0.0004870	67.7042
13	20	1000	1.832	1	200	182	197	193	5.4542	0.0002727	68.5985
14	20	2000	1.465	0.5	586	573	590	583	16.4756	0.0004119	66.7865
15	20	3000	1.0989	2	780	796	791	789	22.2971	0.0003716	71.2102
16	20	4000	0.733	1.5	1301	1299	1288	1296	36.6250	0.0004578	70.2290

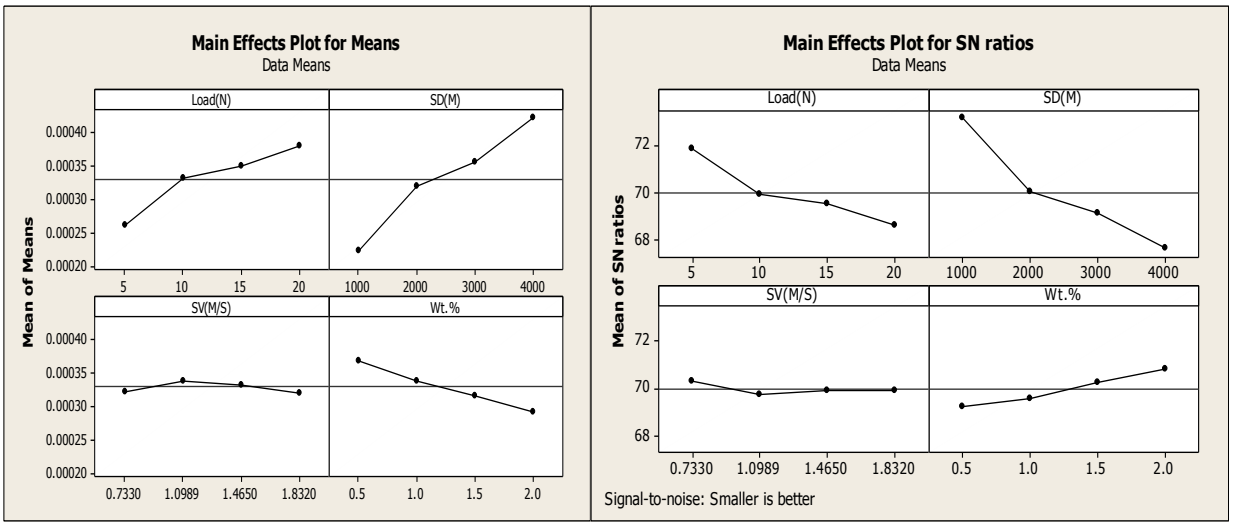

Figure A1 Influence of Process Parameters on SWR (Experimental &S/N data)

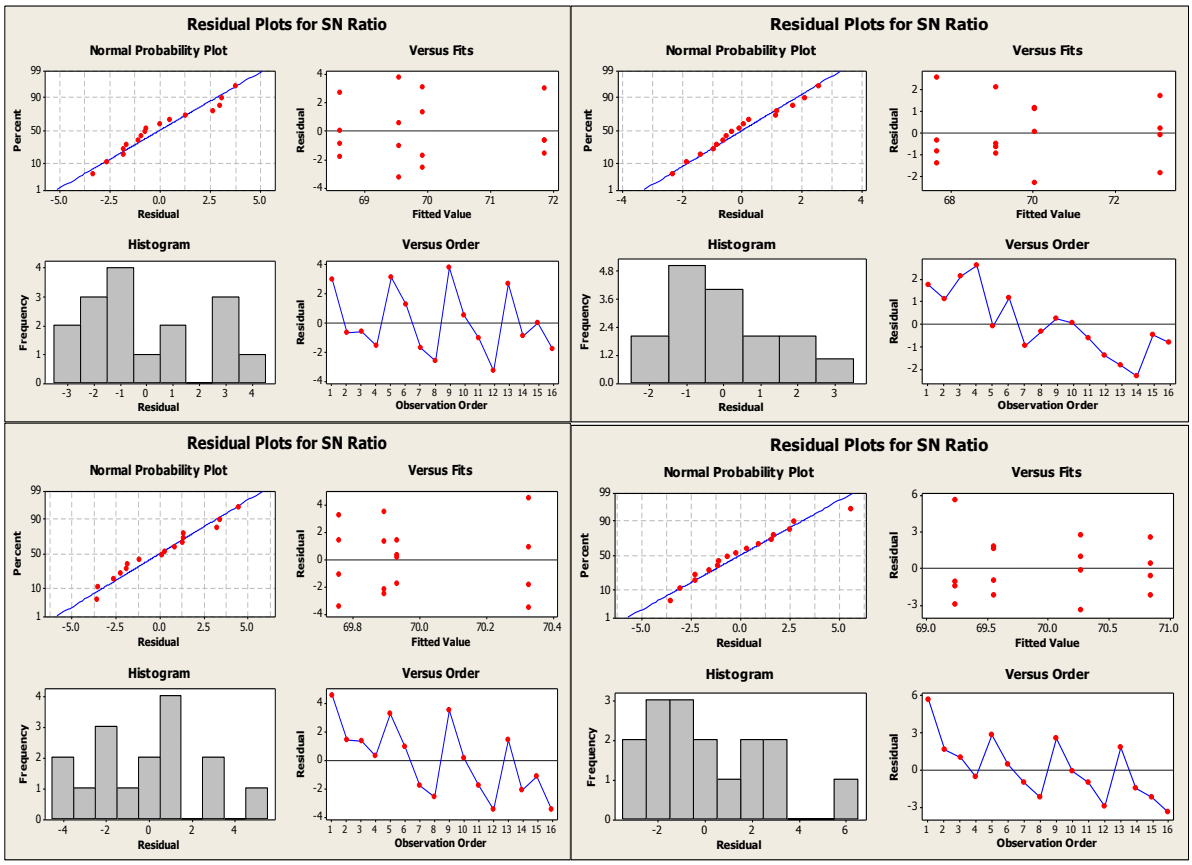

Figure A2 Residual plots for SN Ratios Vs SD,Load,SV and Wt.%

Selection of optimal levels for SWR using MMNC AA2219/Al_2O_3 /50 nm

S = 0.326178 R-Sq = 99.66% R-Sq (adj) = 98.31%

Table A2 Analysis of Variance (ANOVA) for SWR (S/N Data)

Analysis of Variance for SN Ratios							
Source	DF	Seq SS	Adj SS	Adj MS	F	p	% of Contribution
Load(N)	3	22.6216	22.6216	7.5405	70.87	0.003	23.91
SD(M)	3	64.648	64.648	21.5493	202.55	0.001	68.33
SV(M/S)	3	0.7277	0.7277	0.2426	2.28	0.258	0.77
Wt.%	3	6.2901	6.2901	2.0967	19.71	0.018	6.6486
Error	3	0.3192	0.3192	0.1064			
Total	15	94.6066					

S = 9.211530E-06 R-Sq = 99.80% R-Sq (adj) = 98.99%

Table A3 Analysis of Variance for SWR (Experimental Data)

Analysis of Variance for Means						
Source	DF	Seq SS	Adj SS	Adj MS	F	P
Load(N)	3	0.030171*10e-6	0.030171*10e-6	0.010057*10e-6	118.52	0.001
SD(M)	3	0.081783*10e-6	0.081783*10e-6	0.027261*10e-6	321.28	0
SV(M/S)	3	0.000911*10e-6	0.000911*10e-6	0.000304*10e-6	3.58	0.161
Wt.%	3	0.012371*10e-6	0.012371*10e-6	0.004124*10e-6	48.6	0.005
Residual Error	3	0.000255*10e-6	0.000255*10e-6	0.000085*10e-6		
Total	15	0.125491*10e-6				
DF - degrees of freedom, SS - sum of squares, MS - mean squares(Variance), F-ratio of variance of a source to variance of error, P < 0.05 - determines significance of a parameter at 95% confidence level						

Table A4 Response Table for SWR (Experimental Data)

Response table for Means				
Level	Load	SD	SV	Wt.%
1	0.00026	0.000223	0.000323	**0.000368**
2	0.000331	0.00032	0.00034	0.00034
3	0.000348	0.000354	**0.000333**	0.000317
4	**0.000378**	**0.000421**	0.000322	0.000292
Delta	0.000118	0.000198	0.000018	0.000075
Rank	2	1	4	3

The Optimal and Predicted Values for AA 2219/Al_2O_3 /50 nm

Table A5 The optimal and predicted values for AA2219/Al_2O_3/50 nm using Taguchi analysis

Output Response	Optimal set of parameters	Predicted optimal value	Predicted Confidence Interval at 95% confidence Level	Experimental Value (average of three confirmation experiments)
SWR	L4-SD4-SV2-Wt.% 1	0.0005173	0.0004965<η_{SWR}>0.000527	0.0005072

Optimization by using GRA for MMNC AA2219/Al_2O_3 /50 nm

Table A6 Orthogonal Array and Experimental Results Using MMNC AA2219/Al_2O_3 /50 nm

S. No	L	SD	SV	Wt. %	Response (Raw data)			Average WH (μm)	VOW (mm^3) 10e-3	SWR (mm^3/Nm)	S/N Ratio
					WH1 (μm)	WH2 (μm)	WH3 (μm)				
1	5	1000	0.733	0.5	28	33	35	32	0.9043	0.0001809	71.2102
2	5	2000	1.0989	1	101	94	99	98	2.7695	0.0002770	70.2290
3	5	3000	1.465	1.5	153	150	135	146	4.1260	0.0002751	73.0222
4	5	4000	1.832	2	209	225	220	218	6.1607	0.0003080	71.1976
5	10	1000	1.0989	1.5	82	78	77	79	2.2325	0.0002233	68.1365
6	10	2000	0.733	2	184	202	199	195	5.5107	0.0002755	67.2964
7	10	3000	1.832	0.5	420	413	415	416	11.7562	0.0003919	73.3593
8	10	4000	1.465	1	616	608	609	611	17.2669	0.0004317	70.0697
9	15	1000	1.465	2	117	105	120	114	3.2216	0.0002148	68.4778
10	15	2000	1.832	1.5	329	338	332	333	9.4106	0.0003137	66.2494
11	15	3000	0.733	1	595	608	597	600	16.956	0.0003768	71.2863
12	15	4000	1.0989	0.5	1028	1036	1038	1034	29.2208	0.0004870	67.7042
13	20	1000	1.832	1	200	182	197	193	5.4542	0.0002727	68.5985
14	20	2000	1.465	0.5	586	573	590	583	16.4756	0.0004119	66.7865
15	20	3000	1.0989	2	780	796	791	789	22.2971	0.0003716	71.2102
16	20	4000	0.733	1.5	1301	1299	1288	1296	36.6250	0.0004578	70.2290

Optimization steps using Grey Relational Analysis for MMNC AA2219/Al_2O_3 /50 nm

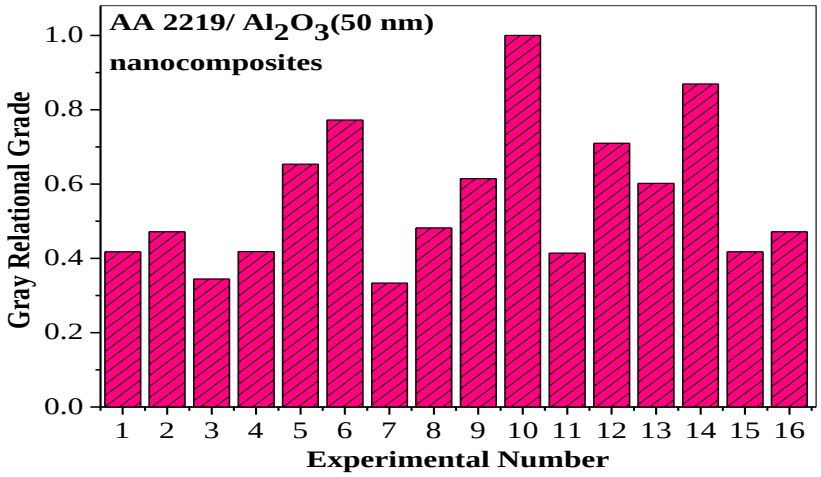

Figure A3 Gray relational grade plot of AA 2219 /Al_2O_3/50 nm composites

Table A7 Gray relational grade

S.No	L	SD	SV	Wt.%	SWR (mm^3/Nm)	S/N Ratio	Normalized S/N Ratio	Δ_{oj}	γ(GRC)	$\overline{\gamma_j}$
1	5	1000	0.733	0.5	0.0001809	71.2102	0.3023	0.6977	0.4175	0.4175
2	5	2000	1.0989	1	0.0002770	70.2290	0.4403	0.5597	0.4718	0.4718
3	5	3000	1.465	1.5	0.0002751	73.0222	0.0474	0.9526	0.3442	0.3442
4	5	4000	1.832	2	0.0003080	71.1976	0.3040	0.696	0.4181	0.4181
5	10	1000	1.0989	1.5	0.0002233	68.1365	0.7346	0.2654	0.6533	0.6533
6	10	2000	0.733	2	0.0002755	67.2964	0.8527	0.1476	0.7721	0.7721
7	10	3000	1.832	0.5	0.0003919	73.3593	0	1	0.3333	0.3333
8	10	4000	1.465	1	0.0004317	70.0697	0.4627	0.5373	0.4820	0.4820
9	15	1000	1.465	2	0.0002148	68.4778	0.6866	0.3134	0.6147	0.6147
10	15	2000	1.832	1.5	0.0003137	66.2494	1	0	1	1
11	15	3000	0.733	1	0.0003768	71.2863	0.2916	0.7084	0.4138	0.4138
12	15	4000	1.0989	0.5	0.0004870	67.7042	0.7954	0.2046	0.7096	0.7096
13	20	1000	1.832	1	0.0002727	68.5985	0.6696	0.3304	0.6021	0.6021
14	20	2000	1.465	0.5	0.0004119	66.7865	0.9245	0.0755	0.8688	0.8688
15	20	3000	1.0989	2	0.0003716	71.2102	0.3023	0.6977	0.4175	0.4175
16	20	4000	0.733	1.5	0.0004578	70.2290	0.4402	0.5598	0.4718	0.4718

Table A8 Average gray relational grade

Input factors	Level 1	Level 2	Level 3	Level 4	Max-Min	rank
Load	0.4129	0.5602	0.5901	**0.6845**	0.2718	2
SD	0.5719	0.5204	0.3772	**0.7782**	0.4010	1
SV	0.5188	**0.5884**	0.5774	0.5631	0.011	4
Wt%	**0.6173**	0.4924	0.5823	0.5556	0.1249	3

General Regression Analysis

Regression Equation

SWR = 0.000148717 + 5.849e-006 Load (N) + 4.8655e-008 SD (M) + 3.43794e-006 SV (M/S) - 6.905e-005 Wt. %

Table A9 The optimal and predicted values for MMNC AA2219/Al_2O_3/50 nm

Response	Optimal Solution of process parameters	Experimental value	Predicted value	% Error
Specific Wear Rate	L4-SD4-SV2-Wt.%1	0.0005163 mm^3/N-m	0.0005072 mm^3/N-m	1.76

B) Specific Wear Rate of AA2219/SiCp/150 nm composite:

Table A10 Wear results for MMNC AA2219/SiCp/150 nm

S.No	L	SD	SV	Wt.%	Response (Raw data) WH1 (μm)	WH 2 (μm)	WH 3 (μm)	Average WH(μm)	VOW (mm^3) 10e-3	SWR (mm^3/Nm)	S/N Ratio
1	5	1000	0.733	0.5	57	59	58	58	1639.08	0.0003278	69.6878
2	5	2000	1.0989	1	149	151	156	152	4295.52	0.0004296	67.3387
3	5	3000	1.465	1.5	236	240	238	238	6725.88	0.0004484	66.9667
4	5	4000	1.832	2	359	350	359	356	10060.56	0.0005030	65.9686
5	10	1000	1.0989	1.5	130	128	114	124	3504.24	0.0003504	69.1087
6	10	2000	0.733	2	327	324	318	323	9127.98	0.0004564	66.8131
7	10	3000	1.832	0.5	736	739	724	733	20714.58	0.0006905	63.2167
8	10	4000	1.465	1	981	975	972	976	27581.76	0.0006895	63.2293
9	15	1000	1.465	2	187	190	178	185	5228.1	0.0003485	69.1559
10	15	2000	1.832	1.5	550	557	552	553	15627.78	0.0005209	65.6649
11	15	3000	0.733	1	963	959	958	960	27129.6	0.0006029	64.3951
12	15	4000	1.0989	0.5	1859	1865	1862	1862	52620.12	0.0008770	61.1400
13	20	1000	1.832	1	297	300	291	296	8364.96	0.0004182	67.5723
14	20	2000	1.465	0.5	1048	1052	1050	1050	29673	0.0007418	62.5943
15	20	3000	1.0989	2	1300	1298	1308	1302	36794.52	0.0006132	64.2480
16	20	4000	0.733	1.5	2161	2166	2153	2160	61041.6	0.0007630	62.3495

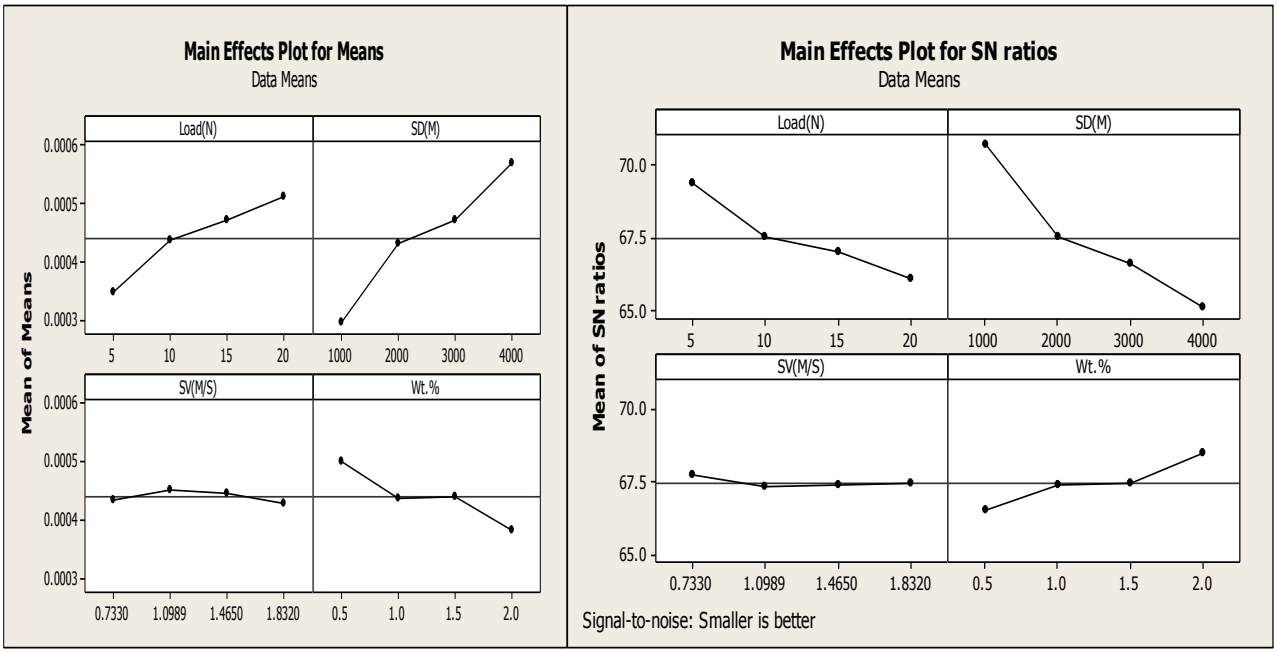

Figure A4 Influence of Process Parameters on SWR (Experimental &S/N data)

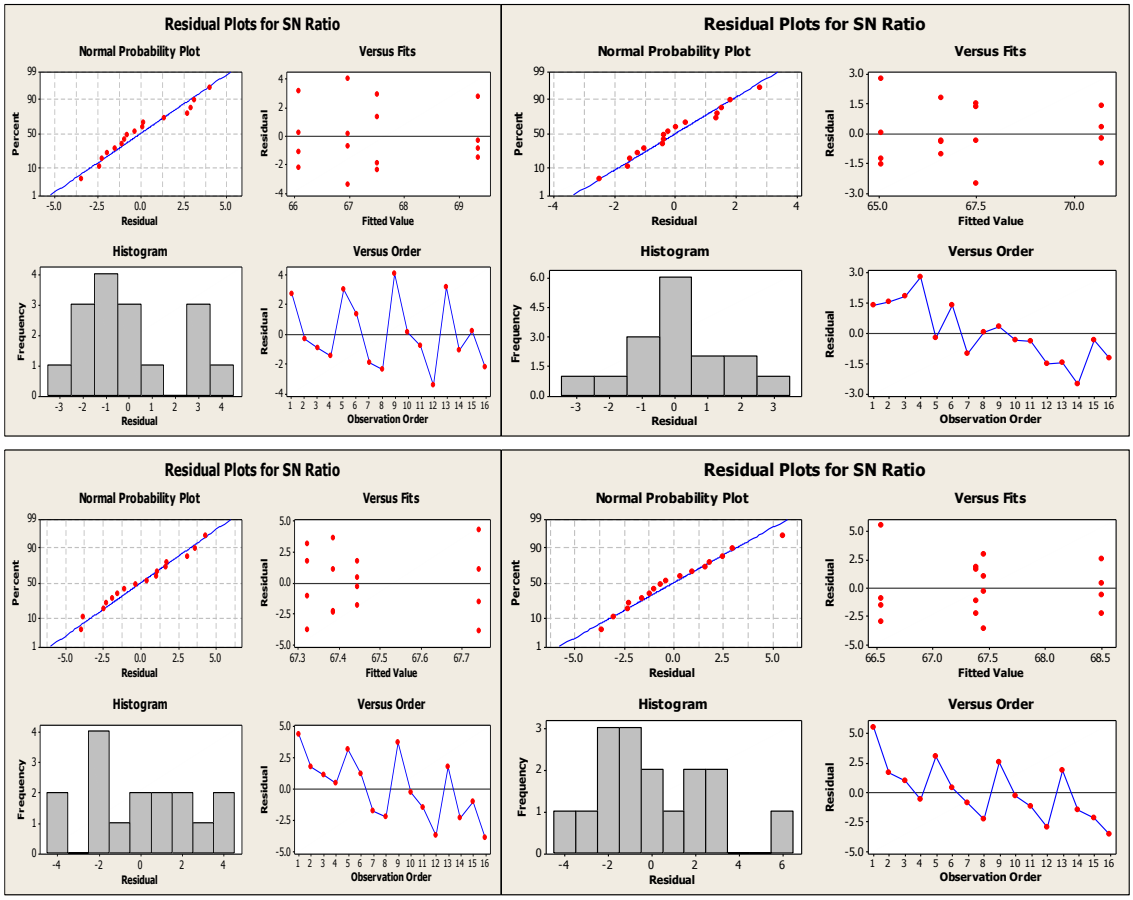

Figure A5 Residual plots for SN Ratios Vs SD,Load,SV and Wt.%

Selection of optimal levels for SWR using MMNC AA2219/SiCp/150 nm

S = 0.254258 R-Sq = 99.80% R-Sq (adj) = 99.02%

Table A11 Analysis of Variance (ANOVA) for SWR (S/N Data)

Analysis of Variance for SN Ratios							
Source	DF	Seq SS	Adj SS	Adj MS	F	p	% of Contribution
Load(N)	3	23.1305	23.1305	7.7102	119.27	0.001	23.35
SD(M)	3	67.5455	67.5455	22.5152	348.28	0	68.19
SV(M/S)	3	0.4151	0.4151	0.1384	2.14	0.274	0.419
Wt.%	3	7.7662	7.7662	2.5887	40.04	0.006	7.84
Error	3	0.1939	0.1939	0.0646			
Total	15	99.0512					

S = 0.0000152084 R-Sq = 99.71% R-Sq (adj) = 98.57%

Table A12 Analysis of Variance for SWR (Experimental Data)

Analysis of Variance for Means						
Source	DF	Seq SS	Adj SS	Adj MS	F	P
Load(N)	3	0.058465*10e-06	0.058465*10e-06	0.019488*10e-06	84.26	0.002
SD(M)	3	0.154822*10e-06	0.154822*10e-06	0.051607*10e-06	223.12	0.001
SV(M/S)	3	0.001155*10e-06	0.001155*10e-06	0.000385*10e-06	1.66	0.343
Wt.%	3	0.028054*10e-06	0.028054*10e-06	0.009351*10e-06	40.43	0.006
Residual Error	3	0.000694*10e-06	0.000694*10e-06	0.000231*10e-06		
Total	15	0.24319*10e-06				

DF - degrees of freedom, SS - sum of squares, MS - mean squares(Variance), F-ratio of variance of a source to variance of error, $P < 0.05$ - determines significance of a parameter at 95% confidence level

Table A13 Response Table for SWR (Experimental Data)

Response table for Means				
Level	Load	SD	SV	Wt.%
1	0.000346	0.000294	0.000436	**0.000501**
2	0.000435	0.00043	**0.000451**	0.000436
3	**0.000469**	0.00047	0.000445	0.000441
4	0.00051	**0.000568**	0.000429	0.000383
Delta	0.000164	0.000274	0.000022	0.000118
Rank	2	1	4	3

The Optimal and Predicted Values for AA 2219/SiCp/150 nm

Table A14 The optimal and predicted values for MMNC's AA 2219/SiCp/150 nm

Output Response	Optimal set of parameters	Predicted optimal value	Predicted Confidence Interval at 95% confidence Level	Experimental Value (average of three confirmation experiments)
SWR	L4-SD4-SV2-Wt. % 1	0.0006924	0.0006429<η_{SWR}>0.0006933	0.0006665

Optimization by using GRA for MMNC AA2219/SiCp /150 nm

Table A15 Orthogonal Array and Experimental Results Using MMNCAA2219/SiCp (150 nm)

S. No	L	SD	SV	Wt. %	Response (Raw data)			Average WH (μm)	VOW (mm^3) 10e-3	SWR (mm^3/N-m)	S/N Ratio
					WH1 (μm)	WH2 (μm)	WH3 (μm)				
1	5	1000	0.733	0.5	43	43	46	44	1243.44	0.0002487	72.0865
2	5	2000	1.0989	1	122	124	129	125	3532.5	0.0003533	69.0371
3	5	3000	1.465	1.5	201	206	196	201	5680.26	0.0003787	68.4341
4	5	4000	1.832	2	288	281	289	286	8082.36	0.0004041	67.8702
5	10	1000	1.0989	1.5	109	102	107	106	2995.56	0.0002996	70.4692
6	10	2000	0.733	2	256	252	257	255	7206.3	0.0003603	68.8667
7	10	3000	1.832	0.5	556	554	564	558	15769.08	0.0005256	65.5869

8	10	4000	1.465	1	784	786	791	787	22240.62	0.0005560	65.0985
9	15	1000	1.465	2	139	152	156	149	4210.74	0.0002807	71.0352
10	15	2000	1.832	1.5	472	467	465	468	13225.68	0.0004409	67.1132
11	15	3000	0.733	1	786	770	784	780	22042.8	0.0004898	66.1996
12	15	4000	1.0989	0.5	1417	1420	1408	1415	39987.9	0.0006665	63.5240
13	20	1000	1.832	1	242	249	2444	245	6923.7	0.0003462	69.2135
14	20	2000	1.465	0.5	797	799	798	798	22551.48	0.0005638	64.9775
15	20	3000	1.0989	2	1030	1033	1036	1033	29192.58	0.0004865	66.2583
16	20	4000	0.733	1.5	1821	1824	1827	1824	51546.24	0.0006443	63.8182

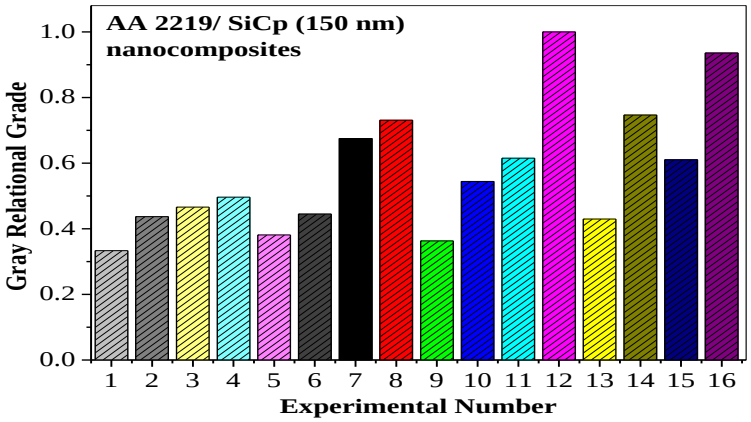

Figure A6 Gray relational grade plot of AA 2219 /SiCp (150 nm) composites

Optimization steps using Grey Relational Analysis for MMNC AA 2219/SiCp/150 nm

Table A16 Gray relational grade

S.No	L	SD	SV	Wt. %	SWR (mm^3/Nm)	S/N Ratio	Normalized S/N Ratio	Δ_{oj}	γ(GRC)	$\overline{\gamma_j}$
1	5	1000	0.733	0.5	0.0002487	72.0865	0	1	0.3333	0.3333
2	5	2000	1.0989	1	0.0003533	69.0371	0.3561	0.6439	0.4371	0.4371
3	5	3000	1.465	1.5	0.0003787	68.4341	0.4266	0.5734	0.4658	0.4658
4	5	4000	1.832	2	0.0004041	67.8702	0.4924	0.5076	0.4962	0.4962
5	10	1000	1.0989	1.5	0.0002996	70.4692	0.1889	0.8111	0.3814	0.3814
6	10	2000	0.733	2	0.0003603	68.8667	0.3760	0.6240	0.4448	0.4448
7	10	3000	1.832	0.5	0.0005256	65.5869	0.7591	0.2409	0.6749	0.6749
8	10	4000	1.465	1	0.0005560	65.0985	0.8161	0.1839	0.7311	0.7311

9	15	1000	1.465	2	0.0002807	71.0352	0.1228	0.8772	0.3631	0.3631
10	15	2000	1.832	1.5	0.0004409	67.1132	0.5808	0.4192	0.5440	0.5440
11	15	3000	0.733	1	0.0004898	66.1996	0.6875	0.3125	0.6154	0.6154
12	15	4000	1.0989	0.5	0.0006665	63.5240	1	0	1	1
13	20	1000	1.832	1	0.0003462	69.2135	0.3355	0.6645	0.4294	0.4294
14	20	2000	1.465	0.5	0.0005638	64.9775	0.8302	0.1698	0.7465	0.7465
15	20	3000	1.0989	2	0.0004865	66.2583	0.6807	0.3193	0.6103	0.6103
16	20	4000	0.733	1.5	0.0006443	63.8182	0.9656	0.0344	0.9356	0.9356

Table A17 Average gray relational grade

Input factors	Level 1	Level 2	Level 3	Level 4	Max-Min	Rank
Load	0.4331	0.5581	0.6306	**0.6805**	0.2474	2
SD	0.3768	0.5431	0.5916	**0.7907**	0.4139	1
SV	0.5823	**0.6072**	0.5766	0.5361	0.0711	4
Wt. %	**0.6887**	0.5533	0.5817	0.4786	0.2101	3

General Regression Analysis:

Regression Equation

SWR = 0.000190007 + 1.0522e-005 Load (N) + 8.6235e-008 SD (M) - 7.21913e-006 SV (M/S) - 7.004e-005 Wt. %

Table A18 The optimal and predicted values for MMNC's AA 2219/SiCp/150 nm

Response	Optimal Solution of process parameters	Experimental value	Predicted value	% Error
Specific Wear Rate	L4-SD4-SV2-Wt.%1	0.0006665mm^3/N-m	0.0006924mm^3/N-m	3.74

C) Specific Wear Rate of AA2219/Al_2O_3/150 nm composite:

Table A19 Wear results for MMNC AA2219/Al_2O_3/150 nm

S. No	L	SD	SV	Wt. %	Response (Raw data)			Average WH(μm)	VOW (mm^3) 10e-3	SWR (mm^3/Nm)	S/N Ratio
					WH1 (μm)	WH2 (μm)	WH3 (μm)				
1	5	1000	0.733	0.5	57	59	58	58	1639.08	0.0003278	69.6878
2	5	2000	1.0989	1	149	151	156	152	4295.52	0.0004296	67.3387
3	5	3000	1.465	1.5	236	240	238	238	6725.88	0.0004484	66.9667
4	5	4000	1.832	2	359	350	359	356	10060.56	0.0005030	65.9686
5	10	1000	1.0989	1.5	130	128	114	124	3504.24	0.0003504	69.1087

6	10	2000	0.733	2	327	324	318	323	9127.98	0.0004564	66.8131
7	10	3000	1.832	0.5	736	739	724	733	20714.58	0.0006905	63.2167
8	10	4000	1.465	1	981	975	972	976	27581.76	0.0006895	63.2293
9	15	1000	1.465	2	187	190	178	185	5228.1	0.0003485	69.1559
10	15	2000	1.832	1.5	550	557	552	553	15627.78	0.0005209	65.6649
11	15	3000	0.733	1	963	959	958	960	27129.6	0.0006029	64.3951
12	15	4000	1.0989	0.5	1859	1865	1862	1862	52620.12	0.0008770	61.1400
13	20	1000	1.832	1	297	300	291	296	8364.96	0.0004182	67.5723
14	20	2000	1.465	0.5	1048	1052	1050	1050	29673	0.0007418	62.5943
15	20	3000	1.0989	2	1300	1298	1308	1302	36794.52	0.0006132	64.2480
16	20	4000	0.733	1.5	2161	2166	2153	2160	61041.6	0.0007630	62.3495

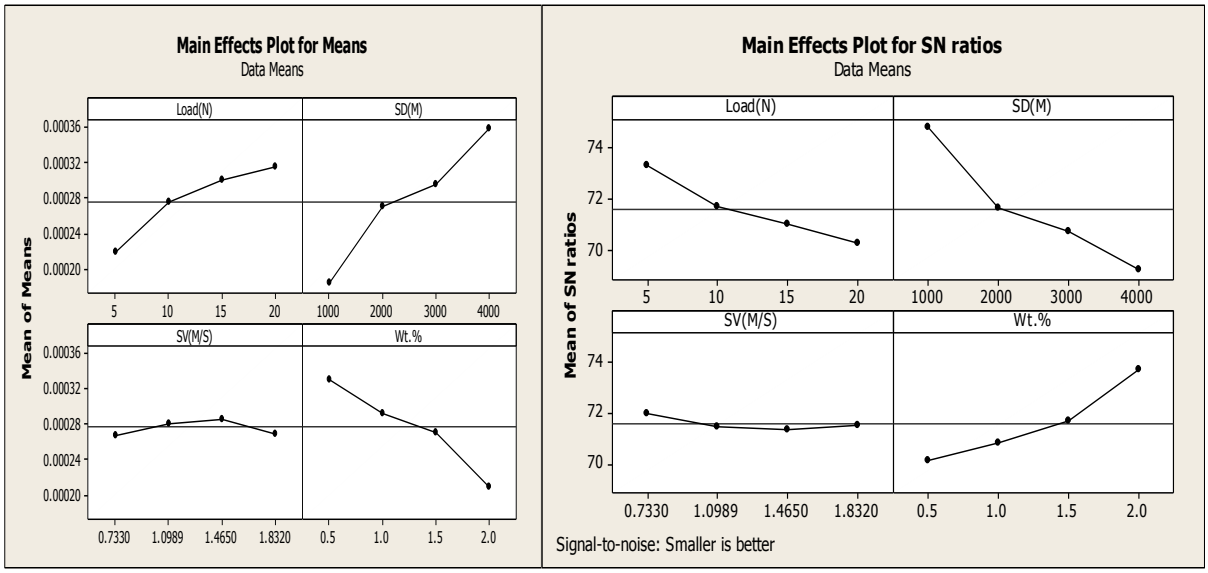

Figure A7 Influence of Process Parameters on SWR (Experimental &S/N data)

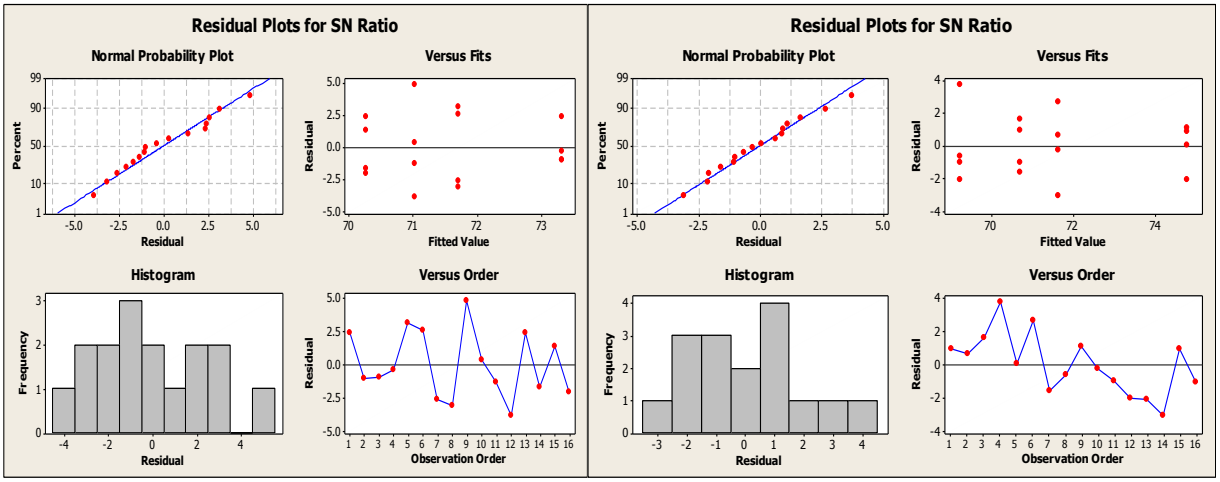

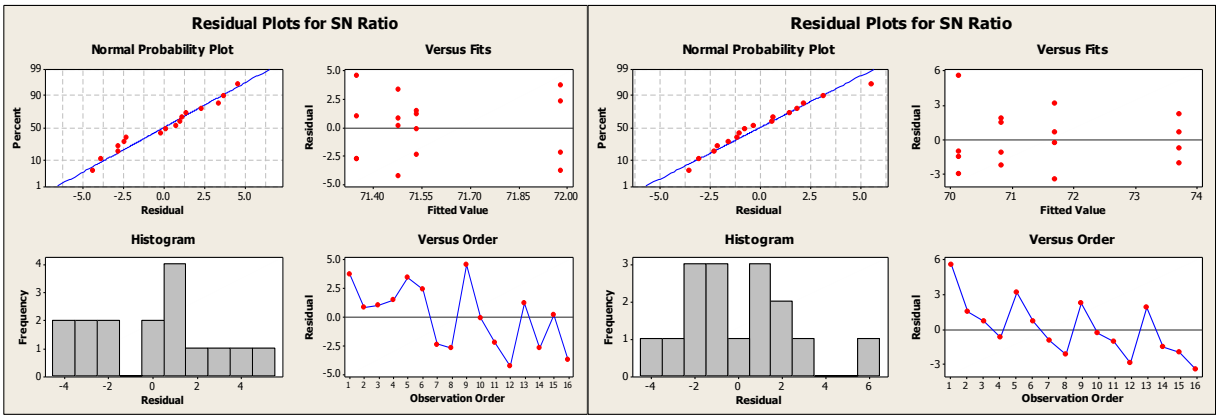

Figure A8 Residual plots for SN Ratios Vs SD,Load,SV and Wt.%

Selection of optimal levels for SWR using MMNC AA2219/Al_2O_3/150 nm

S = 0.185700 R-Sq = 99.90% R-Sq (adj) = 99.51%

Table A20 Analysis of Variance (ANOVA) for SWR (S/N Data)

Analysis of Variance for SN Ratios							
Source	DF	Seq SS	Adj SS	Adj MS	F	p	% of Contribution
Load(N)	3	23.2798	23.2798	7.7599	225.03	0.0000	21.94
SD(M)	3	69.8396	69.8396	23.2799	675.08	0.0000	65.81
SV(M/S)	3	0.3086	0.3086	0.1029	2.98	0.1970	0.291
Wt.%	3	12.5976	12.5976	4.1992	121.77	0.0010	11.87
Error	3	0.1035	0.1035	0.0345			
Total	15	106.129					

S = 0.0165198 R-Sq = 99.80% R-Sq (adj) = 99.02%

Table A21 Analysis of Variance for SWR (Experimental Data)

Analysis of Variance for Means						
Source	DF	Seq SS	Adj SS	Adj MS	F	P
Load(N)	3	0.094171	0.094171	0.03139	115.02	0.001
SD(M)	3	0.2492	0.2492	0.083067	304.38	0.000

SV(M/S)	3	0.003167	0.003167	0.001056	3.87	0.148
Wt.%	3	0.071522	0.071522	0.023841	87.36	0.002
Residual Error	3	0.000819	0.000819	0.000273		
Total	15	0.418878				

DF - degrees of freedom, SS - sum of squares, MS - mean squares (Variance), F-ratio of variance of a source to variance of error, P < 0.05 - determines significance of a parameter at 95% confidence level

Table A22 Response Table for SWR (Experimental Data)

Response table for Means				
Level	Load	SD	SV	Wt.%
1	0.000427	0.000361	0.000538	**0.000659**
2	0.000547	0.000537	**0.000568**	0.000535
3	0.000587	0.000589	0.000557	0.000521
4	**0.000634**	**0.000708**	0.000533	0.00048
Delta	0.000207	0.000347	0.000034	0.000179
Rank	2	1	4	3

The Optimal and Predicted Values for AA 2219/Al_2O_3 /150 nm

Table A23 The optimal and predicted values for MMNC's AA 2219/Al_2O_3/150 nm

Output Response	Optimal set of parameters	Predicted optimal value	Predicted Confidence Interval at 95% confidence Level	Experimental Value (average of three confirmation experiments)
SWR	L4-SD4-SV2-Wt.% 1	0.0008957	0.0008952<η_{SWR}>0.00095	0.0008770

Optimization by using GRA for MMNC AA2219/Al_2O_3 /150 nm

Table A24 Orthogonal Array and Experimental Results Using MMNC AA2219/Al_2O_3 (150 nm)

S. No	L	SD	SV	Wt. %	Response (Raw data)			Average WH (μm)	VOW (mm^3) 10e-3	SWR (mm^3/Nm)	S/N Ratio
					WH1 (μm)	WH 2 (μm)	WH 3 (μm)				
1	5	1000	0.733	0.5	57	59	58	58	1639.08	0.0003278	69.6878
2	5	2000	1.0989	1	149	151	156	152	4295.52	0.0004296	67.3387

3	5	3000	1.465	1.5	236	240	238	238	6725.88	0.0004484	66.9667
4	5	4000	1.832	2	359	350	359	356	10060.56	0.0005030	65.9686
5	10	1000	1.0989	1.5	130	128	114	124	3504.24	0.0003504	69.1087
6	10	2000	0.733	2	327	324	318	323	9127.98	0.0004564	66.8131
7	10	3000	1.832	0.5	736	739	724	733	20714.58	0.0006905	63.2167
8	10	4000	1.465	1	981	975	972	976	27581.76	0.0006895	63.2293
9	15	1000	1.465	2	187	190	178	185	5228.1	0.0003485	69.1559
10	15	2000	1.832	1.5	550	557	552	553	15627.78	0.0005209	65.6649
11	15	3000	0.733	1	963	959	958	960	27129.6	0.0006029	64.3951
12	15	4000	1.0989	0.5	1859	1865	1862	1862	52620.12	0.0008770	61.1400
13	20	1000	1.832	1	297	300	291	296	8364.96	0.0004182	67.5723
14	20	2000	1.465	0.5	1048	1052	1050	1050	29673	0.0007418	62.5943
15	20	3000	1.0989	2	1300	1298	1308	1302	36794.52	0.0006132	64.2480
16	20	4000	0.733	1.5	2161	2166	2153	2160	61041.6	0.0007630	62.3495

Optimization Steps using Grey Relational Analysis for MMNC AA2219/Al_2O_3 /150 nm

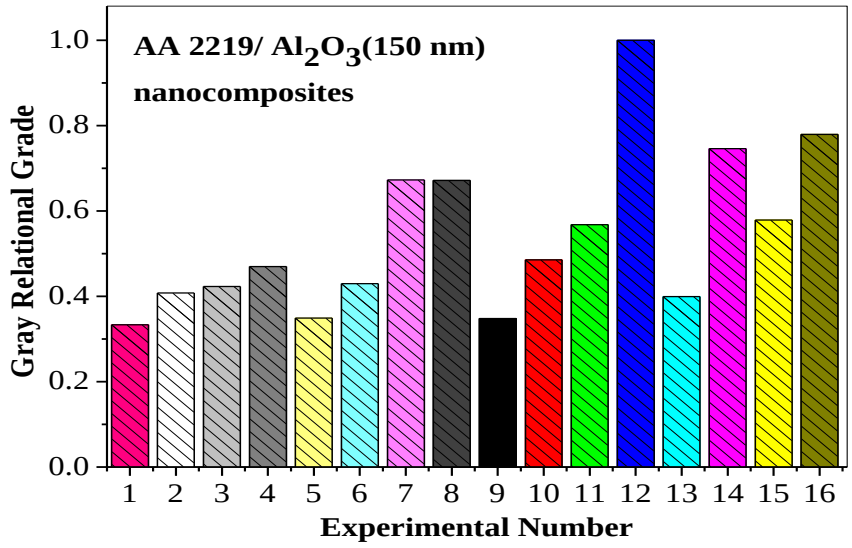

Figure A9 Gray relational grade plot of AA 2219 /Al_2O_3 (150 nm) composites

Table A25 Gray relational grade

S.No	L	SD	SV	Wt. %	SWR (mm^3/Nm)	S/N Ratio	Normalized S/N Ratio	Δ_{oj}	γ(GRC)	$\overline{\gamma_j}$
1	5	1000	0.733	0.5	0.0003278	69.6878	0	1	0.3333	0.3333

2	5	2000	1.0989	1	0.0004296	67.3387	0.2748	0.7252	0.4081	0.4081
3	5	3000	1.465	1.5	0.0004484	66.9667	0.3183	0.6817	0.4231	0.4231
4	5	4000	1.832	2	0.0005030	65.9686	0.4351	0.5649	0.4695	0.4695
5	10	1000	1.0989	1.5	0.0003504	69.1087	0.0677	0.9323	0.3491	0.3491
6	10	2000	0.733	2	0.0004564	66.8131	0.3363	0.6637	0.4297	0.4297
7	10	3000	1.832	0.5	0.0006905	63.2167	0.7570	0.2430	0.6729	0.6729
8	10	4000	1.465	1	0.0006895	63.2293	0.7556	0.2444	0.6717	0.6717
9	15	1000	1.465	2	0.0003485	69.1559	0.0622	0.9378	0.3476	0.3476
10	15	2000	1.832	1.5	0.0005209	65.6649	0.4706	0.5294	0.4857	0.4857
11	15	3000	0.733	1	0.0006029	64.3951	0.6192	0.3808	0.5677	0.5677
12	15	4000	1.0989	0.5	0.0008770	61.1400	1	0	1	1
13	20	1000	1.832	1	0.0004182	67.5723	0.2475	0.7525	0.3992	0.3992
14	20	2000	1.465	0.5	0.0007418	62.5943	0.8299	0.1701	0.7462	0.7462
15	20	3000	1.0989	2	0.0006132	64.2480	0.6364	0.3636	0.5790	0.5790
16	20	4000	0.733	1.5	0.0007630	62.3495	0.8585	0.1415	0.7794	0.7794

Table A26 Average gray relational grade

Input factors	Level 1	Level 2	Level 3	Level 4	Max-Min	Rank
Load	0.4085	0.5309	0.6003	**0.6260**	0.2175	3
SD	0.3573	0.5174	0.5607	**0.7302**	0.3729	1
SV	0.5275	**0.5841**	0.5472	0.5068	0.0773	4
Wt%	**0.6881**	0.5117	0.5093	0.4565	0.2316	2

General Regression Analysis:

SWR = 0.000256596 + 1.32235e-005 Load (N) + 1.09227e-007 SD (M) - 6.47014e-006 SV (M/S) - 0.000110275 Wt. %.

Table A27 The optimal and predicted values for MMNC AA2219/Al_2O_3/150 nm

Response	Optimal Solution of process parameters	Experimental value	Predicted value	% Error
Specific Wear Rate	L4-SD4-SV2-Wt. %1	**0.0008770**	**0.0008957**	**2.09**

D) Specific Wear Rate of AA2014/SiCp/50 nm composite:

Table A28 Wear results for MMNC AA2014/SiCp/50 nm

S. No	L	SD	SV	Wt. %	Response (Raw data)			Average WH (μm)	VOW (mm^3) 10e-3	SWR (mm^3/Nm)	S/N Ratio
					WH1 (μm)	WH2 (μm)	WH3 (μm)				
1	5	1000	0.733	0.5	22	25	22	23	649.98	0.0001299	77.7278
2	5	2000	1.0989	1	70	67	67	68	1921.68	0.0001922	74.3249
3	5	3000	1.465	1.5	106	107	96	103	2910.78	0.0001941	74.2395
4	5	4000	1.832	2	135	133	140	136	3843.36	0.0001922	74.3249
5	10	1000	1.0989	1.5	51	59	52	54	1526.04	0.0001526	76.3289
6	10	2000	0.733	2	116	112	111	113	3193.38	0.0001597	75.9339
7	10	3000	1.832	0.5	293	299	290	294	8308.44	0.0002769	71.1535
8	10	4000	1.465	1	409	415	403	409	11558.34	0.0002889	70.7850
9	15	1000	1.465	2	71	77	68	72	2034.72	0.0001356	77.3548
10	15	2000	1.832	1.5	239	240	244	241	6810.66	0.0002270	72.8795
11	15	3000	0.733	1	411	416	409	412	11643.12	0.0002587	71.7441
12	15	4000	1.0989	0.5	749	742	735	742	20968.92	0.0003495	69.1311
13	20	1000	1.832	1	127	129	128	128	3617.28	0.0001809	74.8512
14	20	2000	1.465	0.5	429	422	412	421	11897.46	0.0002974	70.5332
15	20	3000	1.0989	2	467	470	461	466	13169.16	0.0002195	73.1713
16	20	4000	0.733	1.5	908	911	917	912	25773.12	0.0003222	69.8375

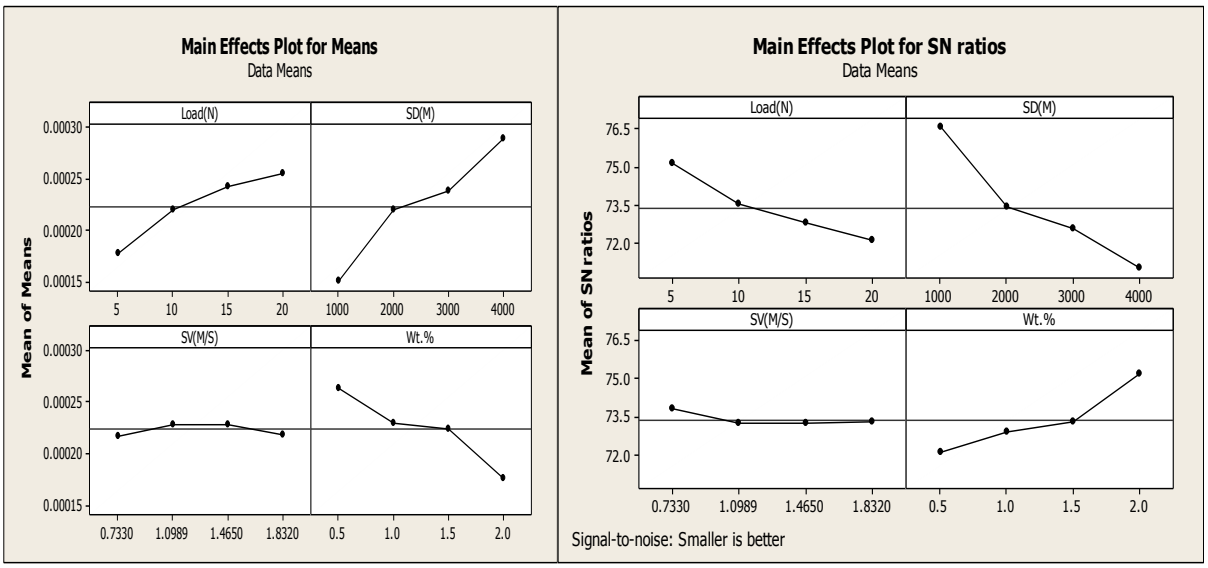

Figure A10 Influence of Process Parameters on SWR (Experimental &S/N data)

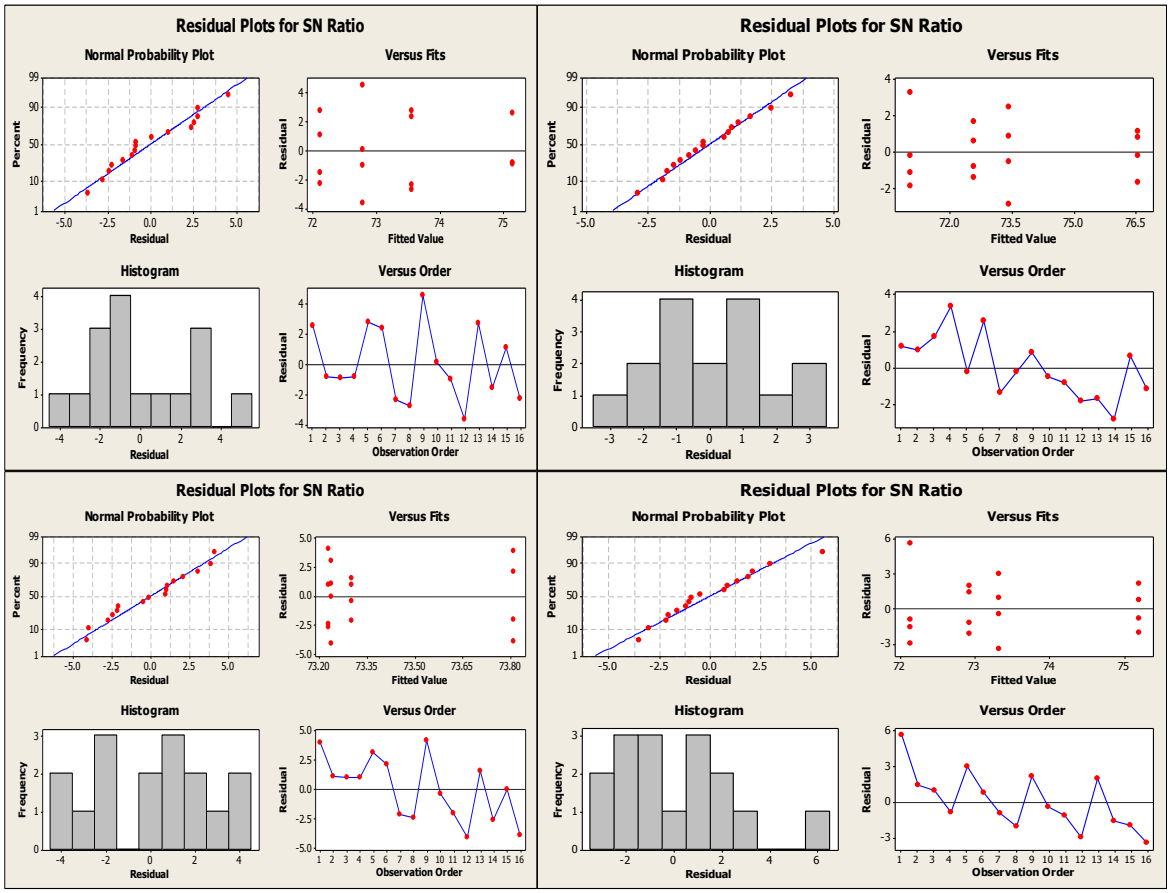

Figure A11 Residual plots for SN Ratios Vs SD,Load,SV and Wt.%

Selection of optimal levels for SWR using MMNC AA2014/SiCp/50 nm

Table A29 Analysis of Variance (ANOVA) for SWR (S/N Data)

Analysis of Variance for SN Ratios							
Source	DF	Seq SS	Adj SS	Adj MS	F	p	% of Contribution
Load(N)	3	20.7286	20.7286	6.9095	32.56	0.009	
SD(M)	3	65.4605	65.4605	21.8202	102.81	0.002	
SV(M/S)	3	0.9347	0.9347	0.3116	1.47	0.38	
Wt.%	3	20.2145	20.2145	6.7382	31.75	0.009	
Error	3	0.6367	0.6367	0.2122			
Total	15	107.975					

S = 0.460685 R-Sq = 99.41% R-Sq (adj) = 97.05%

Table A30 Analysis of Variance for SWR (Experimental Data)

Analysis of Variance for Means						
Source	DF	Seq SS	Adj SS	Adj MS	F	P
Load(N)	3	0.014119*10e-6	0.014119*10e-6	0.004706*10e-6	27.56	0.011
SD(M)	3	0.039341*10e-6	0.039341*10e-6	0.013114*10e-6	76.79	0.002
SV(M/S)	3	0.000429*10e-6	0.000429*10e-6	0.000143*10e-6	0.84	0.556
Wt.%	3	0.015297*10e-6	0.015297*10e-6	0.005099*10e-6	29.86	0.01
Residual Error	3	0.000512*10e-6	0.000512*10e-6	0.000171*10e-6		
Total	15	0.069698*10e-6				
DF - degrees of freedom, SS - sum of squares, MS - mean squares(Variance), F-ratio of variance of a source to variance of error, P < 0.05 - determines significance of a parameter at 95% confidence level						

S = 0.0000130682 R-Sq = 99.26% R-Sq (adj) = 96.32%

Table A31 Response Table for SWR (Experimental Data)

Response table for Means				
Level	Load	SD	SV	Wt.%
1	0.000177	0.00015	0.000218	**0.000263**
2	0.00022	0.000219	0.000228	0.00023
3	0.000243	0.000237	**0.000229**	0.000224
4	**0.000255**	**0.000288**	0.000219	0.000177
Delta	0.000078	0.000138	0.000011	0.000087
Rank	3	1	4	2

The Optimal and Predicted Values for AA2014/SiCp/50 nm

Table A32 The optimal and predicted values for MMNC AA2014/SiCp/50 nm

Output Response	Optimal set of parameters	Predicted optimal value	Predicted Confidence Interval at 95% confidence Level	Experimental Value (average of three confirmation experiments)
SWR	L4-SD4-SV3-Wt.% 1	0.0003668	$0.0003425<\eta_{SWR}>0.0003859$	0.0003495

Optimization by using GRA for MMNC AA2014/SiCp /50 nm

Optimization Steps using Grey Relational Analysis for MMNC AA2014/SiCp/50 nm

Table A33 Grey relational coefficient

S. No	L	SD	SV	Wt. %	SWR (mm^3/Nm)	S/N Ratio	Normalized S/N Ratio	Δ_{oj}	γ (GRC)
1	5	1000	0.733	0.5	0.0001299	77.7278	0	1	0.3333
2	5	2000	1.0989	1	0.0001922	74.3249	0.3958	0.6042	0.4528
3	5	3000	1.465	1.5	0.0001941	74.2395	0.4058	0.5942	0.4570
4	5	4000	1.832	2	0.0001922	74.3249	0.3958	0.6042	0.4528
5	10	1000	1.0989	1.5	0.0001526	76.3289	0.1627	0.8373	0.3789
6	10	2000	0.733	2	0.0001597	75.9339	0.2087	0.7913	0.3872
7	10	3000	1.832	0.5	0.0002769	71.1535	0.7647	0.2353	0.6799
8	10	4000	1.465	1	0.0002889	70.7850	0.8076	0.1924	0.7221
9	15	1000	1.465	2	0.0001356	77.3548	0.0434	0.9566	0.3433
10	15	2000	1.832	1.5	0.0002270	72.8795	0.5640	0.4360	0.5342
11	15	3000	0.733	1	0.0002587	71.7441	0.6960	0.3040	0.6219
12	15	4000	1.0989	0.5	0.0003495	69.1311	1	0	1
13	20	1000	1.832	1	0.0001809	74.8512	0.3346	0.6654	0.4290
14	20	2000	1.465	0.5	0.0002974	70.5332	0.8369	0.1631	0.7540
15	20	3000	1.0989	2	0.0002195	73.1713	0.5300	0.4700	0.5155
16	20	4000	0.733	1.5	0.0003222	69.8375	0.9178	0.0822	0.8588

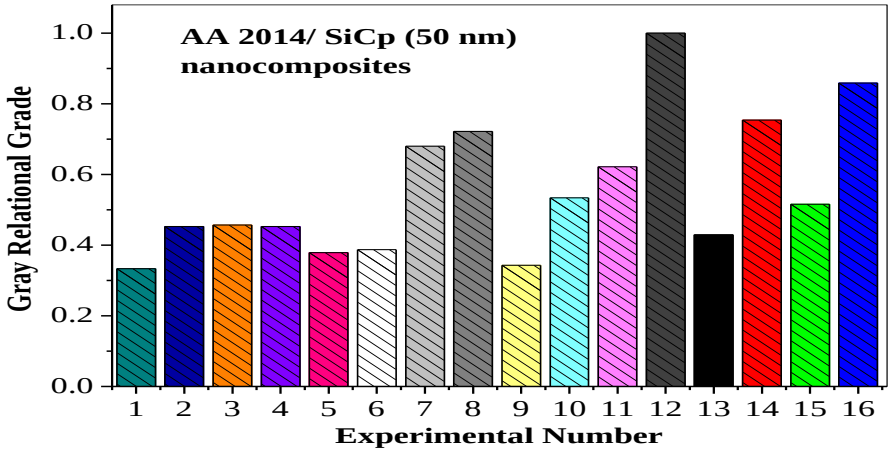

Figure A12 Gray relational grade plot of AA2014/SiCp/50 nm composites

Table A34 Gray relational grade

S.No	L	SD	SV	Wt. %	SWR (mm^3/Nm)	S/N Ratio	Normalized S/N Ratio	Δ_{oj}	γ(GRC)	$\overline{\gamma_j}$
1	5	1000	0.733	0.5	0.0001299	77.7278	0	1	0.3333	0.3333
2	5	2000	1.0989	1	0.0001922	74.3249	0.3958	0.6042	0.4528	0.4528
3	5	3000	1.465	1.5	0.0001941	74.2395	0.4058	0.5942	0.4570	0.4570
4	5	4000	1.832	2	0.0001922	74.3249	0.3958	0.6042	0.4528	0.4528
5	10	1000	1.0989	1.5	0.0001526	76.3289	0.1627	0.8373	0.3789	0.3789
6	10	2000	0.733	2	0.0001597	75.9339	0.2087	0.7913	0.3872	0.3872
7	10	3000	1.832	0.5	0.0002769	71.1535	0.7647	0.2353	0.6799	0.6799
8	10	4000	1.465	1	0.0002889	70.7850	0.8076	0.1924	0.7221	0.7221
9	15	1000	1.465	2	0.0001356	77.3548	0.0434	0.9566	0.3433	0.3433
10	15	2000	1.832	1.5	0.0002270	72.8795	0.5640	0.4360	0.5342	0.5342
11	15	3000	0.733	1	0.0002587	71.7441	0.6960	0.3040	0.6219	0.6219
12	15	4000	1.0989	0.5	0.0003495	69.1311	1	0	1	1
13	20	1000	1.832	1	0.0001809	74.8512	0.3346	0.6654	0.4290	0.4290
14	20	2000	1.465	0.5	0.0002974	70.5332	0.8369	0.1631	0.7540	0.7540
15	20	3000	1.0989	2	0.0002195	73.1713	0.5300	0.4700	0.5155	0.5155
16	20	4000	0.733	1.5	0.0003222	69.8375	0.9178	0.0822	0.8588	0.8588

Table A35 Average gray relational grade

Input factors	Level 1	Level 2	Level 3	Level 4	Max-Min	rank
Load	0.4240	0.5420	0.6249	**0.6393**	0.2153	3
SD	0.3711	0.5321	0.5686	**0.7584**	0.3873	1
SV	0.5503	**0.5868**	0.5691	0.5240	0.0628	4
Wt%	**0.6918**	0.5565	0.5572	0.4247	0.2671	2

General Regression Analysis:

Regression Equation

SWR = 0.000115637 + 5.1375e-006 Load (N) + 4.33575e-008 SD (M) + 1.47255e-006 SV (M/S) - 5.3245e-005 Wt. %.

Table A36 The optimal and predicted values for MMNC AA2014/SiCp/50 nm

Response	Optimal Solution of process parameters	Experimental value	Predicted value	% Error
Specific Wear Rate	L4-SD4-SV3-Wt.%1	**0.0003495**	**0.0003668**	**4.72**

E) Specific Wear Rate of AA2014/Al_2O_3/50 nm composite:

Table A37 Wear results for MMNC AA 2014/Al_2O_3 /50 nm

S. No	L	SD	SV	Wt. %	Response (Raw data)			Average WH (μm)	VOW (mm^3) 10e-3	SWR (mm^3/Nm)	S/N Ratio
					WH1 (μm)	WH2 (μm)	WH3 (μm)				
1	5	1000	0.733	0.5	28	27	32	29	819.54	0.0001639	75.7084
2	5	2000	1.0989	1	89	83	86	86	2430.36	0.0002430	72.2879
3	5	3000	1.465	1.5	127	125	132	128	3617.28	0.0002412	72.3525
4	5	4000	1.832	2	161	156	160	159	4493.34	0.0002247	72.9679
5	10	1000	1.0989	1.5	69	67	56	64	1808.64	0.0001809	74.8512
6	10	2000	0.733	2	136	135	137	136	3843.36	0.0001922	74.3249
7	10	3000	1.832	0.5	371	378	367	372	10512.72	0.0003504	69.1087
8	10	4000	1.465	1	535	529	520	528	14921.28	0.0003730	68.5658
9	15	1000	1.465	2	87	89	79	85	2402.1	0.0001601	75.9122
10	15	2000	1.832	1.5	285	287	289	287	8110.62	0.0002704	71.3599
11	15	3000	0.733	1	522	528	510	520	14695.2	0.0003266	69.7197
12	15	4000	1.0989	0.5	929	938	935	934	26394.84	0.0004399	67.1329
13	20	1000	1.832	1	169	164	159	164	4634.64	0.0002317	72.7015
14	20	2000	1.465	0.5	533	527	524	528	14921.28	0.0003730	68.5658
15	20	3000	1.0989	2	556	555	557	556	15712.56	0.0002619	71.6373
16	20	4000	0.733	1.5	1110	1109	1096	1105	31227.3	0.0003903	68.1720

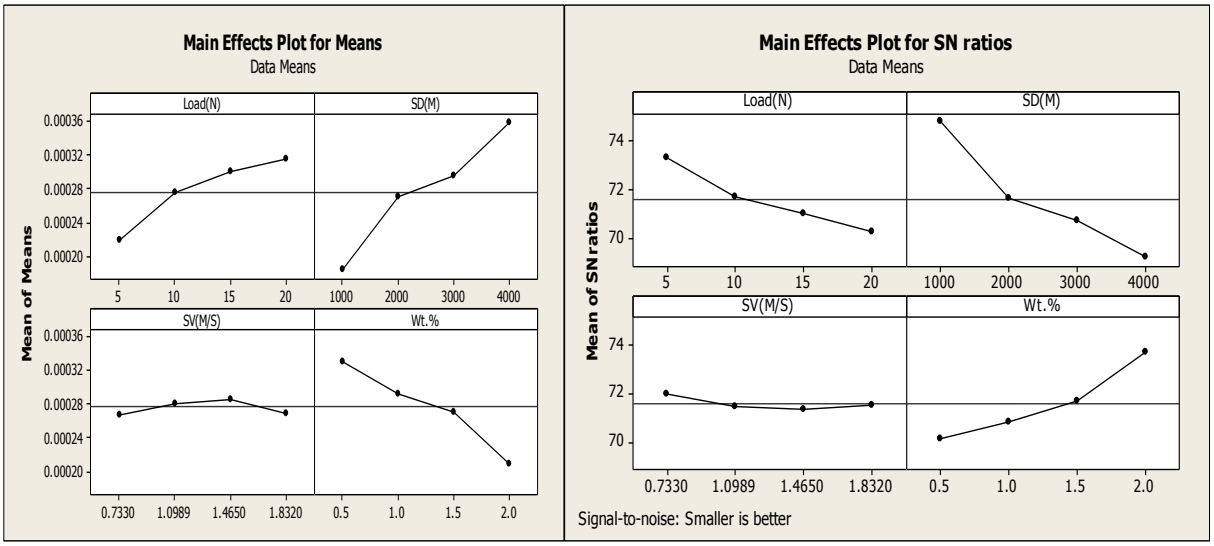

Figure A4 Influence of Process Parameters on SWR (Experimental &S/N data)

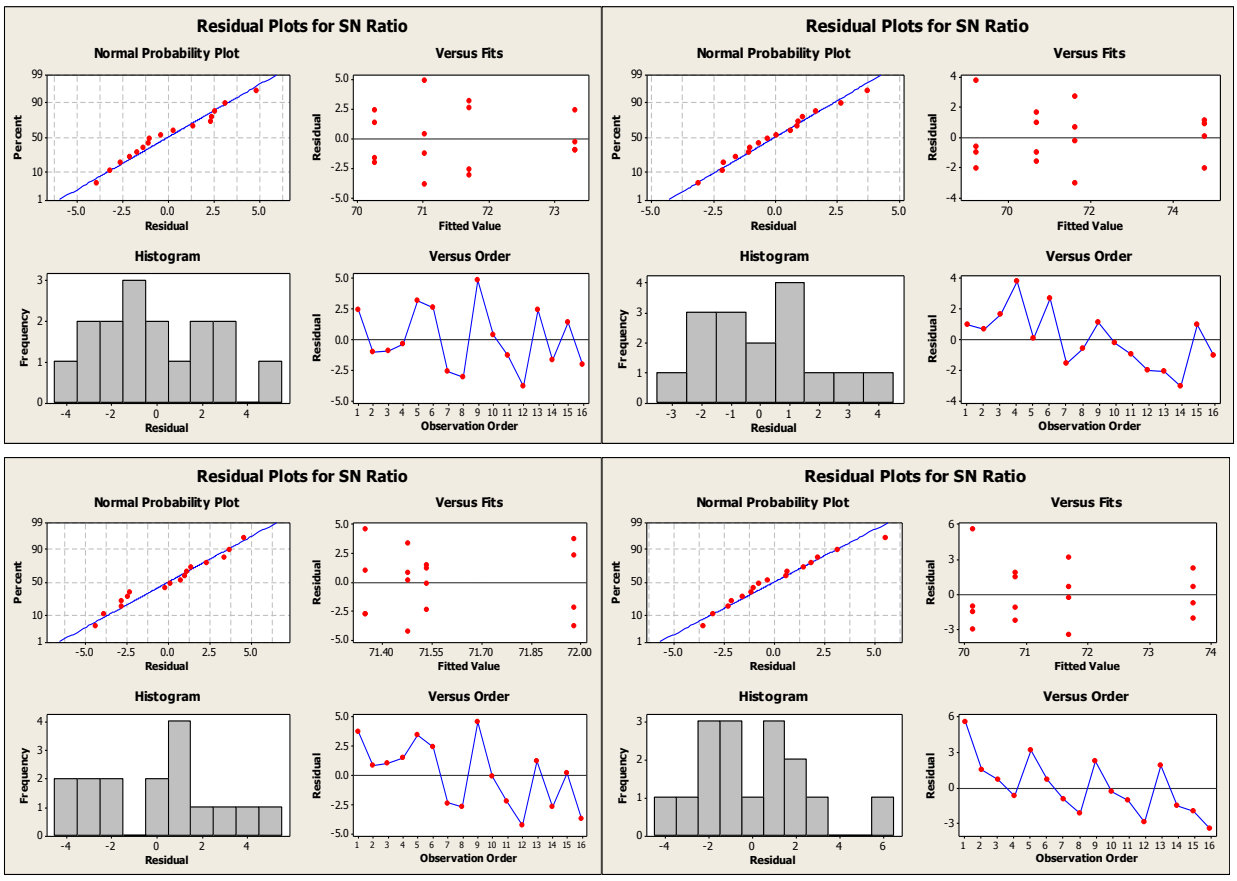

Figure A14 Residual plots for SN Ratios Vs SD,Load,SV and Wt.%

Selection of optimal levels for SWR using MMNC AA 2014/Al_2O_3 /50 nm

S = 0.375346 R-Sq = 99.64% R-Sq (adj) = 98.20%

Table A38 Analysis of Variance (ANOVA) for SWR (S/N Data)

Analysis of Variance for SN Ratios							
Source	DF	Seq SS	Adj SS	Adj MS	F	p	% of Contribution
Load(N)	3	20.3865	20.3865	6.7955	48.23	0.005	
SD(M)	3	66.8528	66.8528	22.2843	158.17	0.001	
SV(M/S)	3	0.9073	0.9073	0.3024	2.15	0.273	
Wt.%	3	28.9404	28.9404	9.6468	68.47	0.003	
Error	3	0.4227	0.4227	0.1409			
Total	15	117.5096					

S = 0.0152331 R-Sq = 99.40% R-Sq (adj) = 97.00%

Table A39 Analysis of Variance for SWR (Experimental Data)

Analysis of Variance for Means						
Source	DF	Seq SS	Adj SS	Adj MS	F	P
Load(N)	3	0.021381	0.021381	0.007127	30.71	0.009
SD(M)	3	0.061579	0.061579	0.020526	88.46	0.002
SV(M/S)	3	0.001003	0.001003	0.000334	1.44	0.386
Wt.%	3	0.031369	0.031369	0.010456	45.06	0.005
Residual Error	3	0.000696	0.000696	0.000232		
Total	15	0.116028				
DF - degrees of freedom, SS - sum of squares, MS - mean squares(Variance), F-ratio of variance of a source to variance of error, P < 0.05 - determines significance of a parameter at 95% confidence level						

Table A40 Response Table for SWR (Experimental Data)

Response table for Means				
Level	Load	SD	SV	Wt.%
1	0.000218	0.000184	0.000268	**0.000332**
2	0.000274	0.00027	0.000281	0.000294
3	0.000299	0.000295	**0.000287**	0.000271
4	**0.000314**	**0.000357**	0.000269	0.00021
Delta	0.000096	0.000173	0.000019	0.000122
Rank	3	1	4	2

The Optimal and Predicted Values for AA 2014/Al_2O_3 /50 nm

Table A41 The optimal and predicted values for MMNCs AA 2014/Al_2O_3 /50 nm

Output Response	Optimal set of parameters	Predicted optimal value	Predicted Confidence Interval at 95% confidence Level	Experimental Value (average of three confirmation experiments)
SWR	L4-SD4-SV3-Wt.% 1	**0.0004629**	0.0004353<η_{SWR}>0.0004873	**0.0004399**

Optimization by using GRA for MMNC AA2014/Al_2O_3 /50 nm

Table A42 Orthogonal Array and Experimental Results Using MMNC AA 2014/Al_2O_3 /50 nm

S. No	L	SD	SV	Wt. %	Response (Raw data)			Average WH (μm)	VOW (mm^3) 10e-3	SWR (mm^3/Nm)	S/N Ratio
					WH1 (μm)	WH2 (μm)	WH3 (μm)				
1	5	1000	0.733	0.5	28	27	32	29	819.54	0.0001639	75.7084
2	5	2000	1.0989	1	89	83	86	86	2430.36	0.0002430	72.2879
3	5	3000	1.465	1.5	127	125	132	128	3617.28	0.0002412	72.3525
4	5	4000	1.832	2	161	156	160	159	4493.34	0.0002247	72.9679
5	10	1000	1.0989	1.5	69	67	56	64	1808.64	0.0001809	74.8512
6	10	2000	0.733	2	136	135	137	136	3843.36	0.0001922	74.3249
7	10	3000	1.832	0.5	371	378	367	372	10512.72	0.0003504	69.1087
8	10	4000	1.465	1	535	529	520	528	14921.28	0.0003730	68.5658
9	15	1000	1.465	2	87	89	79	85	2402.1	0.0001601	75.9122

10	15	2000	1.832	1.5	285	287	289	287	8110.62	0.0002704	71.3599
11	15	3000	0.733	1	522	528	510	520	14695.2	0.0003266	69.7197
12	15	4000	1.0989	0.5	929	938	935	934	26394.84	0.0004399	67.1329
13	20	1000	1.832	1	169	164	159	164	4634.64	0.0002317	72.7015
14	20	2000	1.465	0.5	533	527	524	528	14921.28	0.0003730	68.5658
15	20	3000	1.0989	2	556	555	557	556	15712.56	0.0002619	71.6373
16	20	4000	0.733	1.5	1110	1109	1096	1105	31227.3	0.0003903	68.1720

Optimization Steps using Grey Relational Analysis for MMNC AA 2014/Al_2O_3 /50 nm:

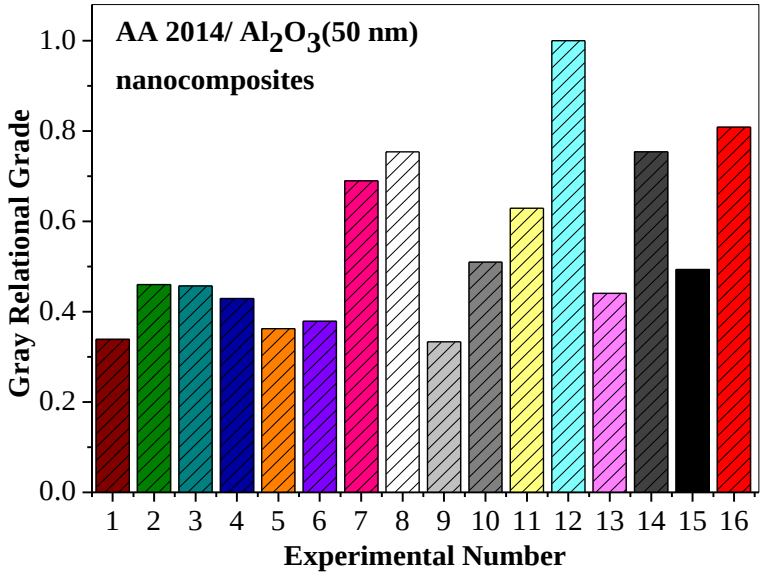

Figure A15 Gray relational grade plot of AA 2014 /Al_2O_3 (50 nm) composites

Table A43 Gray relational grade

S.No	L	SD	SV	Wt. %	SWR (mm^3/N-m)	S/N Ratio	Normalized S/N Ratio	Δ_{oj}	γ(GRC)	$\overline{\gamma_j}$
1	5	1000	0.733	0.5	0.0001639	75.7084	0.0232	0.9768	0.3386	0.3386
2	5	2000	1.0989	1	0.0002430	72.2879	0.4128	0.5872	0.4599	0.4599
3	5	3000	1.465	1.5	0.0002412	72.3525	0.4055	0.5945	0.4568	0.4568
4	5	4000	1.832	2	0.0002247	72.9679	0.3354	0.6646	0.4293	0.4293
5	10	1000	1.0989	1.5	0.0001809	74.8512	0.1209	0.8791	0.3626	0.3626
6	10	2000	0.733	2	0.0001922	74.3249	0.1808	0.8192	0.3790	0.3790
7	10	3000	1.832	0.5	0.0003504	69.1087	0.7749	0.2251	0.6896	0.6896
8	10	4000	1.465	1	0.0003730	68.5658	0.8368	0.1632	0.7539	0.7539
9	15	1000	1.465	2	0.0001601	75.9122	0	1	0.3333	0.3333
10	15	2000	1.832	1.5	0.0002704	71.3599	0.5185	0.4815	0.5094	0.5094

11	15	3000	0.733	1	0.0003266	69.7197	0.7054	0.2946	0.6292	0.6292
12	15	4000	1.0989	0.5	0.0004399	67.1329	1	0	1	1
13	20	1000	1.832	1	0.0002317	72.7015	0.3657	0.6343	0.4408	0.4408
14	20	2000	1.465	0.5	0.0003730	68.5658	0.8368	0.1632	0.7539	0.7539
15	20	3000	1.0989	2	0.0002619	71.6373	0.4869	0.5131	0.4935	0.4935
16	20	4000	0.733	1.5	0.0003903	68.1720	0.8816	0.1184	0.8085	0.8085

Table A44 Average gray relational grade

Input factors	Level 1	Level 2	Level 3	Level 4	Max-Min	rank
Load	0.4212	0.5463	0.6180	**0.6242**	0.2030	3
SD	0.3688	0.5256	0.5673	**0.7479**	0.3791	1
SV	0.5388	**0.5790**	0.5745	0.5173	0.0617	4
Wt%	**0.6955**	0.5710	0.5343	0.4088	0.2867	2

General Regression Analysis:

Regression Equation

SWR = 0.000156487 + 6.264e-006 Load (N) + 5.4385e-008 SD (M) + 2.32071e-006 SV (M/S) - 7.782e-005 Wt. %.

Table A45 The optimal and predicted values for MMNC AA 2014/Al_2O_3 /50 nm

Response	Optimal Solution of process parameters	Experimental value	Predicted value	% Error
Specific Wear Rate	L4-SD4-SV3-Wt. %1	**0.0004399**	**0.0004629**	**4.97**

F) Specific Wear Rate of AA2014/SiCp/150 nm composite:

Table A46 Wear results for MMNC AA2014/SiCp/150 nm:

S. No	L	SD	SV	Wt. %	Response (Raw data)			Average WH(μm)	VOW (mm^3) 10e-3	SWR (mm^3/Nm)	S/N Ratio
					WH1 (μm)	WH2 (μm)	WH3 (μm)				
1	5	1000	0.733	0.5	36	35	40	37	1045.62	0.0002091	73.5929
2	5	2000	1.0989	1	110	105	109	108	3052.08	0.0003052	70.3083
3	5	3000	1.465	1.5	143	150	145	146	4125.96	0.0002751	71.2102
4	5	4000	1.832	2	187	180	176	181	5115.06	0.0002558	71.8420
5	10	1000	1.0989	1.5	82	76	76	78	2204.28	0.0002204	73.1358
6	10	2000	0.733	2	157	160	160	159	4493.34	0.0002247	72.9679
7	10	3000	1.832	0.5	476	469	471	472	13338.72	0.0004446	67.0406

8	10	4000	1.465	1	673	678	677	676	19103.76	0.0004776	66.4187
9	15	1000	1.465	2	100	97	94	97	2741.22	0.0001827	74.7652
10	15	2000	1.832	1.5	331	338	336	335	9467.1	0.0003156	70.0173
11	15	3000	0.733	1	663	669	648	660	18651.6	0.0004145	67.6495
12	15	4000	1.0989	0.5	1199	1189	1188	1192	33685.92	0.0005614	65.0146
13	20	1000	1.832	1	207	211	200	206	5821.56	0.0002911	70.7192
14	20	2000	1.465	0.5	682	679	667	676	19103.76	0.0004776	66.4187
15	20	3000	1.0989	2	649	639	638	642	18142.92	0.0003024	70.3884
16	20	4000	0.733	1.5	1299	1293	1296	1296	36624.96	0.0004578	66.7865

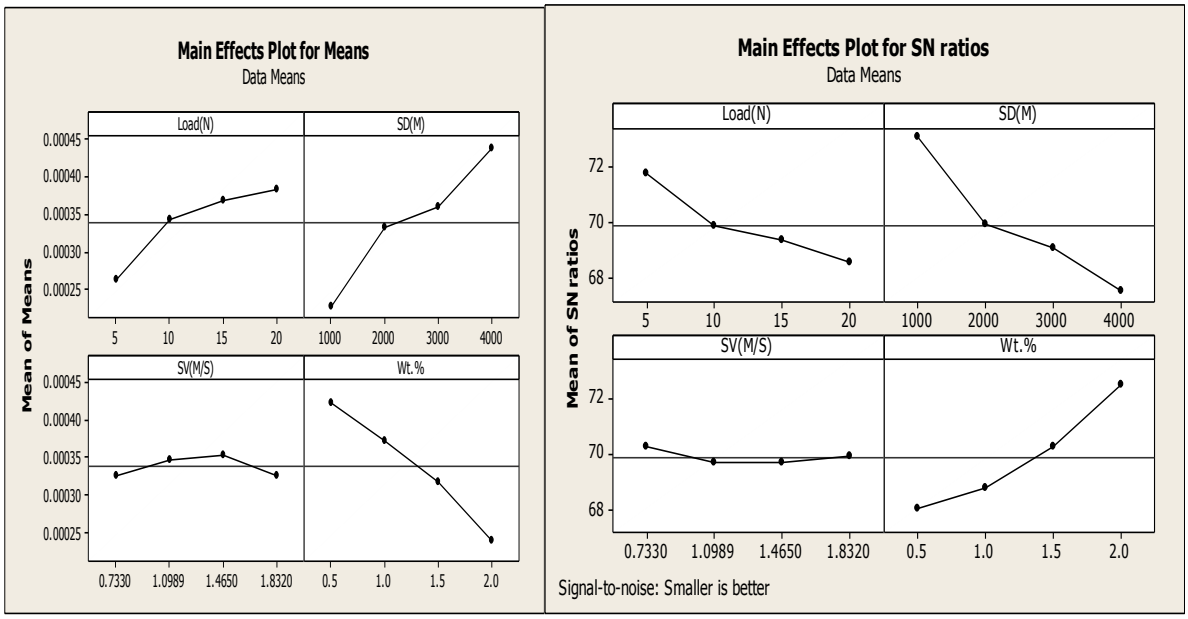

Figure A16 Influence of Process Parameters on SWR (Experimental &S/N data)

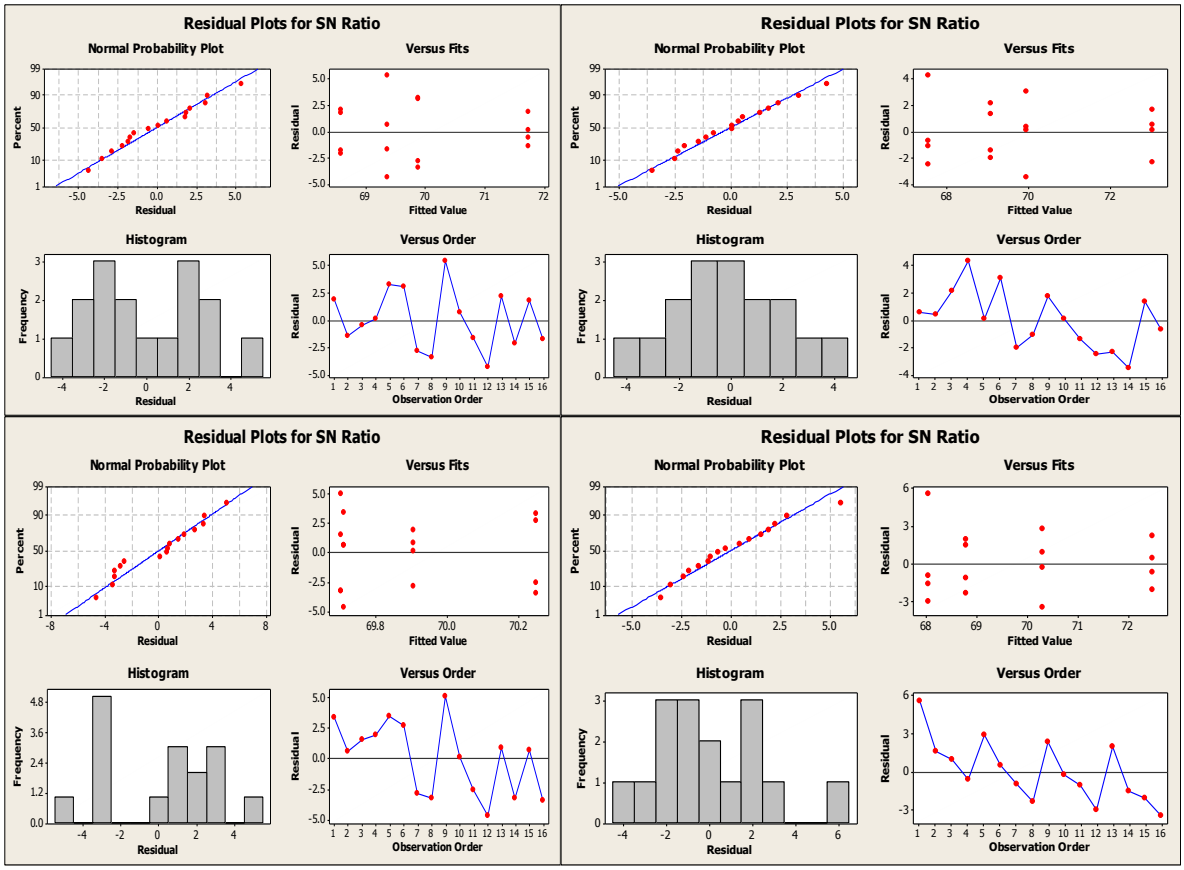

Figure A17 Residual plots for SN Ratios Vs SD,Load, SV and Wt.%

Selection of optimal levels for SWR using MMNC AA2014/SiCp/150 nm

S = 0.360248 R-Sq = 99.71% R-Sq (adj) = 98.56%

Table A47 Analysis of Variance (ANOVA) for SWR (S/N Data)

Analysis of Variance for SN Ratios							
Source	DF	Seq SS	Adj SS	Adj MS	F	p	% of Contribution
Load(N)	3	21.666	21.666	7.222	55.65	0.004	
SD(M)	3	65.26	65.26	21.753	167.62	0.001	
SV(M/S)	3	0.784	0.784	0.261	2.01	0.29	
Wt.%	3	46.71	46.71	15.57	119.97	0.001	
Error	3	0.389	0.389	0.13			
Total	15	134.809					

Table A48 Analysis of Variance for SWR (Experimental Data)

Analysis of Variance for Means						
Source	DF	Seq SS	Adj SS	Adj MS	F	P
Load(N)	3	0.035143*10e-6	0.035143	0.011714	35.54	0.008
SD(M)	3	0.092447	0.092447	0.030816	93.49	0.002
SV(M/S)	3	0.002307	0.002307	0.000769	2.33	0.252
Wt.%	3	0.072719	0.072719	0.02424	73.54	0.003
Residual Error	3	0.000989	0.000989	0.00033		
Total	15	0.203606				
DF - degrees of freedom, SS - sum of squares, MS - mean squares(Variance), F-ratio of variance of a source to variance of error, P < 0.05 - determines significance of a parameter at 95% confidence level						

Table A49 Response Table for SWR (Experimental Data)

Response table for Means				
Level	Load	SD	SV	Wt.%
1	0.000261	0.000226	0.000327	**0.000423**
2	0.000342	0.000331	0.000347	0.000372
3	0.000369	0.000359	**0.000353**	0.000317
4	**0.000382**	**0.000438**	0.000327	0.000241
Delta	0.000121	0.000212	0.000027	0.000182
Rank	3	1	4	2

The Optimal and Predicted Values for AA2014/SiCp/150 nm

Table A50 The optimal and predicted values for MMNC's AA 2014/SiCp/150 nm using Taguchi analysis

Output Response	Optimal set of parameters	Predicted optimal value	Predicted Confidence Interval at 95% confidence Level	Experimental Value (average of three confirmation experiments)
SWR	L4-SD4-SV3-Wt.%1	**0.0005581**	$0.0005504<\eta_{SWR}>0.0006106$	**0.0005614**

Optimization by using GRA for MMNC AA2014/SiCp /150 nm

Table A51 Orthogonal Array and Experimental Results Using MMNC AA2014/SiCp/150 nm

S. No	L	SD	SV	Wt. %	Response (Raw data)			Average WH(μm)	VOW (mm^3) 10e-3	SWR (mm^3/N-m)	S/N Ratio
					WH1 (μm)	WH2 (μm)	WH3 (μm)				
1	5	1000	0.733	0.5	36	35	40	37	1045.62	0.0002091	73.5929
2	5	2000	1.0989	1	110	105	109	108	3052.08	0.0003052	70.3083
3	5	3000	1.465	1.5	143	150	145	146	4125.96	0.0002751	71.2102
4	5	4000	1.832	2	187	180	176	181	5115.06	0.0002558	71.8420
5	10	1000	1.0989	1.5	82	76	76	78	2204.28	0.0002204	73.1358
6	10	2000	0.733	2	157	160	160	159	4493.34	0.0002247	72.9679
7	10	3000	1.832	0.5	476	469	471	472	13338.72	0.0004446	67.0406
8	10	4000	1.465	1	673	678	677	676	19103.76	0.0004776	66.4187
9	15	1000	1.465	2	100	97	94	97	2741.22	0.0001827	74.7652
10	15	2000	1.832	1.5	331	338	336	335	9467.1	0.0003156	70.0173
11	15	3000	0.733	1	663	669	648	660	18651.6	0.0004145	67.6495
12	15	4000	1.0989	0.5	1199	1189	1188	1192	33685.92	0.0005614	65.0146
13	20	1000	1.832	1	207	211	200	206	5821.56	0.0002911	70.7192
14	20	2000	1.465	0.5	682	679	667	676	19103.76	0.0004776	66.4187
15	20	3000	1.0989	2	649	639	638	642	18142.92	0.0003024	70.3884
16	20	4000	0.733	1.5	1299	1293	1296	1296	36624.96	0.0004578	66.7865

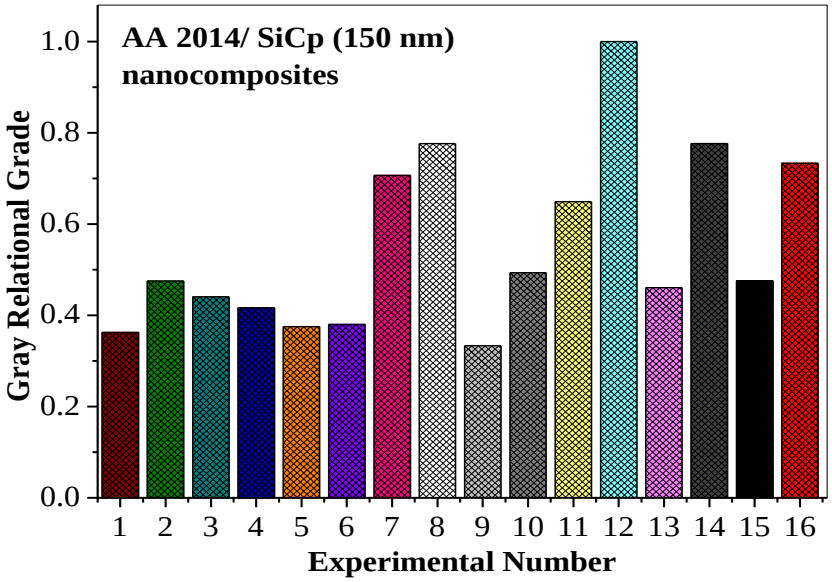

Figure A18 Gray relational grade plot of AA2014/SiCp/150 nm composites

Optimization Steps using Grey Relational Analysis for MMNC AA2014/SiCp/150 nm:

Table A52 Gray relational grade

S.No	L	SD	SV	Wt. %	SWR (mm^3/N-m)	S/N Ratio	Normalized S/N Ratio	Δ_{oj}	γ(GRC)	$\overline{\gamma_j}$
1	5	1000	0.733	0.5	0.0002091	73.5929	0.1202	0.8798	0.3624	0.3624
2	5	2000	1.0989	1	0.0003052	70.3083	0.4571	0.5429	0.4749	0.4749
3	5	3000	1.465	1.5	0.0002751	71.2102	0.3646	0.6354	0.4404	0.4404
4	5	4000	1.832	2	0.0002558	71.8420	0.2998	0.7002	0.4166	0.4166
5	10	1000	1.0989	1.5	0.0002204	73.1358	0.1671	0.8329	0.3751	0.3751
6	10	2000	0.733	2	0.0002247	72.9679	0.1843	0.8157	0.3800	0.3800
7	10	3000	1.832	0.5	0.0004446	67.0406	0.7922	0.2078	0.7064	0.7064
8	10	4000	1.465	1	0.0004776	66.4187	0.8559	0.1441	0.7763	0.7763
9	15	1000	1.465	2	0.0001827	74.7652	0	1	0.3333	0.3333
10	15	2000	1.832	1.5	0.0003156	70.0173	0.4869	0.5131	0.4935	0.4935
11	15	3000	0.733	1	0.0004145	67.6495	0.7298	0.2702	0.6491	0.6491
12	15	4000	1.0989	0.5	0.0005614	65.0146	1	0	1	1
13	20	1000	1.832	1	0.0002911	70.7192	0.4149	0.5851	0.4609	0.4609
14	20	2000	1.465	0.5	0.0004776	66.4187	0.8559	0.1441	0.7763	0.7763
15	20	3000	1.0989	2	0.0003024	70.3884	0.4489	0.5511	0.4757	0.4757
16	20	4000	0.733	1.5	0.0004578	66.7865	0.8183	0.1817	0.7335	0.7335

Table A53 Average gray relational grade

Input factors	Level 1	Level 2	Level 3	Level 4	Max-Min	rank
Load	0.4236	0.5595	0.6116	**0.6190**	0.1954	3
SD	0.3829	0.5312	0.5679	**0.7316**	0.3487	1
SV	0.5313	0.5814	**0.5816**	0.5194	0.0622	4
Wt%	**0.7113**	0.5903	0.5106	0.4014	0.3099	2

General Regression Analysis:

Regression Equation

SWR = 0.000222511 + 7.79e-006 Load (N) + 6.6535e-008 SD (M) + 1.7951e-006 SV (M/S) - 0.00012004 Wt. %.

Table A54 The optimal and predicted values for MMNC AA2014/SiCp/150 nm

Response	Optimal Solution of process parameters	Experimental value	Predicted value	% Error
Specific Wear Rate	L4-SD4-SV3-Wt. %1	0.0005614	0.0005481	0.59

G) Specific Wear Rate of AA2014/Al_2O_3/150 nm composite:

Table A55 Wear results for MMNC AA 2014/Al_2O_3/150 nm

S. No	L	SD	SV	Wt. %	Response (Raw data)			Average WH (μm)	VOW (mm^3) 10e-3	SWR (mm^3/Nm)	S/N Ratio
					WH1 (μm)	WH2 (μm)	WH3 (μm)				
1	5	1000	0.733	0.5	51	56	52	53	1497.78	0.0002996	70.4692
2	5	2000	1.0989	1	139	143	153	145	4097.7	0.0004098	67.7486
3	5	3000	1.465	1.5	222	226	236	228	6443.28	0.0004296	67.3387
4	5	4000	1.832	2	310	307	298	305	8619.3	0.0004309	67.3125
5	10	1000	1.0989	1.5	120	120	117	119	3362.94	0.0003363	69.4655
6	10	2000	0.733	2	272	270	271	271	7658.46	0.0003829	68.3383
7	10	3000	1.832	0.5	670	673	679	674	19047.24	0.0006349	63.9459
8	10	4000	1.465	1	929	936	934	933	26366.58	0.0006592	63.6197
9	15	1000	1.465	2	157	159	158	158	4465.08	0.0002977	70.5244
10	15	2000	1.832	1.5	524	530	527	527	14893.02	0.0004964	66.0834
11	15	3000	0.733	1	925	919	919	921	26027.46	0.0005784	64.7554
12	15	4000	1.0989	0.5	1701	1699	1712	1704	48155.04	0.0008026	61.9100

13	20	1000	1.832	1	280	285	284	283	7997.58	0.0003999	67.9610
14	20	2000	1.465	0.5	963	960	963	962	27186.12	0.0006796	63.3549
15	20	3000	1.0989	2	1099	1093	1096	1096	30972.96	0.0005162	65.7436
16	20	4000	0.733	1.5	2069	2070	2062	2067	58413.42	0.0007302	62.7312

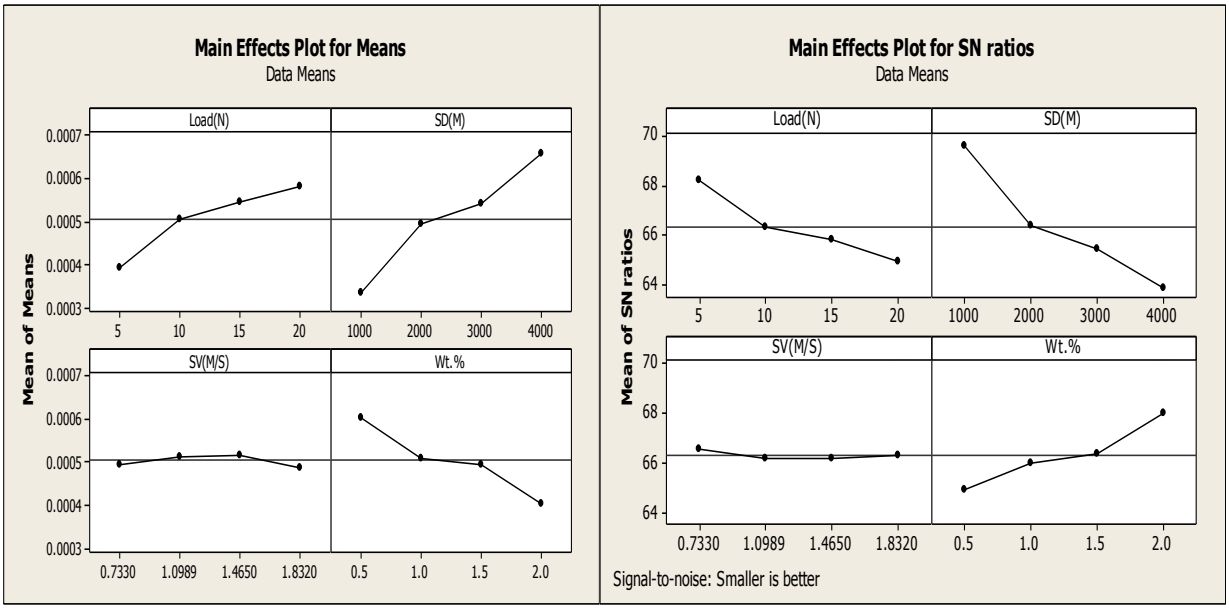

Figure A19 Influence of Process Parameters on SWR (Experimental &S/N data)

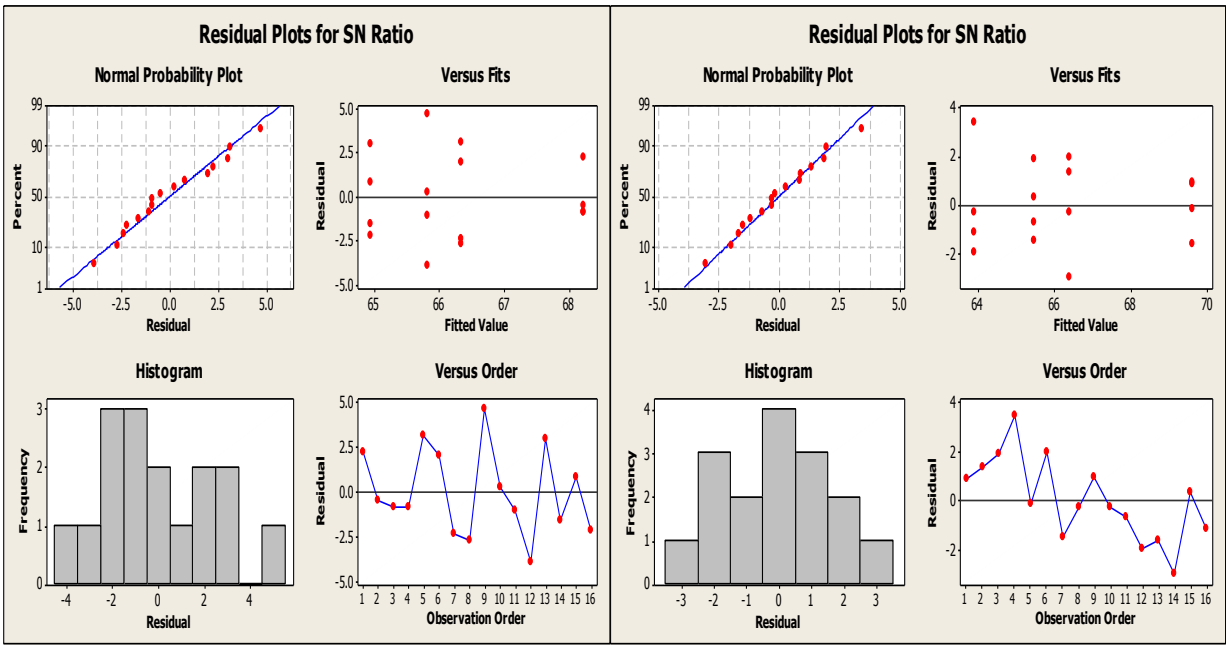

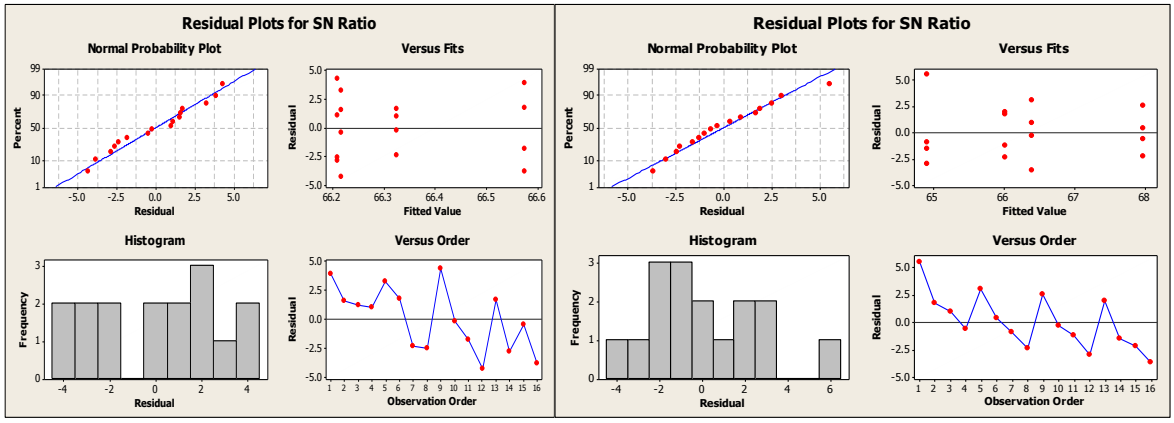

Figure A20 Residual plots for SN Ratios Vs SD,Load,SV and Wt.%

Selection of optimal levels for SWR using MMNC AA 2014/Al_2O_3/150 nm

S = 0.375346 R-Sq = 99.64% R-Sq (adj) = 98.20%

Table A56 Analysis of Variance (ANOVA) for SWR (S/N Data)

Analysis of Variance for SN Ratios							
Source	DF	Seq SS	Adj SS	Adj MS	F	p	% of Contribution
Load(N)	3	20.3865	20.3865	6.7955	48.23	0.005	
SD(M)	3	66.8528	66.8528	22.2843	158.17	0.001	
SV(M/S)	3	0.9073	0.9073	0.3024	2.15	0.273	
Wt.%	3	28.9404	28.9404	9.6468	68.47	0.003	
Error	3	0.4227	0.4227	0.1409			
Total	15	117.5096					

S = 0.0152331 R-Sq = 99.40% R-Sq (adj) = 97.00%

Table A57 Analysis of Variance for SWR (Experimental Data)

Analysis of Variance for Means						
Source	DF	Seq SS	Adj SS	Adj MS	F	P
Load(N)	3	0.021381	0.021381	0.007127	30.71	0.009
SD(M)	3	0.061579	0.061579	0.020526	88.46	0.002
SV(M/S)	3	0.001003	0.001003	0.000334	1.44	0.386

Wt.%	3	0.031369	0.031369	0.010456	45.06	0.005
Residual Error	3	0.000696	0.000696	0.000232		
Total	15	0.116028				

DF - degrees of freedom, SS - sum of squares, MS - mean squares(Variance), F-ratio of variance of a source to variance of error, P < 0.05 - determines significance of a parameter at 95% confidence level

Table A58 Response Table for SWR (Experimental Data)

Response table for Means				
Level	Load	SD	SV	Wt.%
1	0.000218	0.000184	0.000268	**0.000332**
2	0.000274	0.00027	0.000281	0.000294
3	0.000299	0.000295	**0.000287**	0.000271
4	**0.000314**	**0.000357**	0.000269	0.00021
Delta	0.000096	0.000173	0.000019	0.000122
Rank	3	1	4	2

The Optimal and Predicted Values for AA 2014/Al_2O_3/150 nm

Table A59 The optimal and predicted values for MMNC AA 2014/Al_2O_3/150 nm

Output Response	Optimal set of parameters	Predicted optimal value	Predicted Confidence Interval at 95% Confidence Level	Experimental Value (average of three confirmation experiments)
SWR	L4-SD4-SV3-Wt.% 1	**0.0004629**	$0.0004353<\eta_{SWR}>0.0004873$	**0.0004399**

Optimization by using GRA for MMNC AA2014/SiCp /50 nm

Optimization Steps using Grey Relational Analysis for MMNC AA 2014/Al_2O_3/150 nm:

Table A60 Orthogonal Array and Experimental Results Using MMNCAA 2014/Al_2O_3/150 nm

S.No	L	SD	SV	Wt. %	Response (Raw data)			Average WH(µm)	VOW (mm^3) 10e-3	SWR (mm^3/Nm)	S/N Ratio
					WH1 (µm)	WH 2 (µm)	WH3 (µm)				
1	5	1000	0.733	0.5	51	56	52	53	1497.78	0.0002996	70.4692
2	5	2000	1.0989	1	139	143	153	145	4097.7	0.0004098	67.7486
3	5	3000	1.465	1.5	222	226	236	228	6443.28	0.0004296	67.3387
4	5	4000	1.832	2	310	307	298	305	8619.3	0.0004309	67.3125
5	10	1000	1.0989	1.5	120	120	117	119	3362.94	0.0003363	69.4655
6	10	2000	0.733	2	272	270	271	271	7658.46	0.0003829	68.3383
7	10	3000	1.832	0.5	670	673	679	674	19047.24	0.0006349	63.9459
8	10	4000	1.465	1	929	936	934	933	26366.58	0.0006592	63.6197
9	15	1000	1.465	2	157	159	158	158	4465.08	0.0002977	70.5244
10	15	2000	1.832	1.5	524	530	527	527	14893.02	0.0004964	66.0834
11	15	3000	0.733	1	925	919	919	921	26027.46	0.0005784	64.7554
12	15	4000	1.0989	0.5	1701	1699	1712	1704	48155.04	0.0008026	61.9100
13	20	1000	1.832	1	280	285	284	283	7997.58	0.0003999	67.9610
14	20	2000	1.465	0.5	963	960	963	962	27186.12	0.0006796	63.3549
15	20	3000	1.0989	2	1099	1093	1096	1096	30972.96	0.0005162	65.7436
16	20	4000	0.733	1.5	2069	2070	2062	2067	58413.42	0.0007302	62.7312

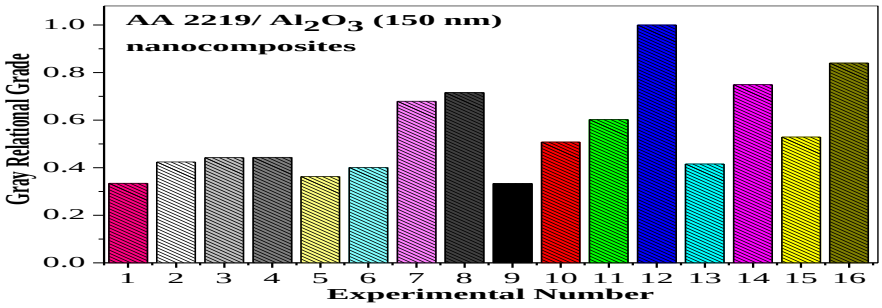

Figure A21 Gray relational grade plot of AA 2014/Al_2O_3/150 nm composites

Table A61 Gray relational grade

S.No	L	SD	SV	Wt. %	SWR (mm^3/Nm)	S/N Ratio	Normalized S/N Ratio	Δ_{oj}	γ(GRC)	$\overline{\gamma_j}$
1	5	1000	0.733	0.5	0.0002996	70.4692	0.0064	0.9936	0.3348	0.3348

2	5	2000	1.0989	1	0.0004098	67.7486	0.3222	0.6778	0.4245	0.4245
3	5	3000	1.465	1.5	0.0004296	67.3387	0.3698	0.6302	0.4424	0.4424
4	5	4000	1.832	2	0.0004309	67.3125	0.3729	0.6271	0.4436	0.4436
5	10	1000	1.0989	1.5	0.0003363	69.4655	0.1229	0.8771	0.3631	0.3631
6	10	2000	0.733	2	0.0003829	68.3383	0.2538	0.7462	0.4012	0.4012
7	10	3000	1.832	0.5	0.0006349	63.9459	0.7637	0.2363	0.6791	0.6791
8	10	4000	1.465	1	0.0006592	63.6197	0.8015	0.1985	0.7158	0.7158
9	15	1000	1.465	2	0.0002977	70.5244	0	1	0.3333	0.3333
10	15	2000	1.832	1.5	0.0004964	66.0834	0.5155	0.4845	0.5079	0.5079
11	15	3000	0.733	1	0.0005784	64.7554	0.6697	0.3303	0.6022	0.6022
12	15	4000	1.0989	0.5	0.0008026	61.9100	1	0	1	1
13	20	1000	1.832	1	0.0003999	67.9610	0.2976	0.7024	0.4158	0.4158
14	20	2000	1.465	0.5	0.0006796	63.3549	0.8323	0.1677	0.7488	0.7488
15	20	3000	1.0989	2	0.0005162	65.7436	0.5550	0.4450	0.5291	0.5291
16	20	4000	0.733	1.5	0.0007302	62.7312	0.9047	0.0953	0.8399	0.8399

Table A62 Average gray relational grade

Input factors	Level 1	Level 2	Level 3	Level 4	Max-Min	rank
Load	0.4113	0.5398	0.6109	**0.6334**	0.2221	3
SD	0.3618	0.5206	0.5632	**0.7498**	0.3880	1
SV	0.5445	**0.5792**	0.5332	0.5116	0.0676	4
Wt. %	**0.6907**	0.5396	0.5383	0.4268	0.2639	2

General Regression Analysis:

Regression Equation

SWR = 0.000258632 + 1.2149e-005 Load (N) + 1.01465e-007 SD (M) - 5.87434e-006 SV (M/S) - 0.00012109 Wt. %.

Table A63 The optimal and predicted values for MMNC AA 2014/Al_2O_3/150 nm using Gray relational analysis

Response	Optimal Solution of process parameters	Experimental value	Predicted value	% Error
Specific Wear Rate	L4-SD4-SV3-Wt.%1	**0.0008026**	**0.0008405**	**4.51**

REFERENCES

1. E. Basiri Tochaee, H. R. Madaah Hosseini, S. M. Seye Reihani, "Fabrication of high strength in-situ Al-Al_3Ti nanocomposite by mechanical alloying and hot extrusion: Investigation of fracture toughness**",** Materials Science and Engineering A 658 (2016) 246-254.
2. Cunguang Chen, Leichen Guo, Ji Luo, Junjie Hao, Zhimeng Guo, Alex A. Volinsky, "Aluminum powder size and microstructure effects on properties of boron nitride reinforced aluminum matrix composites fabricated by semi-solid powder metallurgy", Materials Science and Engineering A, 646 (2015) 306-314.
3. O. Kavian Cooke, I. Tahir Khan, D. Gossett Oliver, "Transient liquid phase diffusion bonding Al-6061 using nano-dispersed Ni coatings", Materials & Design, 33 (2012) 469-475.
4. D.J. Woo, F.C. Heer, L.N. Brewer, J.P. Hooper, " Synthesis of nano diamond-reinforced aluminum metal matrix composites using cold-spray deposition", Corban, 86 (2015) 15–25.
5. S. Pradeep Devaneyan, T. Senthilvelan, "Electro Co-deposition and Characterization of SiC in Nickel Metal Matrix Composite Coatings on Aluminium 7075", Procedia Engineering, 97 (2014) 1496-1505.
6. Adnan Maqbool, F. Ahmad Khalid, M. Asif Hussain, Nabi Bakhsh, "Synthesis of copper coated carbon nanotubes for aluminium matrix composites" Materials Science and Engineering, 60 (2014) 012040.
7. H.G. Prashantha Kumar, M. Anthony Xavior, "Graphene Reinforced Metal Matrix Composite (GRMMC): A Review", Procedia Engineering, 97 (2014) 1033-1040.
8. K. Dash , D. Chaira, B.C. Ray, "Synthesis and characterization of aluminium–alumina micro- and nano-composites by spark plasma sintering", Materials Research Bulletin, 48 Issue 7 (2013) 2535–2542.
9. K. S. artin. Li, Ping Gao , Po-Lock Yue, Xijun Hu, "Synthesis of exfoliated CNT–metal–clay nanocomposite by chemical vapor deposition" Separation and Purification Technology, 67 Issue 2 (2009) 238–243.

10. Kalidindi Sita Rama Raju, Vegesna Ramachandra Raju, Penumetsa Rama Murty Raju, Siriyala Rajesh, Ghosal Partha, "Enhancement of the mechanical properties of an aluminum metal matrix nanocomposite by the hybridization technique", Journal of Materials Research and Technology, 5 Issue 3 (2016) 241–249.
11. Michael Oluwatosin Bodunrin , Kenneth Kanayo Alaneme, Lesley Heath Chown, "Aluminium matrix hybrid composites: a review of reinforcement philosophies; mechanical, corrosion and tribological characteristics", Journal of Materials Research and Technology, 4 Issue 4 (2015) 434–445.
12. Roger Jagdish Narayan, "Pulsed laser deposition of functionally gradient diamond like carbon–metal nanocomposites" Diamond and Related Materials**,** 14 Issue 8 (2005) 1319–1330.
13. M. Dhanashekar, V.S. Senthil Kumar, "Squeeze Casting of Aluminium Metal Matrix Composites-An Overview", Procedia Engineering, 97 (2014) 412-420
14. Tao Li, Lars Schulte, Ole Hansen, Sokol Ndoni, "Nanoporous gyroid TiO_2 and SnO_2 by melt infiltration of block copolymer templates", Microporous and Mesoporous Materials, 210 (2015) 161-168.
15. Y. Yang, J. Lan, XC Li, "Study on bulk aluminium matrix nano-composite fabricated by ultrasonic dispersion of nano-sized SiC particles in molten aluminium alloy", Mater Sci Eng A, 380 (2004) 373-378.
16. X. Jian, H. Xu, T. T. Meek, Q. Han, "Effect of power ultrasound on solidification of aluminium A356 alloy", Mater. Lett, 59 (2005) 190-193.
17. S. Mula, P. Padhi, SC Panigrahi, SK Pabi, S. Ghosh, "On structure and mechanical properties of ultrasonically cast Al-2% Al_2O_3 nanocomposite", Mater Res Bull, 44 (2009) 1154-1160.
18. JC Yan, ZW Xu, L. Shi, X. Ma, SQ Yang, "Ultrasonic assisted fabrication of particle reinforced bonds joining aluminium metal matrix composites", Mater Des, (2011) 343-347.
19. N. V. Murthy, A. P. Reddy, N. Selvaraj, C. S. P. Rao, "Aluminium Metal Matrix Nano Composites (Al-MMNC's)-Manufacturing Methods: A Review" International Journal of Mechanical Engineering, Vol.4 Issue 4 (2015) 29-44.

20. K. Dash, D. Chaira, B. C. Ray, "Synthesis and characterization of aluminium –alumina micro-and nano-composites by spark plasma sintering", Materials Research Bulletin, 48 (2013) 2535-2542.
21. Autar K. Kaw, Mechanics of Composite Materials‖, 2nd Edition, Taylor & Francis Group, (2006) pp 1-2.
22. A.A. Torrance, "The effect of grit size and asperity blunting on abrasive wear", Wear, 253 (2002) 813–819.
23. A. Alahelisten, F. Bergman, M. Olsson, S. Hogmark, "On the wear of aluminum and magnesium metal matrix composites", Wear 165 (1993) 221–226.
24. Abdulhaqq A. Hamid, P.K. Ghosh, S.C. Jain, Subrata Ray, "The influence of porosity and particles content on dry sliding wear of cast in situ Al (Ti)–Al_2O_3(TiO_2) composite", Wear, 265 (2008) 14-26.
25. Abdulhaqq A. Hamid, P.K. Ghosh, S.C. Jain, S. Ray, "Influence of particle content and porosity on the wear behavior of cast in situ Al (Mn)–Al_2O_3 (MnO_2) composite", Wear, 260 (2006) 368–378.
26. Abderrezak Bezazi, S. Gareth Pierce, Keith Worden, El Hadi Harkati, "Fatigue life prediction of sandwich composite materials under flexural tests using a Bayesian trained artificial neural network", International Journal of Fatigue, 29 (2007) 738–747.
27. A. B. Gurcan, T. N. Baker, "Wear behavior of AA6061 aluminum alloy and its composites", Wear, 188 (1995) 185-191.
28. A.K. Prasada Rao, K. Das, B.S. Murty, M. Chakraborty, "Microstructure and the wear mechanism of grain-refined aluminum during dry sliding against steel disc", Wear, 264 (2008) 638-647.
29. Alpas AT, Zhang J, "Effect of SiC particulate reinforcement on the dry sliding wear of aluminum–silicon alloys (A356)", Wear, 155 (1992) 83–104.
30. A.Martin, M.A.Martinez, J.LLorca, "Wear of SiC-reinforced Al-matrix composites in the temperature range 20-2000C", Wear, 193 (1996) 169-179.
31. A. Martin, J. Rodriguez, J. Llorca, "Temperature effects on the wear behavior of particulate reinforced Al-based composites", Wear, 225–229 (1999) 615–620.

32. A. Mandal, M. Chakraborty, B.S. Murty, "Effect of TiB_2 particles on sliding wear behaviour of Al–4Cu alloy", Wear, 262 (2007) 160–166.
33. A.P.Sannino, H.J.Rack, "Dry sliding wear of discontinuously reinforced aluminum composites: review and discussion", Wear, 189 (1995) 1-19.
34. A.Ravikiran, M.K.Surappa, "Effect of Sliding speed on wear behavior of A356 Al 30% SiC_P MMC", Wear, 206 (1997) 33-38.
35. A.R. Riahi, A.T. Alpas, "The role of tribo-layers on the sliding wear behavior of graphitic aluminum matrix composites", Wear, 251 (2001) 1396–1407.
36. Arjula Suresh, A.P. Harsha, M.K. Ghosh, "Solid particle erosion studies on polyphenylene sulfide composites and prediction on erosion data using artificial neural networks", Wear, 266 (2009) 184–193.
37. A.T. Alpas, J. Zhang, "Effect of microstructure (particulate size and volume fraction) and counterface material on the sliding wear resistance of particulate-reinforced aluminum matrix composites", Metall. Mater. Trans. A, 25 (1994) 969–983.
38. A.T.Alpas, S.Wilson, "Effect of temperature on the sliding wear performance of Al alloys and Al matrix composites", Wear, 196 (1996) 270-278.
39. A. Wang, H.J. Rack, "Dry sliding wear in 2124 Al–SiC_w/17-4 PH stainless steel systems", Wear, 147 (1991) 355–374.
40. S. Basavarajappa, G. Chandramohan, R. Subramanian, and Chandrasekar, "Dry sliding wear behavior of Al2219/SiC metal matrix", Materials Science-Poland, 24(2/1) (2006) 357-366.
41. W. Beitz and Kuttner, K. H. (Eds) Dubbel, "Handbook of Mechanical Engineering", Springer-Verlag, London, (1994) p. D8.
42. B.J. Li, C.G. Chao, "Mechanical properties and 95 ° aging characteristics of zircon reinforced Zn-4AI-3Cu alloy", Metall. Mater. Trans. A, 27A (1996) 809–818.
43. B.K. Prasad, "Investigation into sliding wear performance of zinc-based alloy reinforced with SiC particles in dry and lubricated conditions", Wear, 262 (2007) 262–273.
44. B.K. Prasad, O.P. Modi, A.K. Jha, "The effects of alumina fibers on the sliding wear of a cast aluminium alloy", Tribology International, 27 (1994) 153-158.

45. B. Venkataraman, G. Sundararajan, "Correlation between the characteristics of mechanically mixed layer and wear behaviour of aluminum, Al-7075 alloy and Al-MMCs", Wear, 245 (2000) 22–38.
46. Callister Jr. W. D., "Materials Science and Engineering: an introduction", New York, Wiley, (1999).
47. C. Perrin, W.M. Rainforth, "The effect of alumina fiber reinforcement on the wear of an Al-4.3% Cu alloy", Wear, 181–183 (1995) 312.
48. C.S. Ramesh, S.K. Seshadri, "Tribological characteristics of nickel composite coatings", Wear, 255 (2003) 893–902.
49. C.S. Ramesh, A.R. Anwar Khan, N. Ravikumar and P. Savanprabhu, "Prediction of Wear Coefficient of Al6061–TiO2 Composites", Wear, 259 (2005) 602–608.
50. C.S. Ramesh, R. Keshavamurthy, B.H. Channabasappa, Abrar Ahmed, "Microstructure and mechanical properties of Ni–P coated Si_3N_4 reinforced Al6061 composites", Materials Science and Engineering: A, 502 (2009) 99-106.
51. C. Subramanian, "Some considerations towards the design of a wear resistant aluminum alloy", Wear, 155 (1992) 193–205.
52. C. Z. Huang, L. Zhang, L. He, J. Sun, B. Fang, B. Zou, Z. Q. Li and X. Ai, "A study on the prediction of the mechanical properties of a ceramic tool based on an artificial neural network", Journal of Materials Processing Technology, 129 (2002) 399-402.
53. A. Daoud, M.T. Abou-Elkhair, P. Rohatgi, "Wear and friction behavior of near eutectic Al–Si+ZrO2 or WC Particle Composites", Comp Sci., and Tech., 64 (2004) 1029–1040.
54. Debdas Roy, Bikramjit Basu, Amitava Basu Mallick, "Tribological properties of Tialuminide reinforced Al-based in situ metal matrix composite", Intermetallics, 13 (2005) 733–740.
55. D.J. Lloyd, H. Lagace, A. McLeod, P. L. Morris, "Microstructural aspects of aluminumsilicon carbide particulate composites produced by a casting method", Materials Science and Engineering: A, 107 (1989) 73-80.
56. D.M. Aylor, "Metals Handbook V-13", vol. 9, ASM Metals Park, OH, (1982) 859–863.

57. D.P. Mondal, S. Das, A.K. Jha, A.H. Yegneswaran, "Abrasive wear of Al alloy–Al2O3 particle composite: a study on the combined effect of load and size of abrasive", Wear, 223 (1998) 131–138.
58. Elaine Rich, Kevin Knight, "Artificial Intelligence", 2nd Edition, Tata Mc-Graw-Hill publishing company New Delhi, (1999).
59. Ferhat Gul, Mehmet Acilar, "Effect of the reinforcement volume fraction on the dry sliding wear behaviour of Al–10Si/SiCp composites produced by vacuum infiltration technique", Composites Science and Technology, 64 (2004) 1959–1970.
60. Feng Tang, Xiaoling Wu, Shirong Gec, Jichun Ye, Hua Zhu, Masuo Hagiwara, Julie M.Schoenung, "Dry sliding friction and wear properties of B_4C particulate-reinforced Al-5083 matrix composites", Wear, 264 (2008) 555-561.
61. F.S.Rashed, T.S.Mahmoud, "Prediction of wear behavior of A356/SiCp MMCs using neural networks", Tribology International, 42 (2009) 642–648.
62. G. Ganesan, K. Raghukandan, R. Karthikeyan and B.C. Pai, "Development of processing map for 6061 Al/15% SiCp through neural networks", Journal of Materials Processing Technology, 166 (2005) 423-429.
63. R. Gibson, A. J. Clegg, A. A. Das, "Wear of cast Al-Si alloys containing graphite", Wear, 95 (1984) 193-198.
64. G. Partheepan, D.K. Sehgal,R.K. Pandey, "Fracture toughness evaluation using miniature specimen test and neural network", Computational Materials Science, 44 (2008) 523–530.
65. G.Y. Lee, C.K.H. Dharan, R.O. Ritchie, "A physically based abrasive wear model for composite materials", Wear, 252 (3–4) (2002) 322–331.
66. H.C. How, T.N. Baker, "Dry sliding wear behavior of saffil-reinforced AA6061Composites", Wear, 210 (1997) 263-272.
67. H.C. How, T.N. Baker, "Characterization of sliding friction-induced subsurface deformation of Saffil-reinforced AA6061 composites", Wear, 232 (1999) 106–115.
68. Heguo Zhu, Hengzhi Wang, Liangqi Ge, "Wear properties of the composites fabricated by exothermic dispersion reaction synthesis in an Al–TiO2–B2O3 system", Wear, 264 (2008) 967-972.

69. H.L. Lee, W.H. Lu, S. Chan, "Abrasive wear of powder metallurgy Al alloy 6061 –SiC particle composites", Wear, 159 (1992) 223–231.
70. H.R. Hafizpour, M. Sanjari, A. Simchi, "Analysis of the effect of reinforcement particles on the compressibility of Al–SiC composite powders using a neural network model",aterials and Design, 30 (2009) 1518–1523.
71. H. Ribes, M. Suery, G. L Esperance, J.G. Legoux, "Microscopic examination of the interface region in 6061-Al/SiC composites reinforced with as-received and oxidized SiC particles", Metallurgical and Materials Transactions A, 21 (1990) 2489–2496.
72. H. Sekine, R. Chen, "A combined microstructure strengthening analysis of SiCprAl metal matrix composites", Composite, 6 (1995) 183–188.
73. Howell, A. Ball, "Dry sliding wear of particulate-reinforced aluminum alloys against automobile friction materials", Wear, 181-183 (1995) 379-390.
74. Hutchings, Mater. Sci. Technol. 10 (1994) 513–517.
75. H.X. Zhu, S.K. Liu, "Mechanical properties of squeeze-cast zinc alloy matrix composites containing α-alumina fibers", Composites, 5 (1993) 437–442.
76. H. Y. Sohn and S. PalDey, "Synthesis of Ultrafine Particles and Thin Films of Ni4Mo by the Vapor-Phase Hydrogen Co-reduction of the Constituent Metal Chlorides", Materials Science and Engineering A, 247 (1998) 165-172.
77. I.A. Ibrahim, F.A. Mohamed, E.J. Lavernia, "Particulate reinforced metal matrix composites—a review", J. Mater. Sci., 26 (1991) 1137–1156.
78. J.C. Walker, W.M. Rainforth, H. Jones, "Lubricated sliding wear behavior of aluminum alloy composites", Wear, 259 (2005) 577–589.
79. J. Gilbert Kaufman, "Properties of Aluminum Alloys; Tensile, Creep, and Fatigue Data at High and Low Temperatures", ASM International, (2002).
80. Jiahua Zhu, Yijun Shi, Xin Feng, Huaiyuan Wang, Xiaohua Lu, "Prediction on tribological properties of carbon fiber and TiO2 synergistic reinforced polytetrafluoroethylene composites with artificial neural networks", Materials and Design, 30 (2009) 1042–1049.

81. J.K.M. Kwok, S.C. Lim, "High-speed tribological properties of some Al/SiCp composites. I. Frictional and wear-rate characteristics", Composite Science and Technology, 59 (1999) 55–63.
82. J. Llorca, "Failure micro-mechanisms in particulate-reinforced metal matrix composites", J. Phys., 3 (1993) 1793-1798.
83. J.M. Gomez de Salazar, M. I. Barrena, "Influence of heat treatments on the wear behaviour of an AA6092/SiC25p composite", Wear, 256 (2004) 286–293.
84. J.M. Wu, Z.Z. Li, "Contributions of the particulate reinforcement to dry sliding wear resistance of rapidly solidified Al-Ti alloys", Wear, 244 (2000) 147–153.
85. J.Narciso, C.garcia-Cordovilla, E.Louis "Abrasive wear resistance of aluminum alloy/ceramic particulate composites", Wear, 192 (1996) 170-177.
86. Joel Hemanth, "Tribological behavior of cryogenically treated B_4Cp/Al–12% Si composites", Wear, 258 (2005) 1732–1744.
87. B. F. Jogi, P. K. Brahmankara, V. S. Nandab, and R .C Prasad, "Some studies on fatigue crack growth rate of aluminum alloy 6061", Journal of material processing Technology, 201(2008) 380-384.
88. J.P. Tu, Y.Z. Yang, "Tribological behavior of Al18B4O33-whisker reinforced hypoeutectic Al–Si–Mg-matrix composites under dry sliding conditions", Composite Science Technology, 60 (2000) 1801–1809.
89. J.Q. Jiang, R.-S. Tan, A.-B. Ma, "Dry sliding wear behavior of Al2O3–Al composites produced by centrifugal force infiltration", Mater. Sci. Technol, 12 (1996) 483–488.
90. J.R. Gomes, A. Ramalho, M.C. Gaspar, S.F. Carvalho, "Reciprocating wear tests of Al–Si/SiCp composites: A study of the effect of stroke length", Wear, 259 (2005) 545–552.
91. J. Zhang, A.T. Alpas, "Delamination wear in ductile materials containing second phase particles", Materials Science and Engineering: A, 160 (1993) 25-35.
92. J. Zhang, A.T. Alpas, "Transition between mild and severe wear in aluminum alloys", Acta Materia, 45 (2) (1997) 513–528.
93. Kassim S. Al-Rubaie, Humberto N. Yoshimura and Jose Daniel Biasoli de Mello, "Two-body Abrasive Wear of Al–SiC Composites", Wear, 233–235 (1999) 444–454.

94. K.H. Zum Gahr, Met. Prog., 116 (1979), 46.
95. C. K. Kim, S. Y. Park, "A study on the fabrication and mechanical properties of SiC fiber aluminum alloy composites", J Korean Inst Met Mater, (1984) 22:185–92.
96. K. M. Shorowordi, A.S.M.A. Haseeb, J.P. Celis, "Velocity effects on the wear, friction and tribo-chemistry of aluminum MMC sliding against phenolic brake pad", Wear, 256 (2004) 1176–1181.
97. M. D. Kulkarni, P. S. Robi, R. C. Prasad, P. Ramakrishnan, "Deformation and fracture behavior of cast and extruded 7075Al–SiCp composites at room and elevated temperatures", Mater Trans, JIM, 37 (1996) 223–9.
98. L. Ceschini, C. Bosi, A. Casagrande and G.L. Garagnani, "Effect of Thermal Treatment and Recycling on the Tribological Behaviour of an Al Si Mg–SiCp Composite", Wear, 251 (2001) 1377–1385.
99. L. Ceschini, G.S. Daehn h, G.L. Garagnani, C. Martini, "Friction and wear behavior of C 4 Al_20_3/AI composites under dry sliding conditions", Wear, 216 (1998) 229-238.
100. L.E. Nielson and R.F. Landel, "Mechanical properties of polymers and composites", Marcel Dekker, Inc. New York (1994).
101. Lin Ye, Ye Lu, Zhongqing Su, Guang Meng, "Functionalized composite structures for new generation airframes: a review", Composites Science and Technology, 65 (2005) 1436–1446.
102. L.J. Yang, "Wear coefficient equation for aluminum-based matrix composites against steel disc", Wear, 255 (2003) 579–592.
103. L.J. Yang "A test methodology for the determination of wear coefficient", Wear, 259 (2005) 1453–1461.
104. L.J. Yang, "The effect of nominal specimen contact area on the wear coefficient of AA 6061 aluminium matrix composite reinforced with alumina particles", Wear, 263 (2007) 939-948.
105. Lloyd, Int. Met. Rev. 39 (1984) 1–23.
106. L. Las, J.M. Rodrigez-Ibabe, "Wear behavior of eutectic and hypereutectic Al–Si–Cu–Mg casting alloys tested against a composite brake pad", Mater. Sci. Eng., A, 363 (2003) 193–200.

107. Manwar Hussain, Atsushi Nakahira, Shigehiro Nishijima and Koichi Niihara, "Effects of coupling agents on the mechanical properties improvement of the TiO_2 reinforced epoxy system", Materials Letters, 26 (1996) 299-303.
108. Z. Y. Ma, S. C. Tjong, "In situ ceramic particle-reinforced aluminum matrix composites fabricated by reaction pressing in the TiO2 (Ti)–Al–B (B2O3) systems", Metall. Mater. Trans., 28(A) (1997)1931–1942.
109. M. Bai, Q. Xue, X. Wang, Y. Wan, W. Liu, "Wear mechanism of SiC whisker-reinforced 2024 al-alloy matrix composites in oscillating sliding wear tests", Wear, 185 (1995) 197–202.
110. M. Chen, T. Perry, A.T. Alpas, "Ultra-mild wear in eutectic Al–Si alloys", Wear, 263(2007) 552–561.
111. M.D. Bermudez, G. Martinez-Nicolas, F.J. Carri0n, I. Martinez-Mateo, J.A. Rodriguez and E.J. Herrera, "Dry and Lubricated Wear Resistance of Mechanically- Alloyed Aluminum-base Sintered Composites", Wear, 248 (2001) 178–186.
112. M.H. Korkut, "Microstructure and wear behavior of Al2024\SiFe and Al2024\SiFe\Al2O3 composites", Tribology International, 36 (2003) 169–180.
113. M.J. Ghazali, W.M. Rainforth , H. Jones, "Dry sliding wear behavior of some wrought, rapidly solidified powder metallurgy aluminum alloys", Wear, 259 (2005) 490–500.
114. M.K. Surappa, S.V. Prasad, P.K. Rohatgi, "Wear and abrasion of cast Al–alumina particle composites", Wear, 77 (1982) 295–302.
115. Mortensen A, Wong T, Metall Trans A, Vol 21 A (1990) 2257–2263.
116. M.R. Rosenberger, C.E. Schvezov, E. Forlerer, "Wear of different aluminum matrix composites under conditions that generate a mechanically mixed layer", Wear 259 (2005) 590–601.
117. M. Singh, O.P. Modi, Rupa Dasgupta, A.K. Jha, "High stress abrasive wear behavior of aluminium alloy–granite particle composite", Wear, 233–235 (1999) 455–461.
118. M.Y. Chen, M.C. Breslin, "Friction behavior of co-continuous alumina/aluminum composites with and without SiC reinforcement", Wear, 249 (2002) 868–876.

119. Necat Altinkok and Rasit Koker, "Modeling of the prediction of tensile and density properties in particle reinforced metal matrix composites by using neural networks", Materials & Design, 27 (2006) 625-631.
120. O.P. Modi, B.K. Prasad, A.H. Yegneswaran, M.L. Vaidya, "Dry sliding wear behavior of squeeze cast al-alloy–silicon carbide composites", Mater. Sci. Eng. A., 151 (1992) 235– 245.
121. O.P. Modi, R.P. Yadav, B.K. Prasad, A.K. Jha, S. Das, A.H. Yegneswaran, "Three-body abrasion of a cast zinc–aluminum alloy: influence of Al2O3 dispersoid and abrasive medium", Wear, 249 (2001) 792–799.
122. P.C.Pandey, "Composite Materials", Web-Based Course, Dept. of Civil Eng., IISc Bangalore, (2004).
123. Peter J, Blau, "Fifty years of research on the wear of metals", Tribology International, 30 (1997) 321-331.
124. P.H. Shipway, A.R. Kennedy, A.J. Wilkes, "Sliding wear behavior of aluminum-based metal matrix composites produced by a novel liquid route", Wear, 216 (1998) 160 –171.
125. P.K. Rohatgi, Y. Liu, T.L. Barr, Metall. Trans. A., 22 (1991) 1435.
126. P.K. Rohatgi, S. Ray, Y. Liu, "Tribological properties of metal matrix graphite particle composites", Int. Mater. Rev., 37 (1992) 129–149.
127. P.M. Singh, J.J. Lewandowski, "Effects of heat treatment and reinforcement size on reinforcement fracture during tension testing of a SiCp discontinuously reinforced aluminum alloy", Metall. Trans. A., 24 (1993) 2531–2543.
128. P.N. Bindumadhavan, H.K. Wah, O. Prabhakar, "Dual particle size (DPS) composites: effect on wear and mechanical properties of particulate matrix composites", Wear, 248 (2001) 112–120.
129. P. Poza, M.A. Garrido, A. Rico, J. Rodriguez, "Dry sliding wear behavior of aluminum–lithium alloys reinforced with SiC particles", Wear, 262 (2007) 292–300.
130. P.R. Gibson, A.J. Clegg, A.A. Das, Mater. Sci. Technol., 1(1985) 559.
131. P. Vissutipitukul, T. Aizawa, "Short communication; Wear of plasma-nitrided aluminum alloys", Wear, 259 (2005) 482–489.

132. Q.D. Qin, Y.G. Zhao, W. Zhou, "Dry sliding wear behavior of Mg_2Si/Al composites against automobile friction material", Wear, 264 (2008) 654-661.
133. Raimundo Carlos Silverio Freire Jr, Adriao Duarte Doria Neto, Eve Maria Freire de Aquino, "Use of modular networks in the building of constant life diagrams", International Journal of Fatigue, 29 (2007) 389–396.
134. Rajnesh Tyagi, "Synthesis and tribological characterization of in situ cast Al–TiC composites", Wear, 259 (2005) 569–576.
135. R. Chen, G.D. Zhang, "Casting defects and properties of cast A356 alloy reinforced with SiC particulates", Compos. Sci. Technol., 4 (1993) 511–556.
136. Rang Chen, Akira lwabuchi, Tomoharu Shimizu, Hyung Seop Shin, Hidenobu Mifune, "The sliding wear resistance behavior of NiAI and SiC particles reinforced aluminum alloy matrix composites", Wear, 213 (1997) 175-184.
137. Rong Chen , Akira Iwabuchi, Tomoharu Shimizu, "The effect of a T6 heat treatment on the fretting wear of a SiC particle-reinforced A356 aluminum alloy matrix composite", Wear, 238 (2000) 110–119.
138. R. Dwivedi, "Development of Advanced Reinforced Aluminum Brake Rotors", SAE Technical Paper Series, Warrendale, PA, USA, (1995), 8 p.
139. R. Tyagi, S.K. Nath, S. Ray, "Effect of martensite content on friction and oxidative wear behavior of 0.42 Pct carbon dual-phase steel", Metallurgical and Materials Transactions A, 33A (2002) 3479–3488.
140. R.K. Uyyuru, M.K. Surappa, S. Brusethaug, "Effect of reinforcement volume fraction and size distribution on the tribological behavior of Al-composite/brake pad tribocouple", Wear, 260 (2006) 1248–1255.
141. R.K. Uyyuru, M.K. Surappa, S. Brusethaug, "Tribological behavior of Al–Si–SiCp composites/automobile brake pad system under dry sliding conditions", Tribology International, 40 (2007) 365–373.
142. R.L. Deuis, C. Subramaniun, J.M. Yellup, "Abrasive wear of aluminum composites—a review", Wear, 201 (1996) 132–144.

143. R. Tiwari, H. Herman, S. Sampath, B. Gudmundsson, "Plasma spray consolidation of high temperature composites", Materials Science and Engineering: A, 144 (1991) 127-13.
144. Sanjay Kumar Thakur, Brij Kumar Dhindaw, "The influence of interfacial characteristics between SiCp and Mg/Al metal matrix on wear, coefficient of friction and microhardness", Wear, 247 (2001) 191–201.
145. S.C. Sharma, "The sliding wear behavior of Al6061–garnet particulate composites", Wear, 249 (2001) 1036–1045.
146. S. Das, S.V. Prasad, "Microstructure and wear of cast (Al-Si alloy)-graphite composites", Wear, 133 (1989) 173.
147. S. Das, S.V. Prasad, T.R. Ramachandran, "Tribology of Al-Si alloy-graphite composites: tribo induced graphite films and the role of silicon morphology", Materials Science and Engineering: A, 138 (1991) 123.
148. S. Das, "The influence of matrix microstructure and particle reinforcement on the two body abrasive wear of cast Al–Si-alloy composites", J. Mater. Sci. Lett., 16 (1997) 1757–1760.
149. S. Das, D.P. Mondal, S. Sawla, N. Ramakrishnan, "Synergic effect of reinforcement and heat treatment on the two body abrasive wear of an Al–Si alloy under varying loads and abrasive sizes", Wear, 264 (2008) 47–59.
150. Shao-Yun Fu, Guanshui Xu and Yiu-Wing Mai, "On the elastic modulus of hybrid particle/short-fiber/polymer composites", Composites: Part B, 33 (2002) 291-299.
151. S.K. Biswas, "Some mechanisms of tribo-film formation in metal/metal and ceramic/metal sliding interactions", Wear, 245 (2000) 178–189.
152. S.K. Chaudhury, A.K. Singh, C.S. Sivaramakrishnan, S.C. Panigrahi, "Wear and friction behavior of spray formed and stir cast Al–2Mg–11TiO_2 composites", Wear, 258 (2005) 759–767.
153. S. Kumar, V. Balasubramanian, "Developing a mathematical model to evaluate wear rate of AA7075/SiCp powder metallurgy composites", Wear, 264 (2008) 1026-1034.
154. Simon Haykin, "Neural Networks – A Comprehensive Foundation", Second Edition, Pearson Education, Pearson Prentice Hall, (2006).

155. S. Muthukumarasamy, S. Seshan, "Structure and properties of fibre reinforced Zn-27% Al alloy based cast MMCs", Composites, 26 (1995) 387–393.
156. Soon-Chul Kwon, Tadahrru Adachi, Wakako Araki and Akihiko Yamaji, "Thermoviscoelastic properties of silica particulate-reinforced epoxy composites: Considered in terms of particle packing model", Acta Materialia, 54 (2006) 3369-3374.
157. Sug Won Kim, Ui Jong Lee, Sang Won Han, Dong Keun Kim, K. Ogi, "Heat treatment and wear characteristics of Al/SiCp composites fabricated by duplex process", Composites: Part B, 34 (2003) 737–745.
158. S.V. Nair, J.K. Tien, R.C. Bates, "SiC-reinforced aluminum metal matrix composites", Int. Mater. Rev., 30 (6) (1985) 275–290.
159. S.V. Prasad, P.K. Rothagi, "Tribological properties of Al alloy particle composite", J. Metall., 39 (1987) 22.
160. S. Wilson, A.T. Alpas "Wear mechanism maps for metal matrix composites", Wear, 212 (1997) 41-49.
161. Szu Ying Yu, Hitoshi Ishii, Keiichiro Tohgo, Young Tae Cho, Dongfeng Diao, "Temperature dependence of sliding wear behavior in SiC whisker or SiC particulate reinforced 6061 aluminium alloy composite", Wear, 213 (1997) 21-28.
162. T. Miyajima and Y. Iwai; "Effects of Reinforcements on Sliding Wear Behavior of Aluminum Matrix Composites", Wear, 255 (2003) 606–616.
163. T. Zeuner, P. Stojanov, P.R. Saham, H. Ruppert, A. Engels, "Developing trends in disc brake technology for rail application", Mater. Sci. Technol., 14 (1998) 857–863.
164. Uan J Y, Chen LH, Lui TS, "On the extrusion microstructural evolution of Al–Al_3Ni in situ composite", Acta Materialia, 49 (2001) 313-320.
165. U. Sanchez-Santana, C. Rubio-Gonzalez, G. Gomez-Rosas, J.L. Ocana, C. Molpeceres, J. Porro, M. Morales, "Wear and friction of 6061-T6 aluminum alloy treated by laser shock processing", Wear, 260 (2006) 847–854.
166. G. B. Veeresh Kumar, C. S. P. Rao, M. S. Bhagyashekar, N. Selvaraj "Mechanical and Tribological Behaviour of Al6061-SiCp Composites", proceedings of the International Conference ICMM-2008, (2008) pp 1-8.

167. G. B. Veeresh Kumar, C. S. P. Rao, N. Selvaraj, M. S. Bhagyashekar, "Studies on Al6061-SiC and Al7075-Al2O3 Metal Matrix Composites", Journal of Minerals & Materials Characterization & Engineering, (JMMCE), USA volume 9 (2009) pp.47-59.
168. Vencl A., I. Bobi, Z. Mi¡skovi, "Effect of thixo-casting and heat treatment on the tribological properties of hypoeutectic Al–Si alloy", Wear, 264 (2008) 616-623.
169. V. Jayaram, S.K. Biswas, "Wear of Al_2O_3 –SiC [Al, Si] melt oxidized ceramic composites", Wear, 225–229 (1999) 1322–1326.
170. V.V. Bhanu Prasad, K.S. Prasad, A.K Kurovilla, A.B. Pandey, B.V.R.Bhat and Y.R Mahajan, "Composite strengthening in 6061 and Al-4 Mg alloys", Journal of Mat., Sci., 26 (1991) 460.
171. W. Ames, A.T. Alpas, Metall. Mater. Trans. A, 26 (1995) 85.
172. A. Wang and H.J. Rack, "Abrasive wear of silicon carbide particulate and whisker reinforced 7091 aluminum matrix composites", Wear, 146 (1991) 337.
173. W.Q.Song, P.Krauklis, A.P.Mouritz, S.Bandyopadhyay, "The effect of thermal ageing on the abrasive wear behavior of age-hardening 2014 Al/SiC and 6061 Al/SiC composites", Wear, 185 (1995) 125-130.
174. X.Y. Li, K.N. Tandon, "Mechanical mixing induced by sliding wear of an Al–Si alloy against M2 steel", Wear, 225–229 (1999) 640–648.

PUBLICATIONS

1. **N. V. Murthy** [a*], A.P.reddy[b], N. Selvaraj[c], C. S. P. Rao[d“] Preparation of SiC based Aluminium Metal Matrix nano composites by High intensity Ultrasonic Cavitation Process and Evaluation of Mechanical andTribological properties, Materials Science and Engineering 149 (2016) 012106 doi:10.1088/1757-899X/149/1/012106 **(Published).**

2. **N. V. Murthy**, A. P. reddy , n. selvaraj& c. s. p. rao, Aluminum metal matrix nano composites (al mmncs) – manufacturing methods: a review, International Journal of Mechanical Engineering (IJME) ISSN(P): 2319-2240; ISSN(E): 2319-2259 Vol. 4, Issue 4, Jun - Jul 2015, 29-44**.(Published)**

3. **N. V. Murthy**,A. P. reddy,N. selvaraj,c. s. p.rao a review on fabrication of aluminium alloy based metal matrix nano composites through ultrasonic assisted casting , Journal of Metallurgical and Materials Engineering Research(JMMER) Vol. 1, Issue 2, Dec 2015, 1-8**.(Published)**

4. **N. V. Murthy**[a*], N. Selvaraj[b], C. S. P. Rao[c] Dispersion of Alumina Nano Particles in Al 2219 alloy by Ultrasonic Assisted Stir Casting Technique(Materials Today, **Accepted**)

BIO-DATA

Name	:	Vishnumurthy Nallapati
Date of birth	:	04-04-1984
Present Position	:	Research Scholar Department of Mechanical Engineering National Institute of Technology Warangal-506004 Telangana State, India.
Qualification	:	M.Tech (Automobile Engineering)
Permanent Address	:	S/O (Late) N.Ammaiah, H.No 1-76, Kuchinapudi post, Nizampatnam Mandal, Guntur District, Andhra Pradesh,India-522262
E-mail	:	nvm.nitw@gmail.com

ACKNOWLEDGEMENTS

"The Satisfaction and Euphoria that accompany the completion of any task would be incomplete without the mention of people who made it possible, whose constant guidance and encouragement ground my efforts with success".

I consider it a privilege to express my gratitude and respect to **Dr. C.S.P. Rao,** Professor, head , Department of Mechanical Engineering, National Institute of Technology, Warangal, for suggesting the topic and providing constant guidance throughout the course of this research work. He has been a source of direction and encouragement to me in pursuing my long cherished ambition of attaining higher academic levels.

I sincerely thank **Dr. N. Selvaraj**, Professor, Department of Mechanical Engineering, National Institute of Technology, Warangal, for his constant support and continuous motivation during this research work.

I like to extend my sincere thanks to **Prof. C.S.P Rao,** Head of the Mechanical Engineering Department and to the members of my **Doctoral Scrutiny Committee, Dr. DR. Narasimha sarma N V S,** Dean Academic Affairs and Professor, Department of Electrical and Electronics Engineering, **Dr.N.Narasaiah,** Associate Professor, Department of Metallurgical and Materials Engineering, **Dr.R.N.Rao,** Associate Professor, Mechanical Engineering Department, and **Dr.P.S.C.Bose,** Assistant Professor, Mechanical Engineering Department, for all the support bestowed on me by suggesting and verifying the research work.

I sincerely thank the **Director,** National Institute of Technology, Warangal for giving me an opportunity to pursue higher education at such a reputed institute.

I sincerely thank my co-researchers **Mr.A.Prasad Reddy, Mr.K.N.B.Kumar, Dr. Lokeswara Rao Thatuku** and **Mr. Ashok Reddy Komerelli, Mr.Sharath Chandra Palle** and **Mr. Sagar Gullipalli** for their cooperation during the research studies.

The services of the staff of **Mr. Rangilal**, **Mr. Raju and Mr. Ilaiah** Production Engineering Section, Mechanical Engineering Department, National Institute of Technology Warangal are acknowledged with sincere thanks.

I remain grateful to my well wisher **Dasyam Vinay Bhaskar garu (M.L.A)** and to my beloved friends **Mr. D. Ranjith Reddy, Mr. Dasari Srinivas, Mr.G.Mahendar, Mr.A.Ankith Reddy** and **Mr.B.Kranthi kumar** for supporting me in all the directions during this research work.

Above all, I thank the Lord, my family and well wishers who have been an immense support throughout my research work.

(Vishnumurthy Nallapati)